UNIVERSITY OF SHEFFIELD
School of Architectural Studies

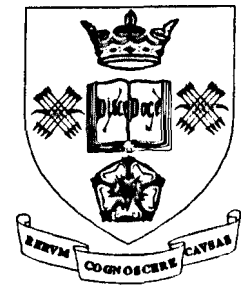

THE BEHAVIOUR OF COMPOSITE BEAMS WITH PARTIAL INTERACTION AT ELEVATED TEMPERATURES

by Vasif Atilla Oven

A thesis submitted in fulfilment of the requirements for the Degree of Doctor of Philosophy.

April, 1996

SUMMARY

When composite slabs are used in conjunction with conventional composite beam construction, the number of shear connectors used along the length of the beam may be limited, resulting in incomplete interaction. This is known to affect the performance of the beam at ambient temperature, but nothing is known about its influence in fire.

This thesis is primarily concerned with the development of a two-dimensional non-linear finite element approach to investigate the structural behaviour of unprotected composite beams at elevated temperatures by considering the influence of slip at the interface. The shear connection is modelled as a linking medium characterised by an assumed force-slip relationship. Semi-rigid connection characteristics are also incorporated as zero length spring elements connected to the steel beam and reinforced concrete slab. A semi-rigid connection model optimising the connection characteristics for a composite beam with partial interaction is proposed, using a pair of rotational springs and a linear spring. The computer model has been validated against experimental data both at ambient temperature and at high temperatures.

A parametric study investigating the influence of shear connection, semi-rigid joint characteristics, reinforcement ratio and different temperature profiles across the cross-section at elevated temperatures has been carried out. It is shown that the failure temperature is little affected by the force-slip characteristics or their spacing. A noticeable improvement in fire resistance is seen when the rigidity of the connection or reinforcement ratio in the concrete slab is increased. It is also found that the failure temperature of composite beams can be significantly higher than that of bare steel beams.

ACKNOWLEDGEMENT

This work was carried out in the School of Architectural Studies at the University of Sheffield. The author would like to express his deepest appreciation and gratitude to Prof. R.J. Plank who supervised this work, for his excellent supervision, support and encouragement throughout. The author gratefully acknowledges the help and support given by Dr. I.W. Burgess for his many helpful criticisms and valuable advice. My sincere thanks are also due to Dr. S.R. Najjar who helped me at critical stages of the development of numerical approach of this study.

My special thanks to Turkish Ministry of Education which made this research and my presence in England possible, and financially supported me throughout my studies.

Words of appreciation are also extended to Prof. B. Lawson, Head of Department and all other members of the academic and secretarial staff in the School of Architectural Studies.

Finally, I wish to thank my beloved wife Handan for her support, patience and understanding during the difficult times of my research.

TABLE OF CONTENTS

LIST OF FIGURES

CHAPTER 1. INTRODUCTION

1.1. General Aspects of Fire Safety and Regulations

Building fires are extremely destructive, causing loss of life and property. Designers must therefore take the necessary precautions to minimise the effects of fire. This includes provision of adequate escape routes, compartmentation, to limit the spread of fire and measures to avoid collapse. Premature structural failure can prevent occupants from reaching their escape route, reduce the speed of evacuation and also precipitate the spread of fire and smoke by destroying compartmentation in the building. This in turn leads to an increase in the rate of injury or death and damage to the property.

The notion of fire safety provision has evolved as a necessity from past experience of fire hazard. The first comprehensive studies on fire safety in buildings in the UK were the two Fire Grading Reports[1,2], published in 1946 and 1952 which form the basis for current fire regulations for buildings. They defined fire safety policies to safeguard life and minimise the damage to property. This was set out in terms of;

1. Minimising the risk of ignition
2. Providing a safe exit for occupants
3. Restricting the spread of fire
4. Minimising the risk of structural collapse.

Both passive and active fire protection measures were considered. Passive measures include fire protection of structural members, means of escape and compartmentation and fire break walls. Active measures such as sprinklers, hand appliances, smoke detectors and dry rising mains are mainly for property protection but they also help to improve life safety.

The Fire Building Regulations[3] in England and Wales were enacted in 1965 and introduced features such as control on linings, space separation and duct penetration. It did not use all of the recommendations of the earlier Fire Grading Reports. For instance, there were no provisions for means of escape and no allowance for active fire extinguishing measures. In 1966 an amendment was introduced to allow compartment size to be doubled if a sprinkler system was used, and in 1973 means of escape were required for every building. In 1985 the regulations[4] were amended to provide a more flexible system. Although technically there were very few changes the framework opened

the way for future modifications and improvements. The regulations were brief and defined functionally, allowing the designer to use solutions other than those prescribed in demonstrating compliance.

In 1986 an important report, Fire Safety in Buildings[5], defined the objectives of fire protection in buildings as, life safety, prevention of conflagration, and property protection. It recommended that all provisions for these three objectives should be under one regulatory system and advocated the use of active fire protection, alternative fire engineering principles and fire safety management, especially in places where a large number of occupants is involved. Legislation and design methods for fire safety in buildings are still evolving, with an increasing facility to allow designers the opportunity of providing satisfactory safety in a variety of ways. A more detailed hierarchy of fire safety strategies is illustrated in Fig. 1.1 covering all aspects of safety. One area of this is the stability of the structure when exposed to fire and it is this aspect which is dealt with in this thesis.

1.2. Fire Safety Requirements for Structural Elements

Current regulations[4,5,6] classify building types into two main categories, namely residential (houses, flats, hospitals, hotels, hostels, etc.) and non-residential. The latter includes assembly (theatres, restaurants, concert halls, etc.), office, shop (shopping malls, department stores, etc.), industrial, and other non-residential (storage, car parks, etc.). Depending on the size, occupancy and use of the building, fire resistance times are specified, typically as 30, 60, 90, 120, 180 and 240 minutes[4,5,6]. In addition, for high rise buildings the key structural elements must have a fire resistance of at least 120 minutes[5].

One way of verifying the fire resistance performance of load-bearing elements is to carry out furnace tests. These are conducted in accordance with BS 476: Part 20 and Part 21[7]. All structural elements within the building must survive the fire for at least the specified fire resistance time without loss of stability, integrity and insulation functions. Integrity is defined as the ability of a specimen to remain free from holes and cracks and insulation is defined as the ability to restrict the temperature rise of the unexposed face of the specimen to below a specified level. Stability is defined as the ability of a specimen to support its test load without excessive deformation.

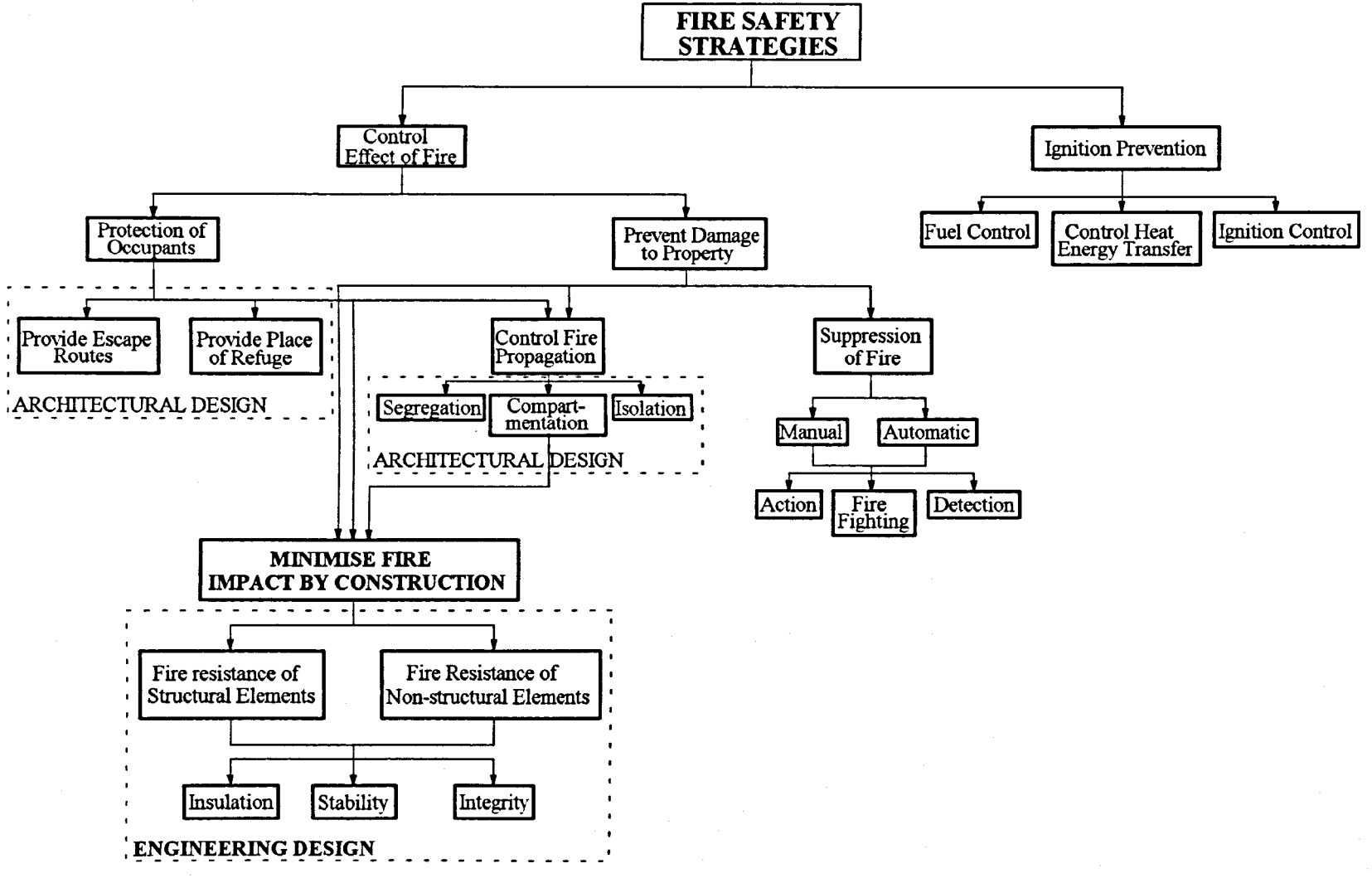

Fig. 1.1 Fire safety strategies.

Regulations which rely on this approach however, have some limitations[8,9,10]. They are generally inflexible, requiring similar fire resistance periods in situations where the fire hazard may be different[8,11]. In addition the required fire resistance times increase in a step-wise manner whilst fire severity in building fires does not. Moreover little account is made for active fire protection measures and no specific provision is made for a fire engineering approach in determining fire severity or designing structural elements.

Fire tests also have some disadvantages. They are costly and time consuming, realistic conditions are difficult to model due to limited dimensions of the furnace, characteristics of the loading device and simplified end restraints[8] and finally the standard heating regime used in these tests is not necessarily representative of real fires[12,13,14].

1.3. Analytical Methods for Predicting the Fire Resistance

The shortcomings of both building regulations and fire tests have led to the development of alternative methods for the specification of fire resistance requirements[8]. Fire engineering approach provides a basis for calculation of fire resistance requirements by considering the severity of a real fire in the context of the particular building. Therefore it can be a cost effective alternative to simple compliance with building regulations in that fire protection may be avoided or reduced in situations where the fire hazard is low and/or sufficient inherent fire resistance of the structure can be demonstrated. Moreover it may be considered as a useful tool in understanding the real structural behaviour in a building fire. The approach can be divided into three stages[8];

1. Modelling the development of a fire in a compartment
2. Prediction of temperature distribution in a structural element
3. Assessment of the structural behaviour.

The temperature rise of structural elements is directly related to the gas temperature of the compartment in which they are placed. The gas temperature in the compartment depends on the time-temperature profile of the fire, characterised by three stages namely, growth, full development and decay. The characteristics of a typical time-temperature profile for a real building fire are affected by the fire load (the amount and type of combustible materials), the available ventilation (size and shape of windows) and the thermal properties of the lining materials. All these factors can be utilised to predict the temperature-time relationship for a fully developed fire in a compartment, for example NATFIR[15], although predicting the growth of the fire is much more difficult.

Because of the temperature-dependent nature of material properties, the temperature distribution within the structural element is crucial for fire conditions. The shielding of parts of an element cross-section, for example the top flange of a steel beam where it is protected on one side by the floor slab, can give rise to temperature gradients. This is most influenced by the detail of the steelwork in relation to the fabric of the building, the configuration of the cross-section and any applied fire protection. Computer programs modelling the appropriate thermal conductivity, specific heat and density for various materials have been developed for predicting temperatures within steel and composite structural elements. For example, FIRES-T2[16,17] and TASEF-2[18] are two-dimensional non-linear finite element models coupled with time-step integration to deal with the heat flow problem, for steel and composite sections.

Assessment of the structural behaviour is concerned with the prediction of deformation and stress history at elevated temperatures. This depends on a number of factors including the load, cross-sectional dimensions, material properties, any composite action, boundary conditions and temperature gradient across the section and along the length. Most structural analysis programs do not carry out thermal analysis to predict temperatures but consider them as input data. Some can deal with whole framed structures, as well as individual members such as beams and columns. CEFICOSS[19,20], FASBUS-2[10,21] and PAFEC[11] are based on two dimensional non-linear finite element models. CEFICOSS is capable of carrying out both thermal and structural analysis on protected and unprotected composite and steel sections and includes the effects of large displacements. FASBUS-2 deals with composite sections and incorporates the effects of creep. NARR[22,23,24] is an efficient, well established computer model based on a secant stiffness method capable of analysing steel frames with composite beams such as conventional floor beams, shelf-angle beams or slim-floor beams. These approaches have been used with some success in modelling the behaviour of simple elements in a fire.

1.4. Composite Construction of Steel and Concrete

In recent years steel framed construction has become very popular for commercial buildings in Britain largely because of faster construction times than for other systems. Composite construction (Fig. 1.2) has also been an important factor offering significant savings in material compared with non-composite frames.

Composite action is usually achieved by connecting the concrete slab to the steel I-section, using shear connectors. The most widely used type of connector is the headed stud. The studs are welded to the flange of the steel I-section and embedded within the

concrete slab. Other types of connectors include bar and channel connectors which have been primarily developed for use in bridges due to their higher strength.

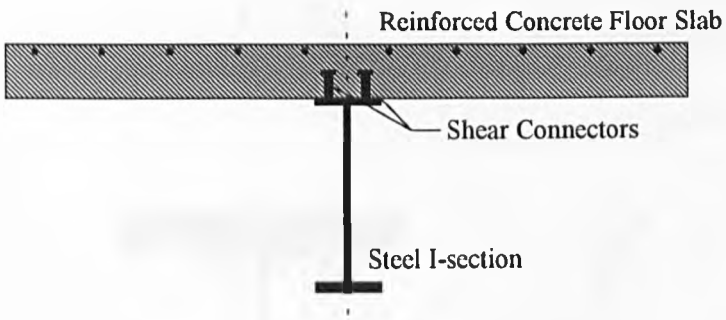

Fig. 1.2 Typical composite beam of steel and concrete.

The amount of slip between the concrete slab and I-section can affect the structural behaviour considerably[25]. If slip is fully free to develop, the concrete slab and steel I-section will bend independently. The distribution of bending stress for this case is illustrated in Fig. 1.3(b). The slip at the interface at mid-span is zero and maximum at the supports. There is an opposite strain in the top fibre of the I-section and bottom fibre in the concrete slab. If slip is completely eliminated by using infinitely stiff shear connection, full interaction develops and plane sections can reasonably be assumed to remain plane (Fig. 1.3(a)). The design of composite beams in practice is often based on the assumption of full interaction. However the degree of interaction depends on the effectiveness of the shear connection. When this is reduced, some slip will inevitably develop at the interface. In such situations partial interaction design methods must be used. The presence of slip results in greater strains than for full interaction with a corresponding increase in stresses, curvatures and deflections. Typical bending stress distribution for this case is shown in Fig. 1.3(c).

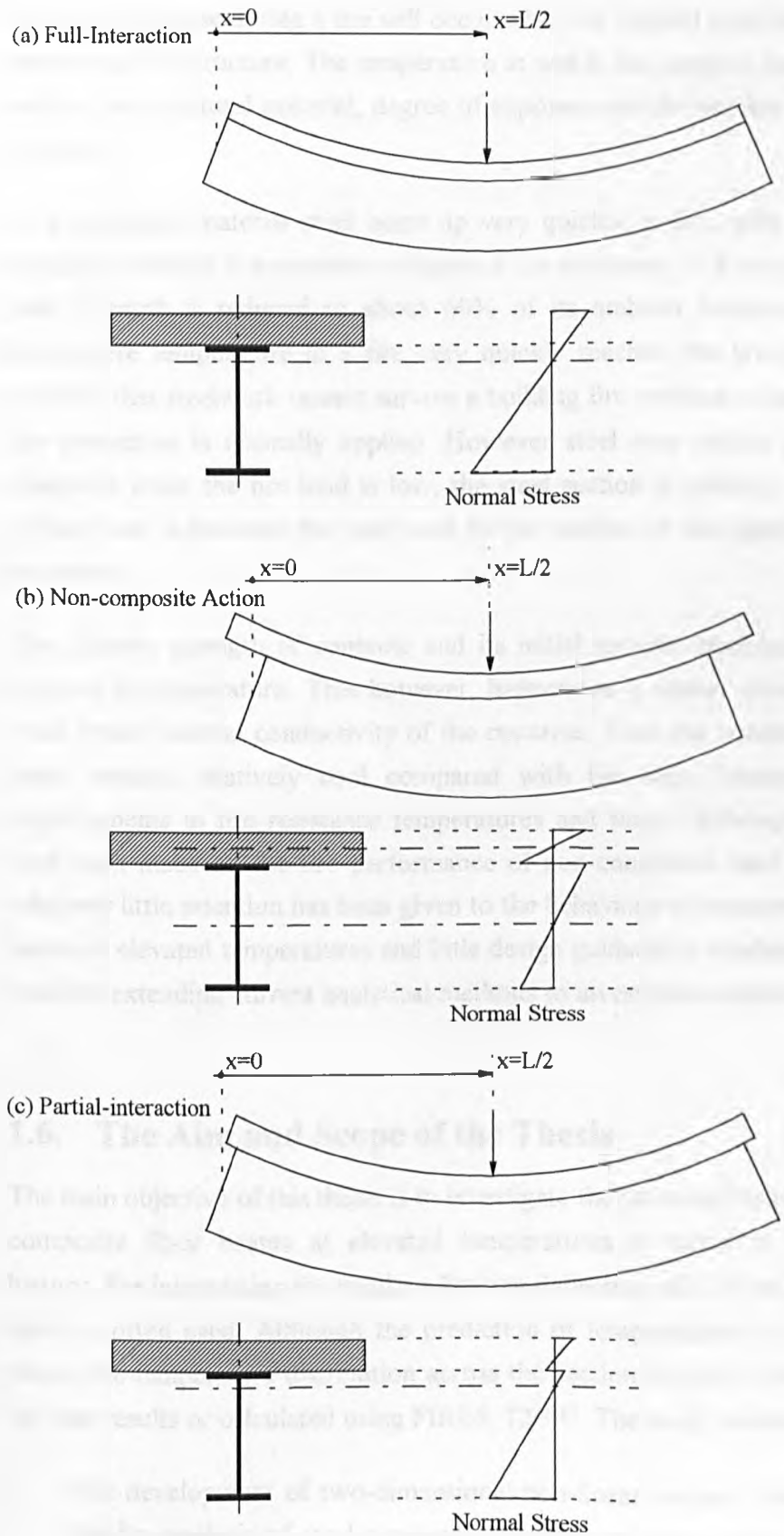

Fig. 1.3 Bending stress distributions.

1.5. The Effect of Fire on Composite Construction

Structural collapse during a fire will occur when the applied load exceeds the load bearing capacity of the structure. The temperature at which this happens depends on many factors such as the structural material, degree of exposure and the precise form and layout of the structure.

As a structural material steel heats up very quickly in fire, with corresponding loss of strength, resulting in premature collapse of the structure. At a temperature of $550^{o}C$[26] its yield strength is reduced to about 60% of its ambient temperature value. Since the atmosphere temperature in a fire very quickly reaches this level it has been generally assumed that steelwork cannot survive a building fire without collapse, and some form of fire protection is normally applied. However steel may exhibit sufficient inherent fire resistance when the fire load is low, the steel section is partially shielded from fire, the applied load is less than the 'safe' load for the section or the rigidity of the connection is increased.

The ultimate strength of concrete and its initial tangent modulus also deteriorate with increase in temperature. This however, happens at a slower rate than for steel due to much lower thermal conductivity of the concrete. Thus the concrete slab in a composite beam remains relatively cool compared with the steel I-section. This can provide improvements in fire resistance temperatures and times. Although a number of studies have been made on the fire performance of non-composite steel beams and deck slabs relatively little attention has been given to the behaviour of composite steel-concrete floor beams at elevated temperatures and little design guidance is available. Therefore there is a need for extending current analytical methods to investigate composite beams in fire..

1.6. The Aim and Scope of the Thesis

The main objective of this thesis is to investigate the structural behaviour of steel-concrete composite floor beams at elevated temperatures in terms of temperature-deflection history. For interpreting the results a limiting deflection of L/20 or L/30 as given in design rules, is often used. Although the prediction of temperatures is not an objective of the thesis, the temperature distribution across the section is either postulated on the basis of fire test results or calculated using FIRES-T2[16,17]. The study involves:

- The development of two-dimensional non-linear inelastic finite element models for the fire analysis of steel-concrete composite structures with fully rigid and flexible shear connection.

- The idealisation of semi-rigid joints for full and partial interaction and the incorporation of these into the finite element analysis.

- Convergence studies to determine the optimum finite element mesh and comparative studies using available experimental data.

- Use of the computer programs developed firstly to determine the influence of certain parameters which might affect the structural response to fire and secondly to gain insight into the behaviour which might lead to simple design methods based on calculations. This may lead to savings in overall construction cost compared with the use of current approaches.

Aspects concerning the integrity and insulation criteria are beyond the scope of this thesis. The analytical part of the thesis (Chapter 4 and 5) describes the derivation of the finite element model for full-interaction and partial-interaction and the treatment of semi-rigid joints. In the validation studies (Chapter 6) convergence studies are presented to optimise the number of elements used and some comparisons are made with experimental data. The parametric studies (Chapter 7) include the influence of semi-rigid connections, shear connectors, reinforcement and temperature distribution across the section.

CHAPTER 2. LITERATURE REVIEW

Although the behaviour of bare steel beams under fire conditions has been studied in reasonable depth both experimentally and analytically, very little research has been conducted on partially or fully composite beams at elevated temperatures. In the first part of this chapter, previous research concerned with experimental studies to determine the material properties and structural behaviour of composite beams will be discussed. In the second part, attention will be focused on analytical research. Most previous work on partially composite beams has been carried out at ambient temperature and studies at high temperatures are very scarce. However, this, together with analytical work which has been conducted on non-composite beams in fire provides a basis for developing elevated temperature studies for composite sections.

2.1. Experimental Studies

The analytical modelling of partially composite beam behaviour under fire conditions requires the high temperature mechanical properties of the materials making up a composite section, namely the steel beam, reinforcing bars, concrete and shear connectors.

The stress-strain-temperature characteristics of steel and related material properties such as yield strength and modulus of elasticity are now quite well established. Generally two different test procedures have been used: the isothermal tensile test in which the specimen is subjected to increasing load under a constant temperature and the anisothermal test in which the specimen is heated under a constant load.

The rate of loading in the isothermal tensile tests and the rate of heating in the anisothermal tests can have a significant influence on these characteristics. Lu, Trubert and Nash[27] conducted isothermal tests on stainless steel. They varied the rate of heating prior to applying load and reported that the yield strength was not affected by this. However, the results were for one temperature only (1200^{o}C). In contrast Willhelm and Kattus[28] presented a family of tensile stress-strain curves at various temperatures from 37^{o}C to 1093^{o}C. Their results for a range of both heating and loading rates showed that these rates did have an influence, particularly on the yield stress. However their studies

were primarily aimed at transient conditions in which both loading and heating vary simultaneously.

There has been some debate about the effect of creep due to different loading rates. The consensus from a number of investigators[29-33] is that the rate of loading has a negligible effect below 370°C but is more important at higher temperatures, particularly above 600°C. Some researchers have recommended that if an isothermal testing procedure was to be adopted, a standard rate of strain must be used so that creep would be accounted for in a consistent way. Jorgensen and Sorensen[29] suggested a rate of 0.05/min whilst Baba and Nagura[32] proposed a much slower rate of 0.01/min. In addition it was concluded that the mechanical properties of steel obtained from such isothermal tensile tests may not be appropriate in situations where the rate of temperature rise within the member was very slow, for example in the case of protected steel elements, in which case the creep effect should be properly accounted for[34,35]. However, based on full-scale beam tests, Harmathy and Stanzak[36-38] studied the effect of creep and concluded that this was not significant for unprotected steel elements because of the rapid rise of temperature.

The results from anisothermal tensile and flexural tests were reported by Witteveen, Twilt and Bijlaard[39]. Although the variation in heating rate (5-50°C/min.) slightly affected the test results at higher temperatures, below 400°C the heating rate had no effect on either collapse temperatures or the stress-strain relationship. In these tests a sudden increase in strain was observed as the temperature was increased from 200°C to 300°C resulting in a rapid deterioration of stress-strain-temperature curves between these temperatures. This is referred to as thermally activated flow. Anisothermal tests are more closely related to real conditions of fire exposure and Kirby and Preston[40] concluded that this testing procedure was more appropriate for determining the material properties of steel for use in fire engineering studies. Although there are some variations in high temperature data for steel, there is now a reasonable consensus about these results, which provide a sound basis for modelling the material characteristics in fire analysis.

Experimental studies at room temperature show that the stress-strain relationship of concrete is highly non-linear and influenced by a number of parameters such as cube strength, particle size and distribution, aggregate/cement ratio, the shape and texture of coarse particles, workability and compaction of the mix[41-45]. This is due to the non-homogenous internal structure and unpredictable cracking mechanisms in concrete[46-48]. Published experimental data defining complete stress-strain relationships for concrete at elevated temperatures is very limited. Furamura[49,50] presented stress-strain-temperature curves for a temperature range between 30°C and 700°C using isothermal compression tests. Similar curves were derived by Anderberg et. al.[51] using anisothermal compression

tests. These studies indicated that both the elastic modulus and compressive strength reduce dramatically for temperatures above 500°C. Anderberg also reported that the stress-strain-temperature characteristics obtained from isothermal tests led to the prediction of unrealistically high thermal stresses and sometimes to an erroneous collapse state when they were used in analytical models[52,53].

Rather more data is available concerning the influence of temperature on specific characteristics notably strengths. Most studies indicate that there is a little change in strength up to a temperature of 300°C whilst above this temperature it reduces significantly[54-57]. However Mohamedbhai[55] showed that the rate of deterioration in strength remained small up to 600°C. Contrasting conclusions have also been drawn concerning the influence of the age of concrete and the water-cement ratio on the compressive strength up to temperatures of 600°C[54,57]. The elastic modulus also decreases markedly as the temperature increases. This reduction has been shown to be influenced by the water-cement ratio, the aggregate type and strength[58,59].

These variations in test results highlight the difficulties in the determination of stress-strain-temperature characteristics for concrete, which are needed in analysing the behaviour of composite beams in fire, and in establishing strength reduction factors for use in design.

The analysis of partially composite beams also requires the force-slip characteristics of the shear connectors. These are normally obtained from push-out tests. Such tests at ambient temperature[60-70] have shown that the relationship is highly non-linear and the force-slip relationship depends on the surrounding concrete strength and the diameter of stud. Both the load-slip characteristics and the ultimate strength of studs from different tests can show a considerable scatter. However some general patterns are evident with slender studs being stiffer[60] and the strength of studs embedded in lightweight concrete being lower than in normal density concrete of an equivalent grade[62]. The strength of studs in metal deck construction has been shown to be less than in solid slabs and the behaviour greatly influenced by the shape of the deck and the stud positions[66,67].

Slutter and Driscoll[61] first suggested that force-slip characteristics from push-out tests might not reflect the exact behaviour in a flexural element. This was confirmed by Lawson[68] and Crisinel[70] who reported that the strength and deformation capacity of studs in beam tests was much greater than in push-out tests. However Robinson[66] reported that the strength of studs from push-out tests and composite beam tests were comparable. Crisinel concluded that results from push-out tests were easier to obtain, more standardised and they gave conservative design values.

The only published research investigating the effect of high temperatures on the force-slip characteristics is a series of push-out tests at elevated temperatures by Kruppa and Zhao[71] for a 19mm headed stud. The results indicated that up to 400°C the reduction in the ultimate shear strength and initial tangent modulus was negligible. However at 500°C, the shear strength was found to decrease by 40%. At 600°C this reduction had increased to 62% and at 700°C was as high as 82%. The authors also noted that the temperature of the studs was around 80% of the upper flange temperature of the steel beam to which they were welded. The differential thermal elongation between the concrete and steel was reported to induce significant levels of shear stress on the studs, but this was not quantified.

It is clear that there is a reasonable amount of data on material properties for steel at high temperatures, and the results from various investigators are in reasonable agreement. However for concrete and shear connectors the effect of high temperatures on their material properties is not so well established. Particularly for concrete these properties are difficult to obtain because of its non-homogeneous internal structure and therefore most work has been done to determine the ultimate strength of concrete rather than full stress-strain-temperature curves. As for the studs, there has been very little research on their properties at elevated temperatures and it would be very useful to conduct more push-out tests on different types and sizes of shear connection under fire conditions.

Structural analysis necessitates the use of mathematical models representing the stress-strain characteristics of the materials used in the analysed structure. These models largely rely on experimental data discussed above and can be in the form of simple and more sophisticated mathematical expressions. For concrete and shear connectors the representation of the-stress-strain characteristics at high temperatures is more difficult because of limited amount of experimental work. For steel these are well established and models have been developed, often on the basis of those used at ambient temperature. At its simplest this is of a multi-linear form[72], but more complex relationships have also been proposed[73]. More precise formulas were proposed by Holmquist and Nadai[74] and Ramberg and Osgood[75] who introduced an exponential expression for describing the stress-strain curve in terms of three parameters, namely Young's modulus and two secant yield strengths.

For high temperatures the yield strength of steel as a proportion of its ambient temperature value can simply be tabulated as a series of strength reduction factors[76,77]. Alternatively simple formulas expressing the reduction in yield strength, modulus of elasticity and coefficient of thermal expansion with increasing temperature have been proposed[29,78]. However such models do not account for the highly non-linear stress-strain

characteristics of the steel at elevated temperatures. Hence more sophisticated expressions, representing the experimental relationship at different temperatures, have also been developed. Dounas and Golrang[79] proposed a linear-elliptic idealisation of the stress-strain-temperature curve. The curve was assumed to be divided into three parts and three mathematical expressions representing each part were described. El-Rimawi[22,23] modified the expression by Ramberg and Osgood[75] by introducing two additional temperature/dependent constants, whilst EC4 Part 1.2[80] uses a curve represented by three different parts, namely elastic, non-linear and plastic. These were defined in terms of the slope of the linear elastic range, the proportional limit and the maximum stress level, with the non-linear transition represented by an elliptical relationship. Such representations are now recognised as giving a reasonable indication of the material characteristics of steel in fire.

Even at ambient temperature representing the stress-strain relationship for concrete mathematically is difficult. The shape of the curve is highly non-linear and dependent on various parameters, requiring the use of complicated mathematical expressions. Early formulas were developed for certain concrete strengths in the form of simple exponential functions considering both the ascending and descending portion of the curve[81-84]. Saenz[85] was first to introduce two separate formulas to represent the two branches. He also introduced the E_o/E ratio (E is the secant modulus and E_o is Young's modulus) as a function of the strength of the concrete and defined the slope of the curve. More recent formulas, which include this ratio[41], have been developed to account for normal and lightweight concrete[42], microcracked concrete[44] and different cube strengths[45]. Further developments of this approach by Tsai[86] use two parameters to control the ascending and descending parts of the curve and have been shown to be in excellent agreement with experimental results for various types of concrete.

Although there are a number of established formulas representing the stress-strain curve of concrete at ambient temperature, there are few corresponding models for high temperatures. The models by Anderberg et. al.[51] and Bresler et. al.[87] consider the different strain components namely, creep strain, thermal strain, transient strain and mechanical strain but mathematical expressions were not explicitly reported. Baldwin and North[88] plotted the experimental stress-strain-temperature data by Furamura[49] as a normalised stress and strain for each temperature level and noticed that all the curves for different temperatures lie along the same course. An empirical formula in terms of the ultimate stress and strain at a given temperature was then fitted to represent this. Kishysh[89] used the stress-strain formula by Saenz[85] to approximate the experimental stress-strain-temperature curves obtained by Furamura[49], both in compression and tension. He also plotted the variation in the modulus of elasticity and compressive strength of concrete

with temperature from previous tests using different water-cement ratios, aggregate and cement types and curing and age of the specimen. An envelope model was developed and a trilinear relationship approximating the upper and lower boundaries of the envelope was proposed. The same basic experimental data[49] has been used as the basis for the material model incorporated into EC4 Part 1.2[80]. This represents the stress-strain-temperature curves of concrete up to a maximum strain of 5% as a non-linear polynomial equation. This consists of two separate forms modelling the ascending and descending parts of the relationship for normal and lightweight concrete.

Partial interaction analysis of composite beams requires the force-slip characteristics of the shear connectors. Based on regression analyses on push-out test data, simple empirical formulas for modelling the force-slip relationship[62,90] or the shear strength of connectors as a function of the strength of concrete[63-65,69] have been proposed for ambient temperature but there is no published data on modelling these characteristics at high temperatures.

An understanding of the effect of high temperature on the materials forming a composite beam is clearly important, and provides a basis for understanding and explaining the behaviour of structures in fire. One way of determining the fire resistance of structural elements is to conduct furnace tests in which the specimen is heated according to a standard time-temperature curve and its deflections are recorded at certain time intervals. However although a significant number of such tests have been conducted many have been performed simply to prove a particular method of achieving fire resistance, and detailed results have often not been fully reported. The specimens in beam tests are typically non-composite construction and in the few tests where composite beams have been used there was no measurement of slip.

Tests have been conducted on both small-scale and full-scale specimens and it has generally been found that the collapse temperature is independent of the heating history and unaffected by thermal expansion[39,91,92]. Cooke[11,93] conducted a series of model tests to study the thermal deformations of an unloaded simply supported bare steel beam and found that the increase in deflections slowed down at 730^{o}C. This was due to the change in the metallurgical composition of the steel at this temperature. He also investigated the collapse temperature of a loaded simply supported steel beam and determined a failure temperature of 550^{o}C.

An extensive programme of full-scale fire tests on individual beams of which two were composite, has been carried out in the U.K by British Steel[94]. Comprehensive temperature and deflection measurements were reported at regular time intervals. These tests included preliminary studies of the influence of beam type, load level, axial restraint and end fixity.

They showed significantly higher failure temperatures than previously reported, partly due to the upper flange in contact with the concrete slab remaining cooler. Where additional shielding is provided, for example in shelf-angle beams or slim floor construction, the failure temperatures are further increased. They also demonstrated the beneficial effect of end restraint and reduced load levels. This is consistent with the findings of Rubert and Schaumann[95] who conducted a series of model tests to show that reducing the load and span/depth ratio resulted in an increase in fire resistance.

Similar tests on individual steel, composite and reinforced concrete beams and columns have also been conducted by a number of authors[19,20,76,78,96]. In some tests[19,20,96] the area between the flanges of the steel section was filled with concrete, essentially providing fire protection, and although the tested section is referred to as composite it was not typical of that used in building construction in the U.K. The results of these tests were reported to show significant scatter due to inconsistencies in material properties and testing procedures[78].

Fire tests on composite concrete slabs have been carried out[97-100] but their results are beyond the scope of this thesis.

Experimental research considering the partial interaction between the concrete slab and steel beam has been undertaken at room temperature. Early studies investigated composite beams with solid concrete slabs while more recent studies have used beams with concrete slabs cast on corrugated metal decks. Most references report end slip measurements but the slip distribution along the length has been measured only by a few authors[60,101,102]. Generally the results show that uniform spacing of shear connectors is appropriate and studs with small diameters are more efficient[60,61,103].

It has been found that large slip deformations have a negligible effect on the load carrying capacity but increase the deflections considerably[60,102,104-106]. Chapman[103] showed that even when the shear connection was designed to provide full interaction the influence of slip on beam deflections in the plastic range was significant. Wright and Francis[102] reported that the stiffness of a composite beam was most affected for interaction levels between 20% and 50%. Increasing the interaction level above 50% was found to have a negligible effect on the beam stiffness under service conditions. The influence of the amount of transverse reinforcement has been studied and shown to have a significant influence on both the failure load and mode[105-107].

It has recently become clear that testing isolated members is unrepresentative of the behaviour of individual members in a highly redundant structure, such as in real building frames. Cooke[93] tested a small-scale two-span continuous beam with rigid supports and

found that the fire resistance is highly influenced by the high temperature strength of the internal support. Cooke and Latham[108] tested a full-scale two dimensional steel frame exposed to a fire of wood cribs and found that the fire resistance temperature was 830°C, significantly higher than suggested by isolated beam tests. Tests on sub-frames have also been conducted by a number of other researchers[19,20,76,96] to validate computer models. These tests on frames are mainly for non-composite beams, Lloyd and Wright[109] tested a full-scale composite frame at ambient temperature and concluded that when additional flexural restraint was provided by the surrounding frame the slip deformations and deflection of a composite beam is significantly lower than for isolated beam tests. However, no corresponding studies have been conducted for fire conditions.

Although these frame tests provide an indication of the interaction between beams and columns they do not reflect the real behaviour of the whole structure of a building. Recognising the need to examine the three-dimensional behaviour of structures, frames including the interaction of slabs, walls, etc. the Building Research Establishment constructed a full-scale eight-storey steel framed building at its Cardington laboratory to carry out static, dynamic and fire tests[110]. The results of these tests will provide invaluable data and will enable comparison with isolated member and sub-frame tests and also predictions from computer models. The building is conventionally framed using composite construction but no measurements have been made of slip. Although a number of fire tests have now been completed unfortunately only very limited test data is available at present.

The characteristics of the end connections of a beam, defined by the moment-rotation relationship are known to influence structural behaviour significantly and now a reasonable amount of data has been assembled for both bare steel and composite connections at ambient temperature. Bare steel connections were studied by Aggarwal[111,112] who determined the moment-rotation characteristics of various connection types including flush and extended endplates. Test results on composite connections are generally very consistent[113-120] and suggest that the ultimate moment capacity of a composite connection is significantly greater (1.5 to 6 times) than the bare steel condition[113-118]. Increasing the slab reinforcement ratio leads to an improvement in moment resistance of flush endplates and the mode of failure is either yielding of the reinforcement or local buckling of the steel beam, depending on the reinforcement ratio[113-118]. For instance Anderson and Najafi[118] reported that varying the reinforcement ratio from 0.55% to 1.65% resulted in an improvement in the moment resistance of approximately 68%. For reinforcement ratios of 0.55% and 1.1% they found that the failure mode was yielding of the reinforcement whereas for 1.65% local buckling of the steel beam was critical.

The influence of partial interaction on the connection characteristics was investigated by Puhali et. al.[119] who concluded that its effect on the moment-rotation curve was very little up to 70% of the plastic moment capacity of the connection. Some contrasting conclusions have also been reported with regard to the influences of concrete on connection stiffness with partial interaction. For example Puhali showed that the contribution of the concrete slab to the connection stiffness was negligible due to early cracking of concrete. However Jarrett and Lennon[120] reported a much higher initial stiffness of the moment-rotation curve, although this reduced significantly after cracking of the concrete.

Only a few studies on limited types of connection have been conducted at elevated temperatures. Lawson and Newman[121,122] presented the results of bare steel and composite connections using flush end plates, extended end plates and double sided web cleats under fire conditions. However due to the limited extent of these tests full moment-rotation-temperature curves could not be derived. The moment capacity of the connection which was found to be about two times greater than for the equivalent bare steel connection was greatly influenced by the strength of the upper bolts which failed at approximately 550^{o}C. The failure temperature of the connection was largely unaffected by the amount of reinforcement. Currently Jones et. al.[123] are conducting fire tests on bare steel and composite connections with flush end plates for small beam and column section sizes. Initial experimental moment-rotation curves for bare steel connections show a gradual degradation as the temperature increases, and a significant moment capacity reduction between 500^{o}C and 600^{o}C. Further results from this work will provide valuable information for modelling connection behaviour under fire conditions.

Structural analysis incorporating the effect of semi-rigid connections at elevated temperatures requires the mathematical modelling of moment-rotation-temperature relationships. This is only possible if sufficient experimental data on a range of connection types is available at high temperatures. At present research in this area is extremely limited and there is clearly a need for more experimental work, particularly concerning composite connections.

It can be seen that although there has been a significant effort in conducting fire tests most of these have been on isolated elements. Frame tests which can provide a better indication of how structures will behave in fire are relatively few. Tests generally provide invaluable data for understanding the behaviour of structures at elevated temperatures but they are generally costly, possibly limited by available furnace characteristics, and often unrepresentative of the real behaviour.

2.2. Analytical Studies

The limitations of tests referred to above have encouraged the development of analytical methods as an alternative way of studying structural response to fire. The approaches adopted can be generally classified into two categories: the calculation of the fire resistance using empirical or semi-empirical methods, and modelling the full behaviour at high temperatures using more comprehensive numerical methods. The former is intended for design purposes whereas the latter is mainly for research purposes.

2.2.1. Simplified Analytical Methods

Simplified models are generally concerned with predicting only the failure temperature or time of the structural element rather than its deformation history prior to collapse. One such method is based on the H_p / A (m^{-1}) concept (section factor) where 'H_p' is the perimeter of the section directly exposed to fire and 'A' is the cross-sectional area of the steel[8,10-12,77,124]. Sections with a high H_p / A ratio heat up faster than those possessing low ratios, resulting in lower fire resistance. Design charts have been prepared, relating failure temperature (determined by tests according to a limiting deflection of L/20 or L/30) to section factor. The same concept is used in similar approaches such as the W/D ratio[14], where 'W' is the weight per metre and 'D' is the heated perimeter of the cross-section, and the U/A factor[125] given by the surface area of the member exposed to the fire (U) divided by the corresponding volume of the member (A). A number of authors[10,12] have adopted this approach using time-temperature characteristics from real fires while others have used the standard heating curve[11,124]. Although the concept of section factor can be used for insulated and uninsulated members[125] and both fully and partly loaded conditions[124], its use is limited to simple structural elements.

Other simplified approaches have been developed based on an ultimate moment capacity concept using the reduced yield strength of steel to predict the collapse temperature[76,77,96,126-128]. Knowing the temperature profile through the critical section, the member is divided into a number of slices of approximately equal temperature. The moment capacity of the member is then calculated by considering the strength properties of the materials in the section. Again this method is generally limited to simply supported beams and can often result in shorter fire resistance times than those measured in tests due to variation in material properties and temperature, geometrical imperfections, and different loading and restraint conditions. Recognising this problem Petterson and Witteveen[129] proposed some correction factors to achieve consistency with experimental results.

The critical temperature of a member, defined as the temperature at which its maximum deflection reaches L/20 or L/30, depends on the load that the member carries. This is accounted for in the load-ratio method[77]. For members in bending, the load-ratio refers to the applied moment at the fire limit state divided by the moment capacity of the member at room temperature. The critical temperature of the member can be obtained using design tables based on fire tests and relating load-ratio to this temperature. An alternative model was also presented by Witteveen[13] who suggested that the quantification of the fire exposure was a problem of heat transfer to the member. The fire resistance was assessed using an empirical formula for calculating the temperature within a uniformly heated element. If the member did not attain the predetermined failure temperature, it was assumed to retain its load bearing capacity.

There are only a few simplified design methods which consider partial interaction and they are only applicable to simply supported beams at room temperature. Crisinel[70] presented an empirical formula expressing design load in terms of the number of shear connectors. The relationship was derived by transforming the partially composite section into an equivalent reduced fully composite section using plastic analysis. An empirical deflection formula which accounts for varying degrees of shear connection was also proposed. Luckyram and Vardy[130] expressed the longitudinal variation of the shear displacement as a second degree differential shear-slip equation which was then integrated to calculate the slip at any section, whilst Bradford and Gilbert[131] calculated the internal forces in a composite section using the non-continuous strain profile due to slip. However, all of these authors have commented that simplified methods are generally inadequate for predicting slip deformations.

Simplified design methods to account for semi-rigidly connected beams at room temperature have been developed by various investigators[114,116,118,119,132-135]. These are typically in the form of empirical formulas expressing the rotational stiffness of the joint derived from regression analyses on experimental moment-rotation curves for various types of connection. These rotational stiffnesses can then be incorporated into first order linear elastic analysis[133] or plastic analysis[134]. Simplified elastic connection models for composite beams have been proposed using an axial spring connected to the reinforcement and a rotational spring connected to the steel beam[135] or three axial springs, representing the reinforcement, the steel connection and the shear stiffness of the studs[118]. The stiffness of the springs was derived from experimental moment-rotation curves. In contrast very little work has been done in developing simplified design approaches specifically for composite beams with semi-rigid support conditions under fire exposure.

2.2.2. Comprehensive Analytical Methods

More sophisticated numerical methods to simulate structural behaviour in fire have been developed mainly for research purposes. These methods, which are typically based on computer modelling using the finite element method, are concerned not only with the fire resistance but also the full deformation history throughout exposure. Most analyses were developed for bare steel sections but some deal with fully composite sections.

Plank[136] presented an analytical method for simply supported steel I-sections with uniform temperature profiles based on a moment-area approach using an iterative procedure to determine the varying neutral axis position with increasing temperature and define the precise stress distribution corresponding to the applied bending moment. From this the modified beam stiffness and mid-span deflections were calculated. The method used a bilinear stress-strain relationship defined by the elastic modulus and yield strength. Using the method the author has shown that the span length and section size have very little influence on failure temperatures. Reducing the design load did increase the failure temperature but it was not recommended because of the less efficient use of the section. Burgess, El-Rimawi and Plank[22] proposed an efficient secant stiffness method of structural analysis for steel beams at elevated temperatures. The method was based on the transformation of the stress-strain-temperature relationships represented using the Ramberg-Osgood equation[75] into moment-curvature-temperature curves. Both uniform and non-uniform temperature profiles across the section were considered. The model was recently extended to analyse two-dimensional steel frames with semi-rigid connections[137,138]. Using the computer model the authors investigated the influence of different support conditions and the P-delta effect on fire performance. They showed that continuous and fixed-ended beams achieved significantly higher failure temperatures than the simply supported case and although the P-delta effect increased the magnitude of beam deflections it had very little effect on failure temperature. A single bay frame with its columns protected was also analysed indicating a fire resistance for the beam of 850^{o}C, an increase of 54% compared with the simply supported case.

Other authors have performed two dimensional analyses using standard finite element computer programs[21,93] demonstrating reasonable accuracy in comparison with test data. Thermal analysis was not incorporated in these studies but material properties were varied with temperature and creep effects were included.

A number of authors have developed special finite element models to deal with two dimensional steel frames[139-141]. All used a similar procedure based on a step-wise constant temperature rise and the incremental variational principle. The stress-strain-temperature

curves of steel were represented by a bilinear relationship with no strain hardening. The effects creep and initial stresses were considered.

Jain and Rao[142] were the first to use the principle of virtual work in a finite element model for structural fire analysis. The model provided an efficient computation for considering the influence of geometrical non-linearity on the behaviour of plane steel frames. The same approach has been adopted by a number of other researchers.

The first computer model (CEFICOSS) capable of an integrated thermal and structural analysis of steel and composite frames was developed by Schleich, Dotreppe and Franssen[19]. The computer model included both thermal analysis using a finite difference method and structural analysis using finite element formulation. The thermal analysis was carried out to determine the temperatures at one minute intervals. At each stage the structure was assumed to be loaded incrementally until the service load was reached. After each step of loading the Newton-Raphson process was employed to restore the equilibrium condition of the structure. The process was repeated until equilibrium could not be maintained. Creep was ignored but the strain hardening effect was considered and reported to have a significant influence on the calculations. A similar method was described by Dotreppe[96] who extended the model to include reinforced concrete structures. Saab et. al.[143] incorporated the effects of elevated temperatures into a previously developed non-linear finite element formulation for plane steel frames at ambient temperature (INSTAF)[144,145] to study the behaviour of steel frames in fire. The equilibrium equations were constructed using the principle of virtual work and solved using the Newton-Raphson iteration method. Large displacements, material non-linearity and residual stresses were considered. The variation in temperature both across the section and along the length of the beam, and thermal stresses were taken into account. The authors analysed a two-bay frame which failed due to excessive sway of columns and concluded that protection of the columns was more important than for beams.

Najjar[146] further extended the computer model by Saab[143] to include three-dimensional behaviour of steel frames and warping deformations. In order to achieve a very accurate treatment of geometric and material non-linearity the formulation was modified to retain all higher-order terms. Bailey[147] further developed the work by Najjar[146] to study the behaviour of composite beams with semi-rigid connections in fire and to account for the cooling phase of a fire. The extension of the program involved the incorporation of shell elements to represent the concrete slab in three dimensions, zero length spring elements accommodating any specified moment-rotation-temperature curve to represent semi-rigid joints, and unloading from an inelastic state to represent the cooling stage of the fire. In addition the geometrical effect of shear deformations within the beam cross-section was

included in the formulation to model lateral-torsional deformations. The temperature variation across the section of the steel beam was considered but it was assumed to be uniform through the thickness of the concrete slab. Some indicative studies were also performed to investigate the influence of continuous floor slab on fire resistance. The examples used in the study were selected to represent the cases used in three fire tests conducted on the full-scale frame at Cardington[110]. It was shown that if cracking of the concrete and thermal strains in the floor slab are ignored, the magnitudes of displacements are much lower and consequently fire resistance is much greater than in situations where they are accounted for. Analyses ignoring these effects predicted no failure of the beam up to a temperature of 950^{o}C and a reversal of direction of vertical displacements at temperatures above 500^{o}C which was attributed to the squashing of the concrete floor slab. For cases where cracking and thermal strains in the slab were represented severe stresses in the concrete slab in hogging caused numerical instability at a temperature of 711^{o}C. Surprisingly extending the floor slab outside the test area for both cases had very little effect on the fire resistance. Regardless of the rotational stiffness of the connection, restraint to thermal expansion resulted in higher vertical displacements and therefore lower fire resistances due to an induced axial force. Most importantly he showed that compared with isolated beams failure temperature for a beam on a three-dimensional frame could be very significantly higher demonstrating the contribution of the membrane and bridging actions of the continuous floor slab.

There has been no published analytical work investigating the influence of partial interaction at elevated temperatures. However, a number of numerical approaches have been proposed to investigate this effect at ambient temperature. Based on tests Siess[148] proposed an equation expressing the slip strain in terms of compressive force in the slab and the applied external moment. Yam et. al.[149] used this to derive a second order non-linear differential equation for the equilibrium of any section along the length of a simply supported beam. The equation was then solved using a step-by-step method of numerical integration. The method assumed that the shear connection acted as a continuous medium along the length of the beam and the concrete slab and steel beam deflected equally so that at any cross-section they had identical curvature. The model was laborious and applicable only to specific end conditions. Hirst and Yeo[150] incorporated an ingenious shear connection element into a standard two-dimensional finite element computer model. Both the steel beam and concrete slab were represented by a grid of standard elements and connected together by means of standard quadrilateral elements representing the shear connection. The connecting elements were assumed to deform in bending as well as in shear and their stiffness was derived empirically.

Roberts et. al.[151] described a finite difference formulation for the analysis of composite beams with partial interaction. The cross-section was divided into two parts, namely the concrete slab and the steel I-section. The influence of uplift forces was taken into account by having independent vertical and rotational displacements for the concrete slab and steel beam. The non-linear material characteristics and the effects of large displacements were incorporated later by Al-Amery et. al.[152] using the layered cross-section approach, but convergence was reported to be poor. Aribert[153] presented a numerical procedure based on the solution of two non-linear equations derived from the equilibrium of normal forces and bending moments in the cross section and two others derived from the strain compatibility at the steel and concrete interface. The boundary conditions at supports were then introduced to evaluate the unknown variables.

The first finite element program specifically designed to consider the effect of partial interaction was proposed by Arizumi, Hamada and Kajita[154]. The model was based on the principle of virtual work and expressed the non-linear equilibrium equations in terms of steel, concrete and shear connectors. The composite section was idealised using two separate elements, namely the steel beam and the concrete slab with identical rotational and vertical deformations but independent axial deformations. The shear connectors were modelled as a continuous medium transferring the shear force. Based on the work by Arizumi et. al.[154], Abdul Wali[155] extended a two-dimensional non-linear finite element model for steel frames[144,145] to incorporate the effect of the concrete slab and shear connection. Material and geometrical non-linearities were considered but the effect of large deformations on slip deformation was ignored. Aribert[153] also reported a finite element model using two parallel beam elements, one for the steel beam and the other for the concrete slab, with shear connectors represented by two diagonal truss elements. However details about the procedure were not presented and the model was found to be inadequate in modelling the local buckling behaviour. Wright[156] proposed a three-dimensional non-linear analytical model for composite beams with profiled metal decking. The method was based on a dummy plate element between the slab and joist whose material properties could be changed to simulate different shear stiffnesses. Details about the procedure were not reported.

There have been relatively few studies on considering the influence of semi-rigid connections under fire conditions[138,148]. The treatment of semi-rigid connections in finite element models can be achieved in two different ways. The first approach is to replace the rotational stiffness coefficients corresponding to the semi-rigid joints with stiffness values defined by the moment-rotation characteristics. This method was adopted in references[155,157] but it was reported to be suitable only for beam analysis and potentially unstable. However based on this approach, El-Rimawi, Burgess and Plank[138,139

incorporated semi-rigid connection characteristics in fire into a secant stiffness method[22]. The rotational stiffness of the connection was represented using a modified version of the Ramberg-Osgood equation[158]. The computer model was validated against the results of a non-sway portal frame test[109]. Although predicted beam deflections showed a reasonable agreement with both the test and another analytical model no details were given about the semi-rigid connections characteristics assumed. El-Rimawi et. al. also conducted a series of studies which included a non-sway portal frame and a three-bay three-storey frame, each with semi-rigid connections. The results for single bay frame suggested that column-led failure results in premature collapse of the structure (575^{o}C) and that beam-led failure was more preferable (680^{o}C). This was also confirmed by the three-storey frame in which column instability occurred at 650^{o}C before beam deflections reached the limiting deflection of L/30. The author concluded that the survival of a structure could be significantly enhanced by properly accounting for the connection stiffness, but that the precise form of the moment-rotation characteristics was not very important in structural analysis.

The second approach for incorporating connection stiffness is to use 'small' spring elements connected to the actual elements using identical degrees of freedom[159,160]. The spring element generally uses a rotational stiffness defined by the moment-rotation curve, and the influence of other stiffnesses and the coupling effect are ignored. Using the same Ramberg-Osgood equation proposed by El-Rimawi[158], Bailey[147] utilised this approach for the treatment of the semi-rigid joints.

The connection characteristics used in these analyses were based largely on assumptions and therefore not conclusively established. Clearly more research in the development of further analytical approaches considering various connection characteristics is needed.

CHAPTER 3. MATERIAL PROPERTIES

3.1. Introduction

The mechanical properties of the materials making up a composite section, namely the steel beam, reinforcing bars, concrete and shear connectors, deteriorate rapidly with increase in temperature losing both strength and stiffness. Structural analysis of composite sections at elevated temperatures therefore requires the mathematical representation of the stress-strain-temperature characteristics of these materials. Material models are based on experimental data and can be highly sensitive to the testing procedures. In addition, with non-homogenous materials such as concrete, there are a large number of other parameters associated with its micro structure which might also affect these characteristics considerably and there are often considerable discrepancies between the results from different investigators. The properties of steel are rather more consistent partly because of the greater homogeneity of its micro structure.

3.2. Material Properties of Steel and Reinforcement at Elevated Temperatures

Several investigators have carried out tests to determine the stress-strain-temperature relationship of steel at elevated temperatures[27,28,30,34,79]. Results indicate a decrease in both yield strength and Young's modulus and a small increase in the coefficient of thermal expansion as the temperature is increased. However the precise relationship between these material properties and temperature varies significantly due to different rates of loading, heating and different steel types as well as the different testing procedures on which the experimental data is based[23,30,34]. In the U.K, a comprehensive anisothermal testing programme was conducted leading to a typical set of stress-strain-temperature curves as shown in Fig. 3.1[40,77].

It can be seen that up to 200^{o}C the effect of temperature on material properties is negligible. Only 14% of the steel's yield strength at ambient temperature is lost and Young's modulus remains unaffected. Above 300^{o}C, however, there is no a clearly defined yield strength. The curve loses its idealised linear elastic-perfectly plastic characteristics at ambient temperature, by developing a rounded transition region between the elastic and plastic region. This relatively sudden loss of strength is attributed to the thermally activated flow[39]. Between 300^{o}C and 400^{o}C there is a little change in material

behaviour, whereas beyond this temperature range the ultimate strength corresponding to a strain of 2% and Young's modulus decrease very rapidly. The stress-strain characteristics become highly non-linear with a very short linear elastic part.

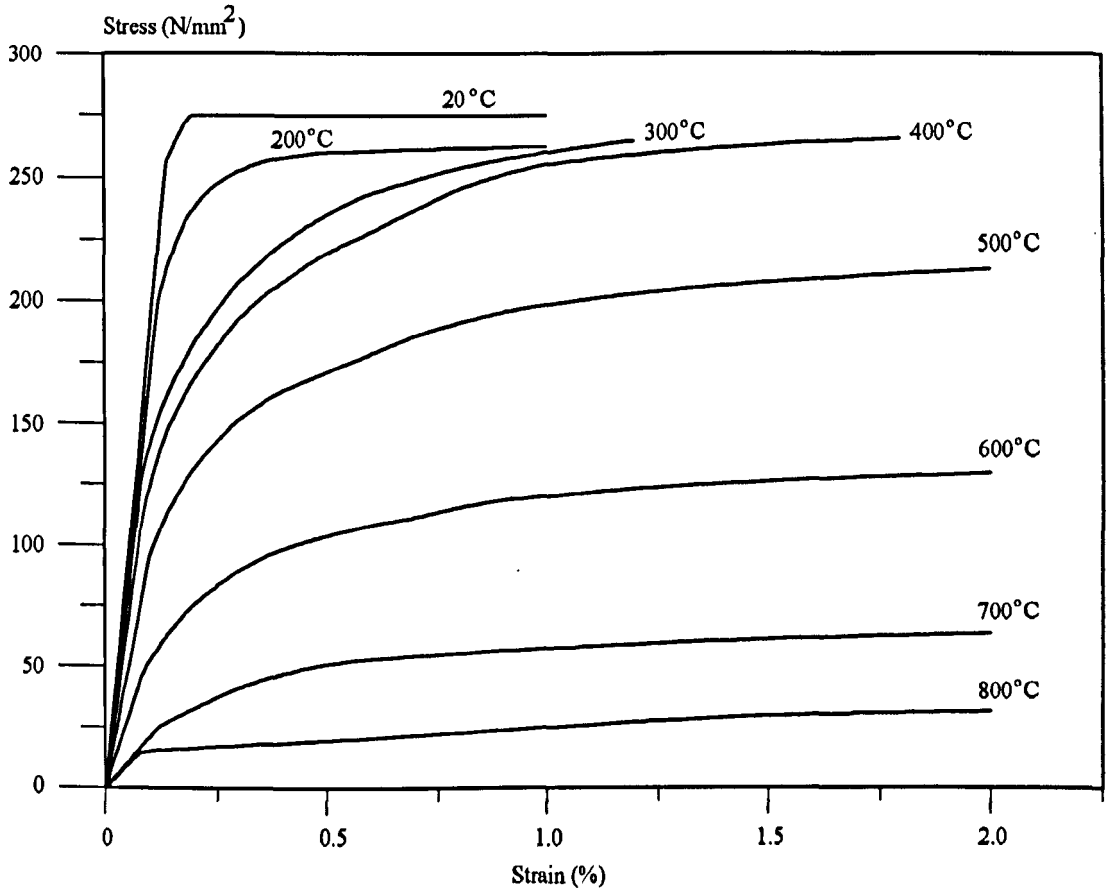

Fig. 3.1 Typical stress-strain-temperature curves for grade 43 steel[77].

Due to the highly rounded shape of the stress-strain curves beyond 200°C it is difficult to represent the material properties using a bi-linear model and therefore a more precise model specified in EC4 Part 1.2[80] has been adopted. The model is based on anisothermal tensile test data for heating rates between 2 and 50°C/min. The effect of high temperature creep is not explicitly considered. As shown in Fig. 3.2(a), the stress-strain-temperature curve consists of three different parts, namely the elastic, transitional and perfectly-plastic parts without strain hardening. The relationship in the transitional part is elliptical and expressed as a polynomial function of proportional limit $\sigma_{apr(\theta)}$, ultimate strength $\sigma_{amax(\theta)}$ and elastic modulus $E_{a(\theta)}$. The same expression is used for steel in both compression and tension.

In structural analysis at high temperatures the effect of thermal deformations must be included. The thermal strains depend on the coefficient of thermal expansion which also

varies with increase in temperature. The model defined in EC4 Part 1.2[80] expressing thermal strains in structural and reinforcing steel as a function of temperature has been used (Fig. 3.2(b)). This is in the form of a second degree polynomial for temperatures up to 750°C. Between 750°C and 850°C the coefficient is constant, and is expressed as a linear function beyond 850°C.

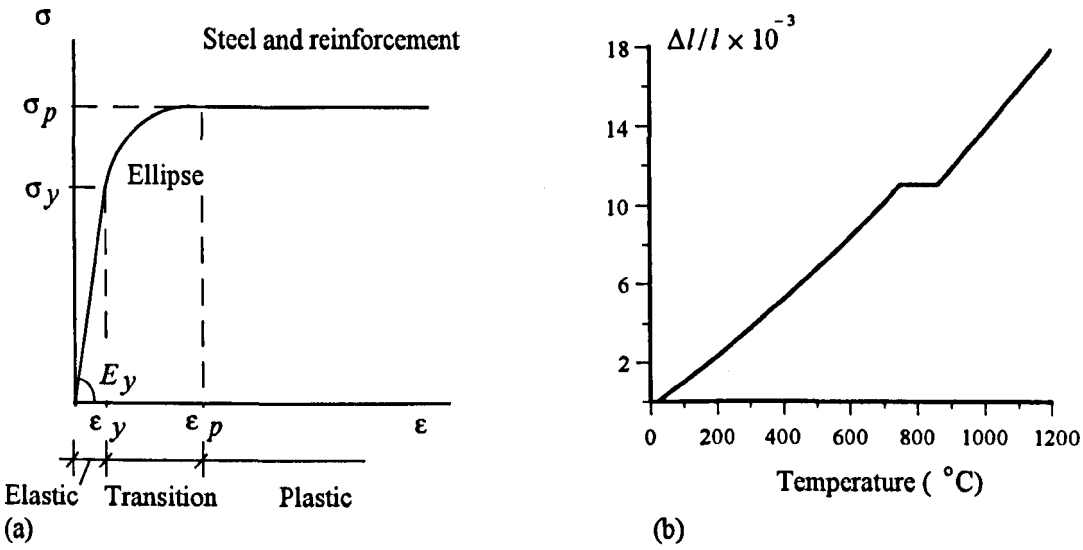

Fig. 3.2 Stress-strain and thermal strain models for the steel and reinforcement (EC4)[80].

3.3. Material Properties of Concrete at Elevated Temperatures

The stress-strain characteristics of concrete at ambient temperatures are highly non-linear because of the gradual deterioration of the bond between the aggregate and mortar with increasing stress. The concrete slab in a composite beam is subjected to a two-dimensional stress state. Therefore the stress-strain characteristics may be more realistically represented if the modelling of these characteristics is based on biaxial testing procedures[161-163]. However these tests are complicated and their results are scattered[48]. Because of this and the fact that ultimate compressive strength under biaxial compression is always higher than the uniaxial strength the concrete material properties used in this work are based on data for uniaxial load conditions.

The influence of isothermal and anisothermal testing procedures on the stress-strain-temperature characteristics of concrete has not been established conclusively[87]. The findings from various investigations are based on isothermal uniaxial compression tests and show a considerable scatter[54-59].

Typical anisothermal stress-strain-temperature curves by Furamura[49] are shown in Fig. 3.3. As can be seen from the figure, there is no change in the ultimate strength up to a temperature of 300°C. This may be attributed to the accelerated hydration of cement[51,54,56,57]. However the failure strain is approximately 50% higher than its value at 20°C. Further increase in temperature results in a steady decrease in both ultimate strength and elastic modulus and strains at maximum stress also increase considerably. At 700°C, 63% of the ultimate strength of concrete at ambient temperature is lost and the strain at maximum stress is increased by approximately four times its value at 20°C.

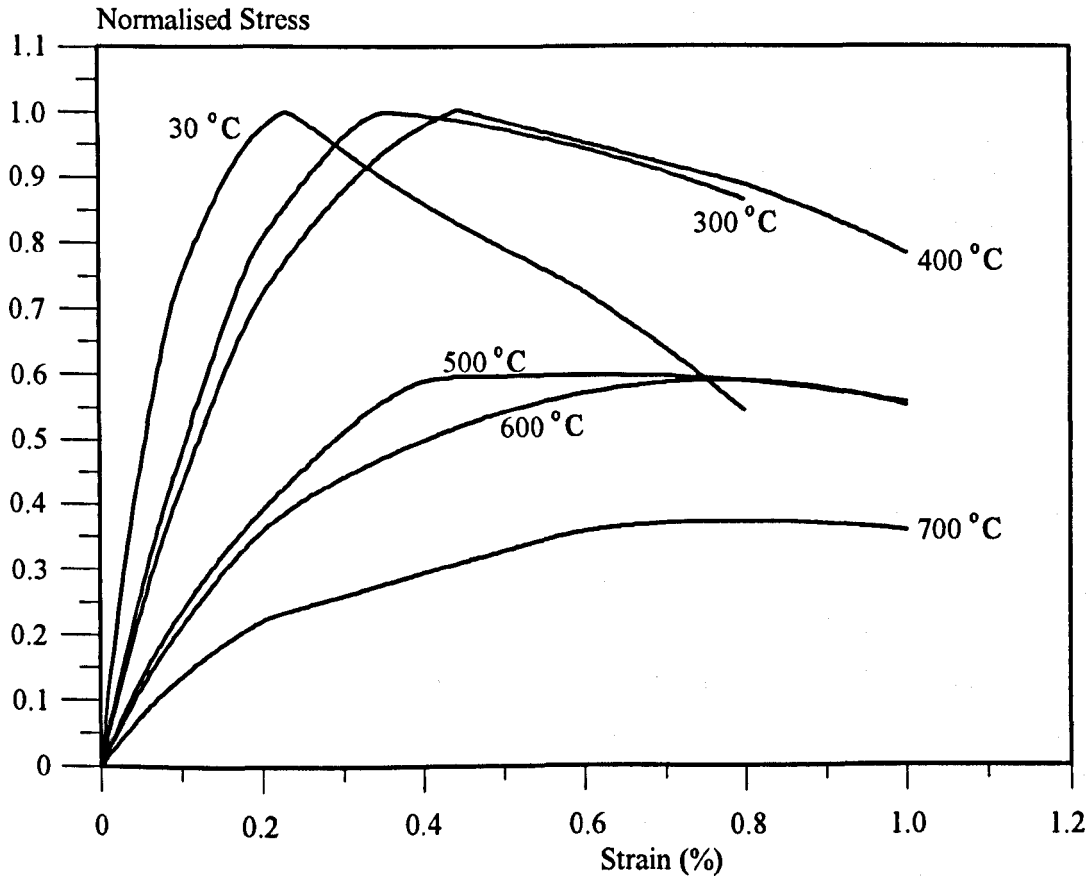

Fig. 3.3 Typical stress-strain-temperature curves for concrete[49].

For the purpose of this investigation a non-linear expression specified in EC4 Part 1.2[80] has been used to represent the relationship as a polynomial equation based on anisothermal test data and expressed as a function of the ultimate compressive strength and corresponding strain as shown in Fig. 3.4(a). The relationship is extended in the opposite direction to include a linear tensile part up to a maximum tensile strength equivalent to 10% of the compressive strength. The formula does not extend beyond the point of maximum stress in compression or tension. A thermal strain-temperature

relationship specified in EC4 Part 1.2[80] and expressed as a third degree polynomial between temperatures 20°C and 700°C and a constant value beyond 700°C has also been adopted (Fig. 3.4(b)).

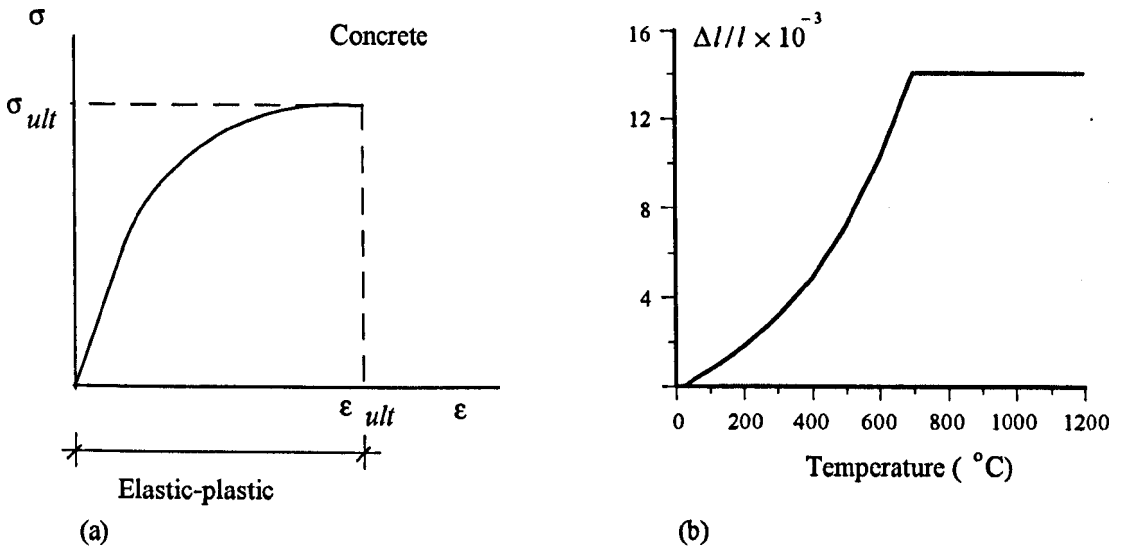

Fig. 3.4 Stress-strain and thermal strain models for the concrete (EC4)[80].

3.4. Material Properties of Shear Connectors at Elevated Temperatures

The structural analysis of composite beams in which the effect of slip between the slab and the steel I-section is included requires the shear force-slip characteristics of shear connection. In modern composite construction welded headed studs of various lengths are most common. The force-slip behaviour of these studs is normally obtained by push-out tests in which they are subjected to pure shear[60-70] even though this testing method is not representative of the behaviour under bending conditions in a composite beam[66,68,70]. In general the strength and ductility of studs in beams are reported to be better than in push-out tests[68]. This is because there is a considerable redistribution of load to the less highly stressed shear connectors. However it is reported that an assessment of the behaviour of studs in beams is difficult and force-slip characteristics from push-out tests are adequate for structural analysis[68].

The force-slip behaviour from push-out tests depends on a number of parameters, such as the compressive strength of concrete, the tensile strength of the stud, the slab reinforcement, the weld collar around the shank of the stud, the size of the stud and the loading conditions, namely cyclic or static loading. Some tests are conducted using profiled metal decks which may result in lower strengths for the studs in a solid concrete

slab due to different stress distributions[67,70]. The direction of the trough profiles parallel or perpendicular to the beam may also have a significant effect on these characteristics[67,68].

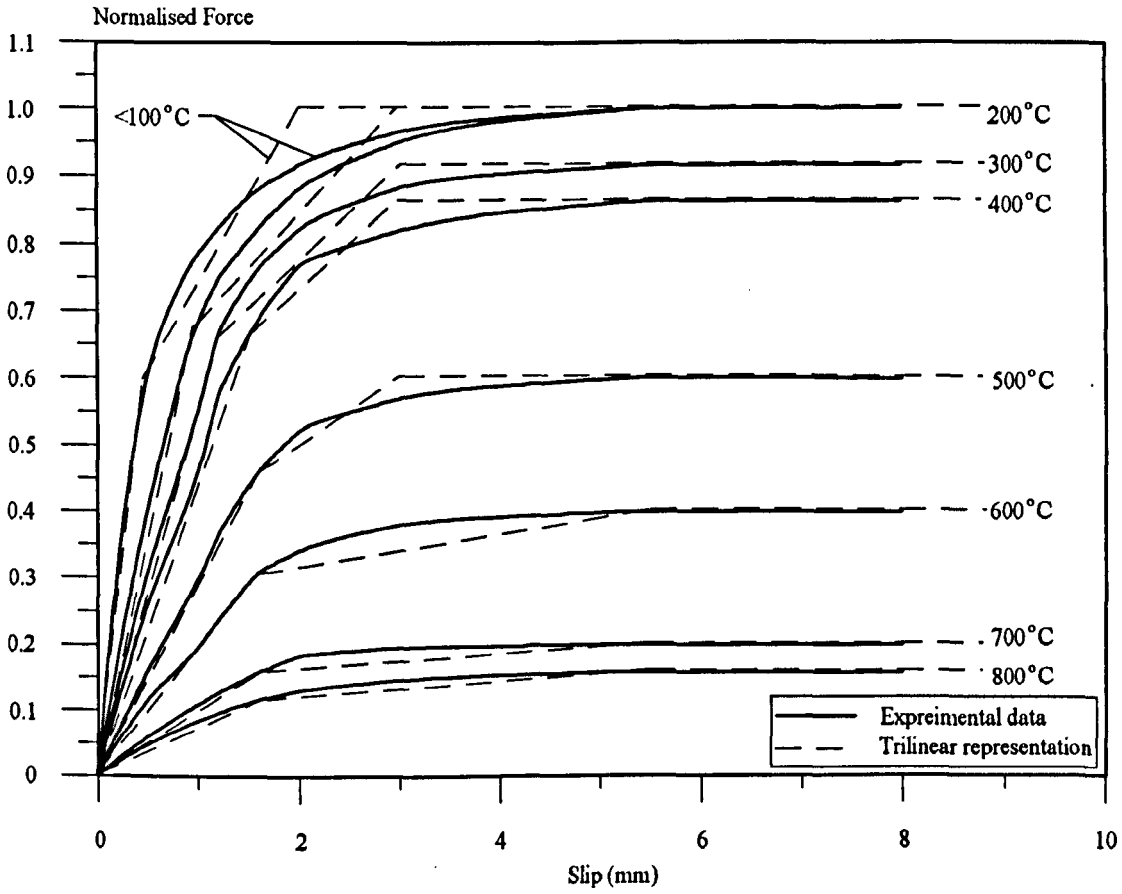

Fig. 3.5 Typical force-slip-temperature curves for shear connectors[71].

Published research on the influence of temperature on the force-slip characteristics of the studs is very limited. Kruppa[71] recently presented some test results for the force-slip-temperature characteristics of a 19×100mm headed stud. These curves are shown in Fig. 3.5 in terms of normalised force and slip. It can be seen that they are highly non-linear and up to 300°C they result in very little reduction in ultimate shear force. Considering that the temperatures within the slab rarely exceed 200°C according to test data[71,97-100], the full range of these characteristics may not be required.

In the present study the option of degrading the force-slip characteristics has been introduced using a trilinear model fit to the experimental data[71] (Fig. 3.5). In situations where the effect of degrading these characteristics is ignored, experimental force-slip curves at ambient temperature by Chapman and Balakrishnan[60] have been utilised. These curves are also idealised as a trilinear model by approximating them into three distinct

parts, a linear-elastic part up to 55% of its ultimate shear capacity, a linear transitional part with a reduced tangent modulus and a perfectly-plastic part beyond 95% of its ultimate load (Fig. 3.6). This is very similar to the representation of the curve for temperatures less than 100°C in Fig. 3.5.

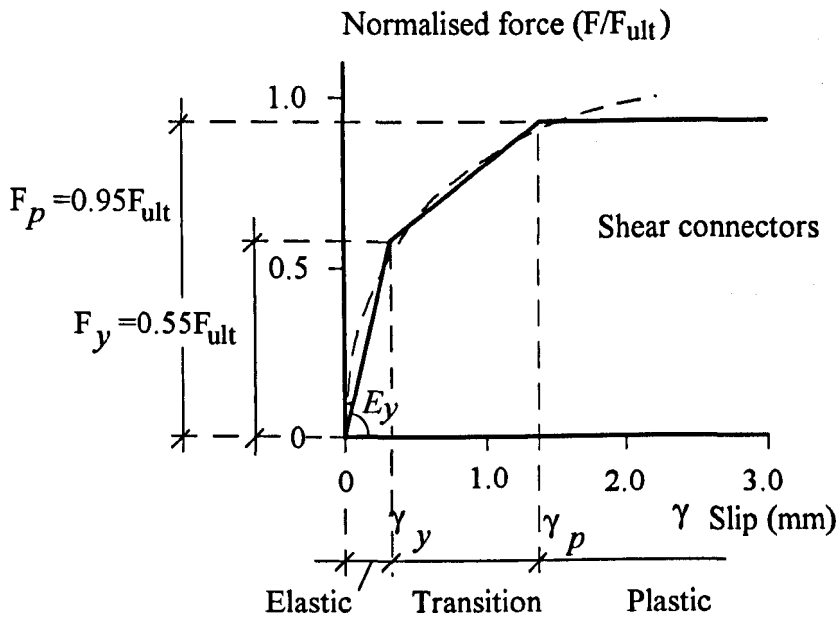

Fig. 3.6 Force-slip model for shear connectors.

CHAPTER 4. THE MATHEMATICAL MODEL

4.1. Introduction

The work presented herein concerns the development of an analytical model for investigating the behaviour of composite beams under fire conditions. A typical section consists of a steel I-section with a reinforced concrete slab connected to its upper flange using flexible shear connectors. The model has been developed in two different directions. In the full interaction model the influence of slip between the concrete slab and steel beam was ignored, assuming full shear connection, whereas in the partial interaction model this is accounted for. Both theoretical models are based on a well established two-dimensional non-linear finite element formulation for steel frames at ambient temperatures (INSTAF)[144,145].

4.2. Full Interaction Formulation

4.2.1. The Concept of the Theoretical Model

The full interaction model incorporates the influence of the reinforced concrete slab and high temperature with minimum modification to the original formulation used in INSTAF. This is described in detail in Reference[144]. The general principles are set out here for completeness and modified parts of the program will be discussed in more detail.

As shown in Fig. 4.1 the proposed model utilises a single line element to represent the composite section with four degrees of freedom at each node, namely the axial displacement, axial strain, vertical displacement and rotation. The effects of material non-linearity of the steel, concrete and reinforcement, geometric non-linearity due to large displacements and a non-linear strain-displacement relationship have been considered. The following assumptions are made:

1. The member is straight, prismatic and symmetric about the Y-Z plane and the Z axis coincides with the centroidal axis of the composite section.
2. All loads are applied in plane at nodal points.
3. Composite action is achieved by an infinitely stiff shear connection so that the slip at any point along the beam is zero.

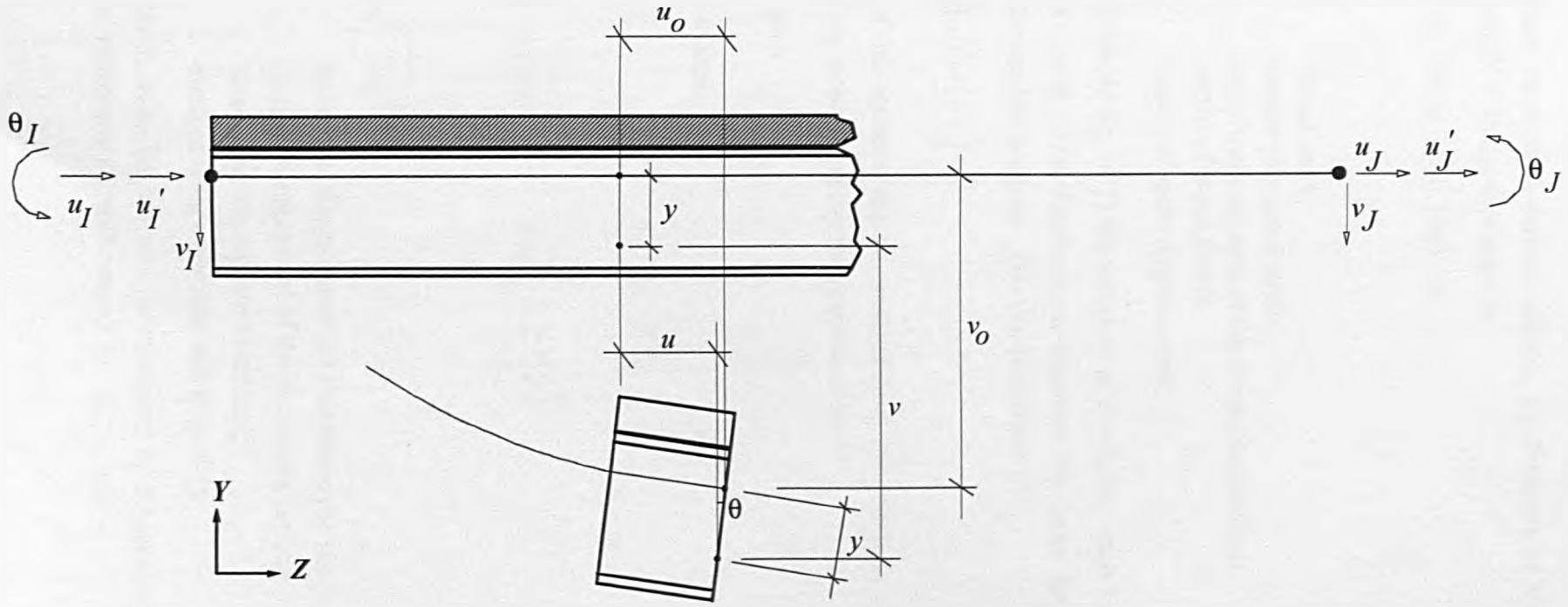

Fig. 4.1 Finite element representation of a composite beam with full interaction.

4.2.2. Basic Formulation

The equilibrium equation is derived utilising the Principle of Virtual Work. For a beam element of length 'l' this is expressed as

$$\delta\omega = \int_l \int_A \sigma_z . \delta\varepsilon_z . dA . dz - \{Q\} . \{\delta q\} = 0 \qquad (4.1)$$

where,

ω= virtual work;
σ_z , ε_z= normal stress and strain;
A= cross-sectional area of the composite section;
$\{Q\}$= vector of nodal forces;
$\{q\}$= vector of nodal displacements.

In order to evaluate Eq. (4.1) the variation of strain, $\delta\varepsilon_z$ must be known. This is done by using Saada's axial strain-displacement equation for large displacements[144,164] as was adopted in the original program. This can be written as

$$\varepsilon_z = u' + \frac{1}{2}\left[(u')^2 + (v')^2\right] \qquad (4.2)$$

The terms of this equation can be obtained from the geometry of Fig. 4.1, assuming that the slope at any point along the reference axes is:

$$v_o' = \frac{\Delta v_o}{\Delta z} = \sin\theta \qquad (4.3)$$

It then follows that

$$u = u_o - y . v_o' \qquad u' = u_o' - y . v_o'' \qquad (4.4)$$

and

$$v = v_o - y(1 - \cos\theta) \qquad v' = v_o' - \frac{y . v_o' . v_o''}{\eta} \qquad (4.5)$$

where,

$$\eta = \cos\theta = \sqrt{1 - (v_o')^2} \qquad (4.6)$$

u , u_o= horizontal displacements of the composite section;
v , v_o= vertical displacement of the composite section;
θ= rotation of the composite section;
y= distance from centroidal axis (Fig. 4.1).

The variation in strain $\delta\varepsilon_z$ can now be evaluated by substituting these relationships into Eq. (4.2) and differentiating with respect to u_o', v_o' and v_o''.

$$\delta\varepsilon_z = \left[\left(1+u_o'\right) - y.v_o''\right]\delta u_o'$$
$$+\frac{1}{\eta^3}\left[\eta^3.v_o' - 2.\eta^2.y.v_o''.v_o' - y.\left(v_o'\right)^3 v_o'' + \eta.\left[\left(y^2.v_o'.\left(v_o''\right)^2\right) - \left(y^2.\left(v_o'\right)^3.\left(v_o''\right)^2\right)\right]\right]\delta v_o'$$
$$+\frac{1}{\eta^2}\left[-\eta^2\left[y.\left(1+u_o'\right) + y^2.v_o''\right] - \eta.y.\left(v_o'\right)^2 + y^2.\left(v_o'\right)^2.v_o''\right]\delta v_o'' \qquad (4.7)$$

Substituting Eq. (4.7) into the virtual work equation (4.1) and using the constants a_1, a_2 and a_3 the equilibrium equation can be rewritten as

$$\delta\omega = \int_l \left[a_1.\delta u_o' + a_2.\delta v_o' + a_3.\delta v_o''\right].dz - \{Q\}.\{\delta q\} = 0 \qquad (4.8)$$

The derivation of these constants is based on the evaluation of stress resultants and described in Reference[144]. Since the displacements u_0', v_o' and v_o'' at any point are functions of a discrete set of six generalised nodal displacements q_i, Eq. (4.8) may be expressed as

$$\psi_i = \frac{\partial\omega}{\partial q_i} = \int_l \left[a_1\frac{\partial u_o'}{\partial q_i} + a_2\frac{\partial v_o'}{\partial q_i} + a_3\frac{\partial v_o''}{\partial q_i}\right].dz - Q_i = 0 \qquad (4.9)$$

where,

ψ_i= partial derivative of virtual work with respect to nodal displacements;
Q_i= nodal force co-ordinate.

Equation (4.9) is non-linear and a solution may be obtained by using the Newton-Raphson method[165] which can be represented in the following form:

$$\frac{\delta\psi_i}{\delta q_j}\Delta q_j = -\psi_i \qquad (4.10)$$

where,

Δq_j= incremental nodal displacement co-ordinate.

Substituting Eq. (4.9) into Eq. (4.10) leads to the general form of non-linear equilibrium equation, which can be expressed in matrix form as

$$[K_T].\Delta q_j = \{\Delta Q\} \qquad (4.11)$$

where $[K_T]$ and $\{\Delta Q\}$ are respectively the stiffness matrix and the incremental unbalanced force vector:

$$[K_T] = \left[\int_l \left[\frac{\partial a_1}{\partial q_j}\frac{\partial u_o'}{\partial q_i} + \frac{\partial a_2}{\partial q_j}\frac{\partial v_o'}{\partial q_i} + \frac{\partial a_3}{\partial q_j}\frac{\partial v_o''}{\partial q_i}\right].dz\right] \qquad (4.12)$$

$$\{\Delta Q\} = Q_i - \int_l \left[a_1\frac{\partial u_o'}{\partial q_i} + a_2\frac{\partial v_o'}{\partial q_i} + a_3\frac{\partial v_o''}{\partial q_i}\right].dz \qquad (4.13)$$

The Gaussian integration method[165] using four Gauss points and weighting factors has been used to determine the above integrals. The iterative procedure is carried out until the incremental unbalanced force vector $\{\Delta Q\}$ is sufficiently small and therefore equilibrium is reached.

In order to evaluate the integrals the displacements at each Gauss point along a finite element are required. These are obtained by multiplying a set of algebraic shape functions, which are cubic polynomials, by the generalised displacements at the nodes[144,145].

4.2.3. The Non-linear Inelastic Formulation at Elevated Temperatures

The constants a_1 to a_3 and their derivatives in the Eqs. (4.12) and (4.13) are functions of internal stress resultants and they need to be determined at each Gauss point over the cross-section. In addition parts of the cross-section may be at different temperatures and the tangent modulus E_t for the corresponding stress-strain curves may be different. Since it is not computationally efficient to use a tangent modulus which varies continuously throughout the cross-section, a transformed-section method has been employed.

The composite cross-section is divided into 11 segments in which the variation in strain is assumed to be linear as shown in Fig. 4.2(b). The strains at the extremities of each segment can be calculated from Eq. (4.2).

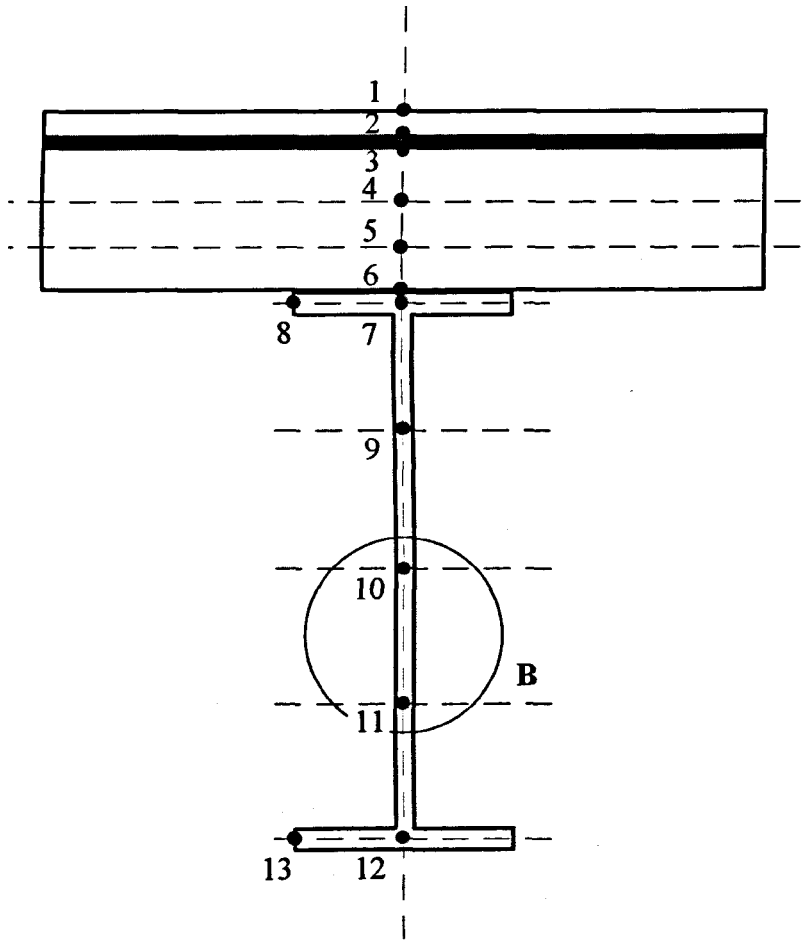

(a) Layered section

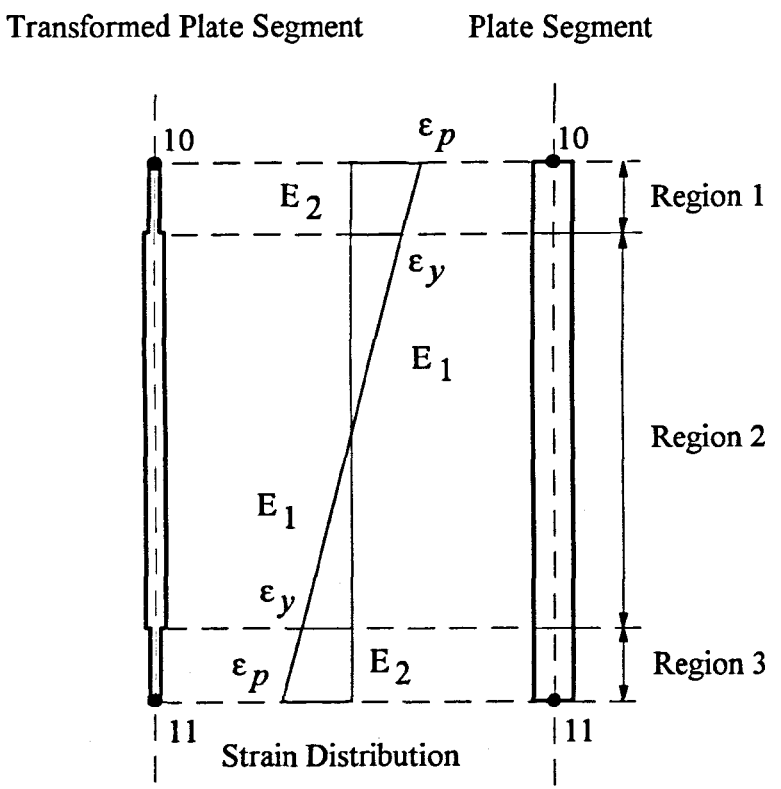

(b) Detail B

Fig. 4.2 Transformation of plate segments.

Any parts of a segment which are strained beyond the plastic limit are ignored, and an average value is calculated for those parts of the segment which are strained less severely. The transformed width of each region is then determined by multiplying the original width by the current tangent modulus divided by the initial elastic modulus of the steel at 20° C (Fig. 4.2(b)).

$$b_{tr} = \frac{E_t}{E_{s_{y20}}} b_{or} \tag{4.14}$$

where,

b_{tr} , b_{or}= transformed and original width of the plate segment;
$E_{s_{y20}}$, E_t= elastic modulus of steel at 20° C and current modulus of a segment.

Once the transformed thickness of each region has been determined, the internal stress resultants, n, m and m^*, can easily be calculated. Using the transformed area, A_{tr}, these can be written in terms of the elastic tangent modulus of steel at 20° C as

$$n = E_{s_{y20}} . \varepsilon_z . A_{tr}$$
$$m = E_{s_{y20}} . \varepsilon_z . y . A_{tr}$$
$$m^* = E_{s_{y20}} . \varepsilon_z . y^2 . A_{tr} \tag{4.15}$$

The above definitions and their derivatives can then be incorporated into the unbalanced force vector and stiffness matrix (Eqs. (4.12) and (4.13)) to solve the nodal displacements at each node.

4.2.4. The Stability Criterion

Solution of the equilibrium equation in global co-ordinates to obtain the displacement vector $\{r\}_G$ requires inversion of the stiffness matrix $[K_T]_G$.

$$[K_T]_G . \{r\}_G = \{R\}_G \tag{4.16}$$
$$\{r\}_G = [K_T]_G^{-1} . \{R\}_G \tag{4.17}$$

When the displacement vector $\{r\}_G$ starts to increase without limit for finite increments of the load vector $\{R\}_G$ the inverse of the stiffness matrix $[K_T]_G$ becomes infinitely large. This can only be true when the determinant of the stiffness matrix $[K_T]_G$ is equal to zero.

The program therefore searches for negative or zero numerical elements on the leading diagonal of the stiffness matrix. Such a condition is considered as structural instability, and as a result the program automatically returns to the previous stable temperature level and increments the temperature using smaller steps. Analysis is terminated when the difference between a stable and unstable temperature level is smaller than a pre-defined tolerance.

4.3. Partial Interaction Formulation

4.3.1. The Concept of the Theoretical Model

The finite element analysis program INSTAF[144-145] has been extended to include the reinforced concrete slab and the slip at its interface with the steel in composite construction. The original program uses a line element to represent the steel I-section with four degrees of freedom at each node, namely the axial displacement, axial strain, vertical displacement and rotation. It considers material non-linearity of the steel, geometric non-linearity due to large displacements and a non-linear strain-displacement relationship. In the modified model the additional effects of material non-linearity in the concrete and shear connectors, and the effect of slip on large displacements, have also been incorporated. The concrete slab and slip at the interface are taken into account by introducing two parallel line elements representing the beam and slab. The model includes two additional degrees of freedom, allowing the concrete and steel to have independent axial displacements and strains. The present mathematical model makes the following assumptions in addition to those in the original version of INSTAF:

1. The distributions of axial strain in the concrete slab and steel I-section are assumed to be linear but different from one another.
2. Shear connectors are assumed to act as a continuous shearing medium along the length of the beam, between the concrete slab and steel I section.
3. The vertical displacement, rotation and curvature of the concrete slab and steel I-section are identical at the end of an element.

4.3.2. Virtual Work Formulation

In the case of partial interaction, the axial deformations of the slab and the beam are different and two line elements representing these two components are therefore used, with axes positioned at the centroids of the concrete slab and steel I-section. Six independent degrees of freedom are considered per node, as illustrated in Fig. 4.3.

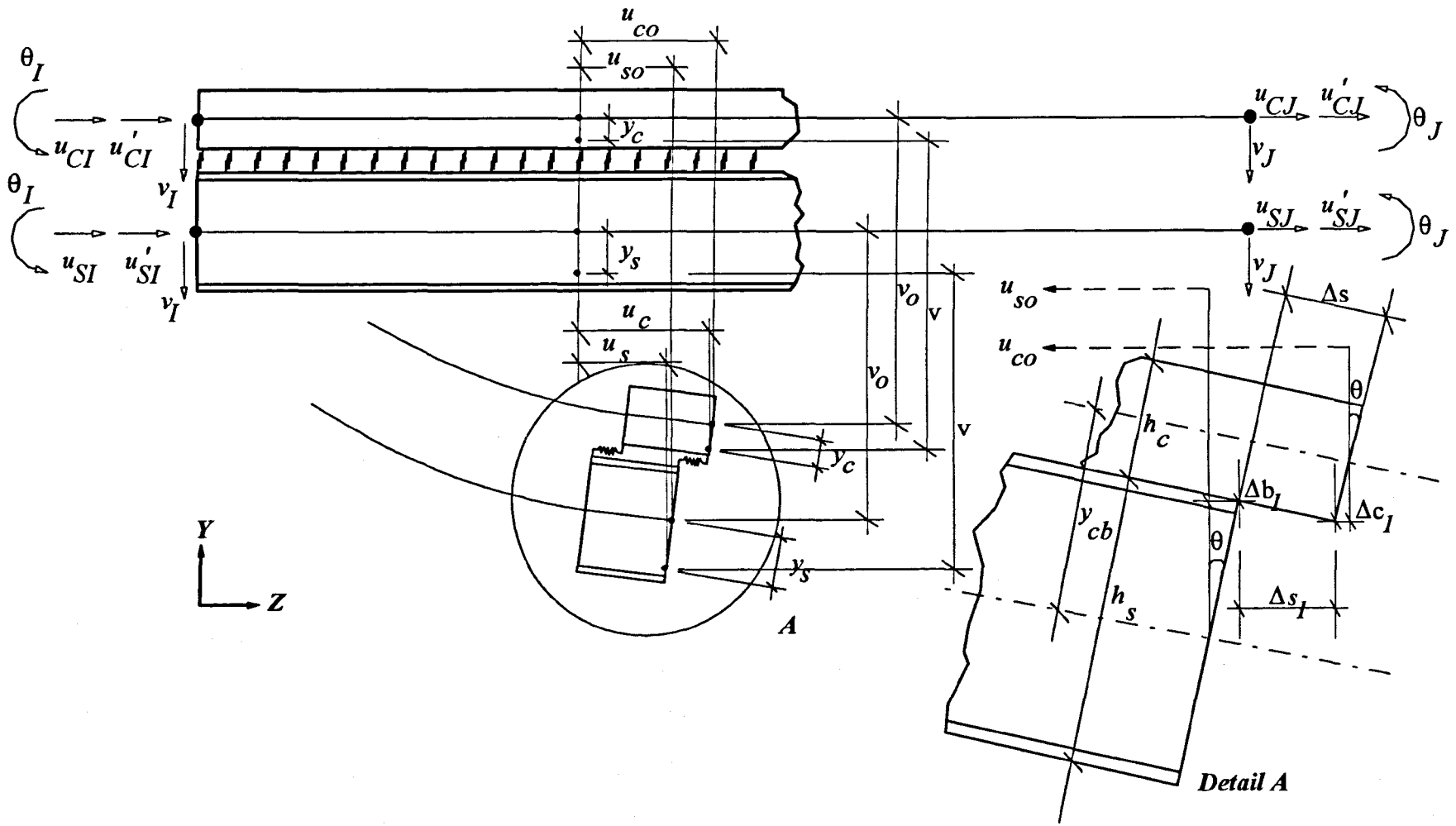

Fig. 4.3 Finite element representation of a composite beam with partial interaction.

The formulation utilises the Principle of Virtual Work. The internal work must be expressed as the sum of the work done by concrete slab, steel I-section and shear connectors. Thus the virtual work equation takes the following form:

$$\delta\omega = \int_l \int_{A_c} \sigma_{cz}.\delta\varepsilon_{cz}.dA_c.dz + \int_l \int_{A_s} \sigma_{sz}.\delta\varepsilon_{sz}.dA_s.dz + \int_l F.\delta\Delta s.dz - \{Q\}.\{\delta q\} = 0 \qquad (4.18)$$

where,

ω=	virtual work;
σ_{sz} , ε_{sz}=	normal stress and strain in the steel I-section;
σ_{cz} , ε_{cz}=	normal stress and strain in the concrete slab;
A_c , A_s=	cross-sectional area of the concrete slab and steel I-section;
F=	shear force per unit length;
Δs=	slip at the interface per unit length.

The first two terms represent the virtual work done by the concrete slab and steel beam. The third term is the virtual work done by shear connectors. If the slip modulus of the shear connection layer is denoted as Q_{sh}, this term may be written as

$$\int_l F.\delta\Delta s.dz = \int_l Q_{sh}.\Delta s.\delta\Delta s.dz \qquad (4.19)$$

In order to evaluate Eq. (4.18) the variation of strain, $\delta\varepsilon_{cz}$ and $\delta\varepsilon_{sz}$, and the slip per unit length, $\delta\Delta s$, must be known. Because of the discontinuity at the interface between the slab and the I-section, the axial strain distributions must be derived separately for the two components using Saada's axial strain-displacement equation[164] (Eq. 4.2). The terms of this equation for the two components can be obtained from the geometry of Fig. 4.3, and Eq. (4.3) as follows

$$u_c = u_{co} - y_c.v_o' \qquad u_c' = u_{co}' - y_c.v_o''$$
$$u_s = u_{so} - y_s.v_o' \qquad u_s' = u_{so}' - y_s.v_o'' \qquad (4.20)$$

and

$$v = v_o - y(1-\cos\theta) \qquad v' = v_o' - \frac{y.v_o'.v_o''}{\eta} \qquad (4.21)$$

where,

u_s , u_{so}=	horizontal displacements in the steel I-section;
u_c , u_{co}=	horizontal displacements in the concrete slab;
v , v_o=	vertical displacement of the composite section;
v_o' , θ=	rotational displacement of the composite section;
y_s , y_c , y=	distance from the centroid of the steel beam and concrete slab (Fig. 4.3).

The variations in strain $\delta\varepsilon_{cz}$ and $\delta\varepsilon_{sz}$ can now be obtained for the two components by substituting these relationships into Eq. (4.2) and differentiating with respect to u'_{co}, u'_{so}, v'_o and v''_o. For the concrete slab this gives

$$\varepsilon_{cz} = u'_{co} + 0.5\left[(u'_{co})^2 + (v'_o)^2\right] - y_c.v''_o\left[1 + u'_{co} + \frac{(v'_o)^2}{\eta}\right] + 0.5.y_c^2(v''_o)^2\left[1 + \frac{(v'_o)^2}{\eta^2}\right] \quad (4.22)$$

$$\begin{aligned}\delta\varepsilon_{cz} = &\left[(1+u'_{co}) - y_c.v''_o\right]\delta u'_{co} \\ &+\frac{1}{\eta^3}\left[\eta^3.v'_o - 2.\eta^2.y_c.v''_o.v'_o - y_c.(v'_o)^3 v''_o + \eta.\left[\left(y_c^2.v'_o.(v''_o)^2\right) - \left(y_c^2.(v'_o)^3.(v''_o)^2\right)\right]\right]\delta v'_o \\ &+\frac{1}{\eta^2}\left[-\eta^2\left[y_c.(1+u'_{co}) + y_c^2.v''_o\right] - \eta.y_c.(v'_o)^2 + y_c^2.(v'_o)^2.v''_o\right]\delta v''_o \end{aligned} \quad (4.23)$$

and for the steel I-section

$$\varepsilon_{sz} = u'_{so} + 0.5\left[(u'_{so})^2 + (v'_o)^2\right] - y_s.v''_o\left[1 + u'_{so} + \frac{(v'_o)^2}{\eta}\right] + 0.5.y_s^2(v''_o)^2\left[1 + \frac{(v'_o)^2}{\eta^2}\right] \quad (4.24)$$

$$\begin{aligned}\delta\varepsilon_{sz} = &\left[(1+u'_{so}) - y_s.v''_o\right]\delta u'_{so} \\ &+\frac{1}{\eta^3}\left[\eta^3.v'_o - 2.\eta^2.y_s.v''_o.v'_o - y_s.(v'_o)^3 v''_o + \eta.\left[y_s^2.v'_o.(v''_o)^2 - y_s^2.(v'_o)^3.(v''_o)^2\right]\right]\delta v'_o \\ &+\frac{1}{\eta^2}\left[-\eta^2.\left[y_s.(1+u'_{so}) + y_s^2.v''_o\right] - \eta.y_s.(v'_o)^2 + y_s^2.(v'_o)^2.v''_o\right]\delta v''_o \end{aligned} \quad (4.25)$$

The slip per unit length Δs at any arbitrary point along the length of the beam can also be determined from Fig. 4.3, as

$$\Delta s = \frac{\Delta s_1}{\cos\theta} = \frac{1}{\eta}(u_{so} - u_{co} + y_{cb}.v'_o) \quad (4.26)$$

where,

y_{cb}= distance between the centroids of the steel I-section and concrete slab.

The variation in slip can similarly be determined by differentiating Eq. (4.26) with respect to u_{co}, u_{so} and v'_o. This yields

$$\delta\Delta s = \frac{1}{\eta}(\delta u_{so} - \delta u_{co}) + \left[\frac{1}{\eta^3}v'_o\left(u_{so} - u_{co} + y_{cb}.v'_o + \frac{\eta^2.y_{cb}}{v'_o}\right)\right]\delta v'_o \quad (4.27)$$

Substituting Equations (4.23), (4.25) and (4.27) into the virtual work equation (4.18) results in the equilibrium equation

$$\delta\omega = \int_l \int_{Ac} \sigma_{cz} \left\{ \left[(1+u'_{co}) - y_c . v''_o \right] \delta u'_{co} \right.$$
$$+ \frac{1}{\eta^3} \left[\eta^3 . v'_o - 2.\eta^2 . y_c . v''_o . v'_o - y_c . (v'_o)^3 v''_o + \eta . \left[y_c^2 . v'_o . (v''_o)^2 - y_c^2 . (v'_o)^3 . (v''_o)^2 \right] \right] \delta v'_o$$
$$\left. + \frac{1}{\eta^2} \left[-\eta^2 . \left[y_c . (1+u'_{co}) + y_c^2 . v''_o \right] - \eta . y_c . (v'_o)^2 + y_c^2 . (v'_o)^2 \right] \delta v''_o \right\} . dA_c . dz$$
$$+ \int_l \int_{As} \sigma_{sz} \left\{ \left[(1+u'_{so}) - y_s . v''_o \right] \delta u'_{so} \right.$$
$$+ \frac{1}{\eta^3} \left[\eta^3 . v'_o - 2.\eta^2 . y_s . v''_o . v'_o - y_s . (v'_o)^3 v''_o + \eta . \left[y_s^2 . v'_o . (v''_o)^2 - y_s^2 . (v'_o)^3 . (v''_o)^2 \right] \right] \delta v'_o$$
$$\left. + \frac{1}{\eta^2} \left[-\eta^2 . \left[y_s . (1+u'_{so}) + y_s^2 . v''_o \right] - \eta . y_s . (v'_o)^2 + y_s^2 . (v'_o)^2 \right] \delta v''_o \right\} . dA_s . dz$$
$$+ \int_l F \left\{ \frac{1}{\eta} (\delta u_{so} - \delta u_{co}) + \left[\frac{1}{\eta^3} v'_o \left(u_{so} - u_{co} + y_{cb} . v'_o + \frac{\eta^2 . y_{cb}}{v'_o} \right) \right] \delta v'_o \right\} dz$$
$$- \{Q\} . \{\delta q\} = 0 \qquad (4.28)$$

The equilibrium equation (4.28) can be expressed using the constants $a_1, a_2, a_3, a_4, a_5, a_6, a_7, a_8$, as

$$\delta\omega = \int_l \left[a_1 . \delta u'_{so} + a_3 . \delta v'_o + a_5 . \delta v''_o \right] . dz + \int_l \left[a_2 . \delta u'_{co} + a_4 . \delta v'_o + a_6 . \delta v''_o \right] . dz$$
$$+ \int_l \left[F \left(a_7 . \delta u_{so} - a_7 . \delta u_{co} + a_8 . \delta v'_o \right) \right] . dz - \{Q\} . \{\delta q\} = 0 \qquad (4.29)$$

The derivation of these constants is based on the evaluation of stress resultants and constants a_1, a_3 and a_5 for the steel I-section are identical to constants a_2, a_4 and a_6 for the concrete slab. Thus only the constants for the steel beam and constants a_7 and a_8 representing the shear connection will be described.

$$a_1 = n_s . (1+u'_{so}) - m_s . v''_o \qquad (4.30)$$

$$a_3 = n_s . v'_o - \frac{1}{\eta^3} m_s . v'_o . v''_o \left[2\eta^2 + \eta (v'_o)^2 \right] + \frac{1}{\eta^4} m_s^* . v'_o . (v''_o)^2 \left[\eta^2 + (v'_o)^2 \right] \qquad (4.31)$$

$$a_5 = \frac{1}{\eta^2} m_s . \left[\eta^2 (1+u'_{so}) - \eta (v'_o)^2 \right] + \frac{1}{\eta^2} m_s^* . v''_o . \left[\eta^2 + (v'_o)^2 \right] \qquad (4.32)$$

$$a_7 = \frac{1}{\eta} \qquad (4.33)$$

$$a_8 = \frac{1}{\eta^3} v'_o \left[u_{so} - u_{co} + y_{cb} . v'_o + \frac{\eta^2 . y_{cb}}{v'_o} \right] \qquad (4.34)$$

where,

n_s= axial stress resultant in the steel I-section;

m_s= bending stress resultant in the steel I-section;

m_s^*= stress resultant due to the higher order terms in Eq. (4.23) and (4.25).

The equilibrium equation (4.29) is approximate only to the extent defined by Eq. (4.3). Considering the displacements u_{co}, u_{so}, u'_{co} u'_{so} v'_o and v''_o at any point as functions of a discrete set of six generalised nodal displacements q_i, it may be expressed as

$$\psi_i = \frac{\partial \omega}{\partial q_i} = \int_l \left[a_1 \frac{\partial u'_{so}}{\partial q_i} + a_3 \frac{\partial v'_o}{\partial q_i} + a_5 \frac{\partial v''_o}{\partial q_i} \right] . dz + \int_l \left[a_2 \frac{\partial u'_{co}}{\partial q_i} + a_4 \frac{\partial v'_o}{\partial q_i} + a_6 \frac{\partial v''_o}{\partial q_i} \right] . dz$$
$$+ \int_l F \left[a_7 \frac{\partial u_{so}}{\partial q_i} - a_7 \frac{\partial u_{co}}{\partial q_i} + a_8 \frac{\partial v'_o}{\partial q_i} \right] . dz - Q_i = 0 \qquad (4.35)$$

Equation (4.35) is highly non-linear and a solution may be obtained by using the Newton-Raphson method[165] which can be represented in the following form:

$$\frac{\delta \psi_i}{\delta q_j} \Delta q_j = -\psi_i \qquad (4.36)$$

Substituting Eq. (4.35) into Eq. (4.36) leads to the general form of non-linear equilibrium equation, which can then be updated by allowing corrections to the displacements until equilibrium is achieved. The equilibrium equations can be expressed in matrix form as

$$[K_T] . \Delta q_j = \{\Delta Q\} \qquad (4.37)$$

where $[K_T]$ and $\{\Delta Q\}$ are respectively the stiffness matrix and the incremental unbalanced force vector and are given below. The iterative procedure is carried out until the incremental unbalanced force vector $\{\Delta Q\}$ is sufficiently small and therefore equilibrium is reached.

$$[K_T] = \left[\int_l \left[\frac{\partial a_1}{\partial q_j} \frac{\partial u'_{so}}{\partial q_i} + \frac{\partial a_3}{\partial q_j} \frac{\partial v'_o}{\partial q_i} + \frac{\partial a_5}{\partial q_j} \frac{\partial v''_o}{\partial q_i} \right] . dz + \int_l \left[\frac{\partial a_2}{\partial q_j} \frac{\partial u'_{co}}{\partial q_i} + \frac{\partial a_4}{\partial q_j} \frac{\partial v'_o}{\partial q_i} + \frac{\partial a_6}{\partial q_j} \frac{\partial v''_o}{\partial q_i} \right] . dz \right.$$
$$\left. + \int_l \left[\frac{\partial (F.a_7)}{\partial q_j} \frac{\partial u_{so}}{\partial q_i} - \frac{\partial (F.a_7)}{\partial q_j} \frac{\partial u_{co}}{\partial q_i} + \frac{\partial (F.a_8)}{\partial q_j} \frac{\partial v'_o}{\partial q_i} \right] . dz \right] \qquad (4.38)$$

$$\{\Delta Q\} = Q_i - \left[\int_l \left[a_1 \frac{\partial u'_{so}}{\partial q_i} + a_3 \frac{\partial v'_o}{\partial q_i} + a_5 \frac{\partial v''_o}{\partial q_i} \right] . dz + \int_l \left[a_2 \frac{\partial u'_{co}}{\partial q_i} + a_4 \frac{\partial v'_o}{\partial q_i} + a_6 \frac{\partial v''_o}{\partial q_i} \right] . dz \right.$$
$$\left. + \int_l F \left[a_7 \frac{\partial u_{so}}{\partial q_i} - a_7 \frac{\partial u_{co}}{\partial q_i} + a_8 \frac{\partial v'_o}{\partial q_i} \right] . dz \right] \qquad (4.39)$$

The Gaussian integration method[165] using four Gauss points and weighting factors has been utilised to determine the above integrals.

4.3.3. The Finite Element Model and Evaluation of Derivatives

At each Gauss point the partial derivatives involving u and v are evaluated using a set of algebraic shape functions which are cubic polynomials. The displacements at each Gauss point along a finite element are determined by interpolation. A typical composite element with partial interaction, its nodal displacements and the cubic shape function in terms of the non-dimensional position co-ordinate ξ, are shown in Fig. 4.4 and may be represented algebraically as

$$u_{so} = \langle \bar{\phi} \rangle \begin{Bmatrix} u_{SI} \\ u'_{SI} \\ u_{SJ} \\ u'_{SJ} \end{Bmatrix} \qquad u_{co} = \langle \bar{\phi} \rangle \begin{Bmatrix} u_{CI} \\ u'_{CI} \\ u_{CJ} \\ u'_{CJ} \end{Bmatrix} \qquad v_o = \langle \bar{\phi} \rangle \begin{Bmatrix} v_I \\ \theta_I \\ v_J \\ \theta_J \end{Bmatrix} \tag{4.40}$$

where the cubic polynomials corresponding to each nodal displacement constitute the shape function vector $\langle \bar{\phi} \rangle$,which is given explicitly in the original development of INSTAF[144,145].

The derivatives in Eqs. (4.38) and (4.39) involving u and v can now be evaluated. The set of derivatives involving a_1 to a_8 must also be determined numerically in order to construct the stiffness matrix. The evaluation of derivatives for the concrete slab and steel I-section (involving a_1 to a_6) are similar so only the terms associated with steel I-section and the interaction force are presented. For the steel beam these can be written as

$$\frac{\partial a_1}{\partial q_j} = \left(1+u'_{so}\right)\frac{\partial n_s}{\partial q_j} + n_s \frac{\partial u'_{so}}{\partial q_j} - v''_o \frac{\partial m_s}{\partial q_j} - m_s \frac{\partial v''_o}{\partial q_j} \tag{4.41}$$

$$\begin{aligned}\frac{\partial a_3}{\partial q_j} &= v'_o \frac{\partial n_s}{\partial q_j} + n_s \frac{\partial v'_o}{\partial q_j} - \frac{v'_o . v''_o}{\eta}\left(2+\frac{\left(v'_o\right)^2}{\eta^2}\right)\frac{\partial m_s}{\partial q_j} \\ &\quad -m_s\left[\frac{v'_o}{\eta}\left(2+\frac{\left(v'_o\right)^2}{\eta^2}\right)\frac{\partial v''_o}{\partial q_j} + \frac{v''_o}{\eta}\left(2+\frac{5.\left(v'_o\right)^2}{\eta}+\frac{3.\left(v'_o\right)^4}{\eta^3}\right)\frac{\partial v'_o}{\partial q_j}\right] + \frac{v'_o.\left(v''_o\right)^2}{\eta^2}\left(1+\frac{\left(v'_o\right)^2}{\eta^2}\right)\frac{\partial m^*_s}{\partial q_j} \\ &\quad -m^*_s\left[\frac{2v'_o.v''_o}{\eta^2}\left(1+\frac{\left(v'_o\right)^2}{\eta^2}\right)\frac{\partial v''_o}{\partial q_j} + \frac{\left(v''_o\right)^2}{\eta^2}\left(1+5.\left(v'_o\right)^2+\frac{4.\left(v'_o\right)^4}{\eta^2}\right)\frac{\partial v'_o}{\partial q_j}\right]\end{aligned} \tag{4.42}$$

$$\begin{aligned}\frac{\partial a_5}{\partial q_j} &= -\left(1+u'_{so}+\frac{\left(v'_o\right)^2}{\eta}\right)\frac{\partial m_s}{\partial q_j} + v''_o\left(1+\frac{\left(v'_o\right)^2}{\eta^2}\right)\frac{\partial m^*_s}{\partial q_j} \\ &\quad -m_s\left[\frac{\partial u_{so}}{\partial q_j} + \frac{v'_o}{\eta}\left(2+\frac{\left(v'_o\right)^2}{\eta^2}\right)\frac{\partial v'_o}{\partial q_j}\right] \\ &\quad +m^*_s\left[\left(1+\frac{\left(v'_o\right)^2}{\eta^2}\right)\frac{\partial v''_o}{\partial q_j} + \frac{2.v'_o.v''_o}{\eta^2}\left(1+\frac{\left(v'_o\right)^2}{\eta^2}\right)\frac{\partial v'_o}{\partial q_j}\right]\end{aligned} \tag{4.43}$$

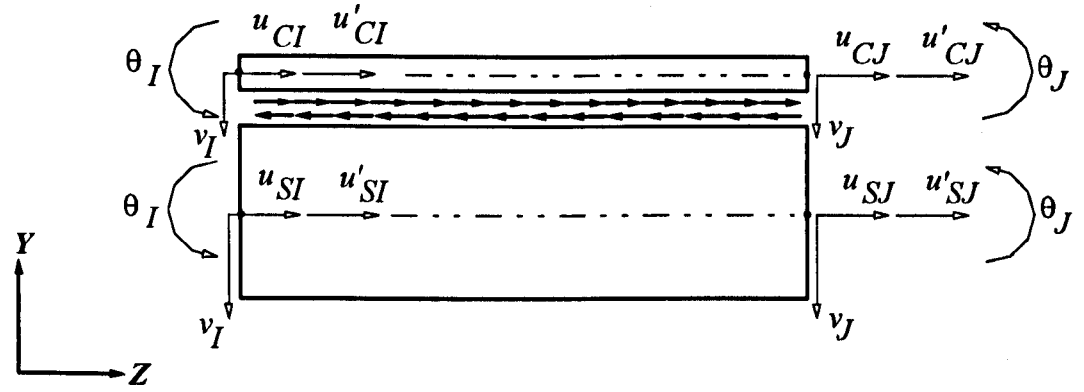

(a) Nodal displacements in local co-ordinate system

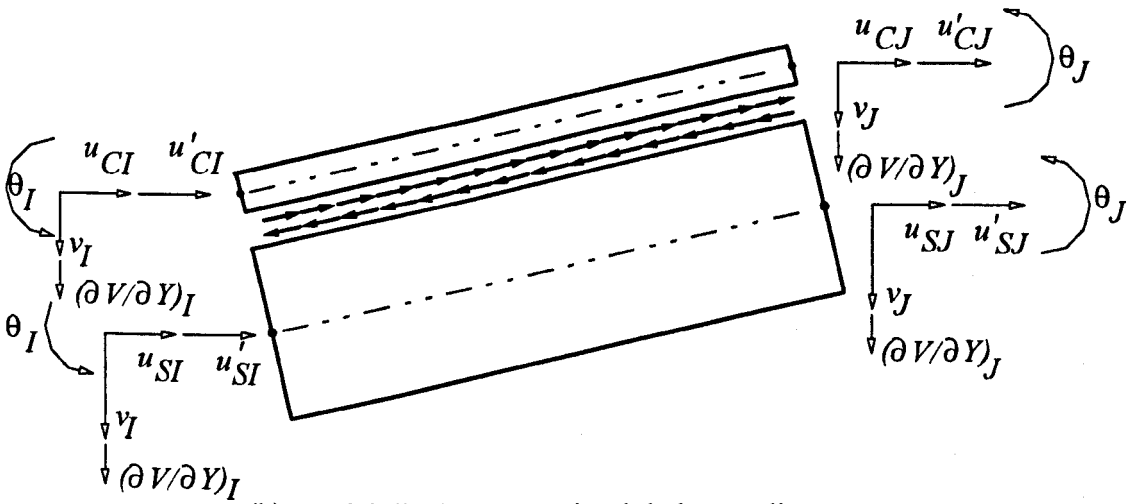

(b) Nodal displacements in global co-ordinate system

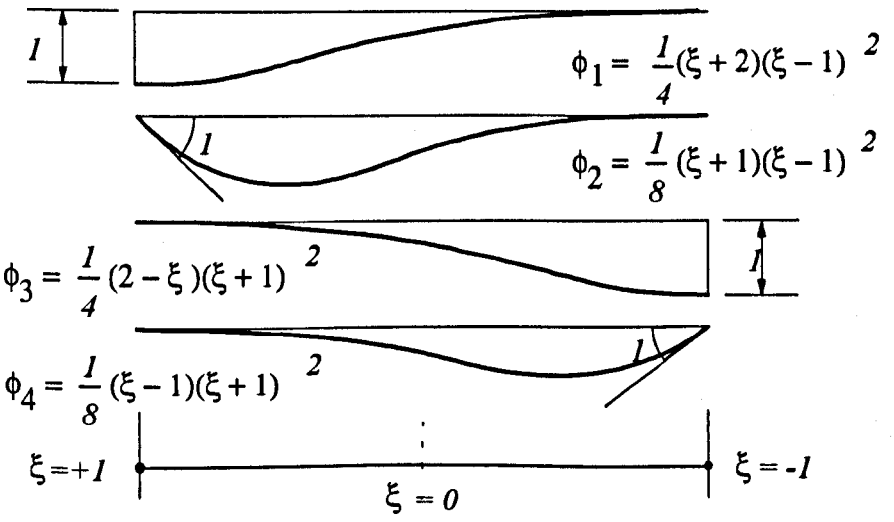

(c) Shape functions

Fig. 4.4 Degrees of freedom and cubic shape functions.

When the interaction force is within the elastic region and Q_{sh} is the elastic modulus which expresses the initial slope of the load-slip relationship (see Fig. 3.6) the derivatives $\frac{\partial(F.a_7)}{\partial q_j}$ and $\frac{\partial(F.a_8)}{\partial q_j}$ corresponding to the shear connection may be calculated using the relationship

$$F = Q_{sh}.\Delta s \tag{4.44}$$

together with Eqs. (4.26), (4.33) and (4.34).

$$\left(\frac{\partial(F.a_7)}{\partial q_j}\right)_{el} = \frac{1}{\eta^2} Q_{sh}\left[\frac{\partial u_{so}}{\partial q_j} - \frac{\partial u_{co}}{\partial q_j} + \left(y_{cb}\left(1+\frac{1}{\eta^2}2.(v_o')^2\right)+\frac{2.v_o'}{\eta^2}(u_{so}-u_{co})\right)\frac{\partial v_o'}{\partial q_j}\right] \tag{4.45}$$

and

$$\begin{aligned}\left(\frac{\partial(F.a_8)}{\partial q_j}\right)_{el} = &\left[\frac{1}{\eta^4} Q_{sh}\left(u_{so}^2+u_{co}^2-2.u_{so}.u_{co}+6.u_{so}.y_{cb}v_o'-6.u_{co}.y_{cb}v_o'\right)\right.\\ &+\left(\frac{1}{\eta^6}4.Q_{sh}.(v_o')^2\right).\left(u_{so}^2+u_{co}^2-2.u_{so}.u_{co}+2.u_{so}.y_{cb}v_o'-2.u_{co}.y_{cb}v_o'\right)\\ &\left.+\frac{1}{\eta^6}Q_{sh}.y_{cb}^2.\left(5.\eta^2.(v_o')^2+4.(v_o')^4+\eta^4\right)\right]\frac{\partial v_o'}{\partial q_j}\\ &+\frac{1}{\eta^4}Q_{sh}\left[v_o'\left(2.u_{so}-2.u_{co}+2.y_{cb}.v_o'\right)+\eta^2.y_{cb}\right].\left[\frac{\partial u_{so}'}{\partial q_j}-\frac{\partial u_{co}'}{\partial q_j}\right]\end{aligned} \tag{4.46}$$

When the interaction force is in the plastic region these partial derivatives become

$$\left(\frac{\partial(F.a_7)}{\partial q_j}\right)_{pl} = \left(\frac{\partial(F.a_7)}{\partial q_j}\right)_{el} + \frac{1}{\eta^3}\left[v_o'\left(F_y - Q_{sp}\Delta s_y\right)\right]\frac{\partial v_o'}{\partial q_j} \tag{4.47}$$

$$\begin{aligned}\left(\frac{\partial(F.a_8)}{\partial q_j}\right)_{pl} = &\left(\frac{\partial(F.a_8)}{\partial q_j}\right)_{el} + \frac{1}{\eta^3}\left(F_y - Q_{sp}\Delta s_y\right)\left[\left(u_{so}-u_{co}+3v_o'y_{cb}\right)\right.\\ &\left.+\frac{3(v_o')^2}{\eta^2}\left(u_{so}-u_{co}+v_o'y_{cb}\right)\right]\frac{\partial v_o'}{\partial q_j}+\frac{v_o'}{\eta^3}\left(F_y-Q_{sp}\Delta s_y\right)\left[\frac{\partial u_{so}}{\partial q_j}-\frac{\partial u_{co}}{\partial q_j}\right]\end{aligned} \tag{4.48}$$

Beyond the plastic limit the derivatives are expressed as

$$\left(\frac{\partial(F.a_7)}{\partial q_j}\right)_{ult} = \frac{F_{ult}v_o'}{\eta^3}\frac{\partial v_o'}{\partial q_j} \tag{4.49}$$

$$\left(\frac{\partial(F.a_8)}{\partial q_j}\right)_{ult} = \frac{F_{ult}}{\eta^3}\left(u_{so} - u_{co} + y_{cb}\left(1+v_o'\right)\right)\left[1+\frac{3\left(v_o'\right)^2}{\eta^2}\right]\frac{\partial v_o'}{\partial q_j}$$

$$+\frac{F_{ult}v_o'}{\eta^3}\left[\frac{\partial u_{so}}{\partial q_j} - \frac{\partial u_{co}}{\partial q_j}\right] \qquad (4.50)$$

where,

F_y , F_{ult}= yield and ultimate strength of the shear connector;
Q_{sp}= tangent modulus in the plastic region;
Δs_y= slip corresponding to yield strength of the shear connector.

4.3.4. The Non-linear Inelastic Formulation at Elevated Temperatures

The stress-strain-temperature behaviour of steel and concrete are highly non-linear and as a result the initial tangent modulus varies significantly with both increasing stress and changing temperature. If parts of the cross-section are subjected to a temperature gradient or different stress levels the corresponding tangent modulus E_t will need to be varied. In order to avoid the use of a continuously varying tangent modulus the transformed-section method described in Section 4.2.3 has been utilised.

4.3.5. Evaluation of Cross-Section Properties and Stress Resultants

Once the transformed area of each region, A_{tr}, has been determined, the first and second moments of area of the total cross section can be calculated as

$$\int_{A_{str}} dA_{s_{tr}} = A_{s_{tr}} \qquad \int_{A_{ctr}} dA_{c_{tr}} = A_{c_{tr}}$$

$$\int_{A_{str}} y_s.dA_{s_{tr}} = I_{1s_{tr}} \qquad \int_{A_{ctr}} y_c.dA_{c_{tr}} = I_{1c_{tr}}$$

$$\int_{A_{str}} y_s^2.dA_{s_{tr}} = I_{2s_{tr}} \qquad \int_{A_{ctr}} y_c^2.dA_{c_{tr}} = I_{2c_{tr}}$$

$$\int_{A_{str}} y_s^3.dA_{s_{tr}} = I_{3s_{tr}} \qquad \int_{A_{ctr}} y_c^3.dA_{c_{tr}} = I_{3c_{tr}}$$

$$\int_{A_{str}} y_s^4.dA_{s_{tr}} = I_{4s_{tr}} \qquad \int_{A_{ctr}} y_c^4.dA_{c_{tr}} = I_{4c_{tr}} \qquad (4.51)$$

The terms a_1 to a_6 are related to the internal stress resultants, n, m and m^*. In the present case both concrete and steel must be represented, and the stress resultants are then defined by

$$n_s = \int_{A_{s_{or}}} E_{s_t}.\varepsilon_{sz}.dA_{s_{or}} \qquad n_c = \int_{A_{c_{or}}} E_{c_t}.\varepsilon_{cz}.dA_{c_{or}}$$
$$m_s = \int_{A_{s_{or}}} E_{s_t}.\varepsilon_{sz}.y_s.dA_{s_{or}} \qquad m_c = \int_{A_{c_{or}}} E_{c_t}.\varepsilon_{cz}.y_c.dA_{c_{or}}$$
$$m_s^* = \int_{A_{s_{or}}} E_{s_t}.\varepsilon_{sz}.y_s^2.dA_{s_{or}} \qquad m_c^* = \int_{A_{c_{or}}} E_{c_t}.\varepsilon_{cz}.y_c^2.dA_{c_{or}} \qquad (4.52)$$

Using the transformed section approach, Eqs. (4.52) can be written in terms of the elastic tangent modulus of each material at 20^o C as,

$$n_s = E_{s_{y20}}.\varepsilon_{sz}.A_{s_{tr}} \qquad n_c = E_{c_{y20}}.\varepsilon_{cz}.A_{c_{tr}}$$
$$m_s = E_{s_{y20}}.\varepsilon_{sz}.y_s.A_{s_{tr}} \qquad m_c = E_{c_{y20}}.\varepsilon_{cz}.y_c.A_{c_{tr}}$$
$$m_s^* = E_{s_{y20}}.\varepsilon_{sz}.y_s^2.A_{s_{tr}} \qquad m_c^* = E_{c_{y20}}.\varepsilon_{cz}.y_c^2.A_{c_{tr}} \qquad (4.53)$$

where,

$A_{s_{or}}$, $A_{s_{tr}}$ = original and transformed area of the steel plate segment;
$A_{c_{or}}$, $A_{c_{tr}}$ = original and transformed area of the concrete plate segment;
$E_{s_{y20}}$, E_{s_t} = initial tangent modulus at 20^o C and current tangent modulus of steel;
$E_{c_{y20}}$, E_{c_t} = initial tangent modulus at 20^o C and current tangent modulus of concrete.

Using Eqs. (4.22), (4.24), (4.51) and the above definitions, the stress resultants and their derivatives can be calculated. The expressions for both steel and concrete are similar but the values E, A, I and u differ for concrete and steel. These are described only for the steel I-section.

$$.n_s = E_{s_{y20}} A_{s_{tr}} \left[u'_{so} + \frac{(u'_{so})^2}{2} + \frac{(v'_o)^2}{2} \right] - E_{s_{y20}} I_{1s_{tr}} v''_o \left[1 + u'_{so} + \frac{(v'_o)^2}{\eta} \right]$$
$$+ \frac{1}{2} E_{s_{y20}} I_{2s_{tr}} (v''_o)^2 \left[1 + \frac{(v'_o)^2}{\eta^2} \right]$$
$$m_s = E_{s_{y20}} I_{1s_{tr}} \left[u'_{so} + \frac{(u'_{so})^2}{2} + \frac{(v'_o)^2}{2} \right] - E_{s_{y20}} I_{2s_{tr}} v''_o \left[1 + u'_{so} + \frac{(v'_o)^2}{\eta} \right]$$
$$+ \frac{1}{2} E_{s_{y20}} I_{3s_{tr}} (v''_o)^2 \left[1 + \frac{(v'_o)^2}{\eta^2} \right]$$
$$m_s^* = E_{s_{y20}} I_{2s_{tr}} \left[u'_{so} + \frac{(u'_{so})^2}{2} + \frac{(v'_o)^2}{2} \right] - E_{s_{y20}} I_{3s_{tr}} v'_o \left[1 + u'_{so} + \frac{(v'_o)^2}{\eta} \right]$$
$$+ \frac{1}{2} E_{s_{y20}} I_{4s_{tr}} (v''_o)^2 \left[1 + \frac{(v'_o)^2}{\eta^2} \right] \qquad (4.54)$$

The derivatives of the stress resultants for the steel I-section can now be calculated as

$$\frac{\partial n_s}{\partial q_j} = E_{s_{y20}} A_{s_{tr}} \left[\left(1+u'_{so}\right)\frac{\partial u'_{so}}{\partial q_j} + v'_o \frac{\partial v'_o}{\partial q_j} \right]$$
$$-E_{s_{y20}} I_{1s_{tr}} \left[v''_o \frac{\partial u'_{so}}{\partial q_j} + \left(1+u'_{so}\right)\frac{\partial v''_o}{\partial q_j} + \frac{v'_o . v''_o}{\eta}\left(2+\frac{\left(v'_o\right)^2}{\eta^2}\right)\frac{\partial v'_o}{\partial q_j} + \frac{\left(v'_o\right)^2}{\eta}\frac{\partial v''_o}{\partial q_j} \right]$$
$$+E_{s_{y20}} I_{2s_{tr}} \left[\frac{v'_o.\left(v''_o\right)^2}{\eta^2}\left(1+\frac{\left(v'_o\right)^2}{\eta^2}\right)\frac{\partial v'_o}{\partial q_j} + v''_o\left(1+\frac{\left(v'_o\right)^2}{\eta^2}\right)\frac{\partial v''_o}{\partial q_j} \right]$$
$$\frac{\partial m_s}{\partial q_j} = E_{s_{y20}} I_{1s_{tr}} \left[\left(1+u'_{so}\right)\frac{\partial u'_{so}}{\partial q_j} + v'_o \frac{\partial v'_o}{\partial q_j} \right]$$
$$-E_{s_{y20}} I_{2s_{tr}} \left[v''_o \frac{\partial u'_{so}}{\partial q_j} + \left(1+u'_{so}\right)\frac{\partial v''_o}{\partial q_j} + \frac{v'_o . v''_o}{\eta}\left(2+\frac{\left(v'_o\right)^2}{\eta^2}\right)\frac{\partial v'_o}{\partial q_j} + \frac{\left(v'_o\right)^2}{\eta}\frac{\partial v''_o}{\partial q_j} \right]$$
$$+E_{s_{y20}} I_{3s_{tr}} \left[\frac{v'_o.\left(v''_o\right)^2}{\eta^2}\left(1+\frac{\left(v'_o\right)^2}{\eta^2}\right)\frac{\partial v'_o}{\partial q_j} + v''_o\left(1+\frac{\left(v'_o\right)^2}{\eta^2}\right)\frac{\partial v''_o}{\partial q_j} \right]$$
$$\frac{\partial m^*_s}{\partial q_j} = E_{s_{y20}} I_{2s_{tr}} \left[\left(1+u'_{so}\right)\frac{\partial u'_{so}}{\partial q_j} + v'_o \frac{\partial v'_o}{\partial q_j} \right]$$
$$-E_{s_{y20}} I_{3s_{tr}} \left[v''_o \frac{\partial u'_{so}}{\partial q_j} + \left(1+u'_{so}\right)\frac{\partial v''_o}{\partial q_j} + \frac{v'_o . v''_o}{\eta}\left(2+\frac{\left(v'_o\right)^2}{\eta^2}\right)\frac{\partial v'_o}{\partial q_j} + \frac{\left(v'_o\right)^2}{\eta}\frac{\partial v''_o}{\partial q_j} \right]$$
$$+E_{s_{y20}} I_{4s_{tr}} \left[\frac{v'_o.\left(v''_o\right)^2}{\eta^2}\left(1+\frac{\left(v'_o\right)^2}{\eta^2}\right)\frac{\partial v'_o}{\partial q_j} + v''_o\left(1+\frac{\left(v'_o\right)^2}{\eta^2}\right)\frac{\partial v''_o}{\partial q_j} \right] \qquad (4.55)$$

These can then be incorporated into the stiffness matrix and unbalanced force vector (Eqs. (4.38) and (4.39)). The solution of the equilibrium equation (4.37) and the stability criterion are identical to that described in the full interaction formulation in Section 4.2.4.

Above analyses form the basis of two computer programs in FORTRAN developed to run on a personal computer. The validation studies and some parametric studies presented in Chapter 6 and 7 have been conducted using the programs.

CHAPTER 5. MATHEMATICAL REPRESENTATION OF SEMI-RIGID JOINTS

5.1. Introduction

The connections which join beams and columns in steel construction are generally classified as simple (pin-jointed), semi-rigid and rigid (fixed). The important difference between these connections, in the context of structural behaviour, lies in their rotational stiffness.

With the exception of portal frame buildings which are treated as rigid frames, most connections are idealised as pinned. This is despite the fact that practical details can provide significant rotational stiffness[132] and that treating the connection as semi-rigid might offer better structural performance with savings in material and therefore lower costs.

A considerable amount of effort has been directed at establishing the connection characteristics for a range of typical details, and a substantial body of data now exist for bare steel conditions[111,112,114,132,133]. Several investigators[115,117] have shown that construction of composite action in semi-rigid connections further improves the moment carrying capacity of the connection by 1.5 to 6 times that of a non-composite one. This is reported to be due to reinforcing bars being continuous over the supports[114,115,118] and the additional resistance to buckling provided by the concrete slab[113,155].

The normal practice of designing connections as pin-jointed provides a degree of redundancy within the structure which may have a significant influence on its performance in fire. In order to investigate this it is necessary to represent the variation of the moment-rotation characteristics of connections with increasing temperature but unfortunately little data is available for this. Some tests have been conducted on the performance of connections in fire[121-123] giving an indication of performance and confirming that the high temperature moment capacity of composite connections is greater than that of the equivalent non-composite connection.

In order to investigate the influence of connection rigidity on the performance of the complete structure in fire semi-rigid connections have been incorporated with both full and partial interaction analysis models described in Chapter 4. Although there is a need for further experimental work with large-scale specimens and newer fastening

techniques[113], the computer model is aimed at providing a preliminary tool for understanding the influence of such connections on structural behaviour in fire.

5.2. Mathematical Representation of Connection Characteristics

5.2.1. Non-Composite Beams

The structural performance of a connection is generally described by its in plane moment-rotation characteristics obtained from tests on beam-column assemblies. The behaviour is generally non-linear with an initially stiff region followed by a marked reduction in stiffness. Although the ambient temperature characteristics for steel-to-steel connections are reasonably well established there is little published experimental work at elevated temperatures.

In the present analysis, the moment-rotation-temperature characteristics are modelled using a Ramberg-Osgood equation derived by El-Rimawi[158], which is fitted to the available data and an assumed end point corresponding to a rotation of 100mrad. At this rotation the reduction in moment capacity of the connection is calculated on the basis of the material strength reduction factors at 0.5% strain as given in BS5950 Part 8[77].

The moment-rotation characteristics are represented by

$$\phi = \frac{M}{A} + 0.01\left(\frac{M}{B}\right)^n \qquad (5.1)$$

where ϕ is the rotation, M is the moment and A, B, and n are temperature dependent constants and are given in reference[158]. The corresponding curves as derived by El-Rimawi and the experimental points on which they are based are shown in Fig. 5.1(a) and (b) for flush end plate and extended end plate connections respectively. These are based on a 305×165 UB40 section and for different sections El-Rimawi proposed the following modifications to the temperature-dependent constants.

$$A_m = A \times f;\ B_m = B \times f^2 \qquad (5.2)$$

where A_m and B_m are the constants to be used in Eq. (5.1) for a section depth D_c and

$$f = (D_c - 50)/(303.8 - 50) \qquad (5.3)$$

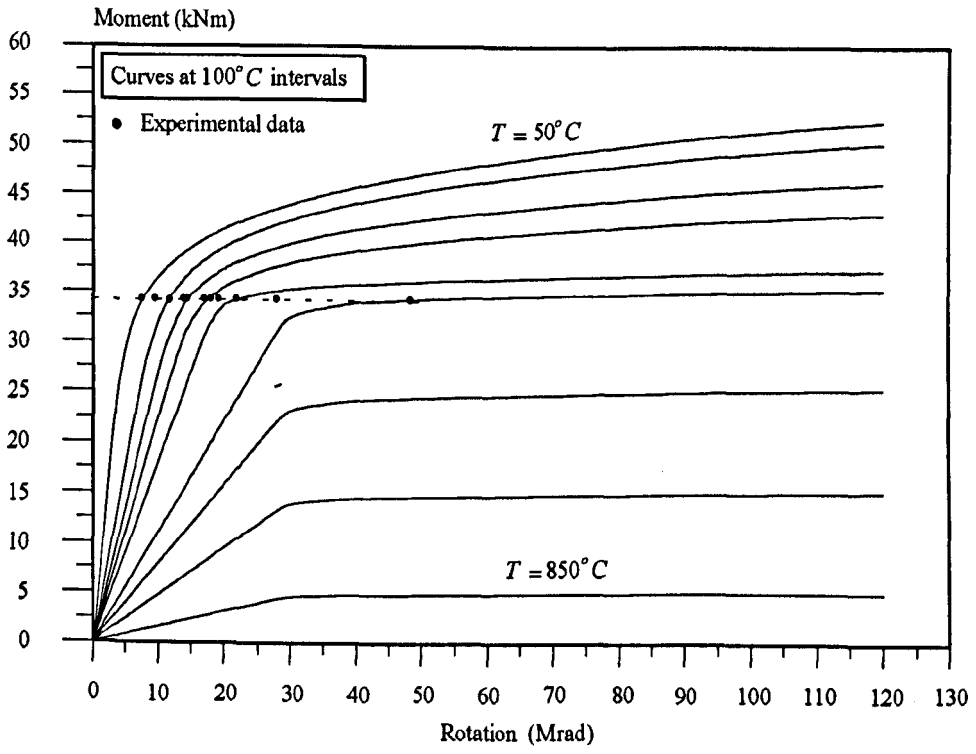

(a) Theoretical Moment-Rotation curves for flush end plate connections.

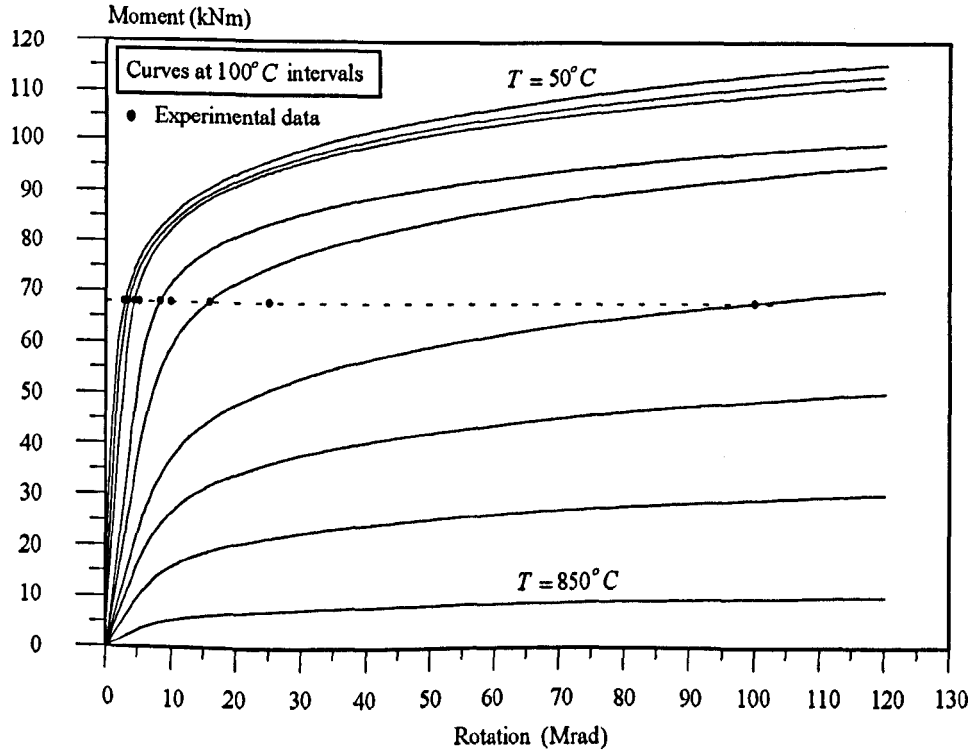

(b) Theoretical Moment-Rotation curves for extended end plate connections.

Fig. 5.1 Moment-rotation-temperature curves for flush and extended end plates.

5.2.2. Composite Beams with Full interaction

Because of the limited data available for composite connections, the steel-to-steel connection characteristics described above have been adopted for full interaction analysis ignoring any stiffening effect of the slab and reinforcement.

The connections have been modelled as zero length spring elements with four degrees of freedom to ensure compatibility with the beam elements as shown in Fig. 5.2(a). The coupling effect between rotational, shear and axial displacements is ignored since its influence on the overall behaviour is small in comparison with the direct stiffnesses[160]. The spring element stiffness matrix can therefore be represented as follows:

$$\begin{bmatrix} K_u & 0 & 0 & 0 & -K_u & 0 & 0 & 0 \\ 0 & K_u' & 0 & 0 & 0 & -K_u' & 0 & 0 \\ 0 & 0 & K_v & 0 & 0 & 0 & -K_v & 0 \\ 0 & 0 & 0 & K_\theta & 0 & 0 & 0 & -K_\theta \\ -K_u & 0 & 0 & 0 & K_u & 0 & 0 & 0 \\ 0 & -K_u' & 0 & 0 & 0 & K_u' & 0 & 0 \\ 0 & 0 & -K_v & 0 & 0 & 0 & K_v & 0 \\ 0 & 0 & 0 & -K_\theta & 0 & 0 & 0 & K_\theta \end{bmatrix}_{8\times 8} \begin{bmatrix} u_I \\ u_I' \\ v_I \\ \theta_I \\ u_J \\ u_J' \\ v_J \\ \theta_J \end{bmatrix}_{1\times 8}$$

For full interaction, only the rotation is modelled, and the corresponding stiffness, K_θ, is defined by Eq. (5.1). The stiffnesses corresponding to the remaining degrees of freedom, K_u, K_u', K_v, are assumed rigid and accordingly are represented by a very large numerical value.

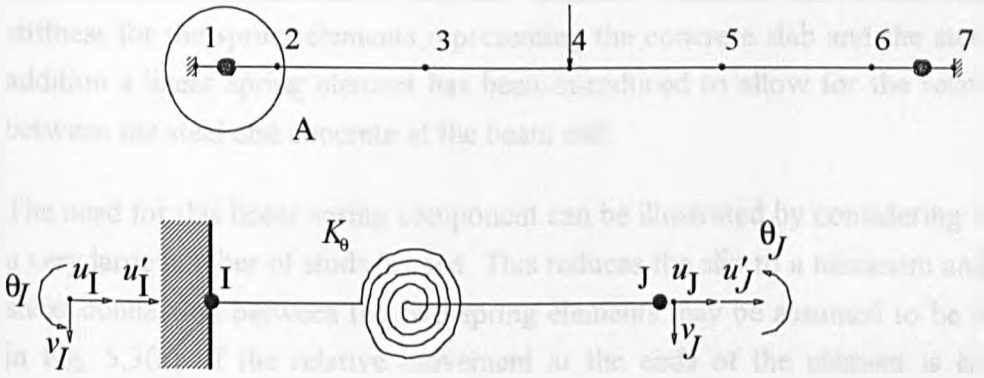

Detail A

(a) Spring element for full interaction analysis.

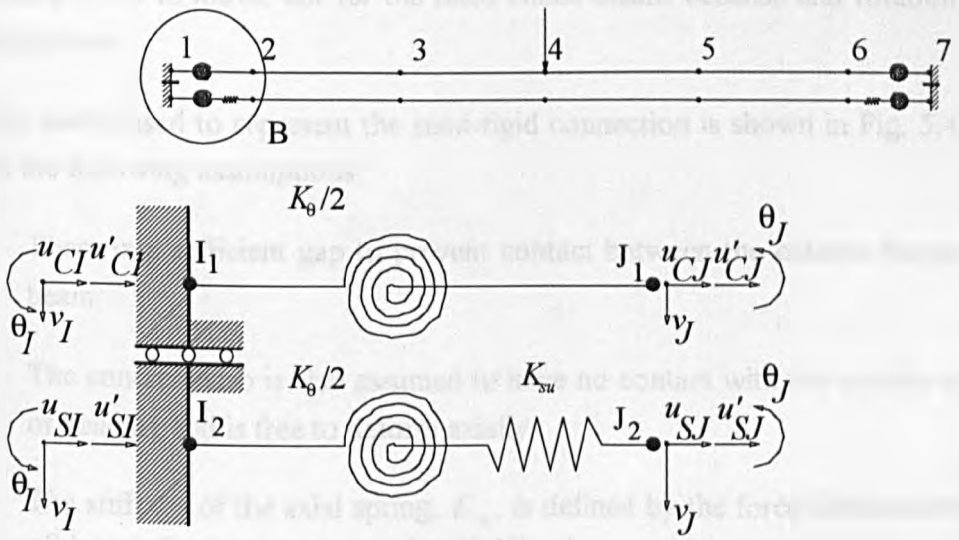

Detail B

(b) Spring element for partial interaction analysis.

Fig. 5.2 Semi-rigid connection models for full and partial interaction analyses.

5.2.3. Composite Beams with Partial interaction

In the partial interaction analysis two parallel elements represent the steel beam and concrete slab, each contributing to the stiffness of the connection. Therefore the connection has been modelled as a pair of rotational springs. As seen in Fig. 5.2(b), the finite element representation requires identical rotations and hence equal rotational stiffness for the spring elements representing the concrete slab and the steel I-section. In addition a linear spring element has been introduced to allow for the relative movement between the steel and concrete at the beam end.

The need for this linear spring component can be illustrated by considering the case where a very large number of studs is used. This reduces the slip to a minimum and therefore the shear connection between the two spring elements may be assumed to be rigid as shown in Fig. 5.3(a). If the relative movement at the ends of the element is constrained this results in a normal reaction force N' inducing an additional reaction moment which in turn increases the rotational stiffness of the connection compared with the full-interaction model (Fig. 5.3(b)). This does not arise in the case of simply supported beams because the ends are free to move, nor for the fixed ended beams because end rotation is completely suppressed.

The model used to represent the semi-rigid connection is shown in Fig. 5.4, and is based on the following assumptions:

- There is a sufficient gap to prevent contact between the column flange and the steel beam.
- The concrete slab is also assumed to have no contact with the column in the direction of bending and is free to deform axially.
- The stiffness of the axial spring, K_{su}, is defined by the force-displacement relationship of the reinforcing bars over a length '$D_{r\exp}$'.
- The centre of rotation of the connection is at point J_1 for the concrete slab and at point J_2 for the steel I-section as shown in Fig. 5.2(b).
- The extension of reinforcement is concentrated within a distance between the centre line of the column and the first shear connector.
- The characteristics of the reinforcement are modelled using a bilinear stress-strain relationship with a yield strain of 2% (Fig. 5.5).

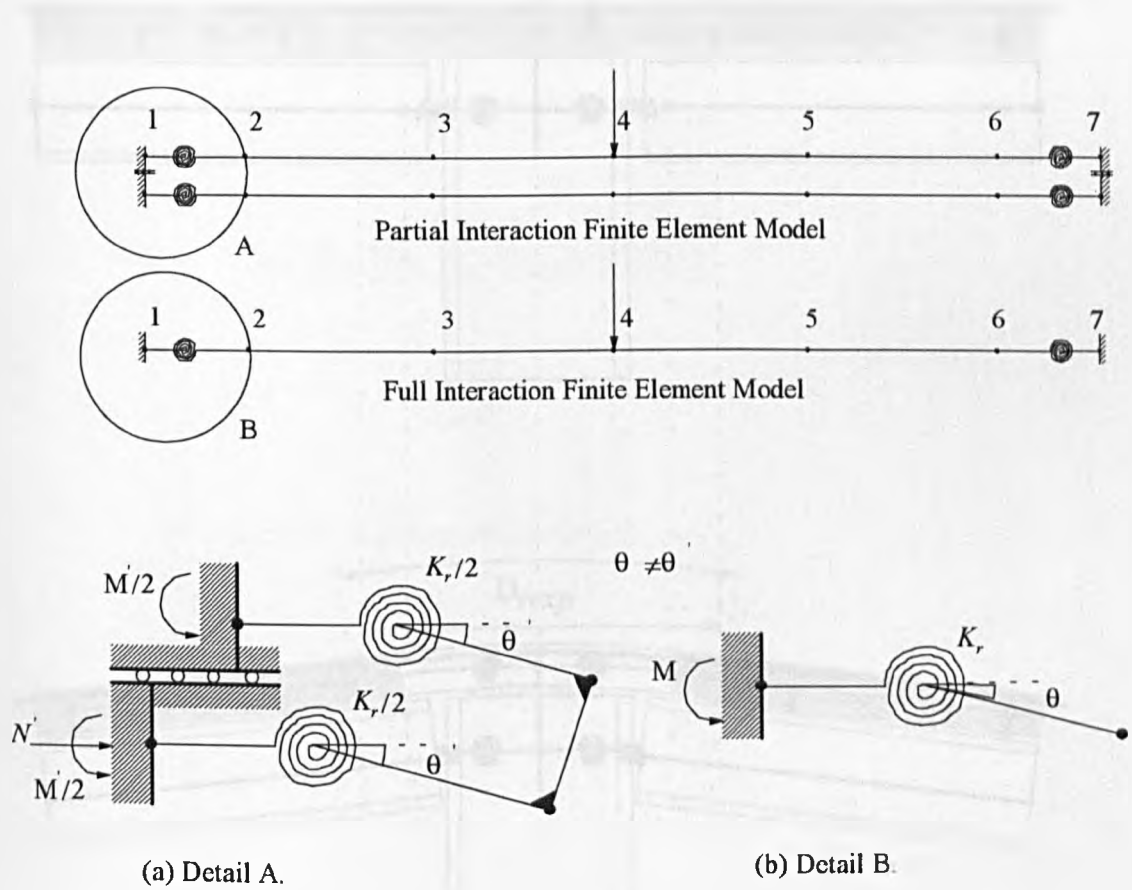

(a) Detail A.

(b) Detail B.

Fig. 5.3 The influence of the axial force due to the absence of a linear spring.

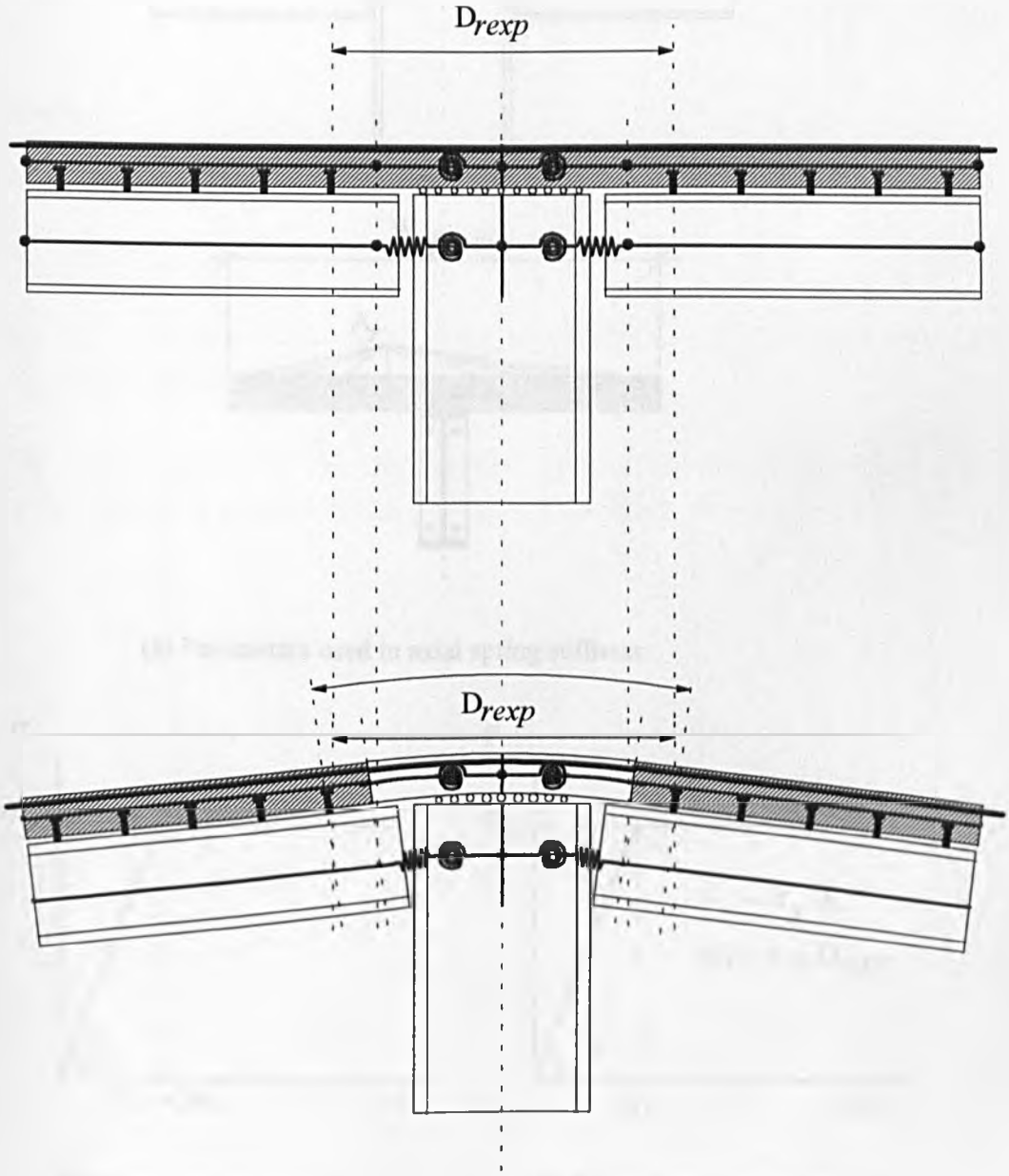

Fig. 5.4 Assumptions for the semi-rigid model for partial interaction analysis.

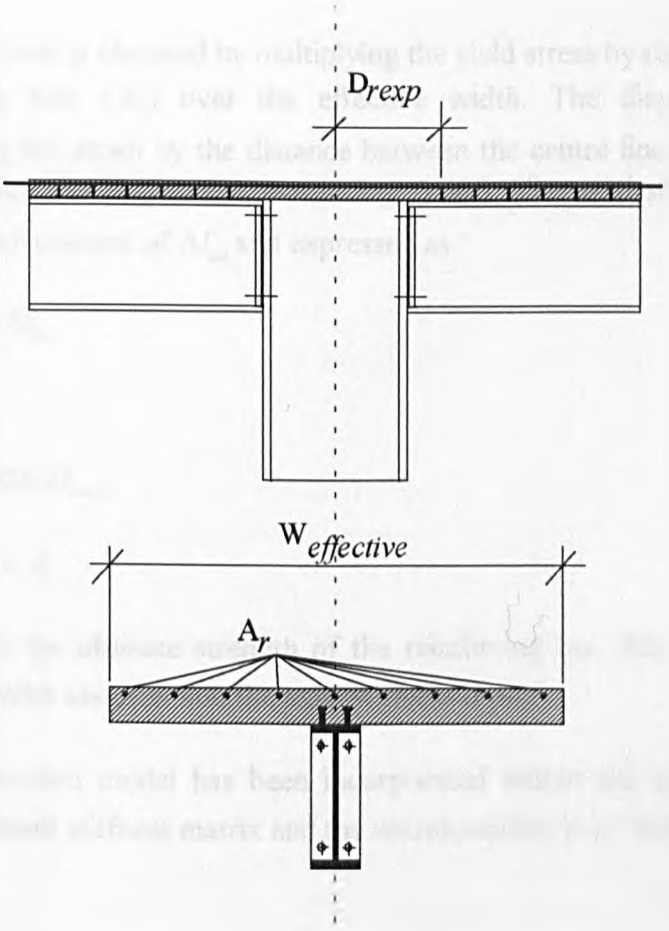

(a) Parameters used in axial spring stiffness.

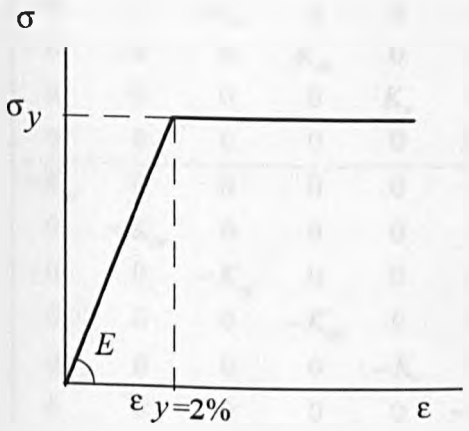

(b) Stress-strain model.

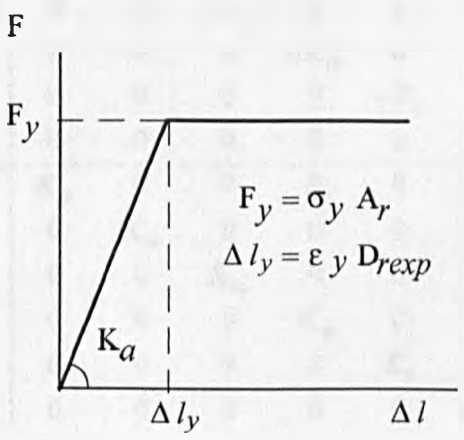

(c) Force-displacement model.

Fig. 5.5 Force-displacement model for the linear spring.

The axial force is obtained by multiplying the yield stress by the cross-sectional area of the reinforcing bars (A_r) over the effective width. The displacement is calculated by multiplying the strain by the distance between the centre line of the column and the first shear connector ($D_{r\exp}$) as shown in Fig. 5.5(a). The axial stiffness is therefore constant up to a displacement of Δl_{ult} and expressed as

$$K_a = F_{ult} / \Delta l_{ult} \tag{5.5}$$

where

$$\Delta l_{ult} = 0.02 \times D_{r\exp} \tag{5.6}$$

$$F_{ult} = \sigma_{ult} \times A_r \tag{5.7}$$

and σ_{ult} is the ultimate strength of the reinforcing bar. For displacements greater than Δl_{ult} the model assumes that the axial stiffness is zero.

This connection model has been incorporated within the analysis using a zero length spring element stiffness matrix and the corresponding is as follows:

$$\begin{bmatrix}
K_{su} & 0 & 0 & 0 & 0 & 0 & -K_{su} & 0 & 0 & 0 & 0 & 0 \\
0 & K'_{su} & 0 & 0 & 0 & 0 & 0 & -K'_{su} & 0 & 0 & 0 & 0 \\
0 & 0 & K_{cu} & 0 & 0 & 0 & 0 & 0 & -K_{cu} & 0 & 0 & 0 \\
0 & 0 & 0 & K'_{cu} & 0 & 0 & 0 & 0 & 0 & -K'_{cu} & 0 & 0 \\
0 & 0 & 0 & 0 & K_v & 0 & 0 & 0 & 0 & 0 & -K_v & 0 \\
0 & 0 & 0 & 0 & 0 & K_\theta & 0 & 0 & 0 & 0 & 0 & -K_\theta \\
-K_{su} & 0 & 0 & 0 & 0 & 0 & K_{su} & 0 & 0 & 0 & 0 & 0 \\
0 & -K'_{su} & 0 & 0 & 0 & 0 & 0 & K'_{su} & 0 & 0 & 0 & 0 \\
0 & 0 & -K_{cu} & 0 & 0 & 0 & 0 & 0 & K_{cu} & 0 & 0 & 0 \\
0 & 0 & 0 & -K'_{cu} & 0 & 0 & 0 & 0 & 0 & K'_{cu} & 0 & 0 \\
0 & 0 & 0 & 0 & -K_v & 0 & 0 & 0 & 0 & 0 & K_v & 0 \\
0 & 0 & 0 & 0 & 0 & -K_\theta & 0 & 0 & 0 & 0 & 0 & K_\theta
\end{bmatrix}_{12\times12}
\begin{bmatrix}
u_{SI} \\ u'_{SI} \\ u_{CI} \\ u'_{CI} \\ v_I \\ \theta_I \\ u_{SJ} \\ u'_{SJ} \\ u_{CJ} \\ u'_{CJ} \\ v_J \\ \theta_J
\end{bmatrix}_{1\times12}$$

If the full rotational stiffness from the moment-rotation curve is applied to both the steel and concrete the overall rotational stiffness of the connection will be doubled and hence the stiffness, K_θ, defined by the moment-rotation relationship in Eq. (5.1) was distributed equally between the concrete slab and the steel beam. All other degrees of freedom are

suppressed and hence the corresponding stiffnesses, $K_{su}^{'}, K_{cu}, K_{cu}^{'}, K_{v}$, are represented by a very large numerical value. Again the coupling stiffnesses are ignored.

In order to validate this connection model load-deflection analyses were conducted at ambient temperature for a 6m beam with a centre point load (Fig. 5.6). Different connection models as shown in Fig. 5.7 were used to represent the extended end plate characteristics Fig. 5.1(b). In order to compare with full interaction, a very stiff shear connection (100 studs along the length of the beam) was considered. The results are shown in Fig. 5.8.

Connection types 1 to 4 consist of only rotational spring elements. In connection type 3 and 4, the rotational stiffness was equally distributed between the concrete and the steel beam while in connection type 1 and 2 the full stiffness is applied to both. In connection types 2 and 4 the axial displacement of concrete slab is freely allowed whereas it is fully restrained in Types 1 and 3.

Type 1 is the stiffest connection since the axial movement of the concrete slab is fully restrained and the total rotational stiffness of the connection is effectively doubled. As a result the mid span deflections are much lower than the full interaction case and the predicted failure load is 723kN. Although releasing axial movement of the concrete slab (Type 2) clearly results in slightly greater end rotations and mid-span deflections the differences are negligible. Types 3 and 4 are both more flexible because of the reduced effective rotational stiffness. This results in increased deflections and reduced failure loads of 687kN for Type 3 and 676kN for Type 4.

However the behaviour is still significantly stiffer than the full interaction case, due to the end moment induced by the axial forces (Fig. 5.3(a)). Connection types 5, 6 and 7 introduce a linear spring with a constant stiffness value of 31500N/mm defined by the bilinear force-displacement relationship of reinforcing bars as shown in Fig. 5.5(c). For this particular example the variables $D_{r\exp}$ and A_r in Eq. (5.6) and (5.7) were assumed to be 216mm and $226mm^2$ respectively. The rotational spring stiffness is identical to those used for connection types 3 to 5.

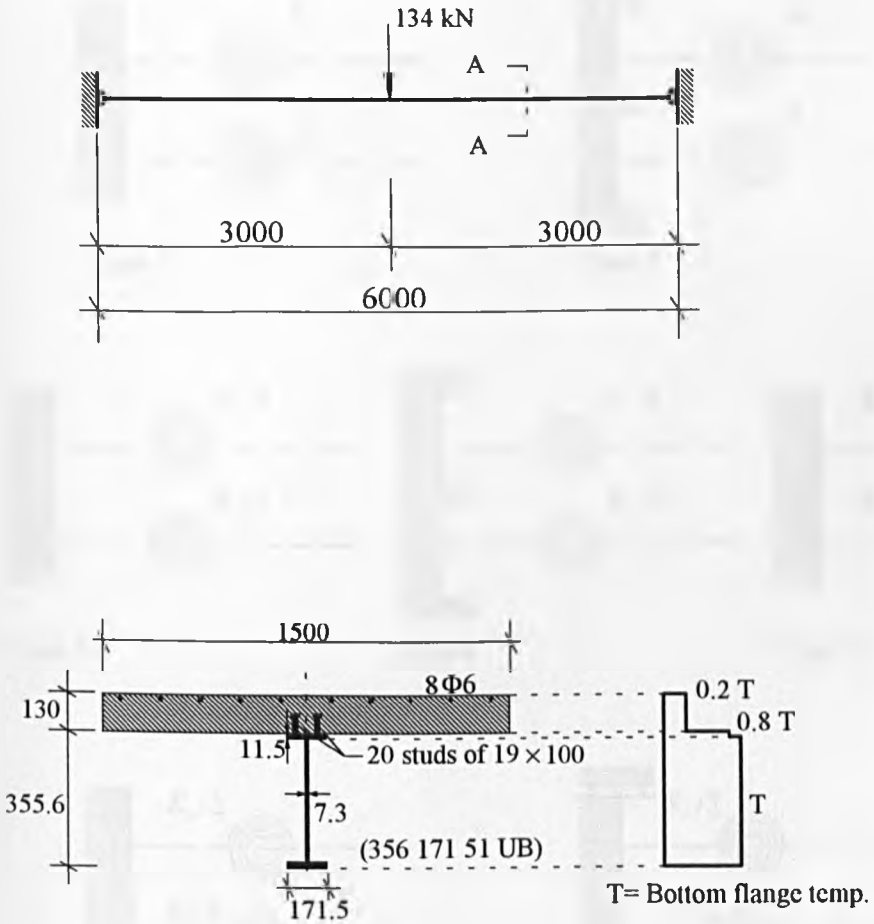

Section A-A and assumed temperature profile.

Fig. 5.6 Typical of the main beams used in the large building test frame by BRE[154].

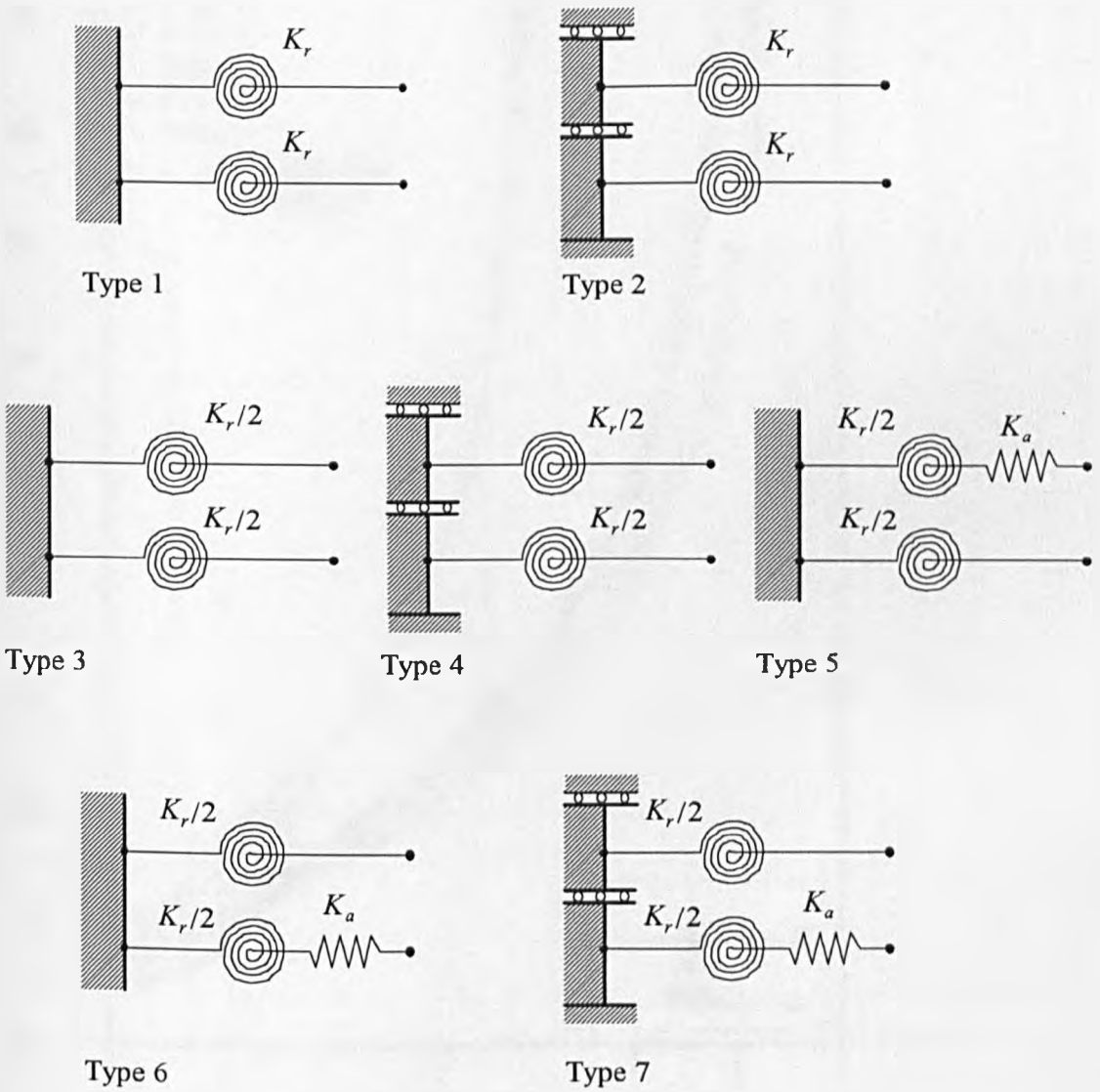

Fig. 5.7 Connection models used for the optimum representation of semi-rigid joints

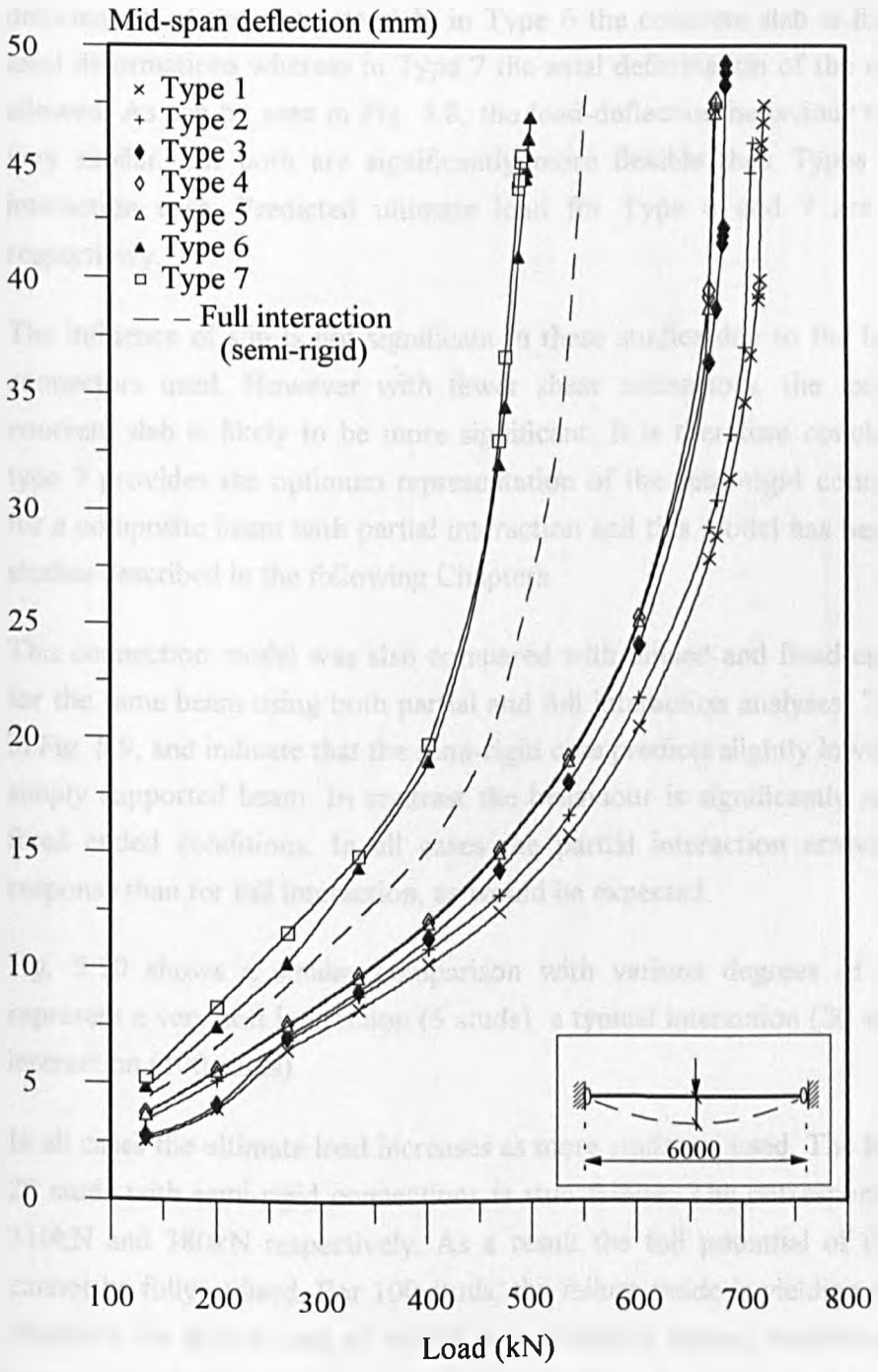

Fig. 5.8 Load-deflection behaviour for various types of connection.

As expected the load-deflection behaviour for Type 5 is intermediate between Type 3 and 4 with a predicted failure load of 678kN. In Types 6 and 7, the linear spring was connected to the steel I-section. In order to determine the influence of the axial deformation of the concrete slab, in Type 6 the concrete slab is fully restrained against axial deformations whereas in Type 7 the axial deformation of the concrete slab is freely allowed. As can be seen in Fig. 5.8, the load-deflection behaviour for these two cases is very similar, but both are significantly more flexible than Types 1 to 5 and the full interaction case. Predicted ultimate load for Type 6 and 7 are 500kN and 490kN respectively.

The influence of slip is not significant in these studies due to the large number of shear connectors used. However with fewer shear connectors, the axial movement of the concrete slab is likely to be more significant. It is therefore concluded that connection type 7 provides the optimum representation of the semi-rigid connection characteristics for a composite beam with partial interaction and this model has been used in the further studies described in the following Chapters.

This connection model was also compared with pinned and fixed-end support conditions for the same beam using both partial and full interaction analyses. The results are shown in Fig. 5.9, and indicate that the semi-rigid case predicts slightly lower deflections than the simply supported beam. In contrast the behaviour is significantly more flexible than for fixed ended conditions. In all cases the partial interaction analysis indicates a softer response than for full interaction, as would be expected.

Fig. 5.10 shows a similar comparison with various degrees of shear connection to represent a very soft interaction (5 studs), a typical interaction (20 studs), and a very stiff interaction (100 studs).

In all cases the ultimate load increases as more studs are used. The failure mode for 5 and 20 studs with semi-rigid connections is stud failure. The corresponding failure loads are 310kN and 380kN respectively. As a result the full potential of the composite section cannot be fully utilised. For 100 studs, the failure mode is yielding of the steel beam and therefore the failure load of 495kN is significantly higher, indicating an improvement of more than 30%. These results suggest that the structural behaviour at ambient temperature is equally sensitive to the changes in end conditions and the shear connection.

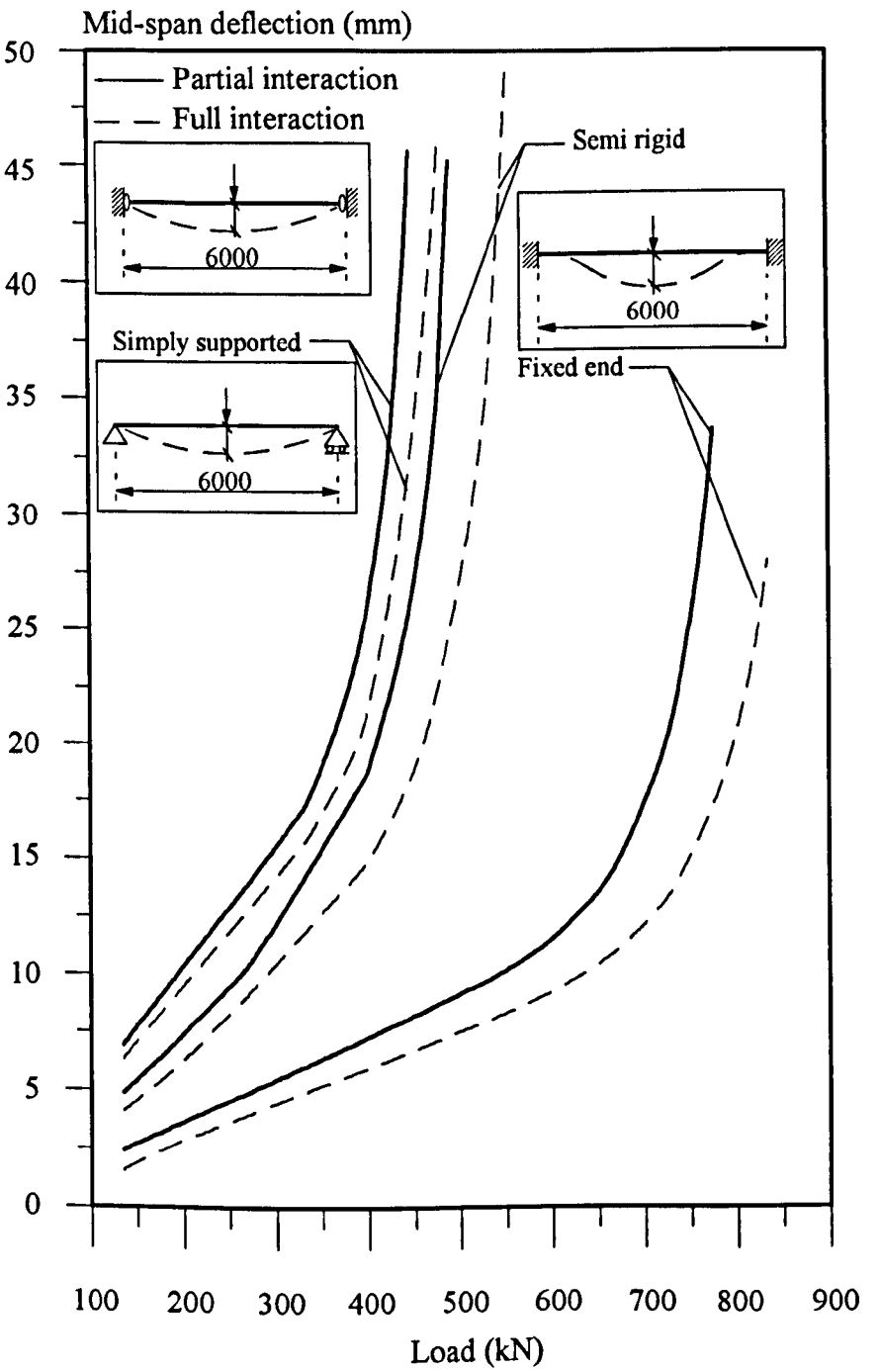

Fig. 5.9 Comparisons with idealised end conditions.

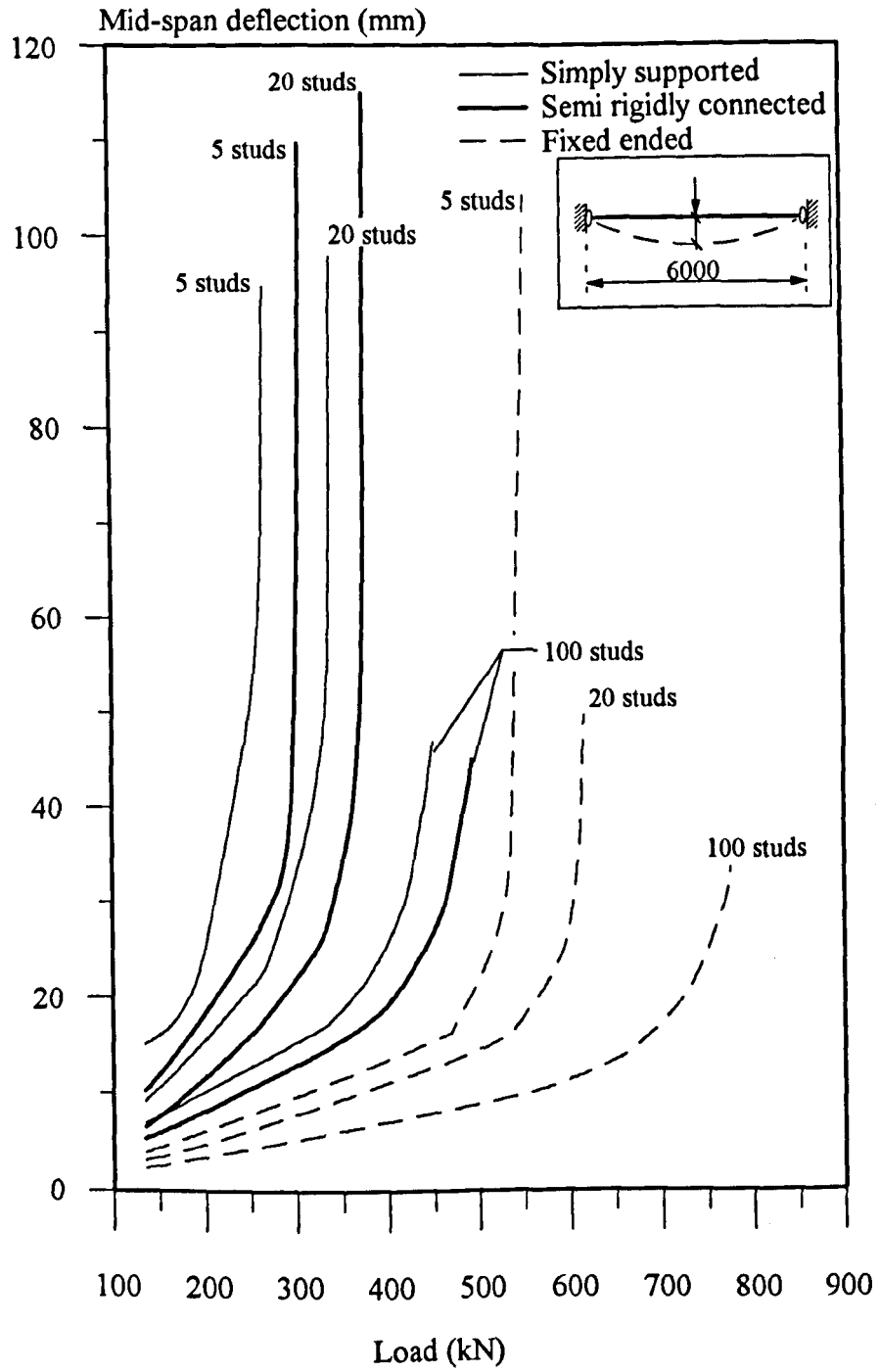

Fig. 5.10 The influence of the number of studs on different end conditions.

In the absence of suitable independent data, these indicative studies provide a degree of validation for the case of partially composite beams with semi-rigid support conditions, at ambient temperature. This is further supported by Fig. 5.11 which compares the results for idealised end conditions with those obtained by using very flexible springs (to represent simple supports) and very stiff rotational springs (to represent fixed ended supports).

In order to represent fire conditions, the comparison between partial and full interaction analyses using three different types of connection was repeated at elevated temperatures. The beam utilised in the analysis is similar to the one in the ambient temperature studies but with one support free to deform axially to prevent any axial force due to restraint to thermal expansion. The assumed temperature profile is shown in Fig. 5.6.

The results are shown in Fig. 5.12, as plots of temperature-deflection and demonstrate a similar pattern to the load-deflection curves (Fig. 5.9). Using both partial and full interaction analysis, the failure temperatures, defined by a limiting deflection of L/20, for the simply supported and fixed ended beams are 700^{o}C and 800^{o}C respectively. The agreement between the partial and full interaction analysis for the semi-rigid beam is also satisfactory, with failure temperatures of 750^{o}C and 786^{o}C respectively. The improvement in the failure temperature over the simply supported beam is approximately 10%. The slight difference in predicted temperature is mainly because of the axial force due to the partial restraint to thermal expansion in the semi-rigid model used in partial interaction analysis. Nevertheless both the full interaction and partial interaction analyses indicate comparable failure temperatures and where similar end connections are used they result in consistent temperature-deflection behaviour.

A comparison in terms of temperature-deflection behaviour using various degrees of shear connection namely, a very soft interaction (5 studs), a typical interaction (20 studs), and a very stiff interaction (100 studs) is shown in Fig. 5.13. The structural behaviour for 5, 20 and 100 studs is identical up to a temperature of 550^{o}C. The difference in predicted failure temperatures of 749^{o}C and 725^{o}C, for 100 and 20 studs respectively, is negligible. The failure temperature for 5 studs is 682^{o}C, approximately 7.5% less than for 20 and 100 studs. This is a relatively small reduction suggesting structural behaviour at high temperatures is not very sensitive to the number of studs used. Because of relatively cooler temperatures, the studs retain greater strength than the steel beam thus yielding of the steel becomes more critical.

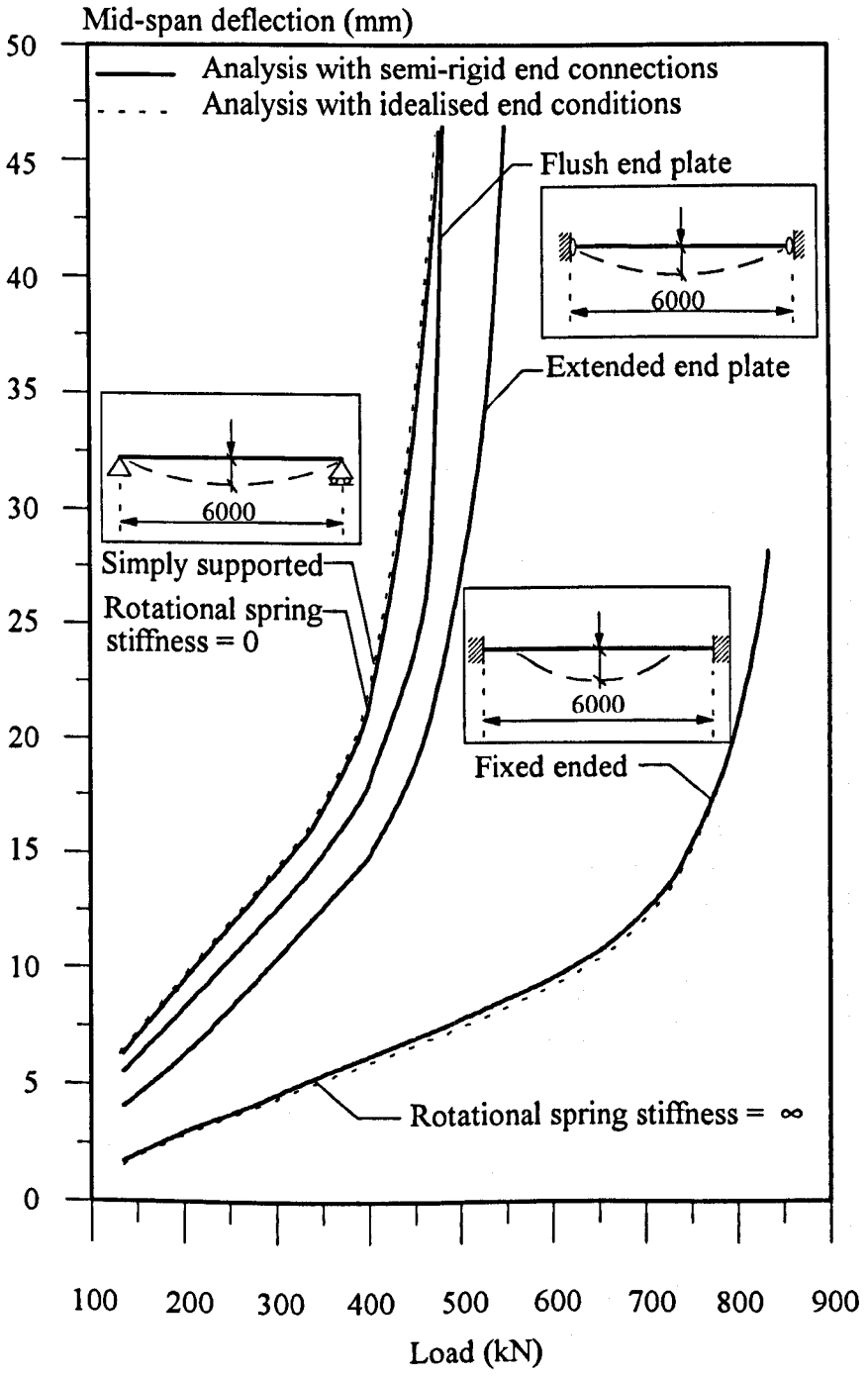

Fig. 5.11 Comparisons between analyses with idealised and semi-rigid end conditions.

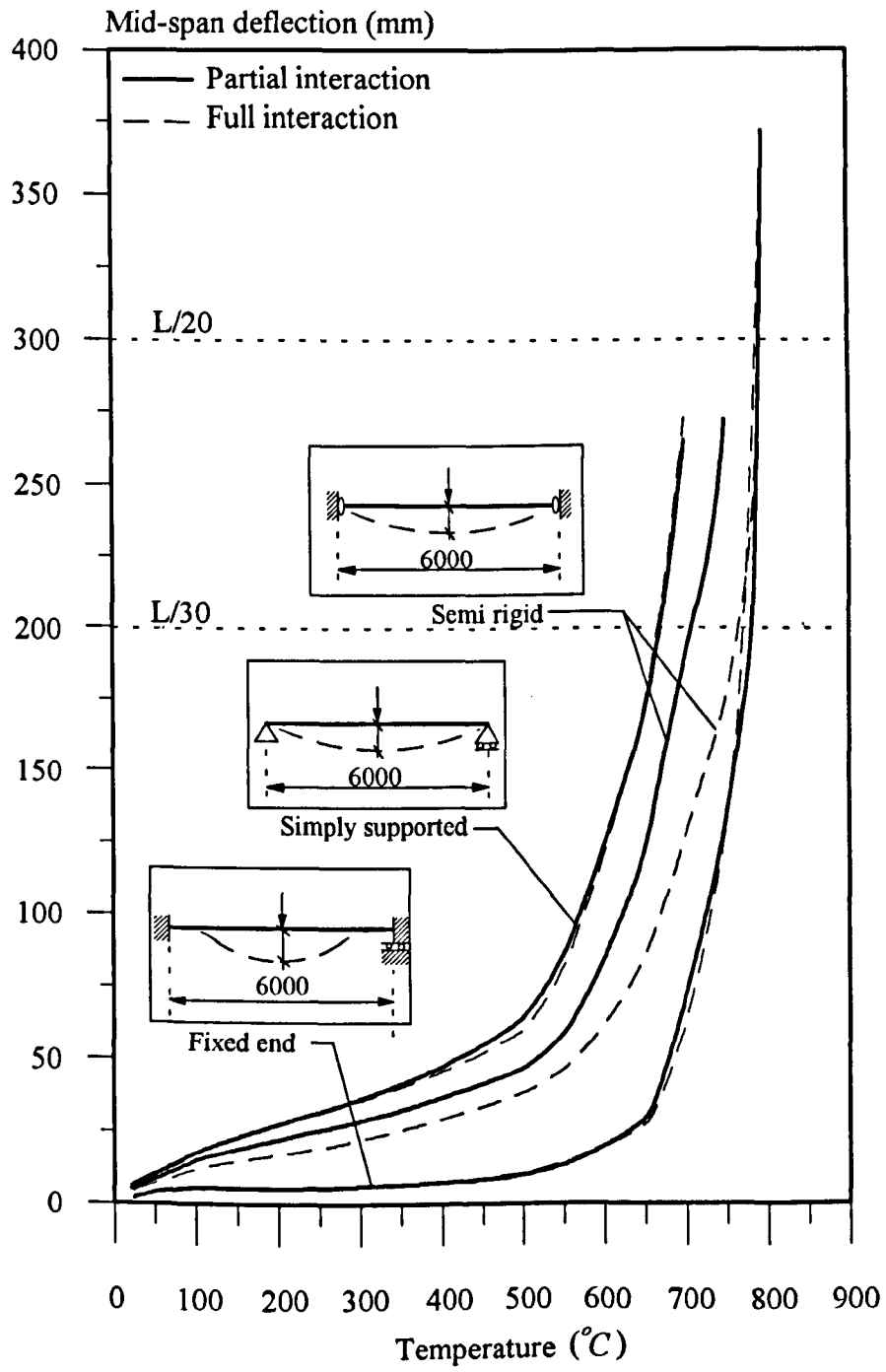

Fig 5.12 Comparisons with idealised end conditions at elevated temperatures.

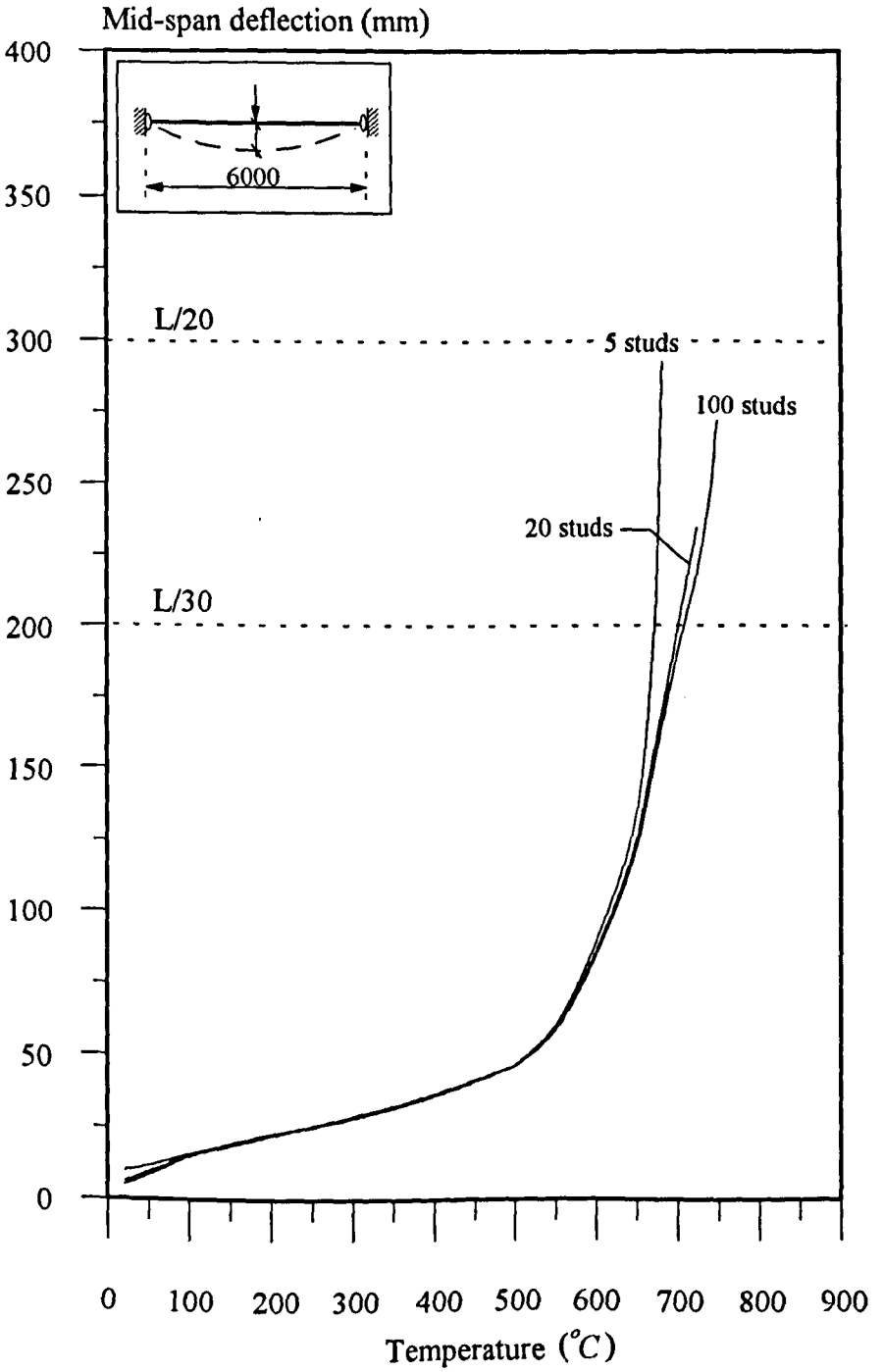

Fig 5.13 The effect of number of studs on semi-rigid joints at elevated temperatures.

These preliminary studies suggest that model adopted for representing the semi-rigid connection characteristics is reasonable. More rigorous validation of the approach will only be possible when more detailed experimental data is available. The studies also emphasise the fact that the elevated temperature behaviour of the beam may be different from the behaviour at ambient temperature. Even when the shear connection is very stiff, the semi-rigid connection model used in full interaction analysis may not be fully adequate in representing the structural behaviour.

CHAPTER 6. VALIDATION OF THE MATHEMATICAL MODEL

6.1. Introduction

With any finite element model it is necessary to carry out a series of convergence studies and comparisons with experimental data to demonstrate the validity of the analytical approach and to assess numerical stability and running speed during the execution of the program.

The accuracy and processing speed of a finite element model depend upon the mesh density. A convergence study has therefore been conducted with a varying number of elements in order to determine an optimum mesh density as well as to expose any possible mistakes in the code. In this study different types of beam have been used with both full and partial interaction.

In order to verify the applicability of the material and structural models utilised in the analytical model, some comparisons have also been made with published experimental data for fully and partially composite beams using various end connections at both ambient and elevated temperatures.

6.2. Convergence Studies at Elevated Temperatures

In finite element analysis the displacements and internal forces are evaluated at the nodes of each element. The accuracy of the numerical integration used to determine the stiffness matrix and stress resultants depends on the number of elements. Consequently this has a significant influence on the results. It is generally accepted that as the number of elements increases a better representation of the structural behaviour is achieved. The use of too many elements, on the other hand, can be time consuming and may lead to potential numerical instability. Therefore it is necessary to determine the optimum number of elements to be used with different types of beam. For this purpose a convergence study using different beam types has been undertaken by increasing the number of elements and comparing the predicted temperature-deflection behaviour.

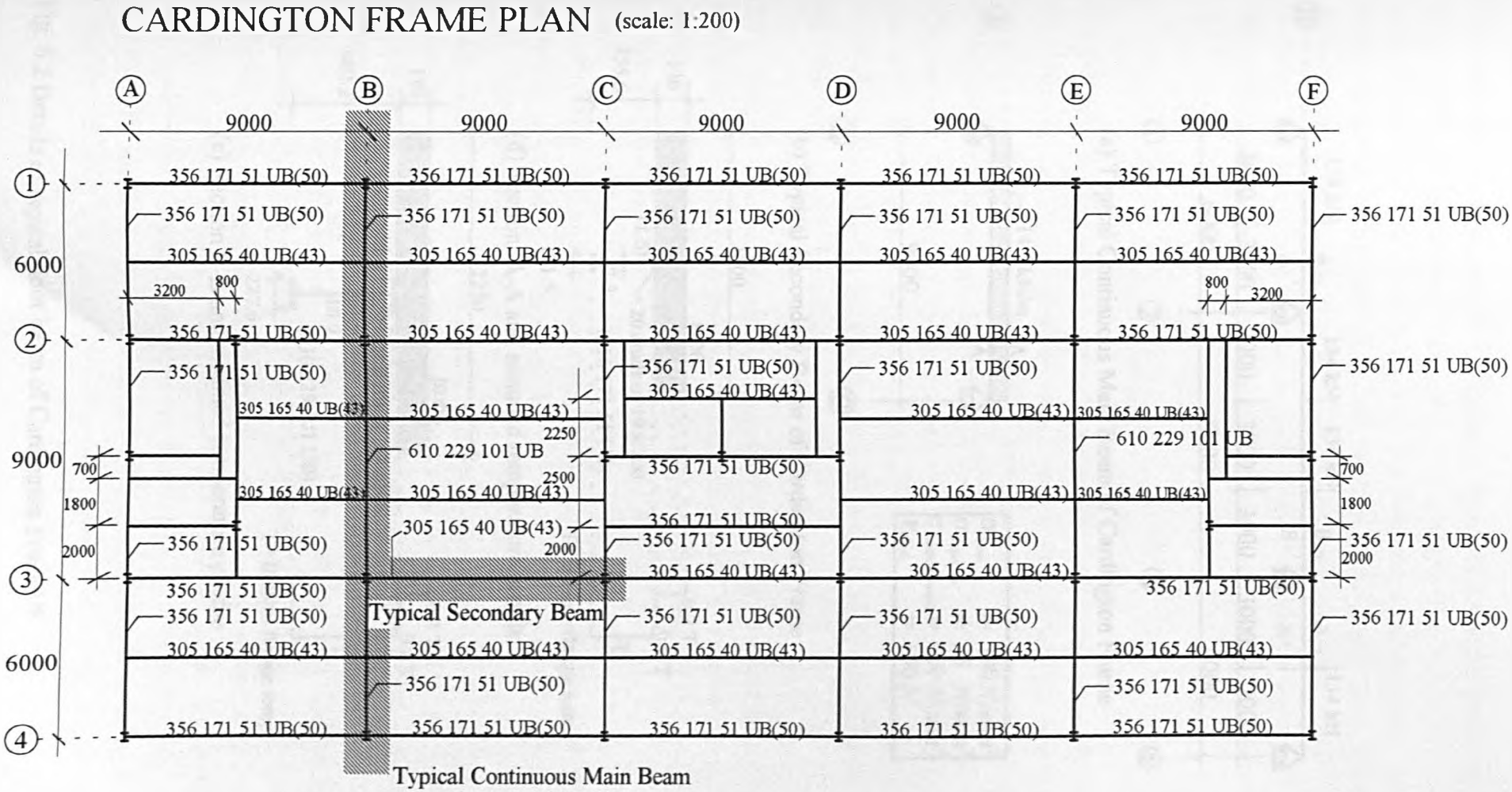

Fig. 6.1 Typical floor plan of Cardington frame.

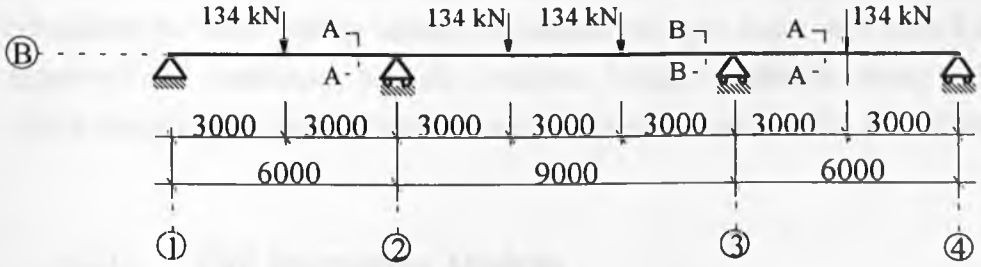

(a) Typical Continuous Main Beam of Cardington Frame

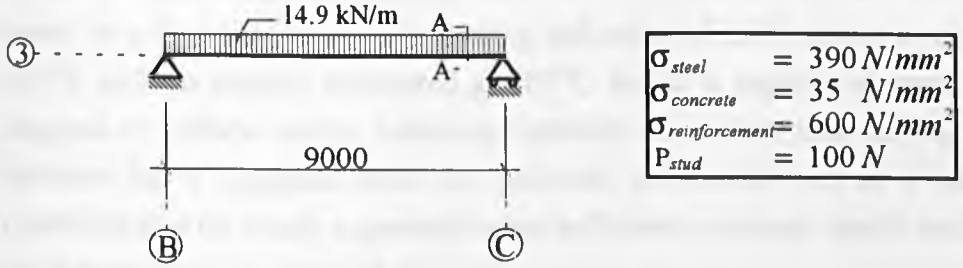

(b) Typical Secondary Beam of Cardington Frame

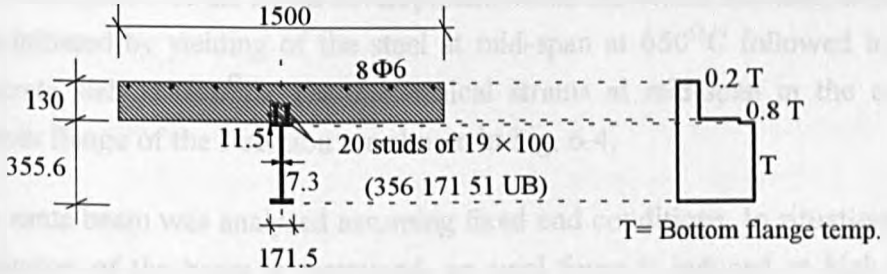

(d) Section A-A and assumed temperature profile

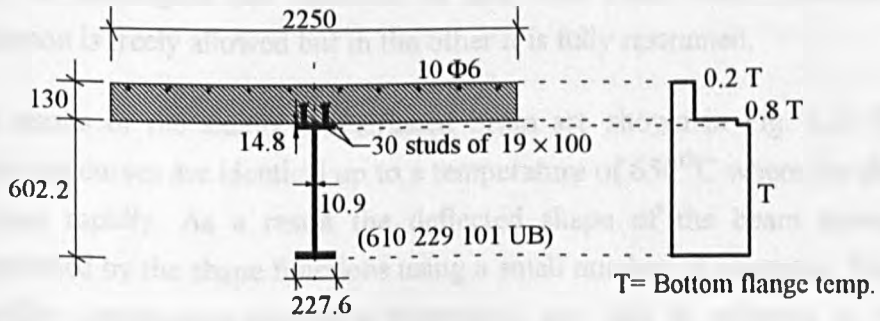

(c) Section B-B and assumed temperature profile

Fig. 6.2 Details of typical floor beam of Cardington Frame[110].

A typical floor arrangement of the Building Research Establishment's experimental 8-storey composite steel-framed building[110] at Cardington (Fig. 6.1) has been used as the basis of this study. The frame is typical of a commercial office block. The main cross frames consist of a 9m inner span and two 6m outer spans. Two cases have been considered for these studies, namely an isolated 6m span beam with both fixed and simply supported end conditions, and the complete 3-span continuous beam. Details together with average material properties and assumed temperature profiles are shown in Fig. 6.2.

6.2.1. Full Interaction Analysis

The temperature-deflection behaviour for the simply supported beam is shown in Fig. 6.3 for increasing numbers of elements from 2 to 16. In all cases the critical temperature based on a failure criterion of a limiting deflection of L/30 occurs at a temperature of 650°C and the analysis terminated at 700°C due to a negative element on the leading diagonal of stiffness matrix, indicating instability. It is clear that varying the number of elements has a negligible effect on predicted deflections, and as a result it may be concluded that for simply supported beams sufficiently accurate results can be obtained by using the minimum number of elements.

An investigation of the strain development within individual elements indicated that failure was initiated by yielding of the steel at mid-span at 650°C followed by crushing of the concrete slab at 700°C. The mechanical strains at mid-span in the concrete slab and bottom flange of the I-section are shown in Fig. 6.4.

The same beam was analysed assuming fixed end conditions. In situations where the axial expansion of the beam is restrained, an axial force is induced at high temperatures. In order to investigate the influence of this, two cases were considered. In one case expansion is freely allowed but in the other it is fully restrained.

The results of the axially unrestrained beam are shown in Fig. 6.5. The temperature-deflection curves are identical up to a temperature of 650°C where the deflections start to increase rapidly. As a result the deflected shape of the beam cannot be accurately represented by the shape functions using a small number of elements. This generally leads to stiffer temperature-deflection behaviour, and this is reflected in the temperature-deflection curves. However, the differences are relatively small. The predicted failure temperatures using 2 and 16 elements are 800°C and 770°C respectively, a discrepancy of only 4%, and the corresponding deflections for all analyses exceed the limiting deflection of L/30. The use of more than four elements along the length results in only

negligible differences in the behaviour. Hence it may be concluded that the four element representation of the beam provides satisfactory accuracy.

As can be seen from the strains in the top of concrete slab at the supports (Fig. 6.6), the concrete cracks under tension at temperatures above 20°C and has very little influence on the structural behaviour. The strains in the bottom flange (Fig. 6.6) indicate that above 650°C the steel near to the supports yields and the stresses at mid-span then increase rapidly. The failure corresponds to the formation of third plastic hinge at this point.

The temperature-deflection behaviour for the axially restrained fixed ended beam is shown in Fig. 6.7. In all cases the predicted deflections are identical up to 500°C. As with the axially unrestrained fixed ended beam, at higher temperatures the deflections increase rapidly due to yielding of the steel near to the supports (Fig. 6.8). As the number of elements is decreased the structural behaviour becomes stiffer because the deflected shape of the beam is less accurately modelled.

The failure temperature is about 9% lower than the axially unrestrained case due to the influence of axial force. All analyses terminated as a result of negative elements on the leading diagonal of the stiffness matrix, with deflections slightly in excess of L/30 and failure temperatures ranging between 725°C and 700°C indicating an error of less than 3.5%. These results suggest that the use of four elements for fixed ended beams is satisfactory.

The results for the continuous beam are shown in Fig. 6.9. The deflections are for the mid-span of the 9m centre span. The number of elements representing this span is 4, 6, 12 and 16 whereas each of the two 6m outer spans is represented using 2, 4, 8 and 10 elements respectively.

It can be seen that up to 600°C all cases are identical. At this temperature plastic hinges form at the supports and bending is redistributed towards the middle of each span. The beam fails when a third plastic hinge forms at the centre of the inner span. The predicted failure temperature varies between 675°C and 725°C depending on the number of elements used along the length, representing a range of less than 7.5%. The results indicate that six elements in the 9m inner span and four elements in the 6m outer spans give a satisfactory representation for the beam.

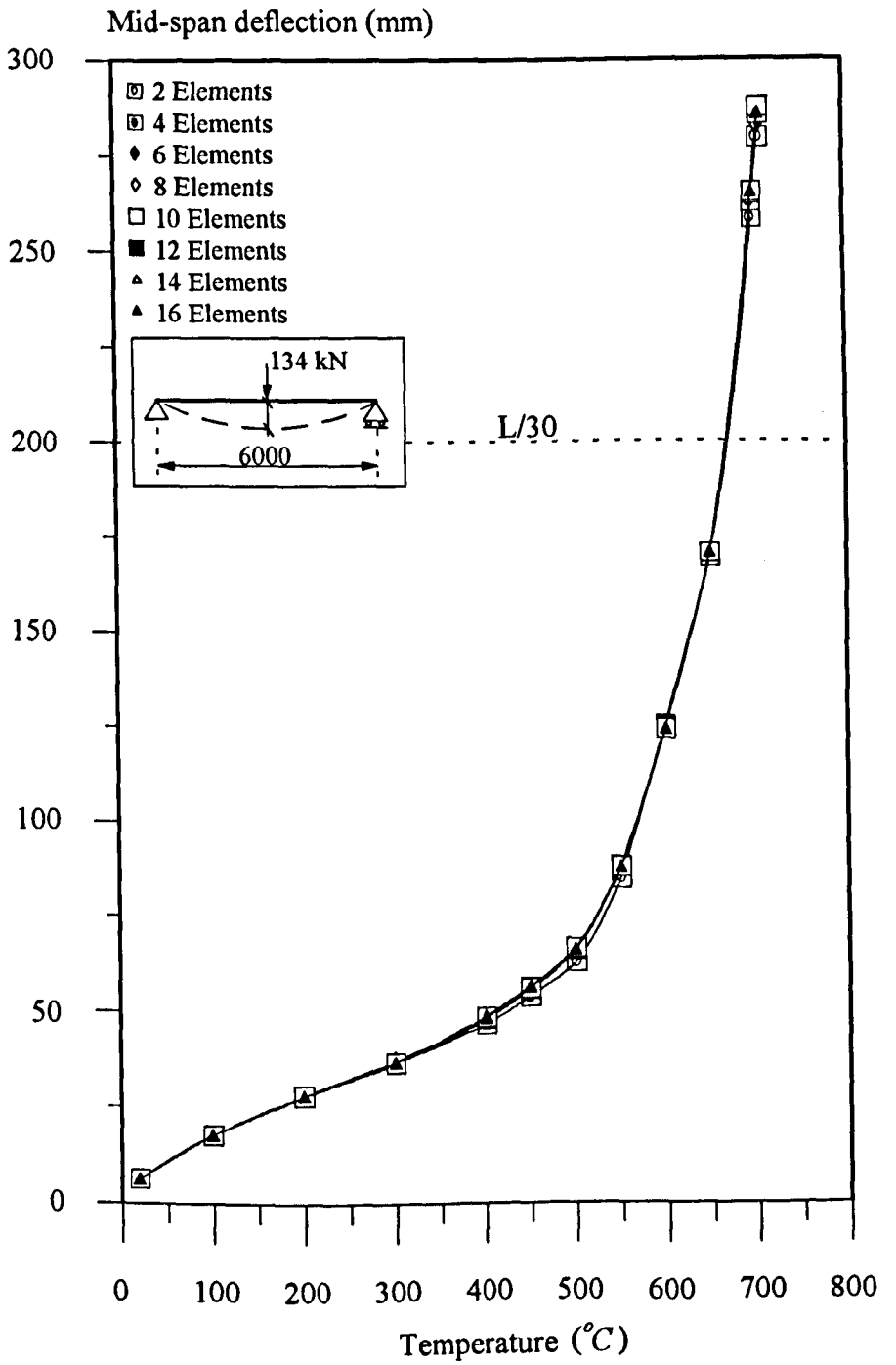

Fig. 6.3 Convergence study for simply supported beam with full interaction.

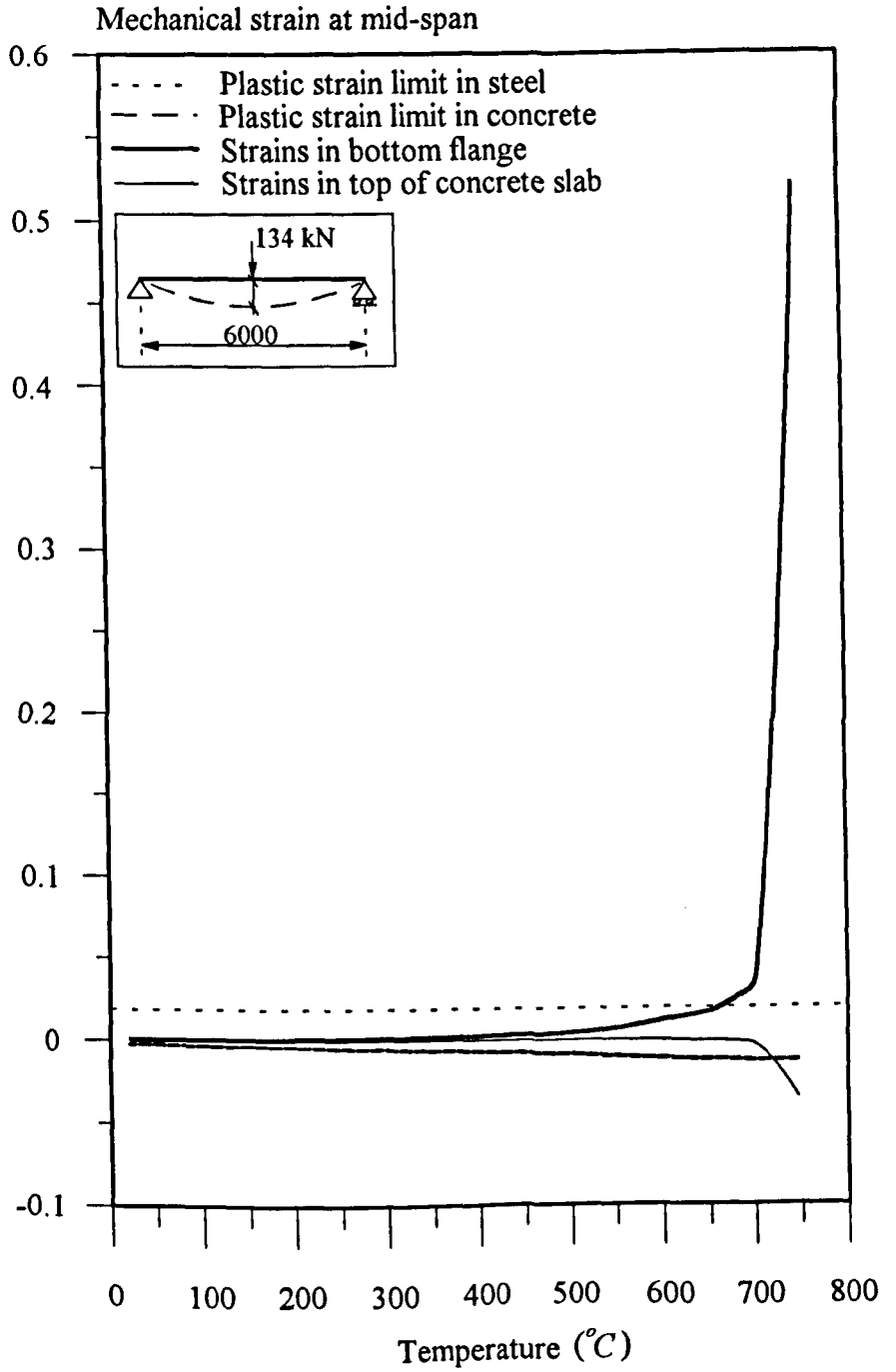

Fig. 6.4 Mechanical strains for simply supported beam with full interaction.

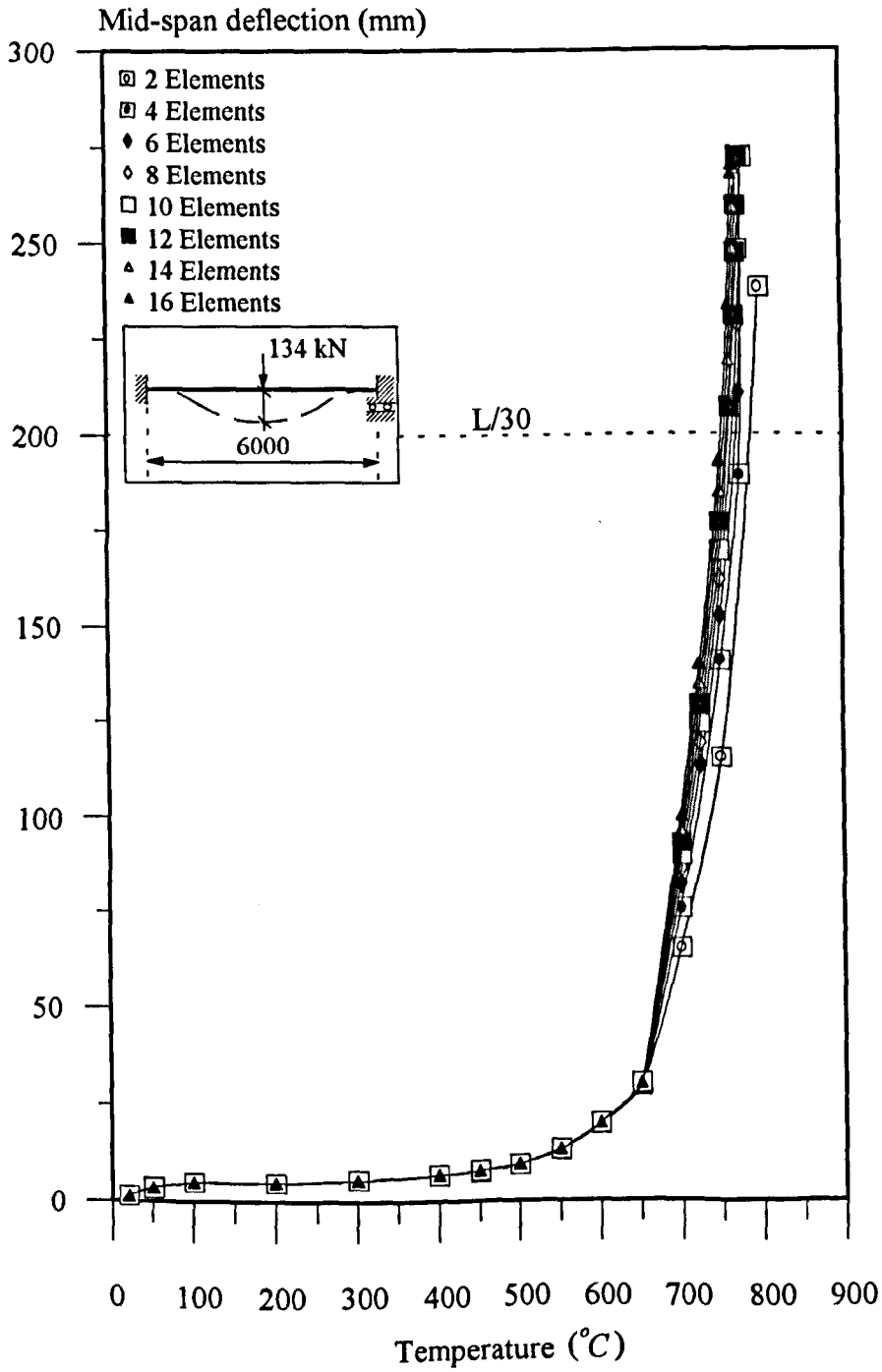

Fig. 6.5 Convergence study for axially unrestrained fixed end beam with full interaction.

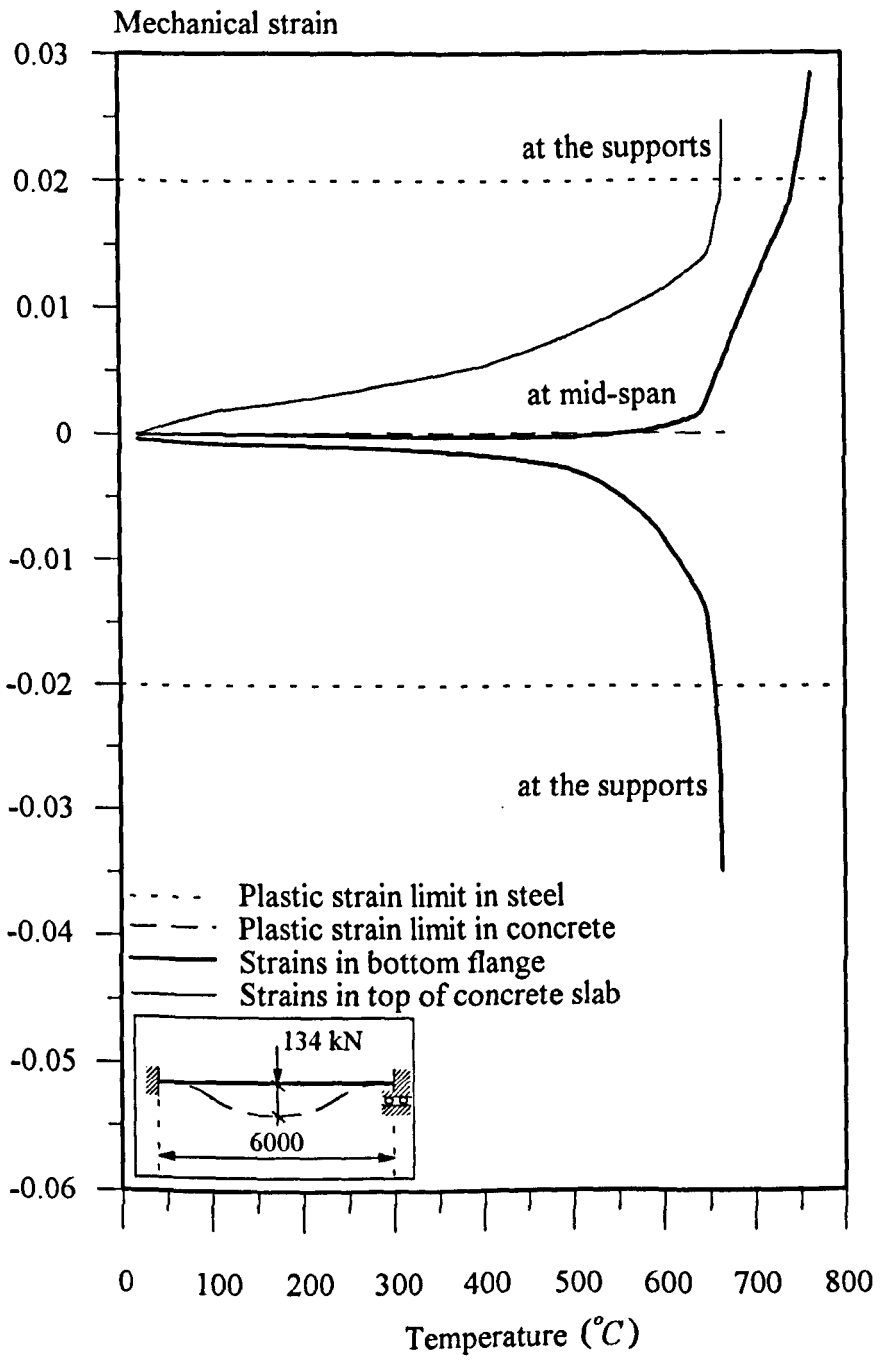

Fig. 6.6 Mechanical strains for axially unrestrained fixed end beam with full interaction.

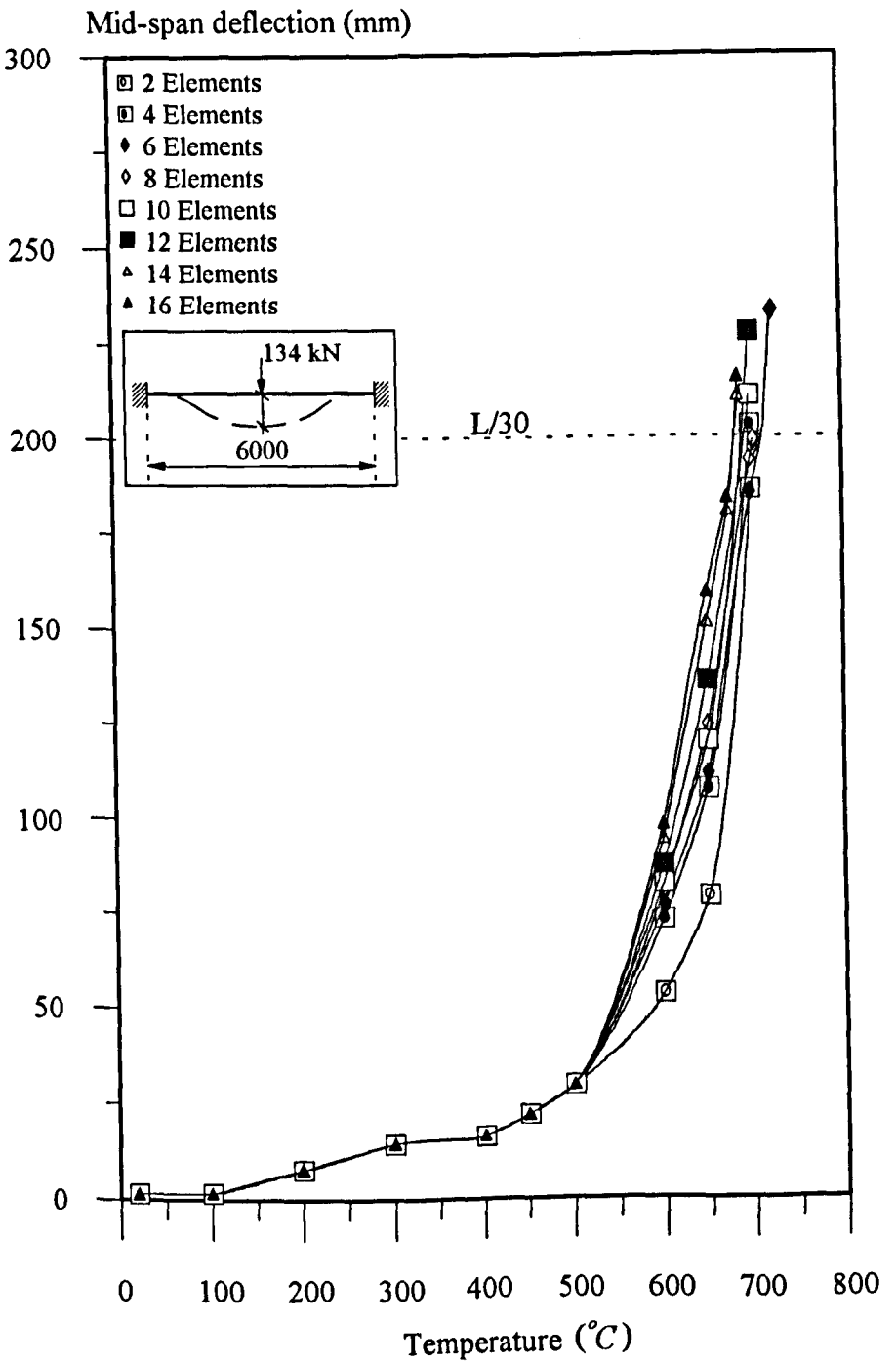

Fig. 6.7 Convergence study for axially restrained fixed end beam with full interaction.

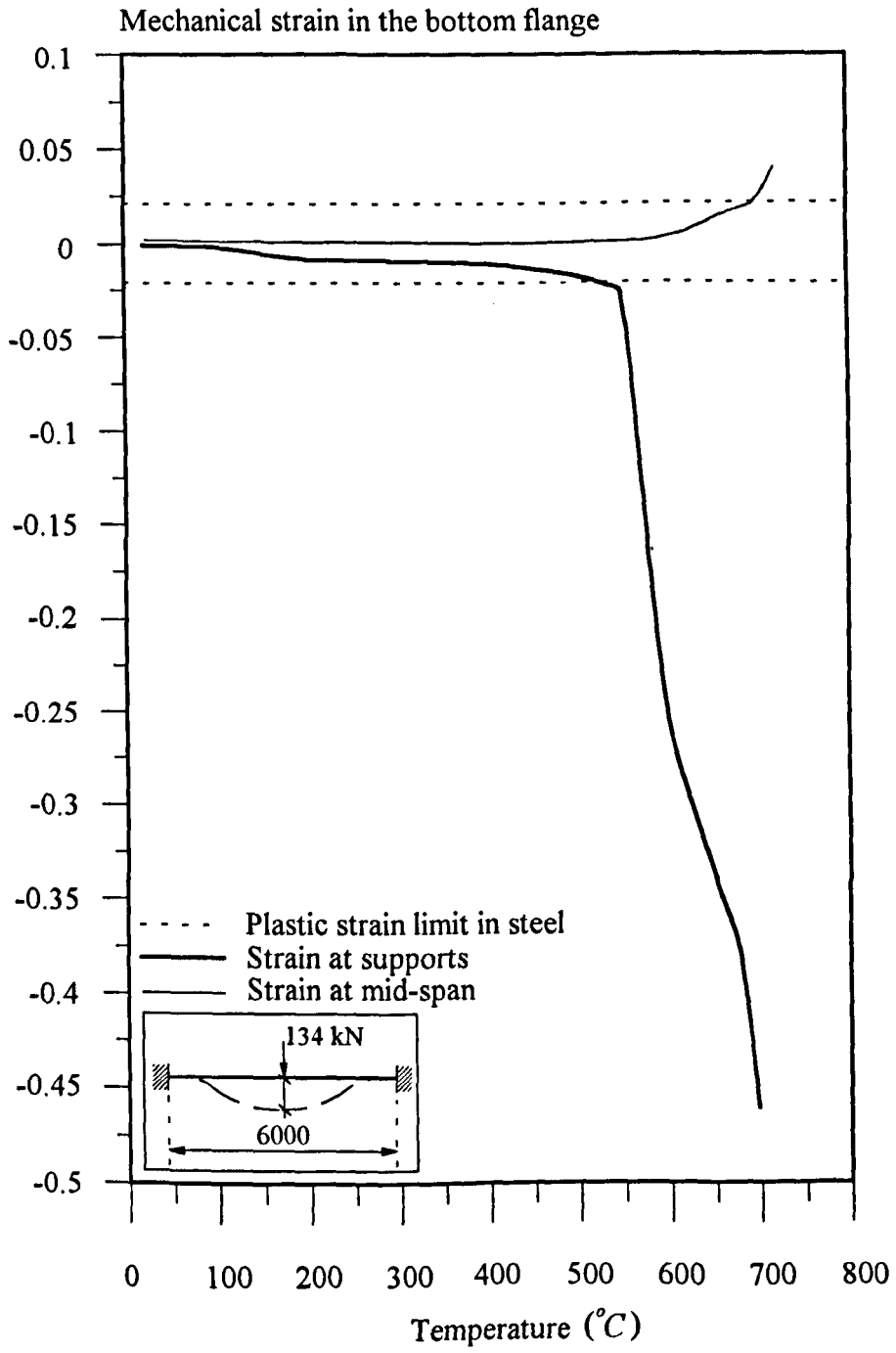

Fig. 6.8 Mechanical strains for axially restrained fixed end beam with full interaction.

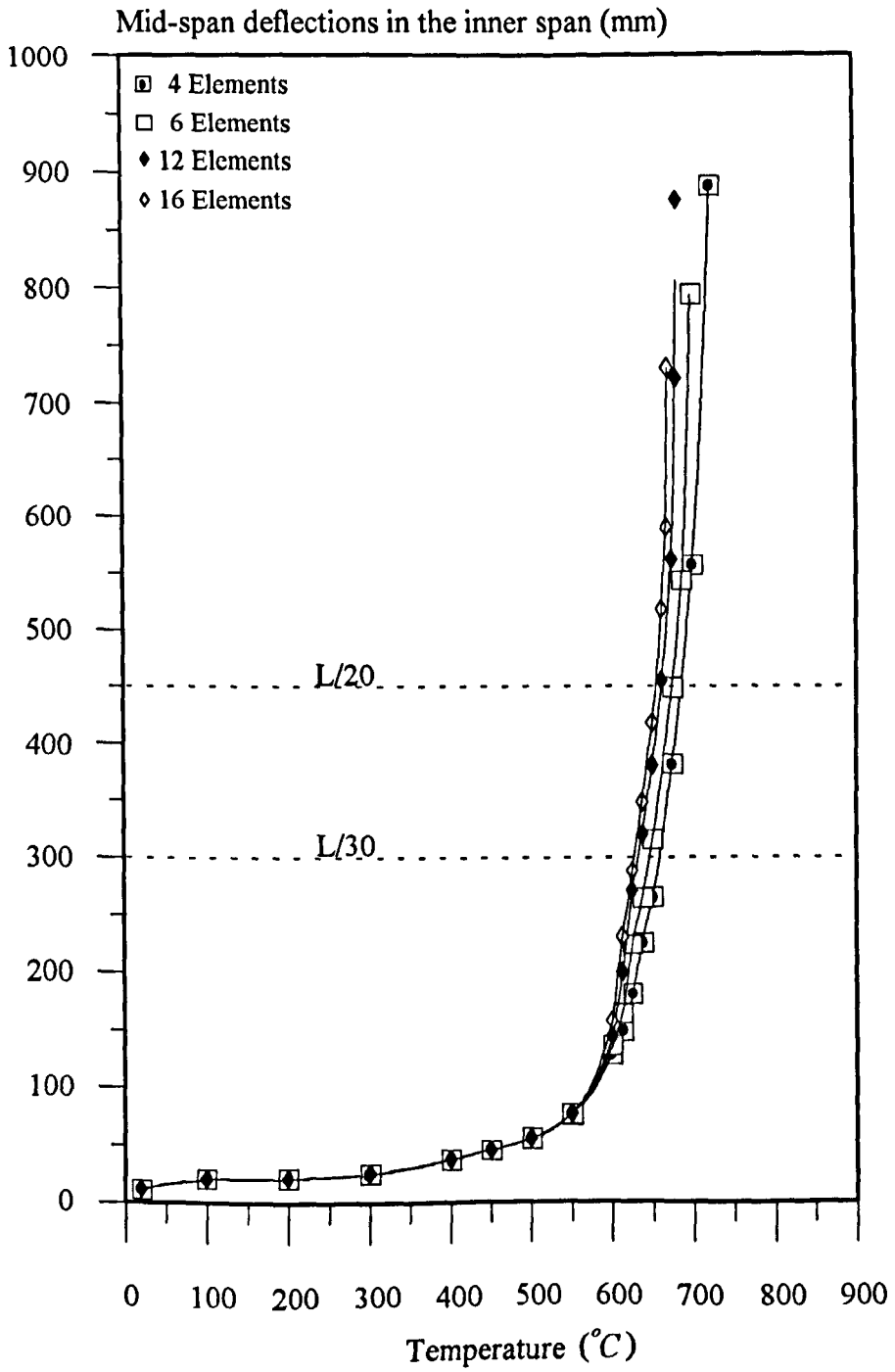

Fig. 6.9 Convergence study for continuous beam with full interaction.

6.2.2. Partial Interaction Analysis

The above convergence studies for simply supported and fixed ended beams, with full interaction, have been repeated using partial interaction analysis. The same beam size, loading conditions and temperature regime were used, but the connection between the steel I-section and concrete slab was assumed to be provided by 20 headed studs along the length.

The temperature-deflection behaviour for the simply supported beam is shown in Fig. 6.10 and is clearly identical regardless of the number of elements used. The predicted failure temperature is 665^{o}C and the corresponding deflection is 223mm, exceeding the limiting deflection of L/30. Typical slip patterns at 20^{o}C and 500^{o}C are shown in Fig. 6.11 and again indicate negligible difference. This implies that the minimum number of elements is sufficient to represent the beam.

Fig. 6.12 and 6.13 show similar results for the fixed ended beam. Up to 400^{o}C the temperature-deflection behaviour is identical for all cases whereas above this temperature a slight variation in predicted deflections is observed. The steel at the supports yields at 500^{o}C and mid-span deflections increase rapidly. As before fewer elements lead to a stiffer response. The variation in failure temperatures is however less than 2%, with 2 element analysis predicting a temperature of 700^{o}C compared with 688^{o}C for 16 elements. The corresponding deflections at failure for all analyses are in excess of L/20.

The slips at 300^{o}C are beyond the plastic slip value of 0.5mm indicating that all shear connectors along the length fail due to differential thermal elongation of the steel and concrete slab. Compared with the slip pattern for the simply supported case it may be concluded that the influence of thermal elongation of the beam on shear connectors is more severe for fully fixed end conditions than for simply supported end conditions. Once again the predicted slip patterns are almost identical and it can be concluded that the four number of elements are sufficient for predicting the structural behaviour within a reasonable accuracy.

Fig. 6.14 shows similar comparisons for the same beam using semi-rigid end conditions characterised by the model in Fig. 5.2(b). The stiffness of the rotational spring is defined by the moment-rotation characteristics of an extended end plate shown in Fig. 5.1(b) and the stiffness of the axial spring is defined by the force-elongation model shown in Fig. 5.5(c) using a constant stiffness value of 31500N/mm.

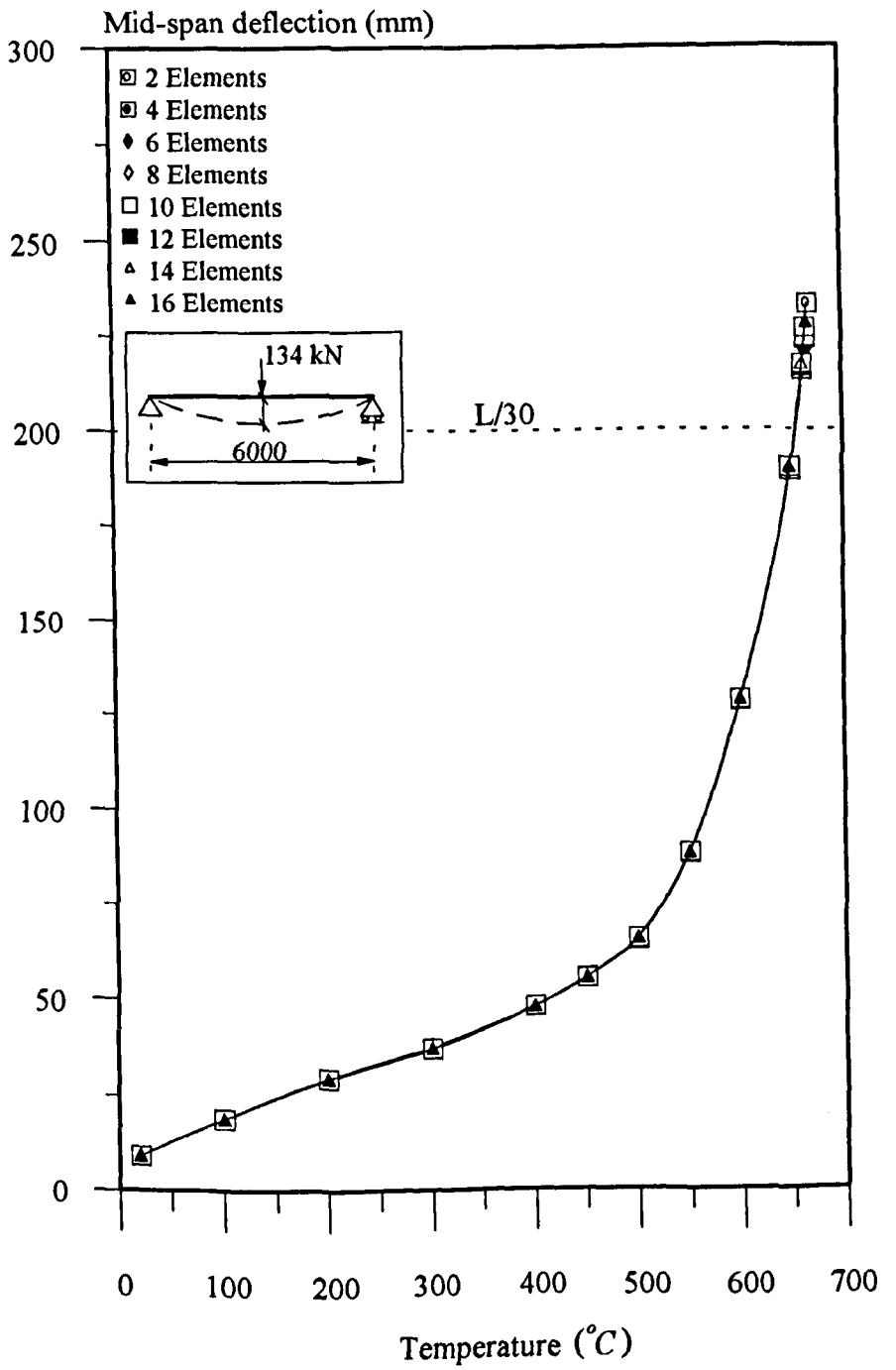

Fig. 6.10 Convergence study for simply supported beam with partial interaction.

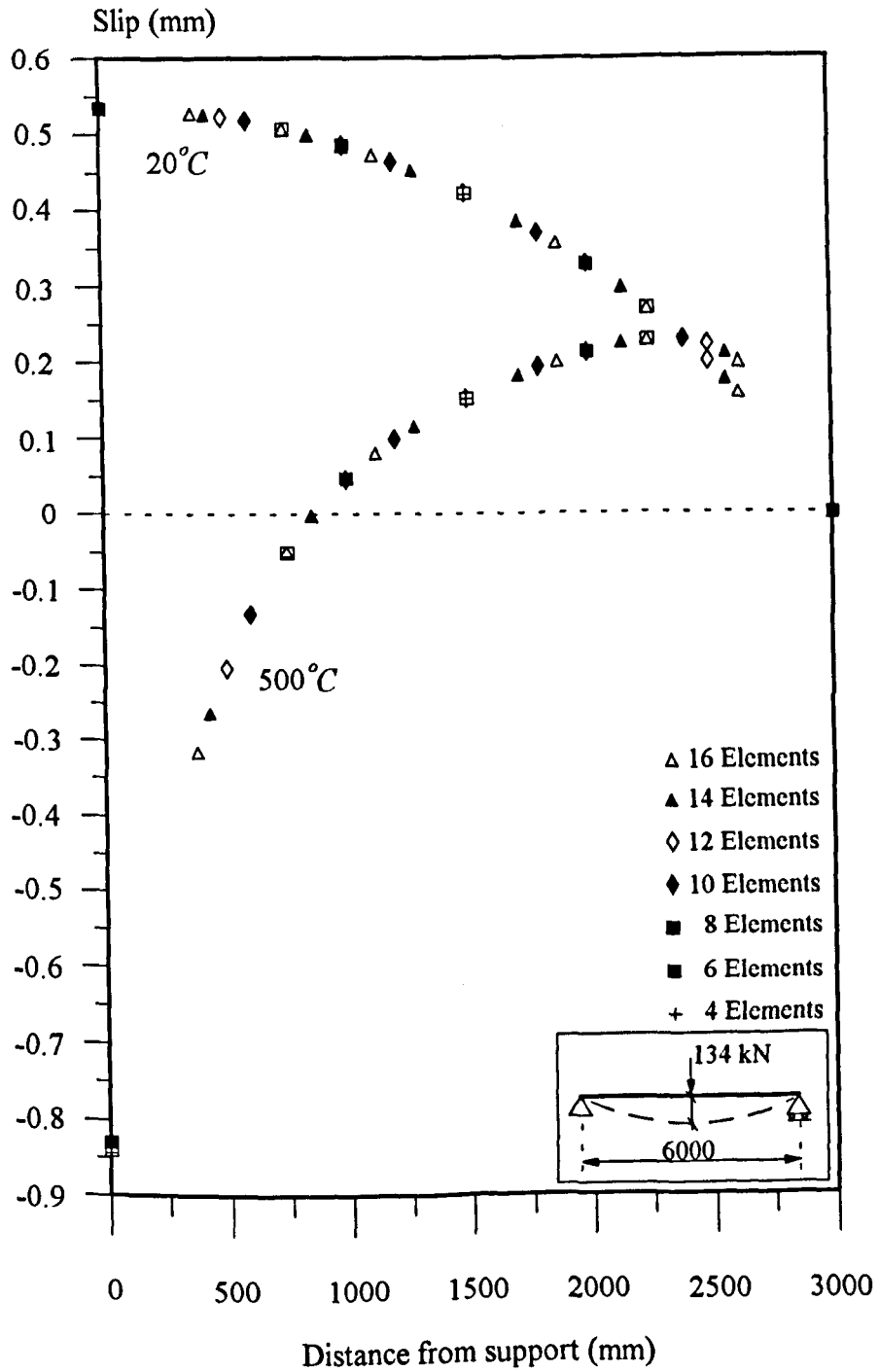

Fig. 6.11 Slip convergence for simply supported beam with partial interaction.

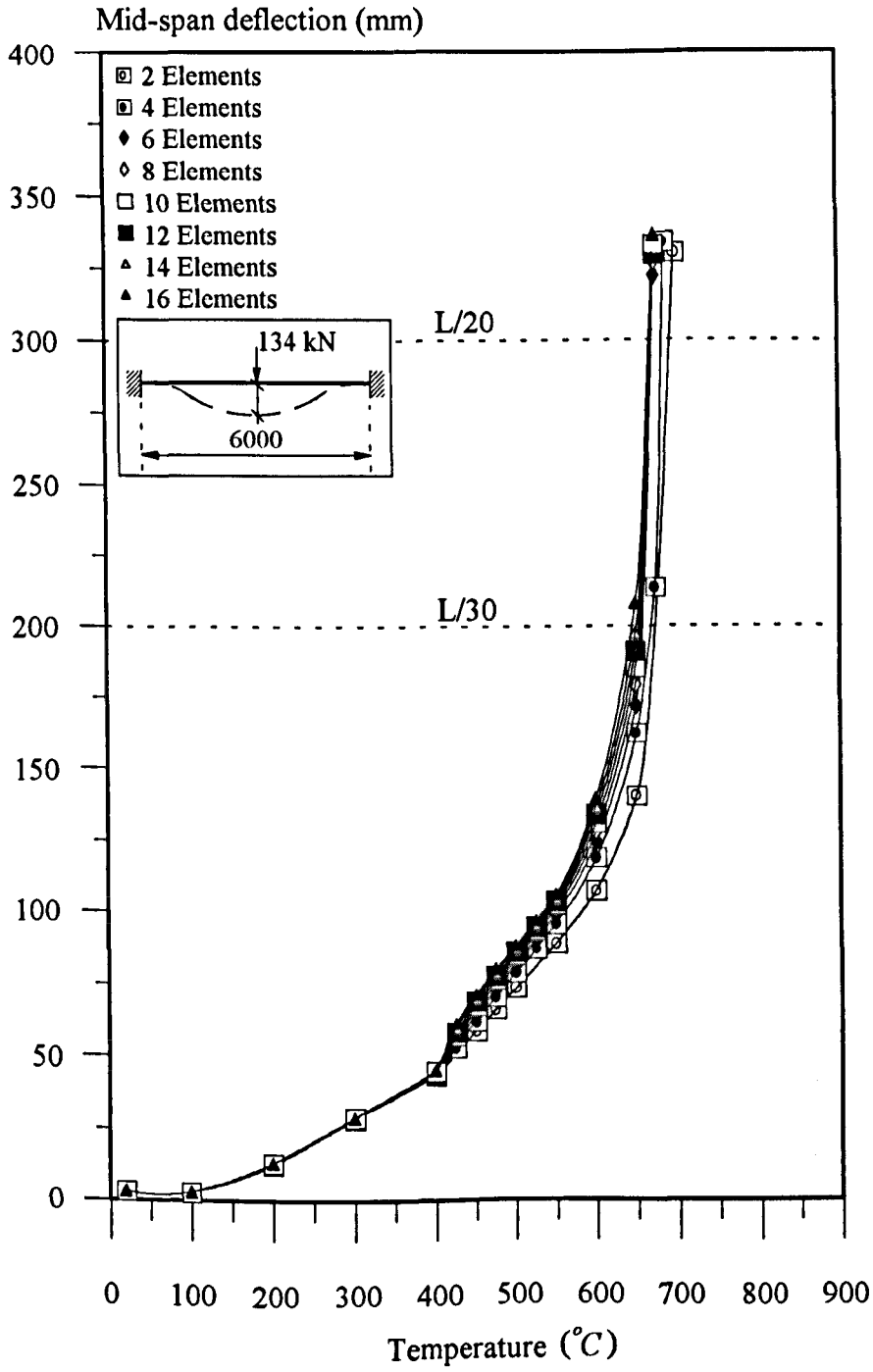

Fig. 6.12 Convergence study for fixed end beam with partial interaction.

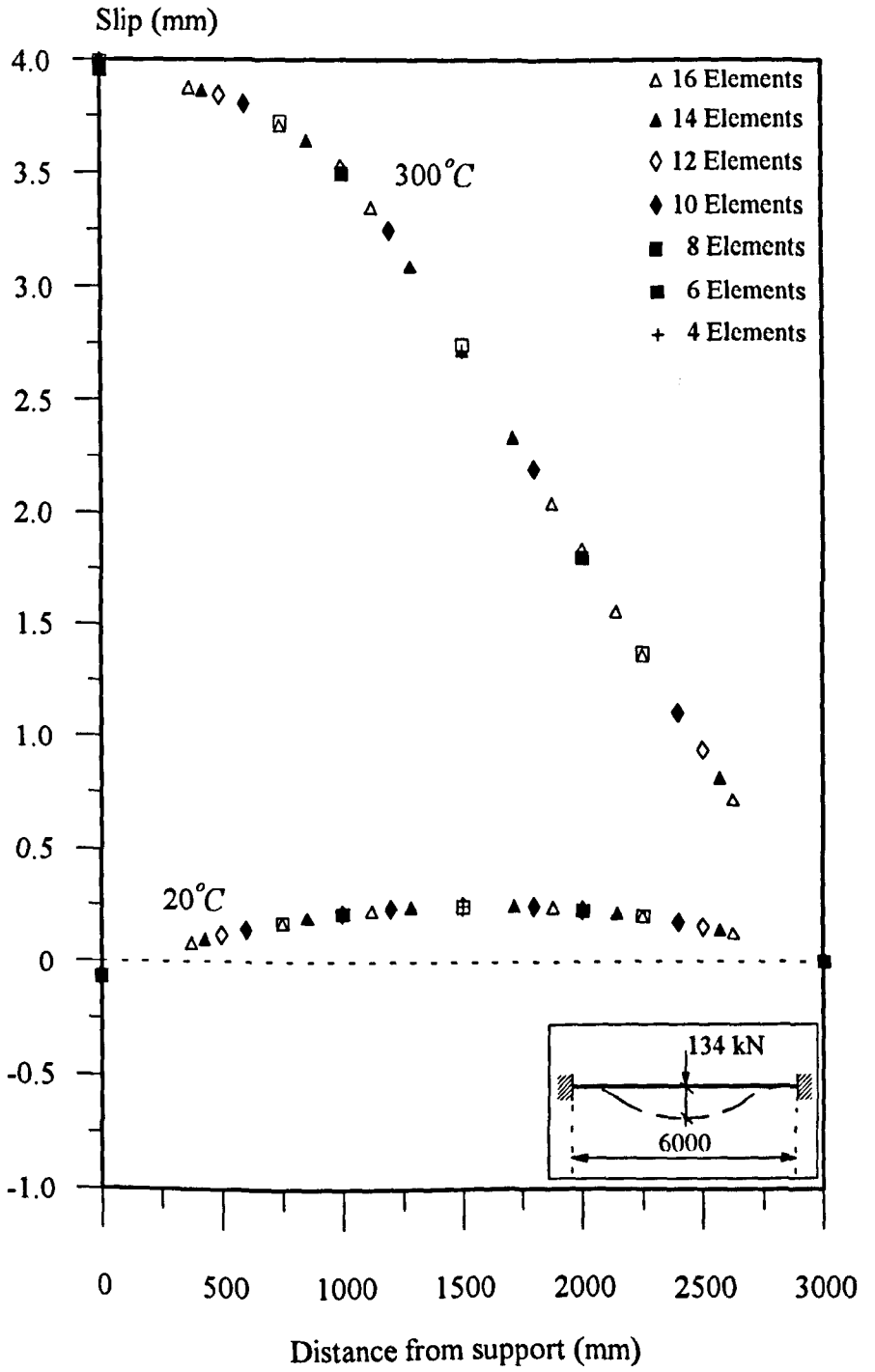

Fig. 6.13 Slip convergence for fixed end beam with partial interaction.

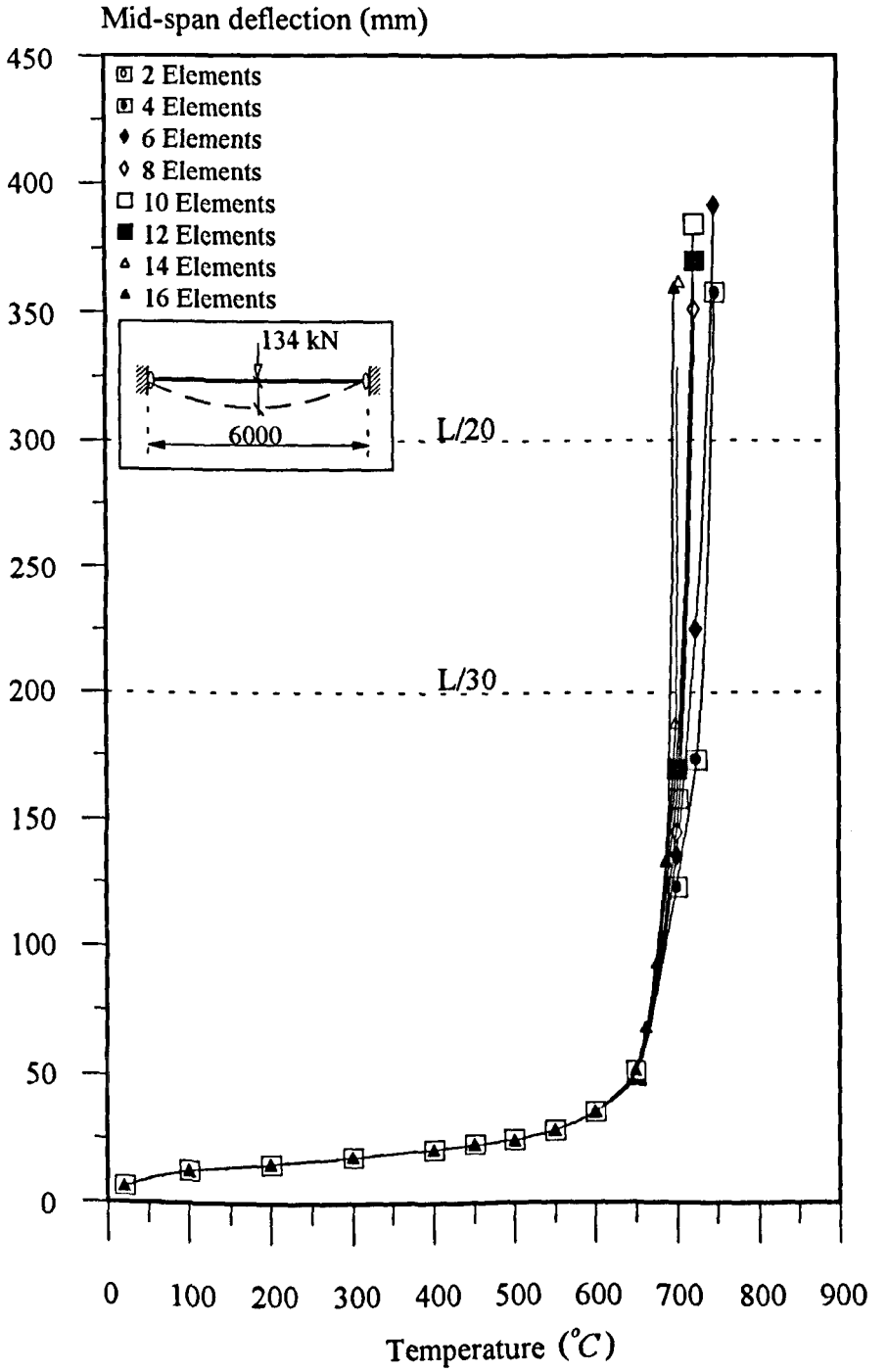

Fig. 6.14 Convergence study for semi-rigidly connected beam with partial interaction.

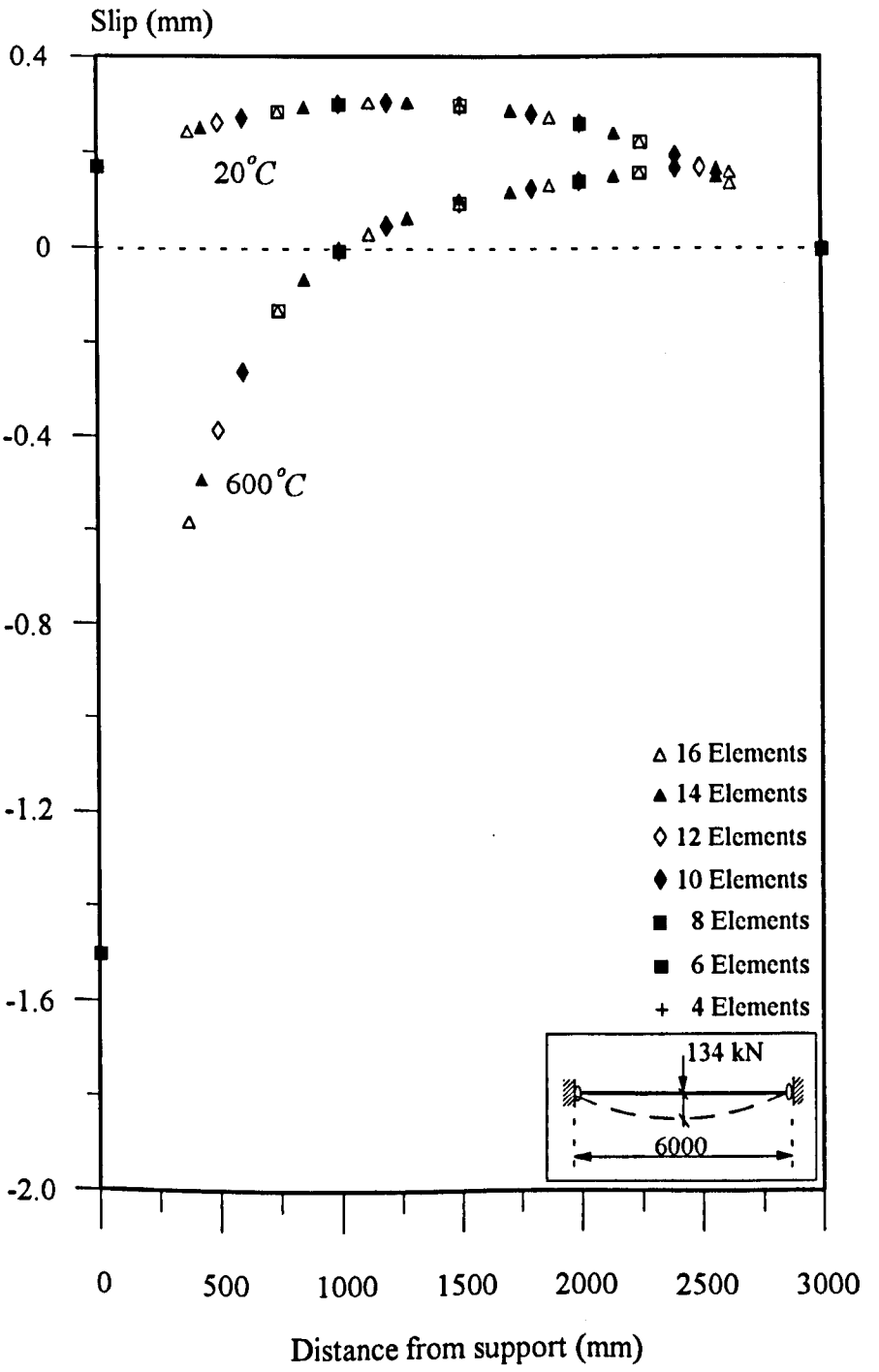

Fig. 6.15 Slip convergence for semi-rigidly connected beam with partial interaction.

As for the fixed ended beam, the temperature-deflection behaviour for all cases is identical up to 650°C. At this point the steel yields at the supports and the bending is redistributed towards the mid-span of the beam. Above this temperature analyses using denser meshes predict more rapidly increasing deflections. Nevertheless, the difference in predicted failure temperature and corresponding deflection is very small. The failure temperatures for the 2 and 16 element analyses are 750°C and 725°C respectively a discrepancy of about 3.5%.

Fig. 6.15 shows the typical slip distributions at 20°C and 600°C which show negligible influence of the number of elements used. It can be seen that the effect of differential thermal elongation on slips is considerably less than for the fixed ended beam.

These convergence studies demonstrate a consistency in the analytical results and indicate that a relatively small number of elements is sufficient to give reliable results. In the remaining studies four to six elements have been used to represent individual beam spans.

6.3. Comparison with Experimental Data at Ambient Temperature

Some comparisons have been made with published test results for composite beams at ambient temperature assuming full and partial interaction. Both simply supported and continuous beams have been included in this validation, and where possible both load-deflection history and slip patterns have been compared.

6.3.1. Full Interaction Analysis

A comparison for the case of full interaction has been based on tests where sufficient studs have been used to minimise the influence of slip. Slutter and Driscoll[61] carried out tests on twelve simply supported composite beams of 4572mm span. The shear connection for all beams was reported to provide full interaction, although the measured maximum end slip values were negligible in only three tests. These have been chosen for comparison.

The beams referenced as B4-T2 and B4-T4 were loaded symmetrically with two concentrated loads, applied 228.6mm and 457.2mm from the centre line of the beam. The third beam B10-T13 was loaded with four concentrated loads at 1143mm spacing. The cross-section of the beams and the reinforcement of five 8mm diameter bars were the same for all cases. The configuration of the beams and physical properties of the materials used are illustrated in Fig. 6.16.

The test results were plotted as deflection against moment ratio and are shown in Figs. 6.17 to 6.19 together with the current analytical results. The moment ratio was defined as the applied test moment divided by the theoretical ultimate moment. In all cases at load levels up to 50% of the ultimate moment capacity of the beams the agreement between the analytical and test deflections is excellent. Between 50% and 90% of the ultimate moment capacity, an increase in the end slips of the test specimens is reported[61] and as a result tests show greater deflections than the full interaction analyses. However the comparisons remain very good with a discrepancy in deflection of less than 15%. Beyond 90% of the ultimate moment capacity analysis and test results agree less well possibly because of increasing slips although the general pattern of behaviour is consistent. The reported ultimate moments for beams B4-T2 and B4-T4 were 311kNm and for beam B10-T13, 312kNm. The predicted ultimate moment for all cases is 317kNm, an overestimate of only 2%. The predicted mode of failure is yielding of the steel at the point loads whereas the failure of test specimens was reported to be due to shearing of the studs. This shows that the influence of slip may be significant even with 'fully composite' beams.

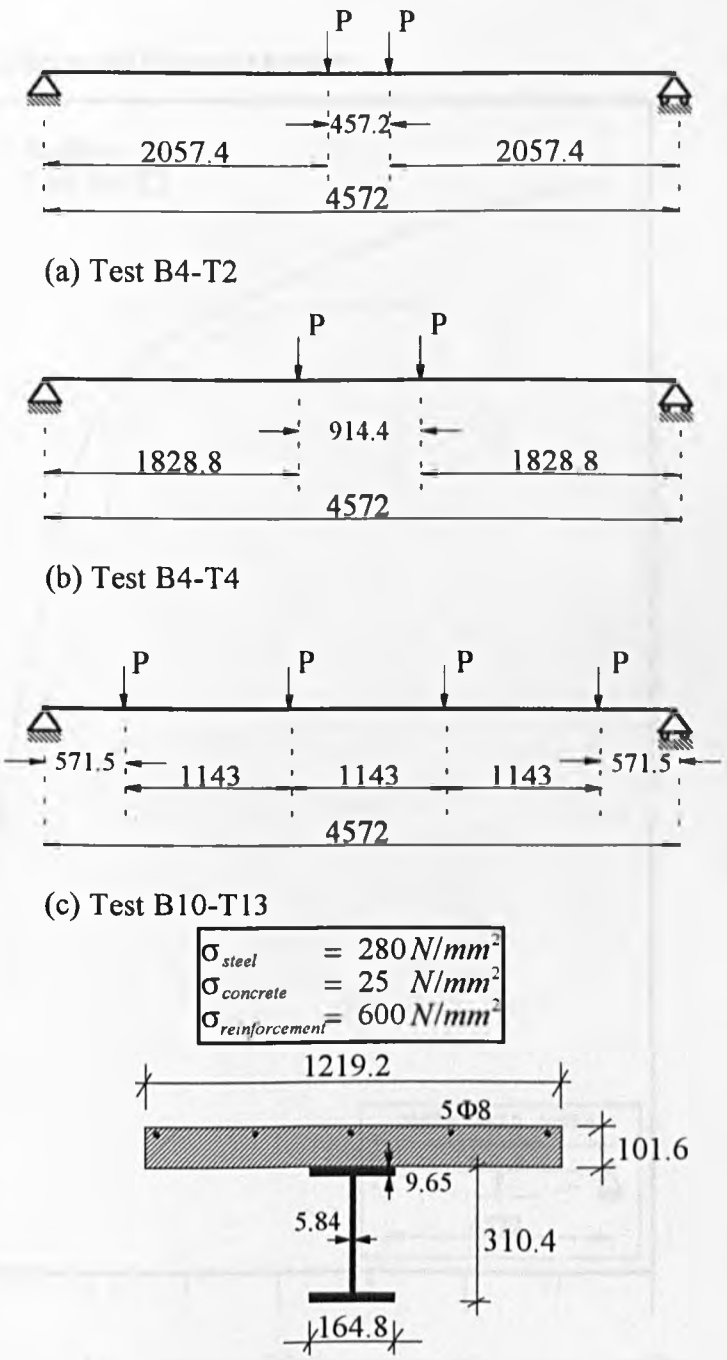

Fig. 6.16 Details of test beams used for validating full interaction analysis.

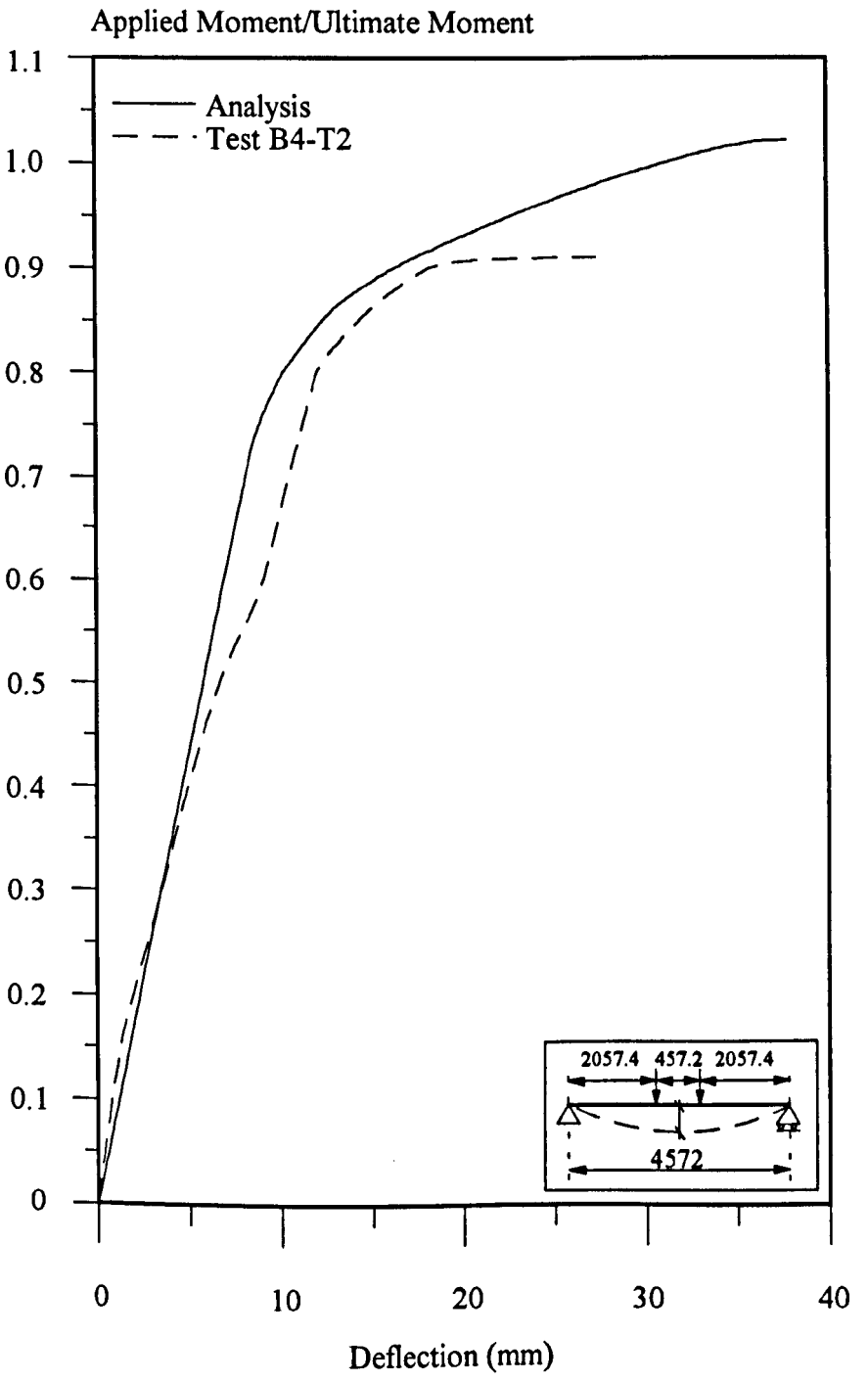

Fig. 6.17 Comparison between analysis and test beam B4-T2.

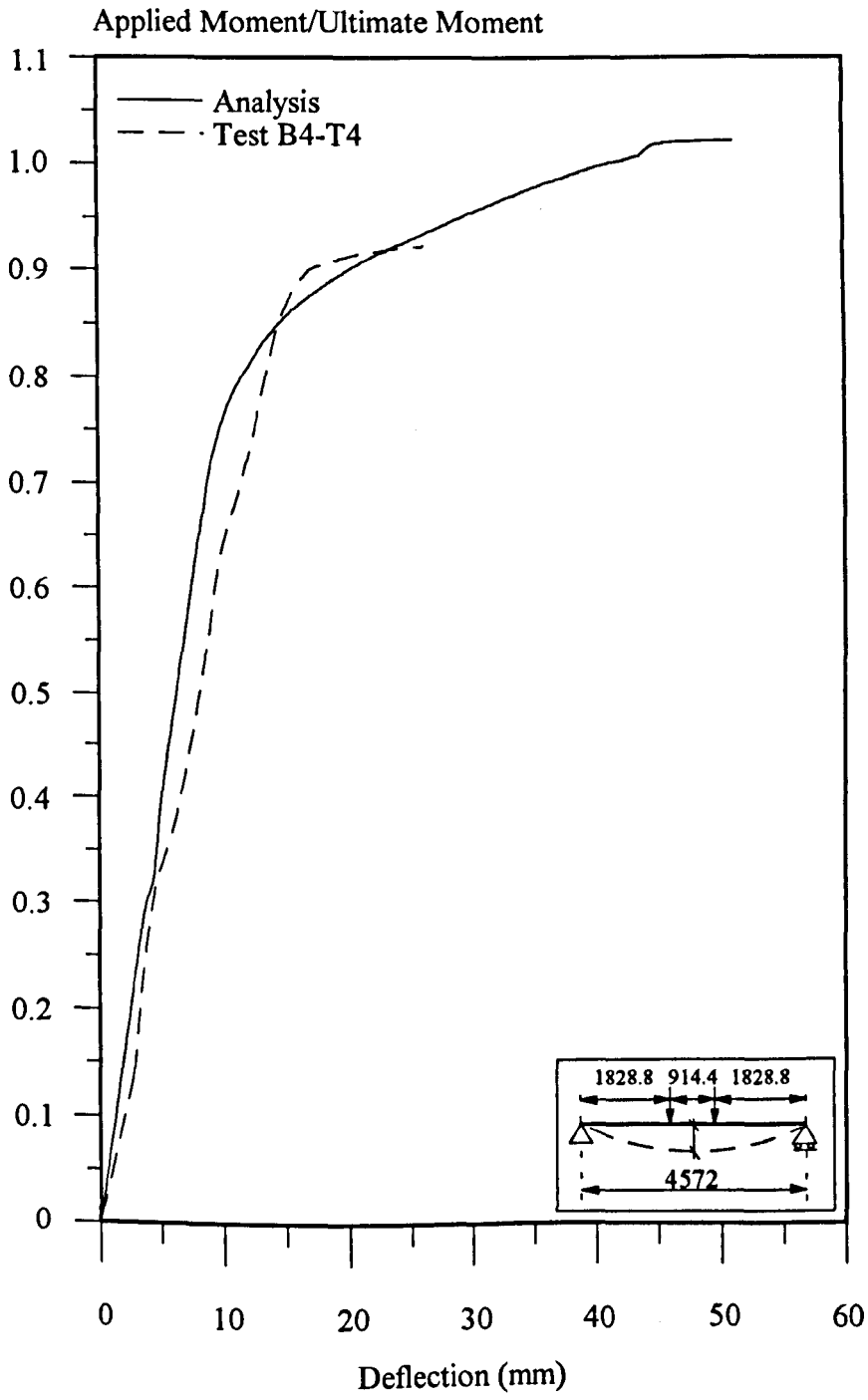

Fig. 6.18 Comparison between analysis and test beam B4-T4.

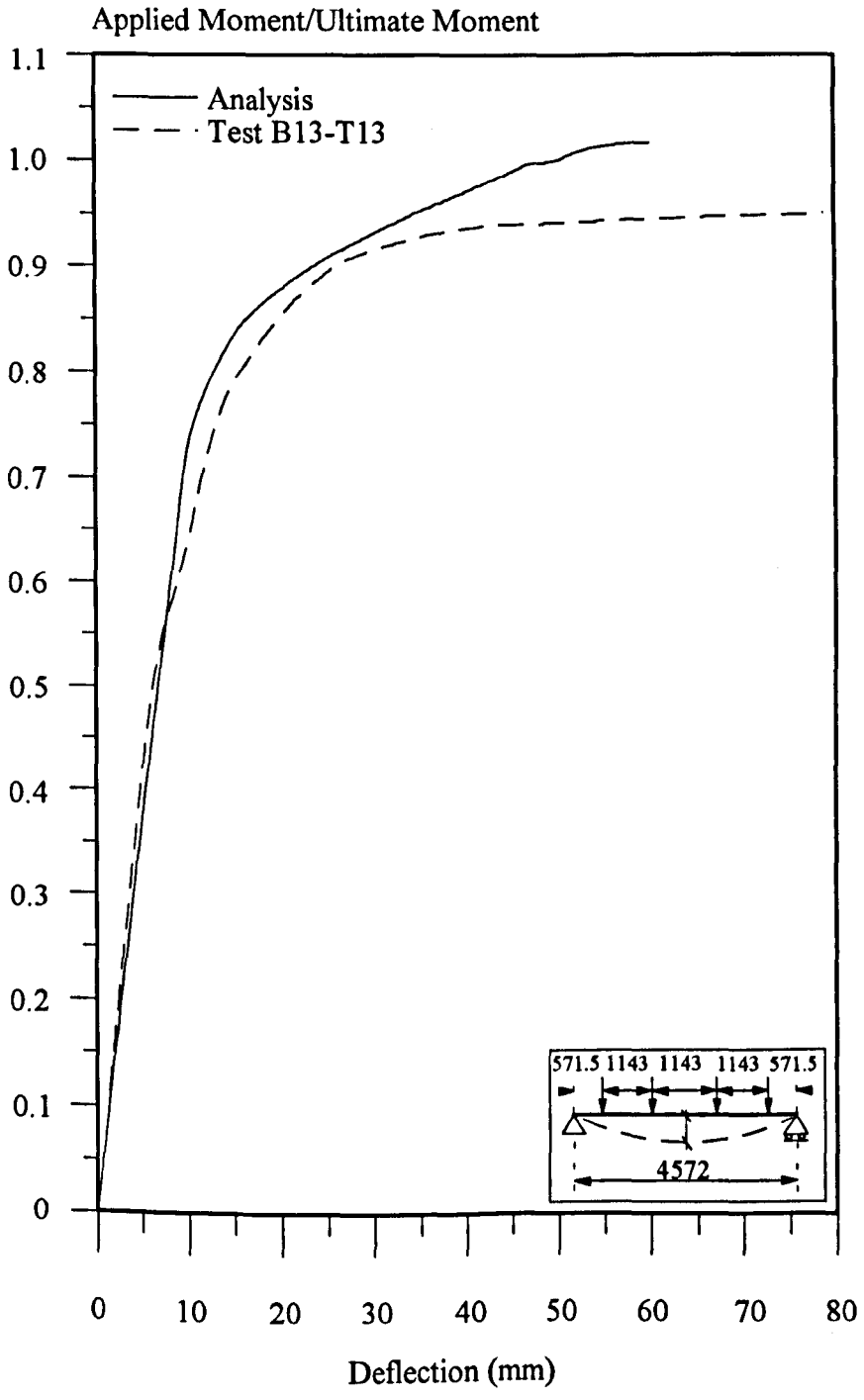

Fig. 6.19 Comparison between analysis and test beam B13-T13.

6.3.2. Partial Interaction Analysis with Idealised End Conditions

In partial interaction analysis the influence of slip on beam behaviour is considered. The program was verified by comparing both the load-deflection behaviour and the slip patterns with available experimental results for simply supported and continuous beams. The results of these comparisons are discussed separately as below.

6.3.2.1. Load-Deflection Behaviour

Six simply supported beams were tested by Chapman and Balakrishnan[60] with results presented as load-deflection plots. All beams have a length of 5500mm and the same cross-sectional dimensions and reinforcement details as shown in Fig. 6.20. The beams referenced as E1 and A1 to A6 were loaded with a central point load, whereas U4 was uniformly loaded. The variables in these tests were the number of studs, and the material properties of studs, steel I-section and concrete.

Analytical and test results are compared in Figs. 6.21 to 6.25. For all cases the analytical and experimental results are in reasonable agreement and predicted failure loads are within 6%. For tests A1 and A6 predicted failure loads are 424kN and 425kN respectively compared with results of 419kN and 408kN, indicating an overestimate of 1.2% and 4% respectively. The predicted failure loads for tests E1 and A3 are 472kN and 418kN and are also in good agreement with test values of 498kN and 436kN indicating an underestimate of 5.5% and 4.2% respectively. For tests A5 and U4 the predicted ultimate loads of 448kN and 900kN were the same as those observed in the tests. The predicted pattern of deflections also correlates reasonably with test data up to about 70% of the failure load. As failure is approached, observed deflections start to increase rapidly. Given the uncertainties associated with modelling the behaviour of concrete at high strains and the uplift of the concrete slab reported during the testing it might be expected that the calculated and test deflections will diverge. As seen in Fig. 6.25, for test U4, the discrepancy in deflections near failure is significantly less because of the load being applied through 18 interconnected hydraulic jacks restricting the uplift of concrete. Nevertheless the overall pattern of behaviour in all tests is well represented.

Test	σ_{steel} (N/mm^2)	$\sigma_{concrete}$ (N/mm^2)	$\sigma_{reinforcement}$ (N/mm^2)	No of Studs	P_{stud} (N)
E1	462	51	600	100	64
A1	414	30.5	600	84	112
A3	452	26	600	68	112
A5	451	42	600	44	122
A6	445	41	600	32	122
U4	474	43	600	32	122
U5	434	32	600	32	112

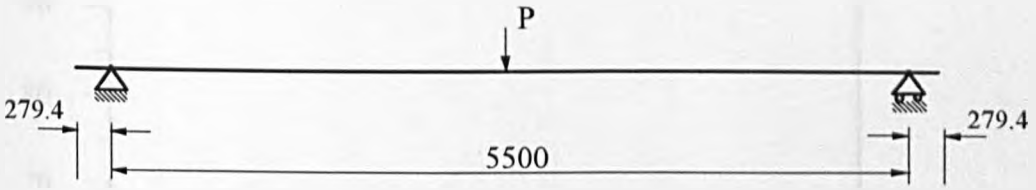

(a) Centre loaded case

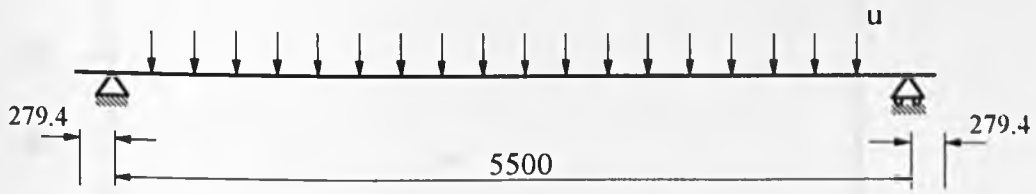

(b) Uniformly loaded case

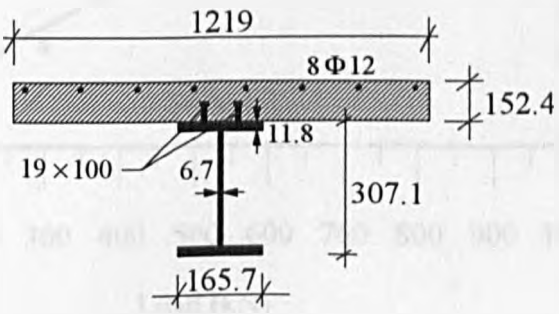

Fig. 6.20 Details of simple beams used for validating partial interaction analysis.

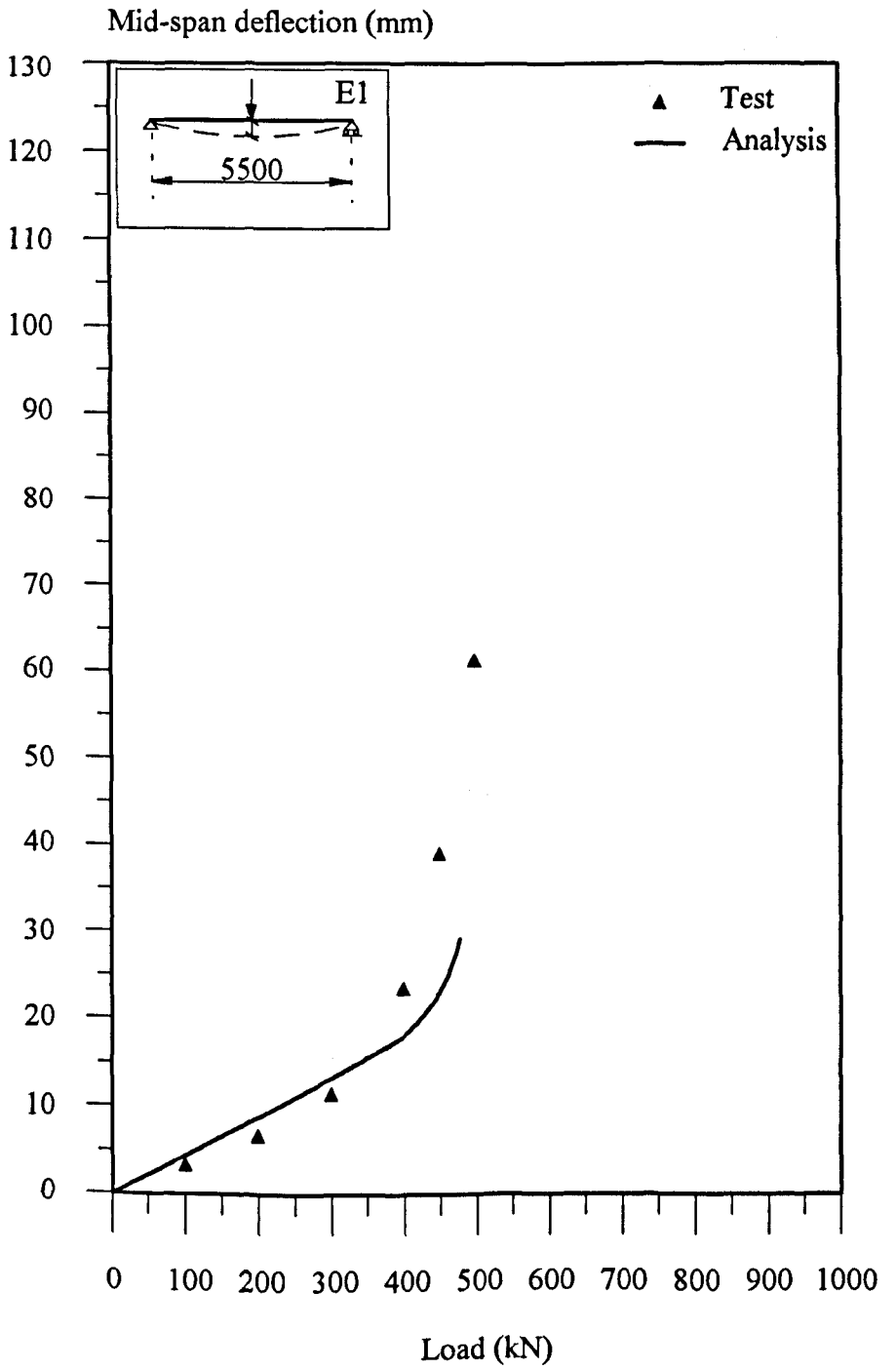

Fig. 6.21 Comparison between analysis and test beam E1.

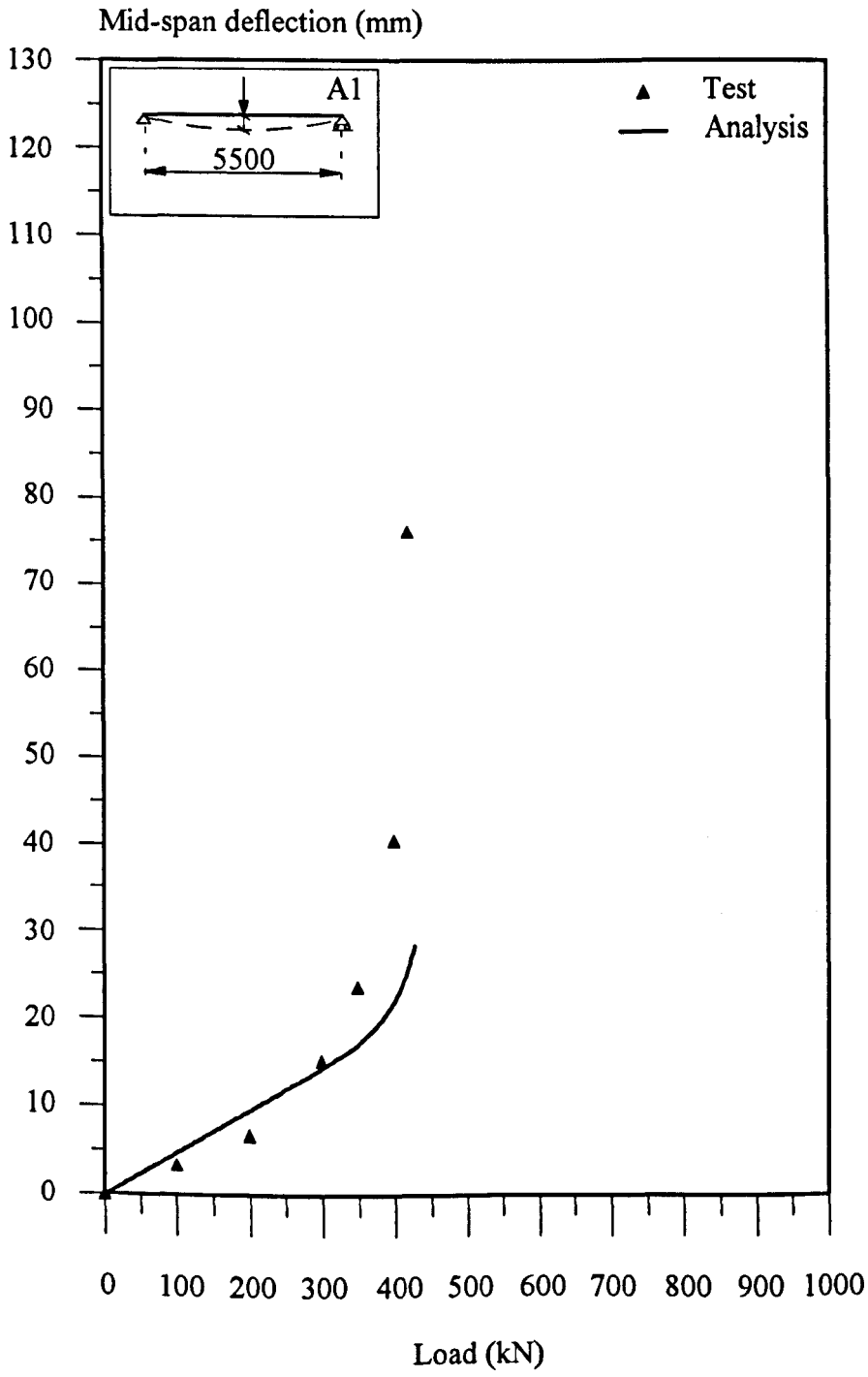

Fig. 6.22 Comparison between analysis and test beam A1.

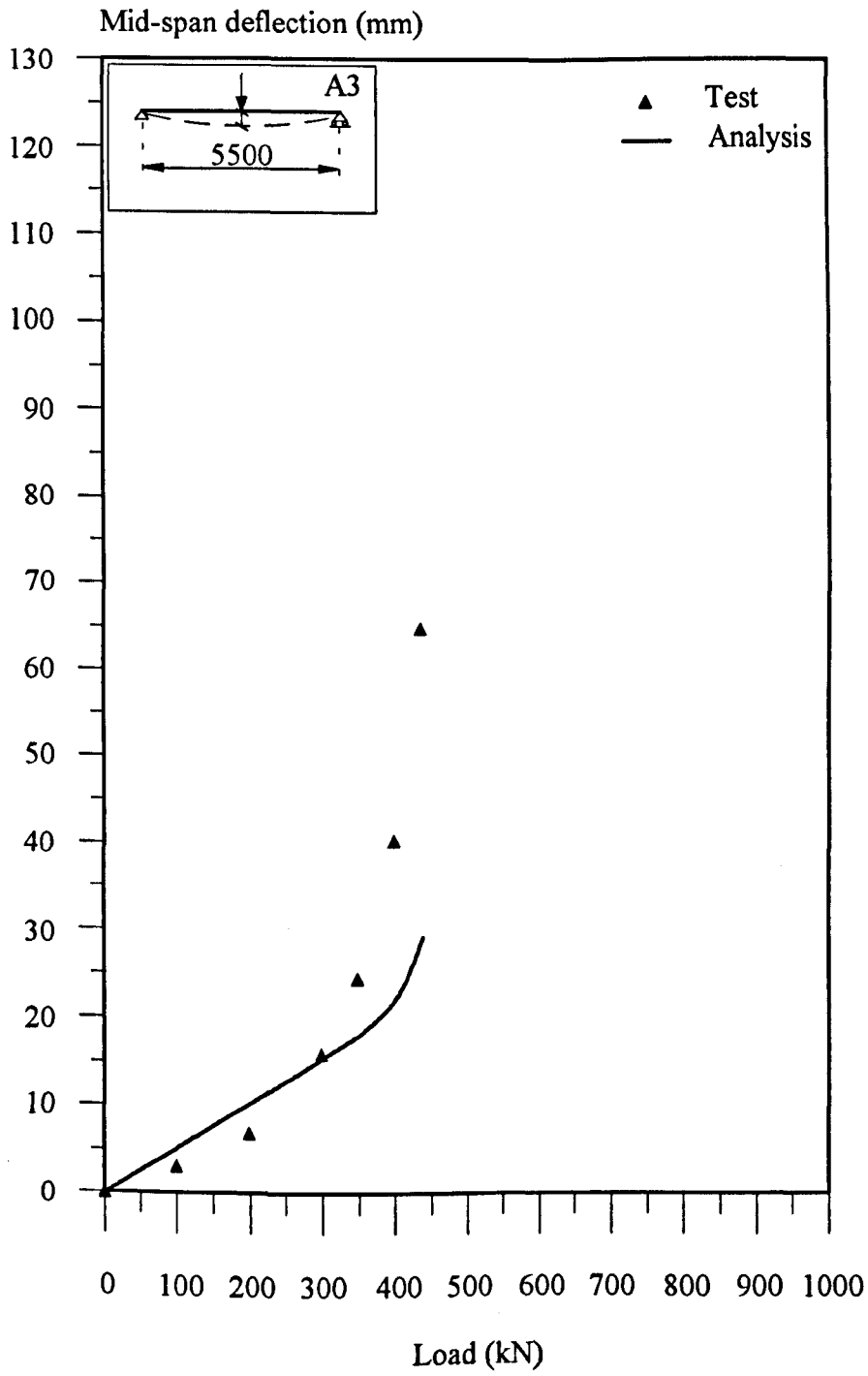

Fig. 6.23 Comparison between analysis and test beam A3.

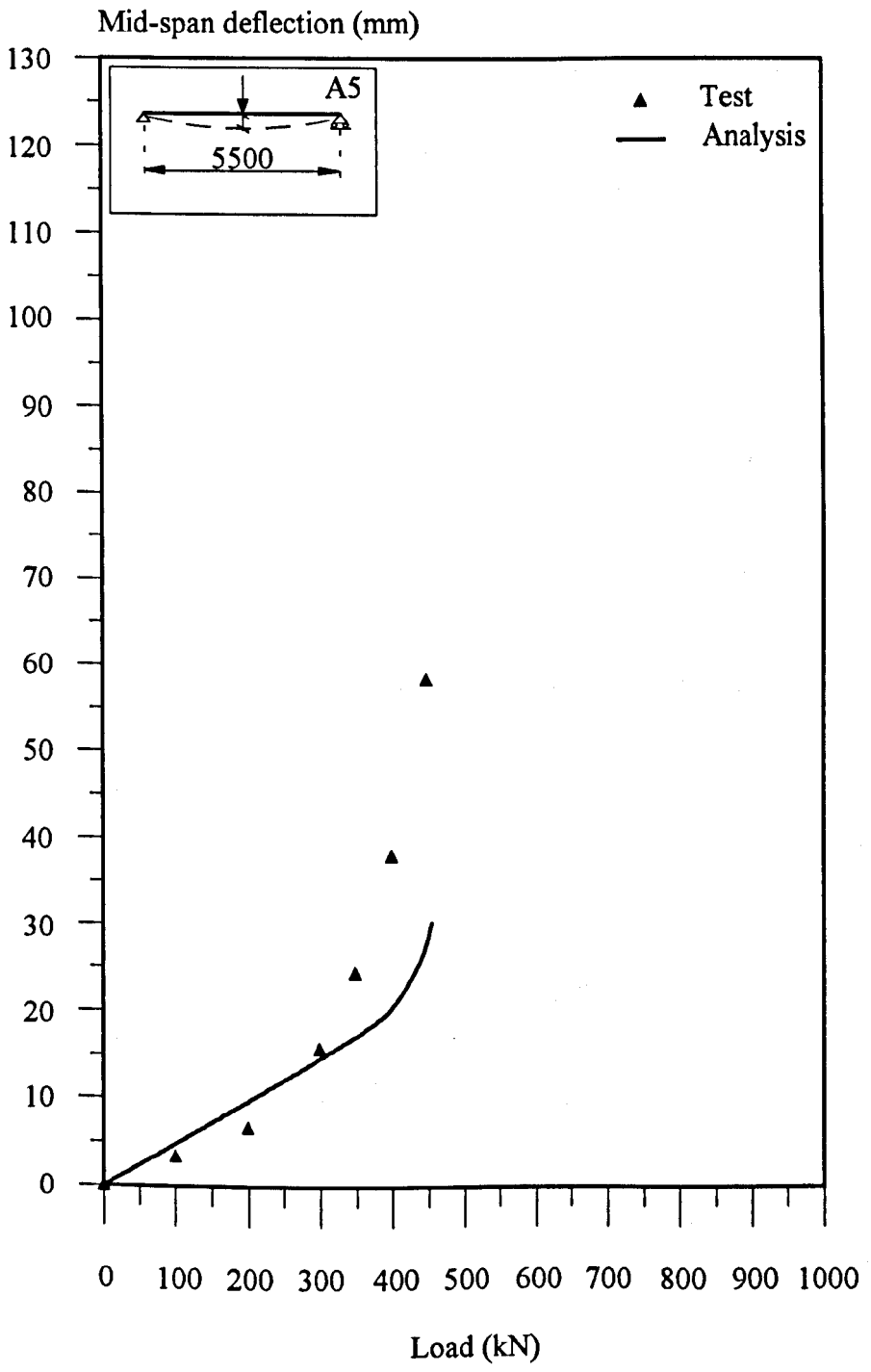

Fig. 6.24 Comparison between analysis and test beam A5.

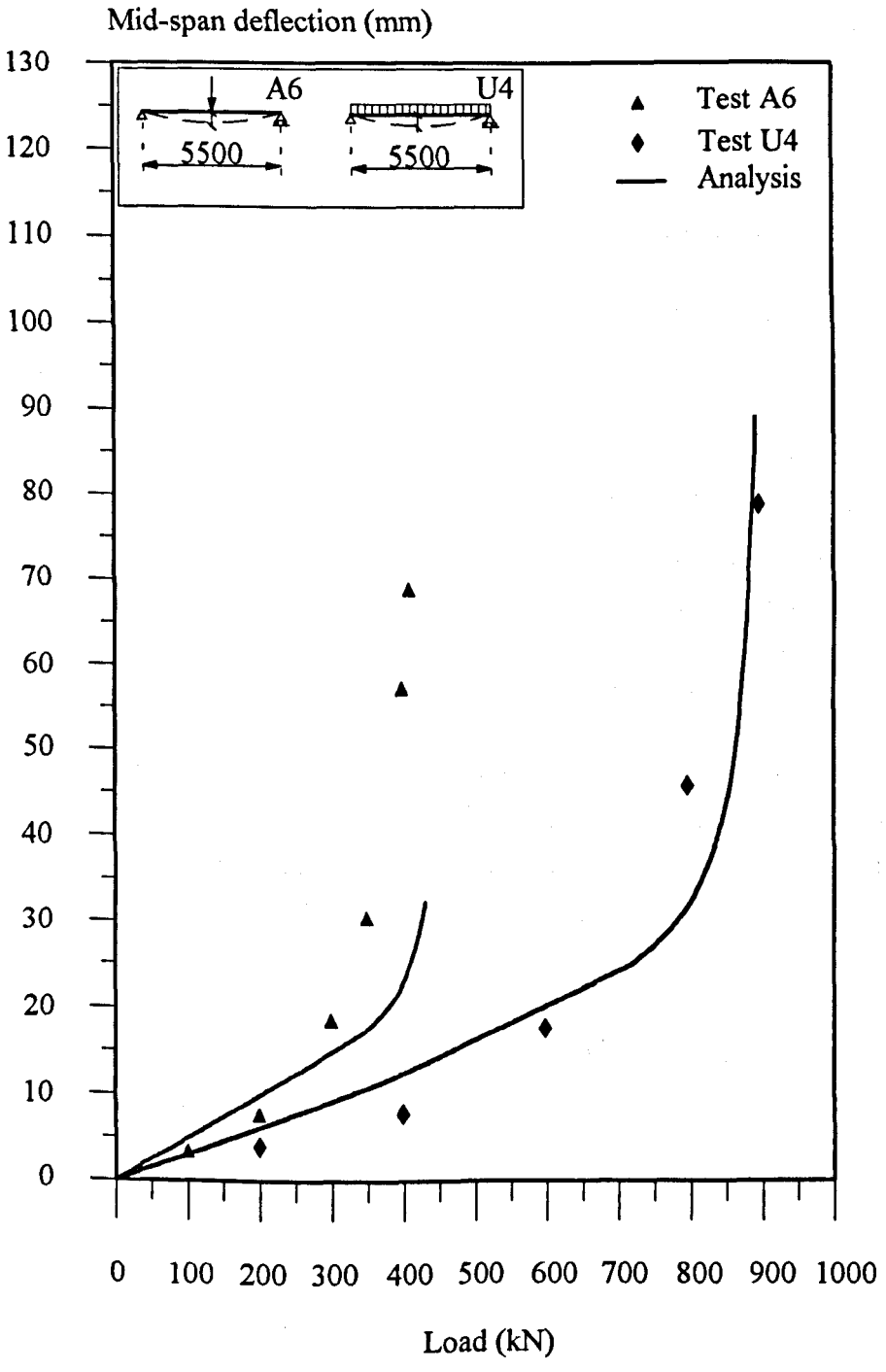

Fig 6.25 Comparison between analysis and test beams A6 and U4.

Three continuous test beams, B13 by Slutter and Driscoll[61], CB1 by Barnard and Johnson[106] and CB2 by Teraszkiewics[101,155], have also been used for comparison studies. Tests B13 and CB2 used a two-span beam with two concentrated loads on each span, whereas test CB1 was based on a three-span beam with a concentrated load on the inner span. The configurations of these beams and material properties are illustrated in Fig. 6.26.

Comparisons of analytical and test load-deflection behaviours are shown in Figs. 6.27 to 6.29. Force-slip relationships were reported only for test specimen CB2, and so the same values as used in the comparison for simply supported beams have been assumed.

Slutter and Driscoll[61] presented their test results as plots of deflection against load ratio. The latter was defined as the applied test load divided by the ultimate load, and it is unfortunate that the precise value for this was not reported. For the purpose of this comparison the ultimate load used in determining the load ratio was simply the value, 168kN, calculated by the program at collapse. The ultimate load based on simple plastic analysis and calculated design bending strengths for the composite beam of 250kNm (mid-span) and 95kNm (support) is 142kN. Subject to this assumption it can be seen that there is good correlation between the test results and the predicted behaviour with a maximum discrepancy of 8% throughout the load history.

For test CB1, the experimental data was presented as a moment-curvature relationship at the loaded point. For the purpose of comparison the analytical results are presented in a similar form in Fig. 6.28. The predicted ultimate moment is 31.5kNm compared with the test result of 37kNm. This means correlation is less good than the previous case with the ultimate moment being underestimated by 17%. However when account is taken of the uncertainties associated with testing composite beams, and the assumptions which have been made concerning various parameters, the comparison provides support for the analytical predictions.

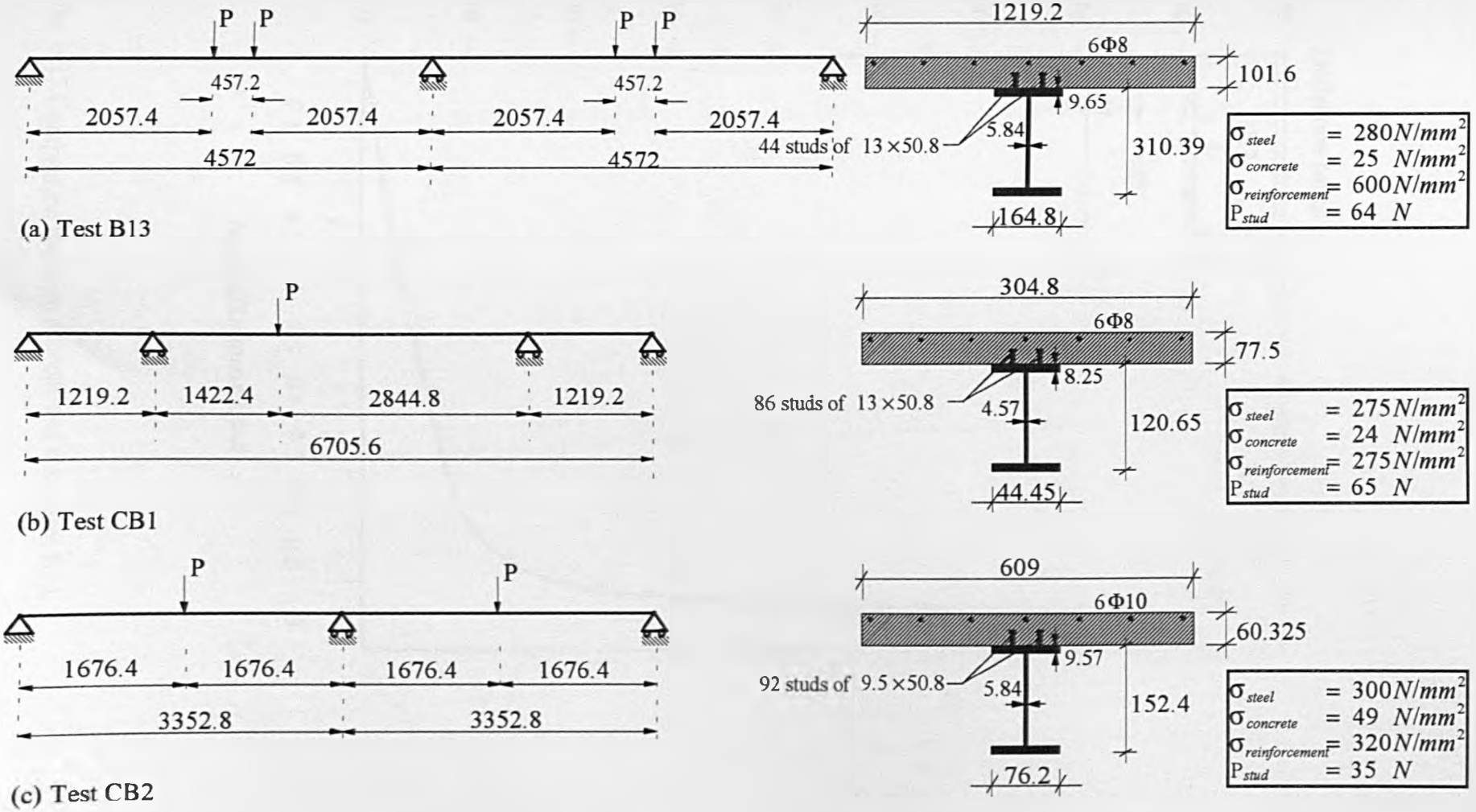

Fig. 6.26 Details of continuous beams used for validating partial interaction analysis.

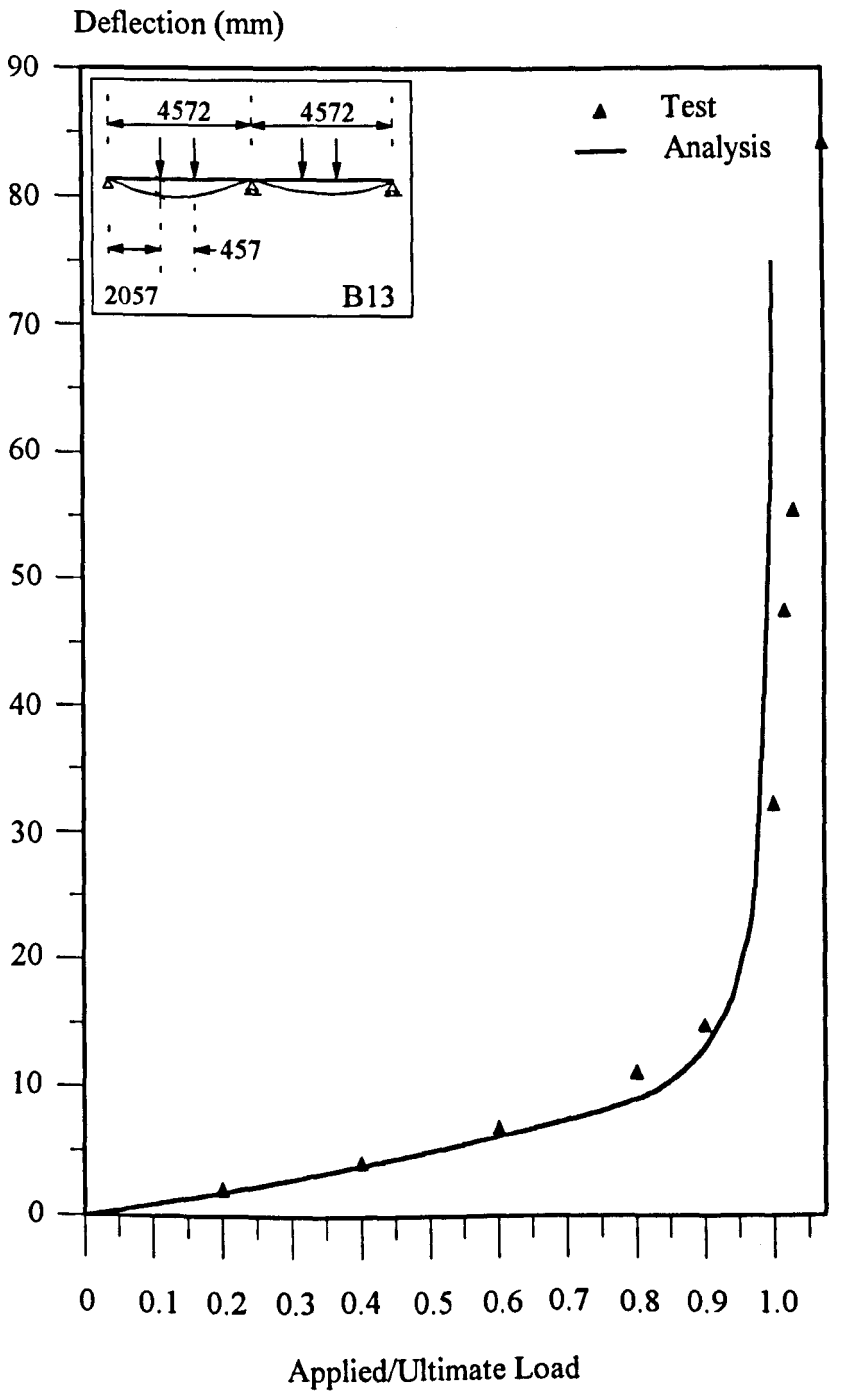

Fig. 6.27 Comparison between analysis and test beam B13.

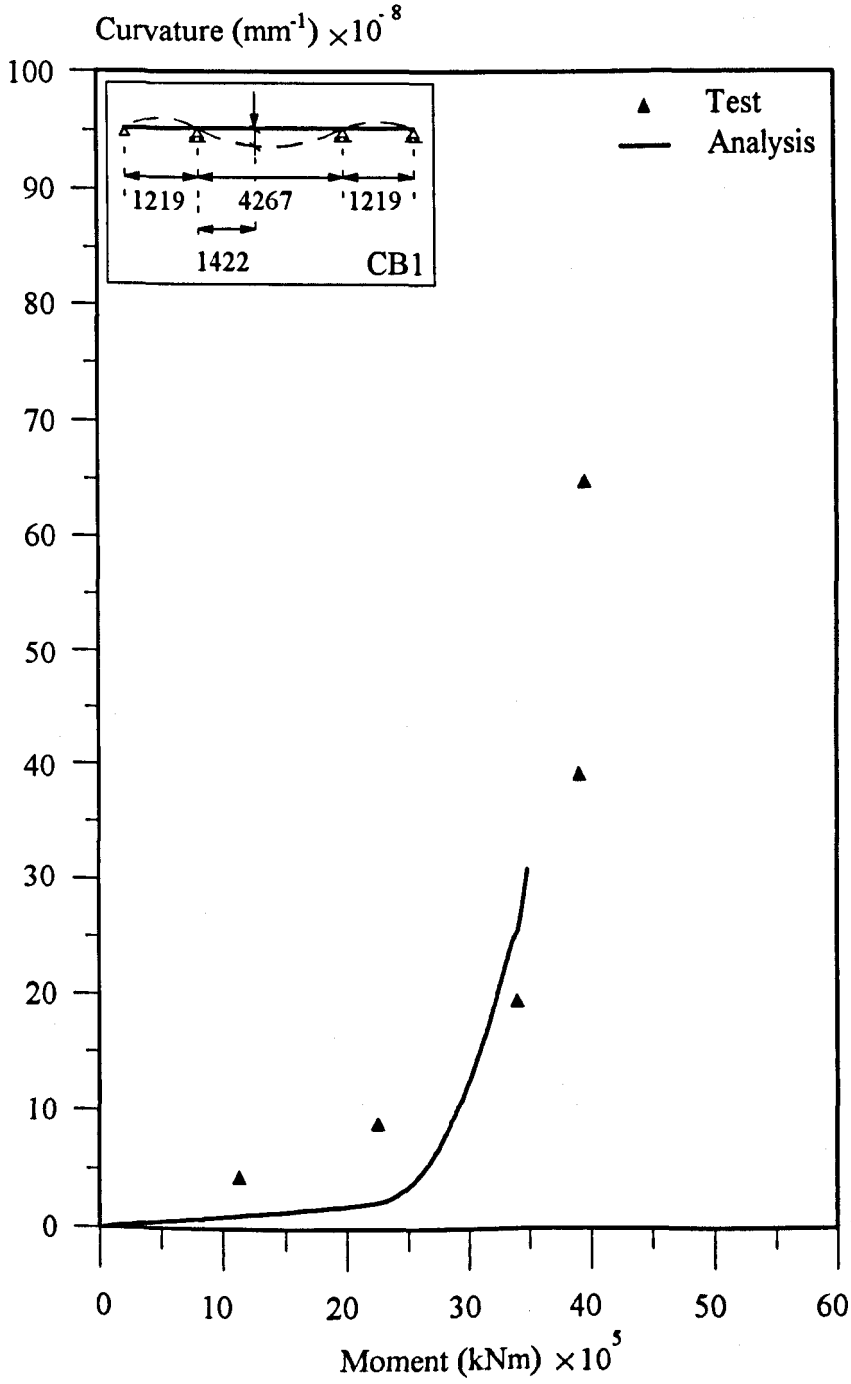

Fig. 6.28 Comparison between analysis and test beam CB1.

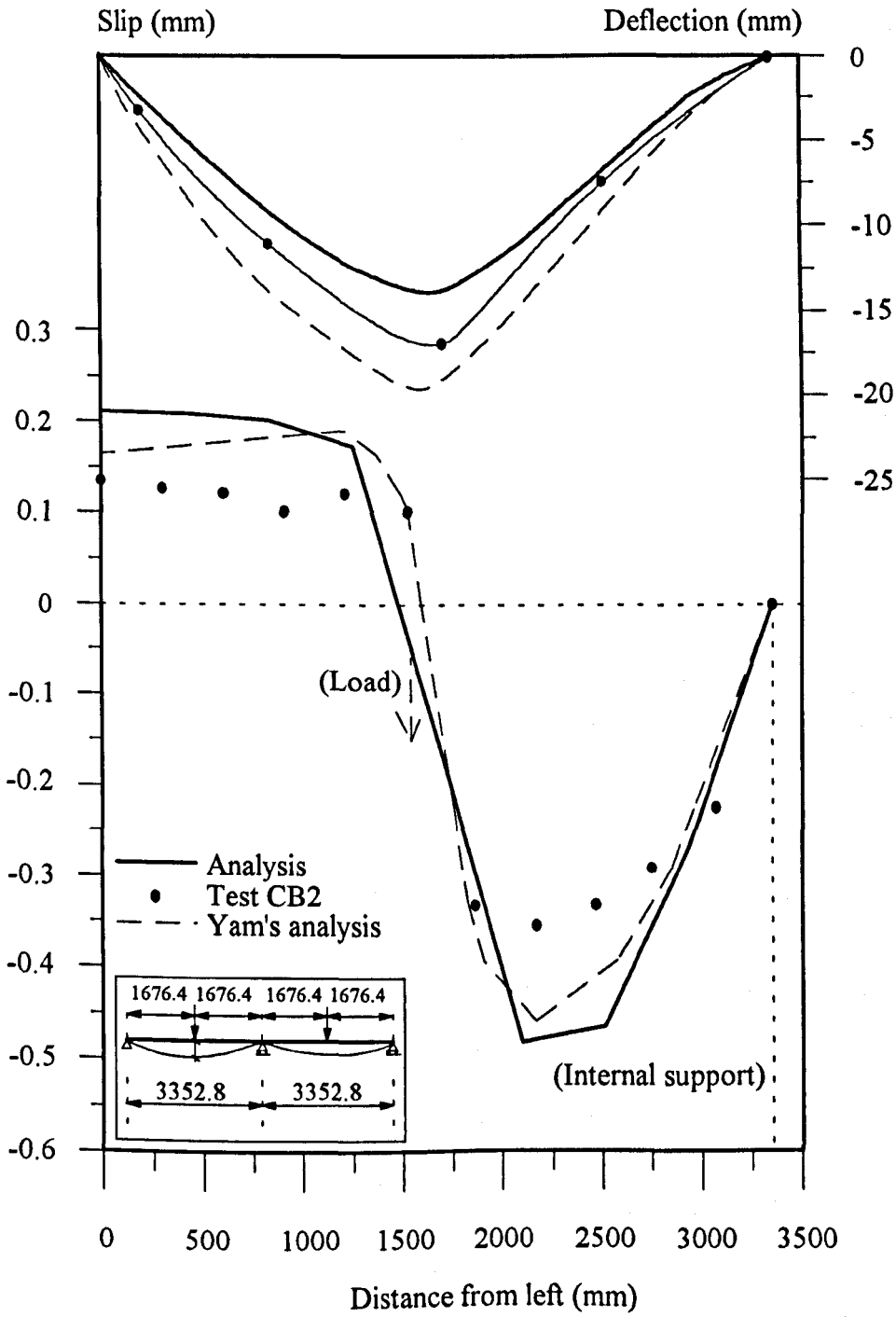

Fig. 6.29 Comparison between analysis and test beam CB2.

The test beam CB2 was also used by Yam and Chapman[149] to validate their analysis of composite beams with partial interaction. The experimental ultimate load of 150kN compares with predicted values of 139kN (current) and 137kN (Yam). Although both analyses underestimate the experimental ultimate load by 9%, the computed values from both analyses are consistent. The mode of failure was reported to be shear failure of the studs and this is also confirmed by the present analysis, since at 137kN the maximum computed slips exceed the plastic limit of 1.4mm. A complete load-deflection behaviour of this test was not available. Instead a deflection pattern along the length, at 120kN, was used for comparison as shown in Fig. 6.29. The maximum predicted deflections are 14mm (current) and 19.6mm (Yam) compared with a measured deflection of 17mm. The difference in predicted deflections may be attributed to the different material models used in the analyses. Moreover, 120kN corresponds to 88% of the failure load predicted by both analyses and a small increase in load at this level will result in a considerable increase in slip and hence deflection. As a consequence, it may concluded that although precise agreement between test and analyses cannot be achieved, the predicted deflection pattern from the present analysis compares satisfactorily with both the test and Yam's analysis.

6.3.2.2. Load-Slip Behaviour

In some of the tests referred to above the very small slip between the steel flange and the concrete slab which characterises partial interaction has been measured, both at the ends of the beam and along the span.

Figs. 6.30 and 6.31 show the predicted end slip-load behaviour compared with test results for simply supported beams A1, A3, A5, A6 and E1 respectively. As can be seen there is reasonable agreement between analytical and experimental data in all cases, despite the very small magnitude of the slips. In the case of test A6, the calculated end slips at failure are beyond the plastic limit of the studs, indicating stud failure. This is consistent with the test observations reported[60]. In tests A3 and A5 the studs are stressed beyond their elastic limit but they have not reached the plastic limit. This is consistent with analytical slips for test A3 but not for test A5 in which they are underestimated. The mode of failure for test A5 was reported to be simultaneous stud failure and crushing of the concrete[60]. However the analysis predicts that the concrete crushes before any significant shear slip occurs. This might be due to the fact that the force-slip characteristics of studs from push-out tests are different from that under bending conditions[66,68,70]. The observed failure mode for all other tests with a central load is concrete crushing, and as expected the end slips are much lower. The discrepancy at low load levels, for all tests, may be explained by the

underestimation of the shear rigidity of the cantilevers extending beyond the supports, and the difficulty in measuring small slips accurately.

The distribution of slip along the length of the beam was recorded for tests E1, U4 and U5. These are shown in Figs. 6.32 to 6.34 respectively together with the corresponding analytical results. The magnitudes of the slips are very small and precise agreement cannot be expected. The predicted slip patterns compare well with the tests in qualitative terms. For Test E1 the predicted slip pattern at 448.2kN, does not correlate well with Yam's analysis or test. This is because near failure a small increase in load causes a rather large increase in slip. As can be seen from Fig. 6.32, at 476kN predicted end slips are in much better agreement with test and Yam's analysis. In tests E1 and U4, the extra studs beyond the support clearly lead to a reduction in slip towards the beam ends, but the rate of reduction is not quite the same as those measured in tests. This may again be attributed to an underestimation of the shear rigidity of the cantilevers in the analysis. In test U5 the length of test beam U4 has been increased so that all studs lie within the span. As seen from Fig. 6.34, the slip does not reduce towards the ends, as was seen in the other cases. Both the analytical and experimental slips increase by flattening towards the support position. At load levels of 89.5kN and 179.5kN the predicted slip distribution compares very well with the test, while at 269kN the analysis predicts higher slips. This may be due to underestimation of slip modulus of the shear connectors at this load level.

No experimental slip measurements were reported for the continuous beams B13 and CB1, and hence only the analytical slip distributions are presented in Figs. 6.35 and 6.36 respectively. The slip distribution for test B13 is symmetrical about the centre support where the slip is zero. Maximum slip occurs at both ends, indicating that studs near the end supports are stressed beyond their elastic limit. The slip behaviour of Test CB1 is asymmetrical and the concrete slab in the left outer span moves to the right relative to the joist. However, the slip near the inner joints appears to change direction and not to give a clear pattern of slip progression. This may be attributed to the complex nature of slip distribution taking place in such beams. The predicted slip patterns indicate that the maximum slip occurs near to the load and that the shear connectors are stressed to levels well within their capacity.

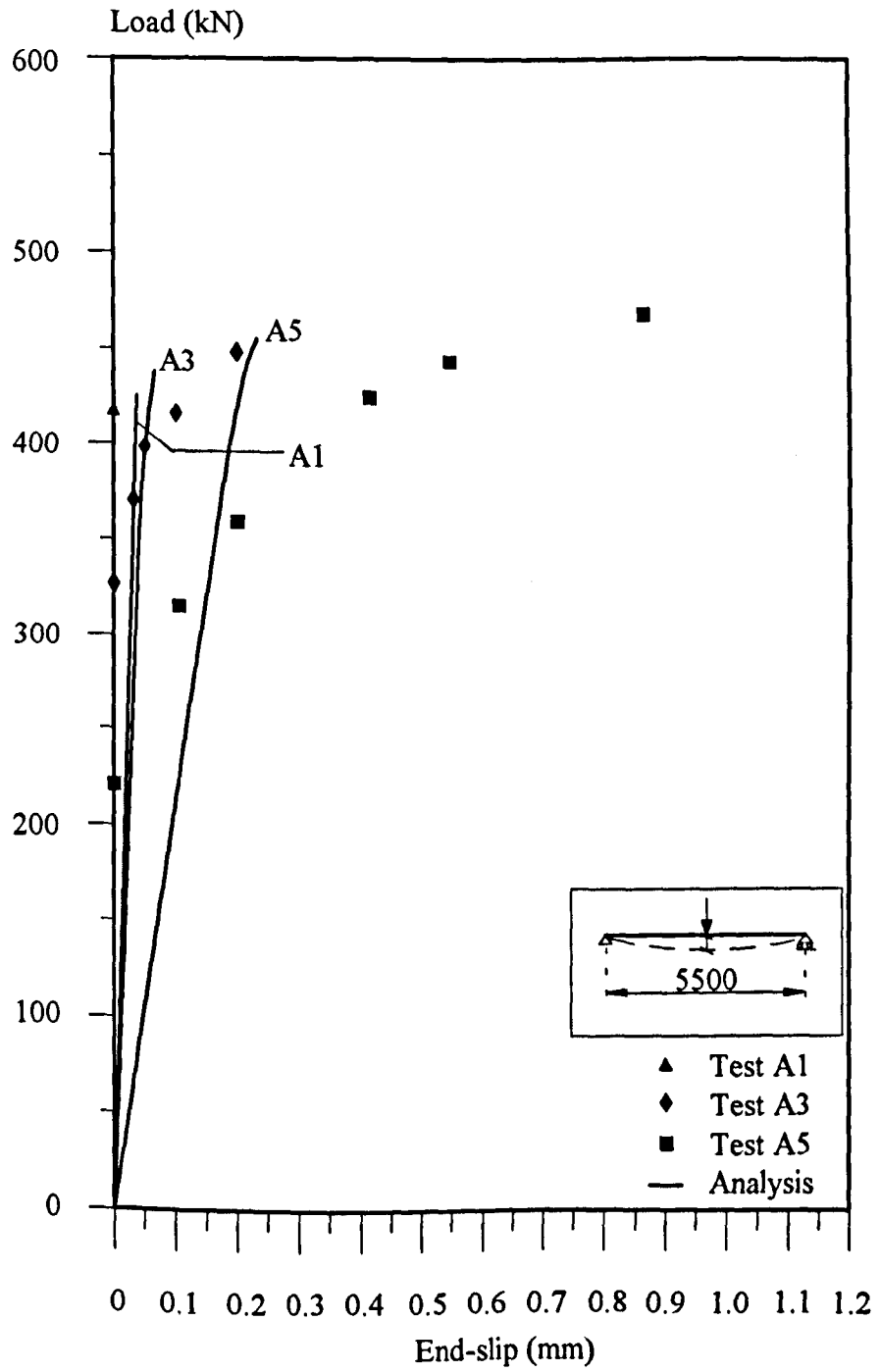

Fig. 6.30 Analytical and test load-end-slip behaviour for tests A1, A3 and A5.

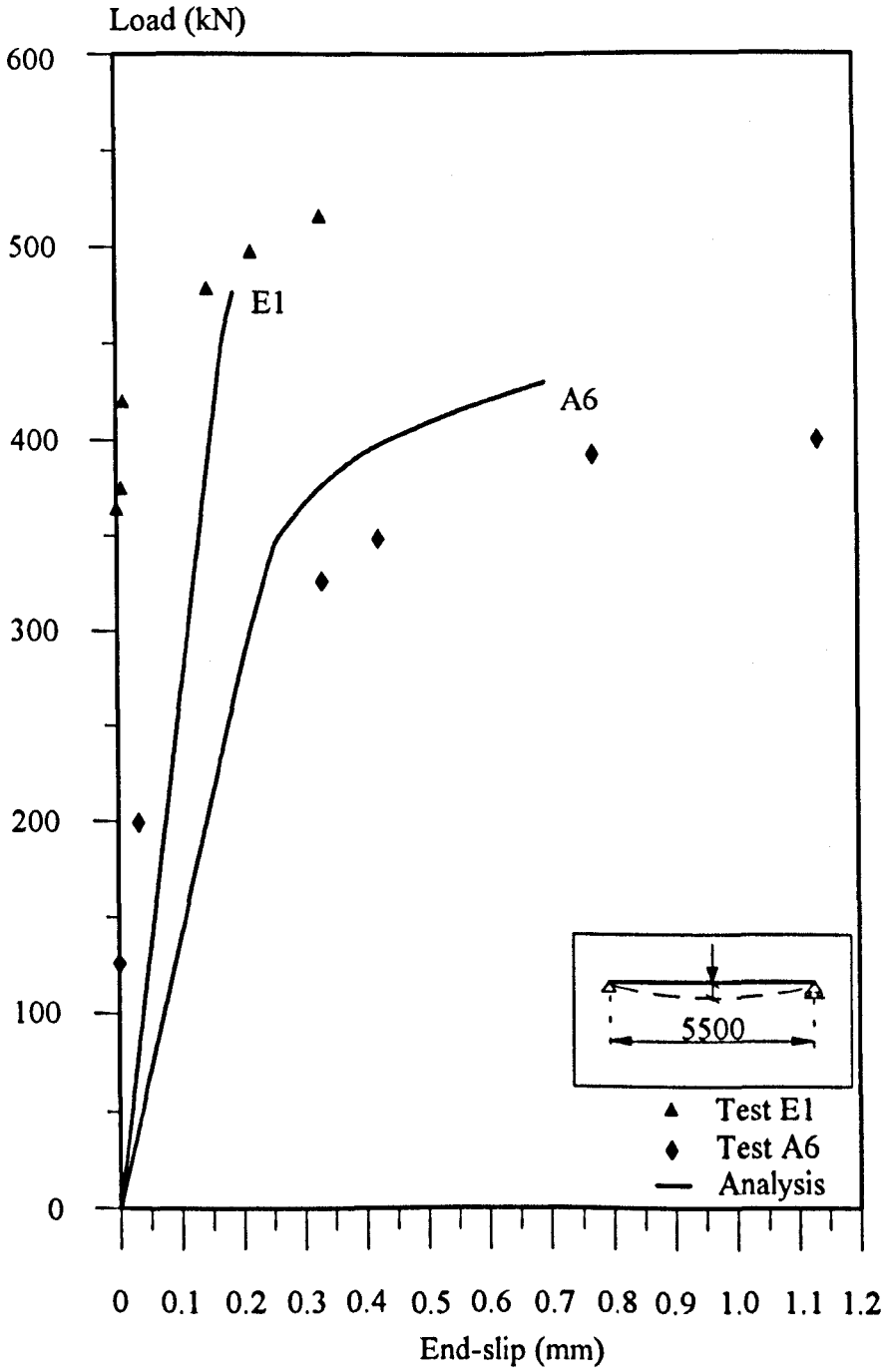

Fig. 6.31 Analytical and test load-end-slip behaviour for tests E1 and A6.

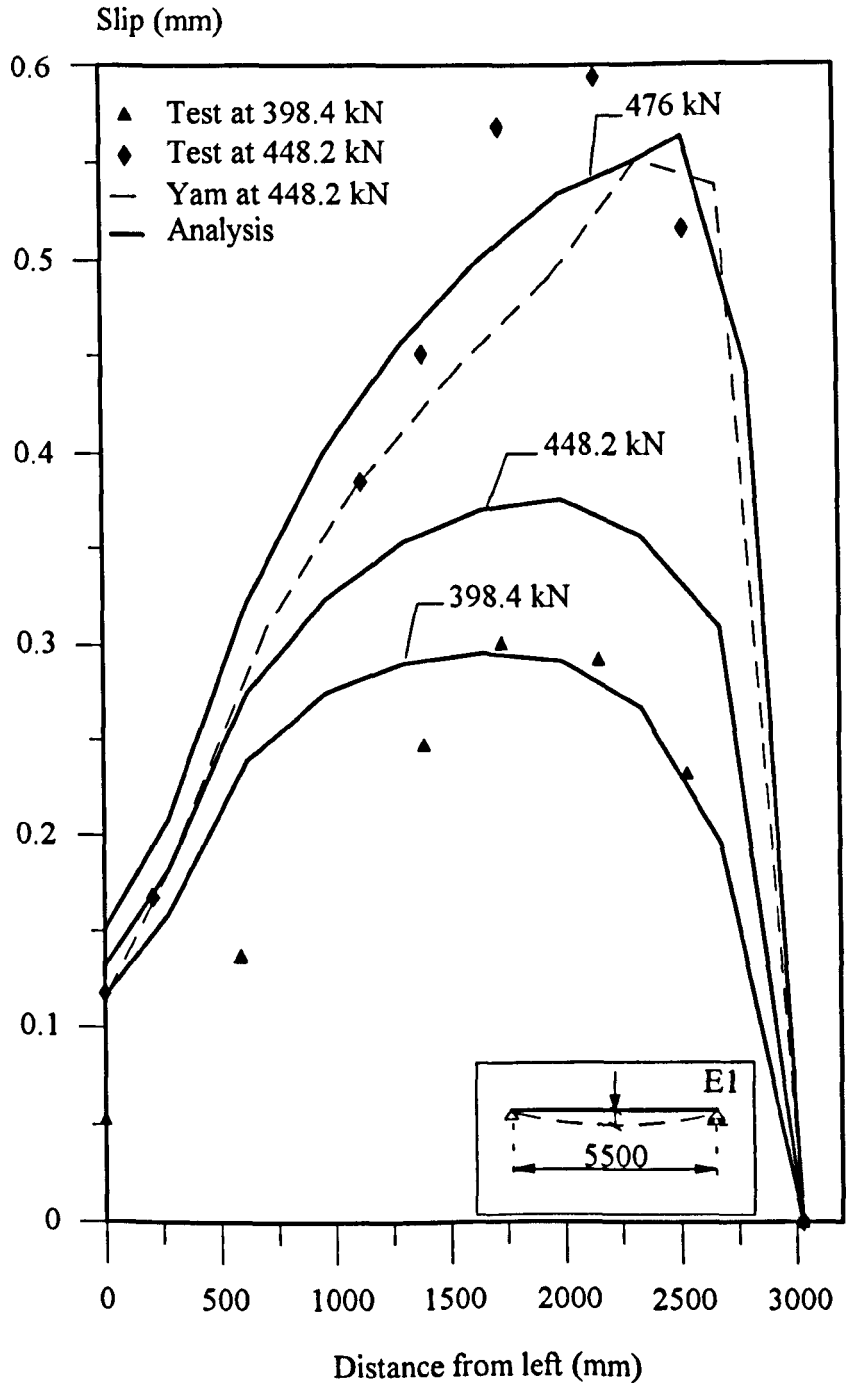

Fig. 6.32 Analytical and test slip distribution for test beam E1.

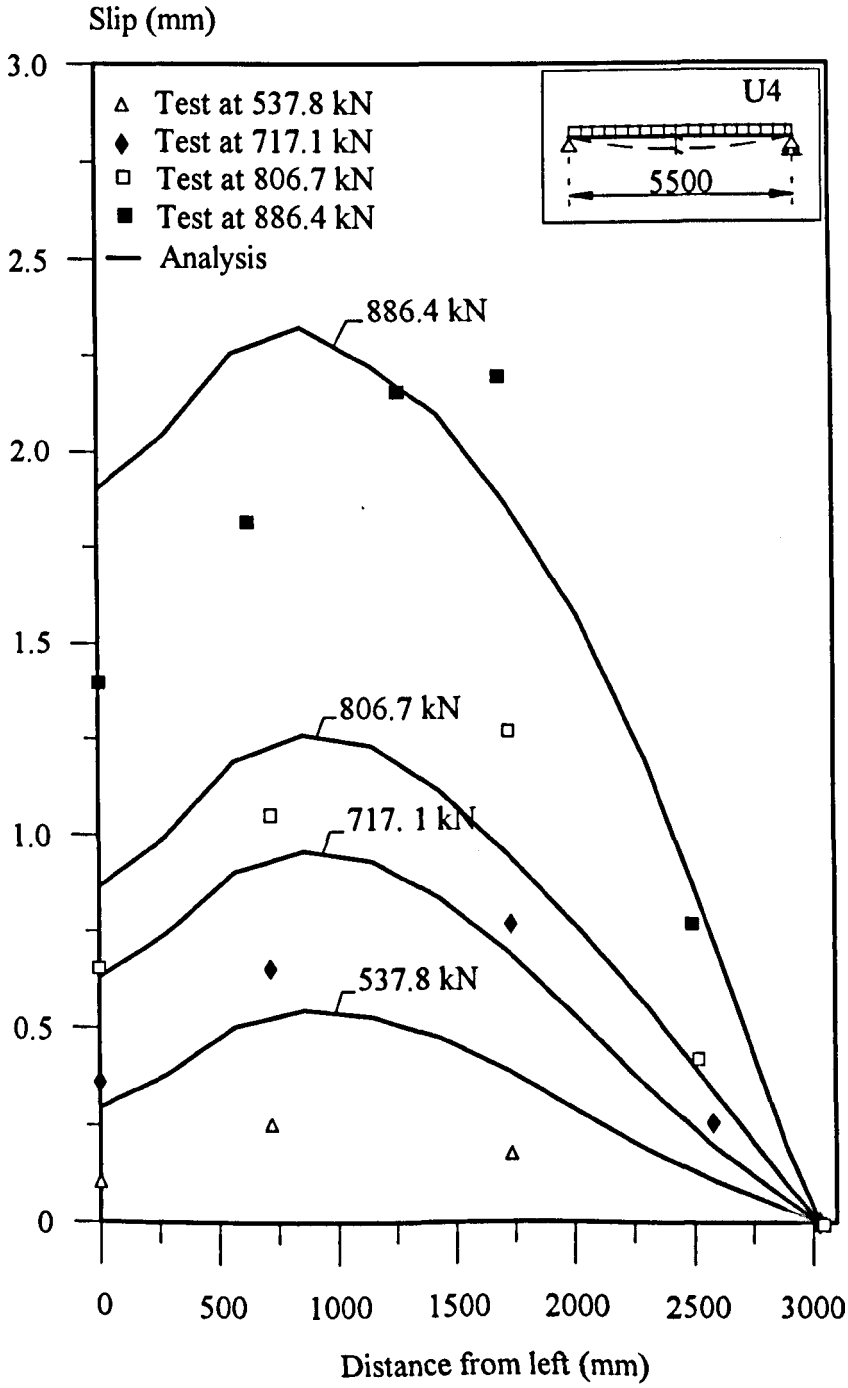

Fig. 6.33 Analytical and test slip distribution for test beam U4.

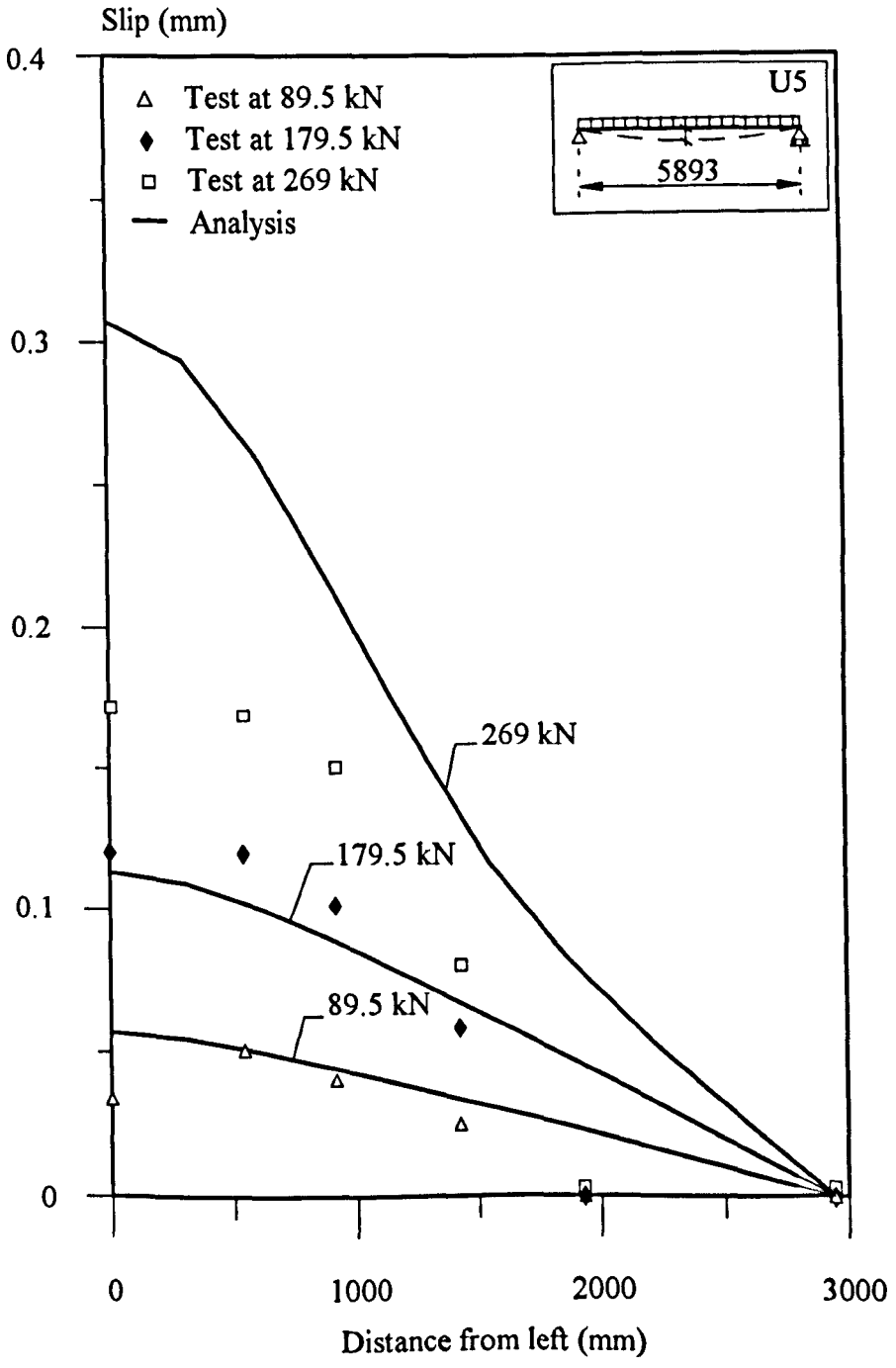

Fig. 6.34 Analytical and test slip distribution for test beam U5.

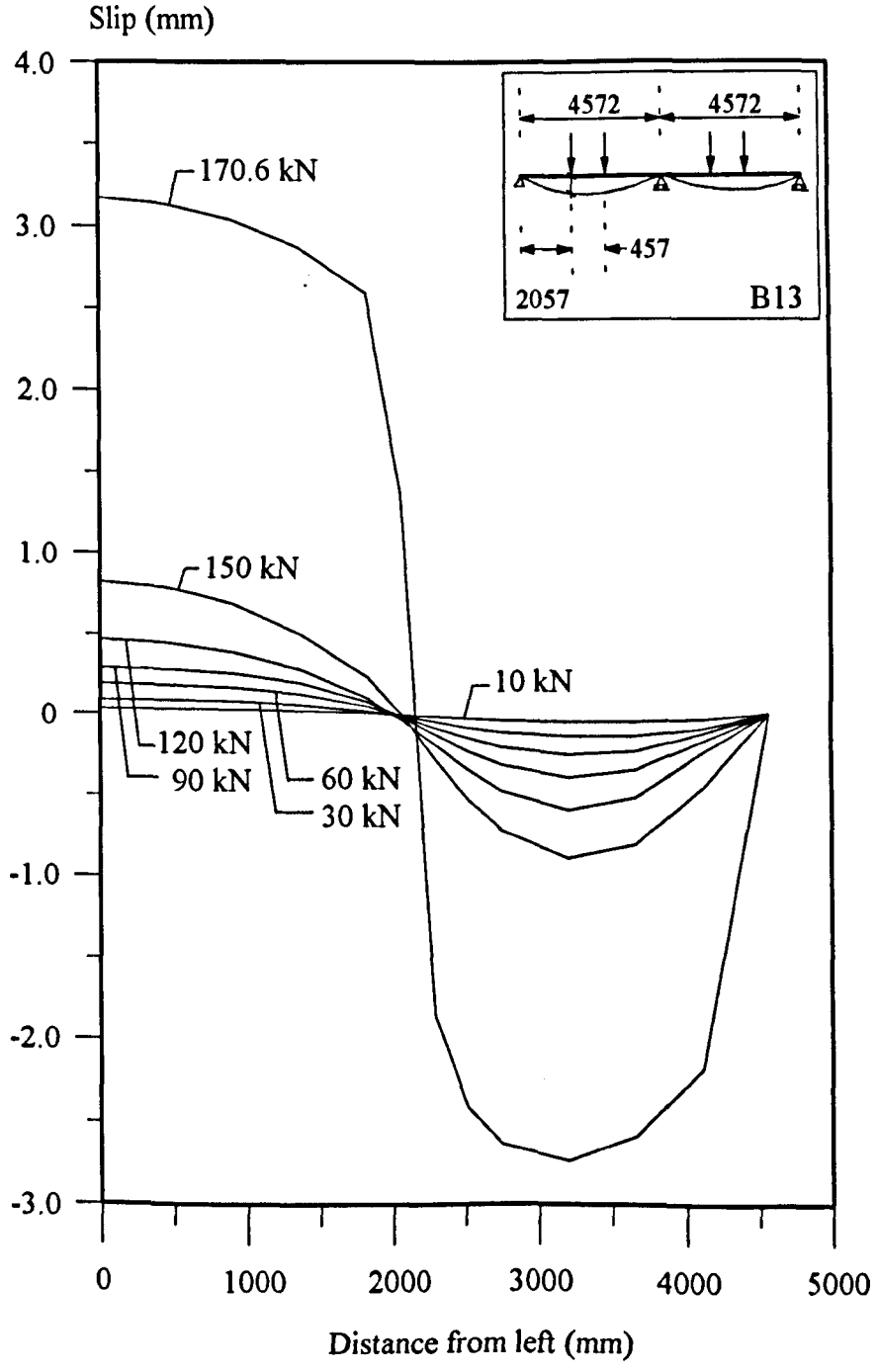

Fig. 6.35 Analytical slip distribution for test beam B13.

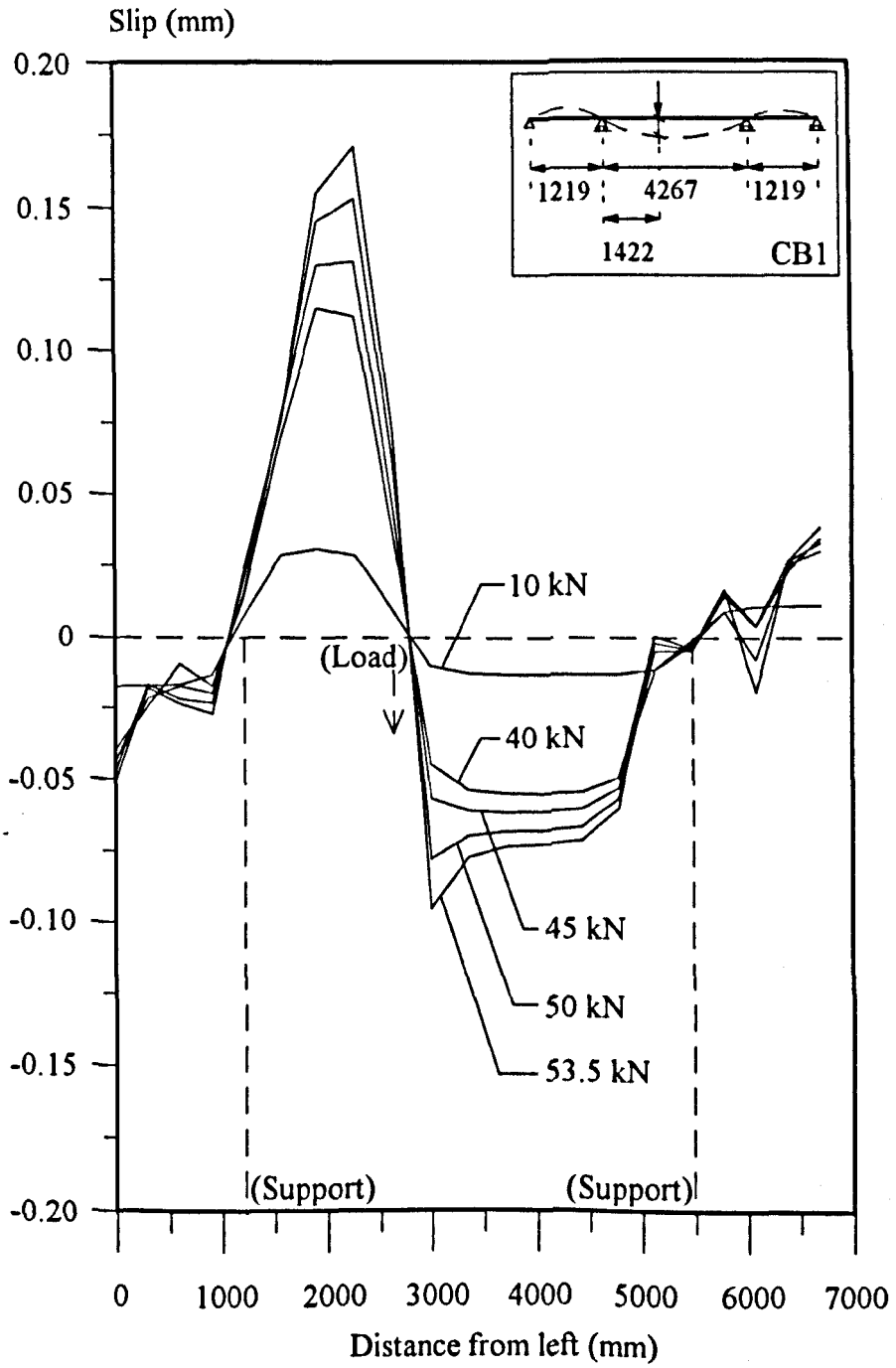

Fig. 6.36 Analytical slip distribution for test beam CB1.

The comparison between the experimental and analytical slip distribution at 120kN for test CB2 is presented in Fig. 6.29 together with predictions of Yam's analysis. The measured and computed slips from both analyses indicate that the maximum slip occurs at a distance 1153mm from the internal support in both spans near to the load. The present analysis predicts a maximum slip of 0.482mm, the computed slip by Yam's analysis is 0.46mm and the measured slip is 0.36mm. The agreement between analytical and test slips at the beam ends is also good with the present analysis and Yam's analysis predicting a slip of 0.21mm and 0.17mm respectively compared with a measured value of 0.14mm. Again the reason why both analyses overestimate the test may be that at this stage of loading the slips increase very rapidly and the accuracy in measuring these slips in tests may be affected. In general the correlation between the measured and computed slip values throughout the whole length of the span is very good and this gives confidence in the ability of the program to model complicated slip patterns.

The partial-interaction computer model cannot be considered as validated until it is compared with sufficient experimental and analytical data. However, the above comparisons with a variety of different test data show that the analysis gives consistent results. Although there is a lack of information on recorded slips, especially for continuous beams, the analysis appears to predict the deflection and slip behaviour at various load levels quite well. Discrepancies may be associated with the difficulty of measuring the very small slip deformations during a test, which therefore may not be entirely reliable. The results of push-out tests may also introduce some uncertainties if used as load-slip characteristics with the shear connectors stressed in bending under real conditions.

6.3.3. Partial Interaction Analysis with Semi-Rigid End Conditions

Generally beams are designed assuming fully rigid or pinned ends. However, in reality these idealised conditions are seldom achieved and the beam behaviour is not the same as initially designed for. The partial interaction program is capable of investigating the combined influence of slip and semi-rigid joints to give a more realistic insight into structural behaviour of composite beams.

In order to validate the computer model, three cruciform specimens consisting of two composite cantilevers 1500mm long as tested by Anderson and Najafi[118], and a single 7000mm long composite beam tested in a sub-frame by BRE[120] have been used for comparison. In all specimens the beam-to-column connection was a flush end plate and the concrete slab was cast on a metal deck. The partial interaction computer model, in its

present form, is not capable of analysing frames or composite beams with metal decks, and hence all analyses have been conducted on isolated cantilevers or beams with solid concrete slabs. The semi-rigid model used in the analyses is illustrated in Fig. 5.2(b). The moment-rotation characteristics of the rotational spring for the cruciform specimens are as shown in Fig. 6.37(a). For the BRE test however, these have not been specified and therefore the relationship for a flush end plate proposed by El-Rimawi[158] has been adopted. This is illustrated in Fig. 6.37(b). The stiffness of the axial spring is defined by the model shown in Fig. 5.5(c). Details of the specimens and material properties for both tests are shown in Fig. 6.38.

The experimental data for the cantilever beams was plotted as a moment-rotation relationship at the connection. For the purpose of comparison the analytical results are presented in a similar form in Fig. 6.39. The correlation between the test and predicted behaviour is excellent up to about 80% of the ultimate moment whereas for higher moments the analysis overestimates rotations. The predicted ultimate moment capacities for S4F and S12F are 170kNm and 292kNm respectively and compare very well with the corresponding test values of 175kNm and 300kNm. For test S8F however the agreement is less good. Analysis predicts a maximum moment capacity of 226kNm whereas the test moment is 250kNm, an underestimate of 12%. It was reported that in all tests the slip at the free end was negligible[118]. However the analysis indicates shearing of the studs at a moment of approximately 80% of the maximum test moment and it is this point that the test and analytical results start to diverge. This may be due to the fact that force-slip characteristics based on push-out tests underestimate the true behaviour in bending[68].

The experimental load-deflection behaviour, together with analytical predictions for the BRE composite beam (referred to as NR2) are shown in Fig. 6.40. Predicted deflections are in very good agreement with test deflections up to 200kN whereas beyond this load the test deflections increase much faster than predicted. The ultimate loads are 324kN (analysis) and 240kN (test). This discrepancy may be attributed to the excessive rotations of the column around the joint when the beam flanges contact the column flange. Indeed it was reported that both end plates yielded and deformed sufficiently for contact to be made between the lower flange of the beam and the column flange[120]. Another reason for this discrepancy might be the fact that the assumed moment-rotation characteristics used in the analysis overestimate the rotational stiffness of joint. It was also reported that there was extensive deformation of the studs close to the connection[120]. This is consistent with the predicted slip at the joint being beyond the plastic limit at failure.

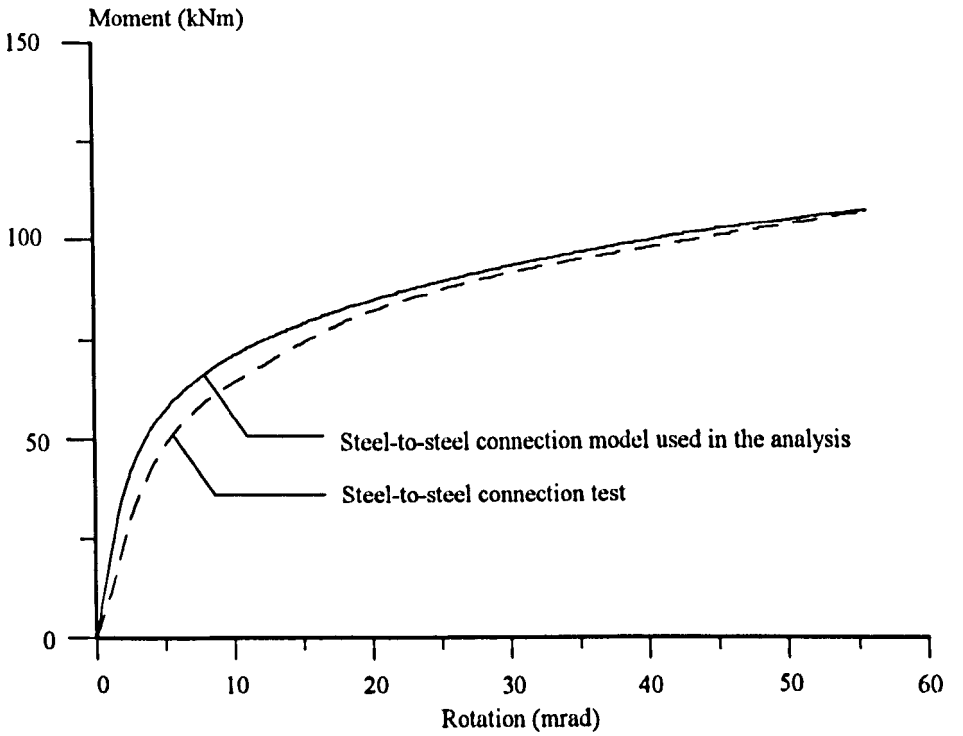

(a) Moment-rotation characteristics for test beams S4F, S8F and S12F.

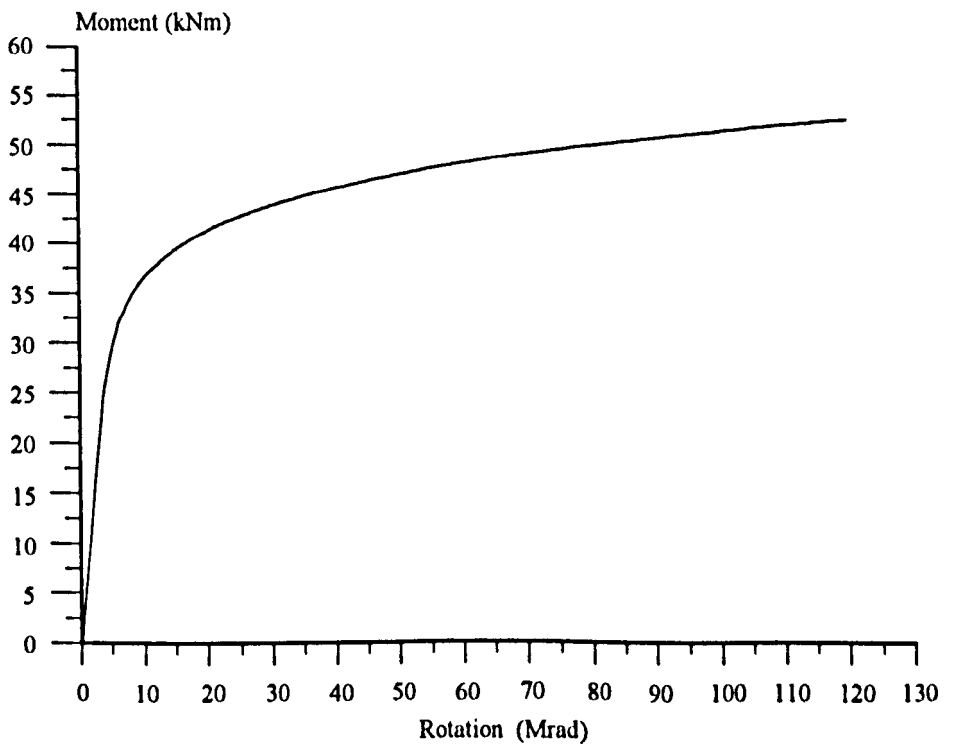

(b)Assumed moment-rotation characteristics used in the analysis of test beam NR2.

Fig. 6.37 Moment-rotation characteristics used for the semi-rigid connection model.

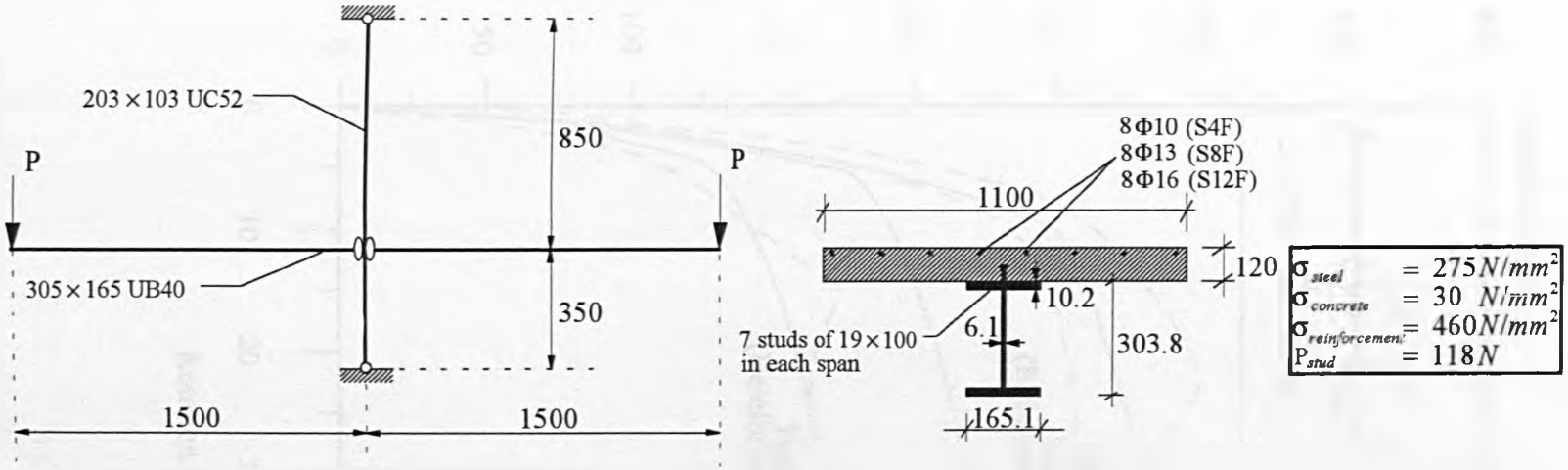

(a) Cruciform Tests

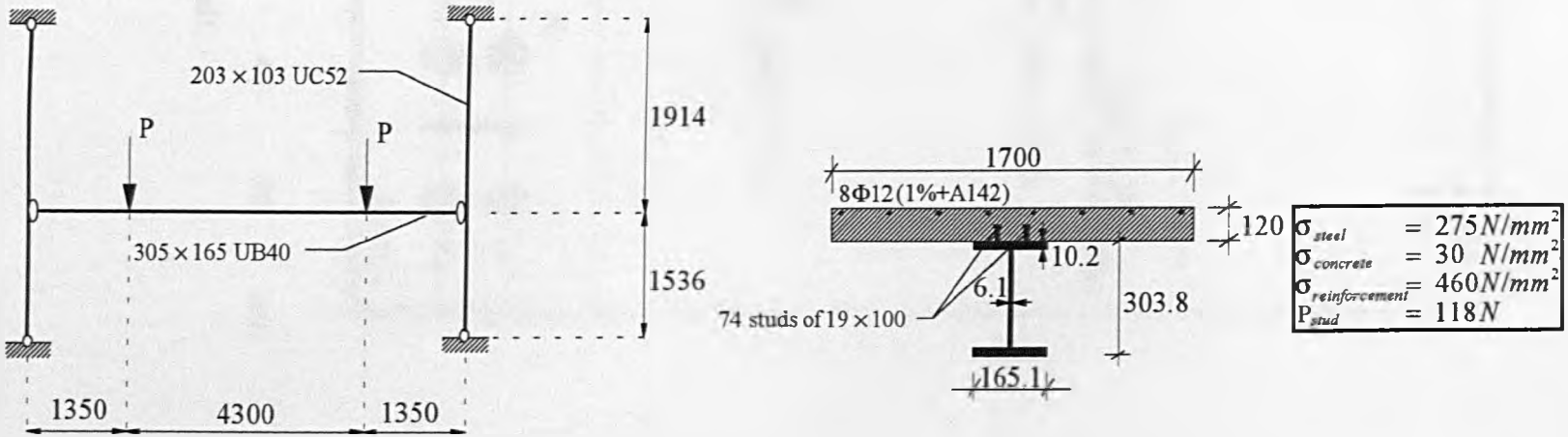

(b) BRE Test

Fig. 6.38 Details of semi-rigid beams used for validating partial interaction analysis.

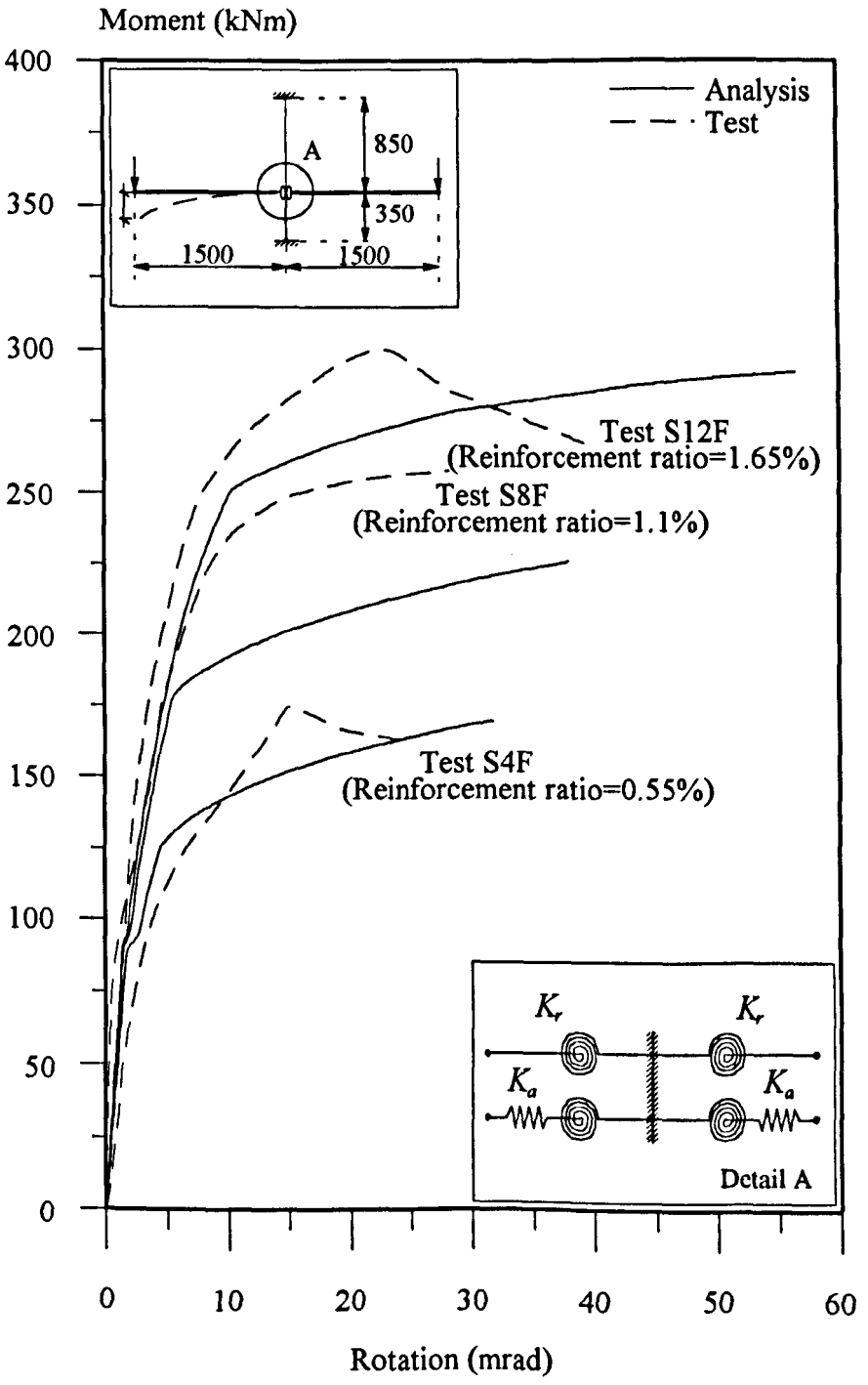

Fig. 6.39 Comparison between analysis and semi-rigid joint tests S4F, S8F and S12F.

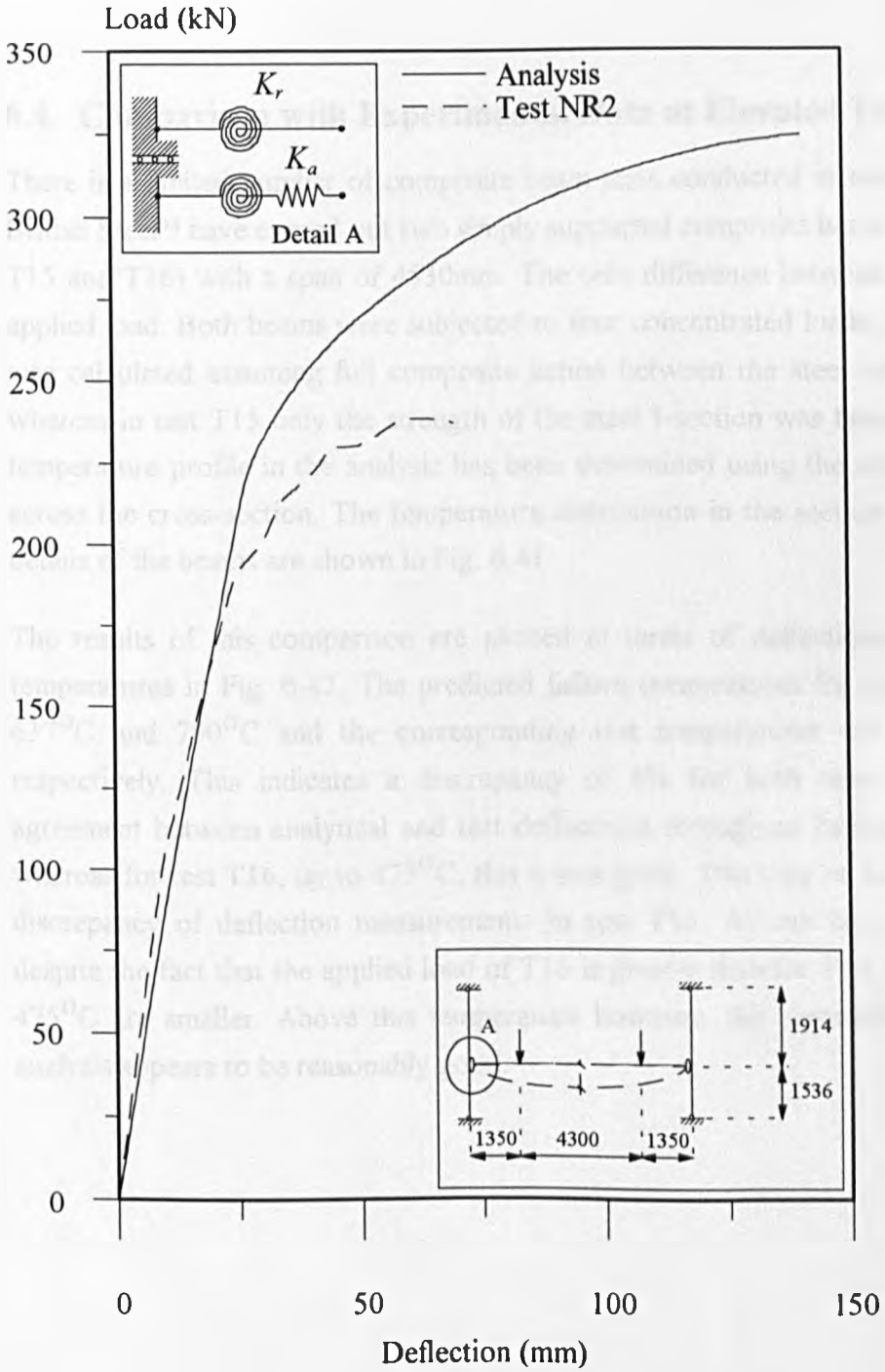

Fig. 6.40 Comparison between analysis and semi-rigidly connected test beam NR2.

Given the uncertainties associated with the modelling of stud behaviour and connection characteristics the partial interaction analysis with semi-rigid connections compares sufficiently well with previously published test data and therefore justifying its use for further analytical studies.

6.4. Comparison with Experimental Data at Elevated Temperatures

There is a limited number of composite beam tests conducted at elevated temperatures. British Steel[94] have carried out two simply supported composite beam tests (referred to as T15 and T16) with a span of 4530mm. The only difference between these tests was the applied load. Both beams were subjected to four concentrated loads. In test T16 the load was calculated assuming full composite action between the steel and the concrete slab whereas in test T15 only the strength of the steel I-section was taken into account. The temperature profile in the analysis has been determined using the recorded temperatures across the cross-section. The temperature distribution in the section together with other details of the beams are shown in Fig. 6.41.

The results of this comparison are plotted in terms of deflections and bottom flange temperatures in Fig. 6.42. The predicted failure temperatures for test T16 and T15 are 637^{o}C and 790^{o}C and the corresponding test temperatures are 666^{o}C and 762^{o}C respectively. This indicates a discrepancy of 4% for both tests. For test T15, the agreement between analytical and test deflections throughout heating is also very good whereas for test T16, up to 475^{o}C, this is less good. This may be attributed to the slight discrepancy of deflection measurements in test T16. As can be seen from Fig. 6.42, despite the fact that the applied load of T16 is greater than for T15, the deflections up to 475^{o}C are smaller. Above this temperature however, the correlation between test and analysis appears to be reasonably good.

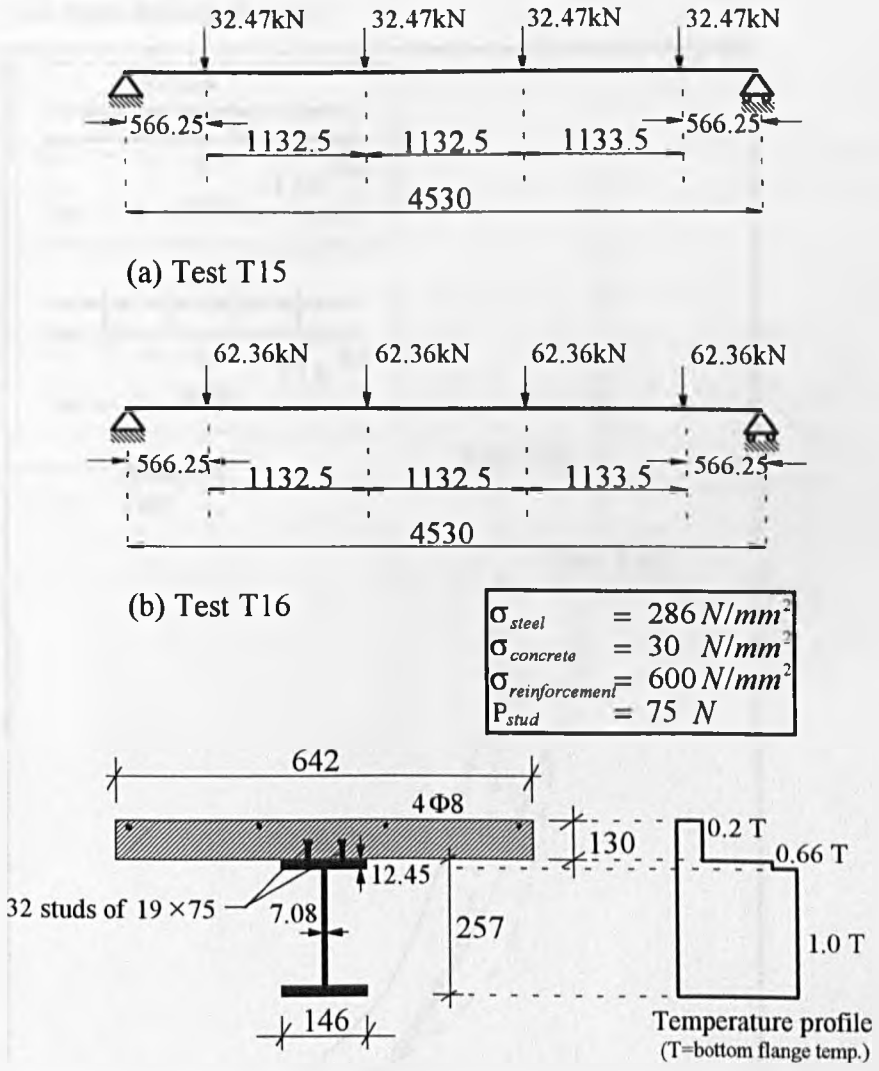

Fig. 6.41 Details of beams used for validating partial interaction analysis at elevated temperatures.

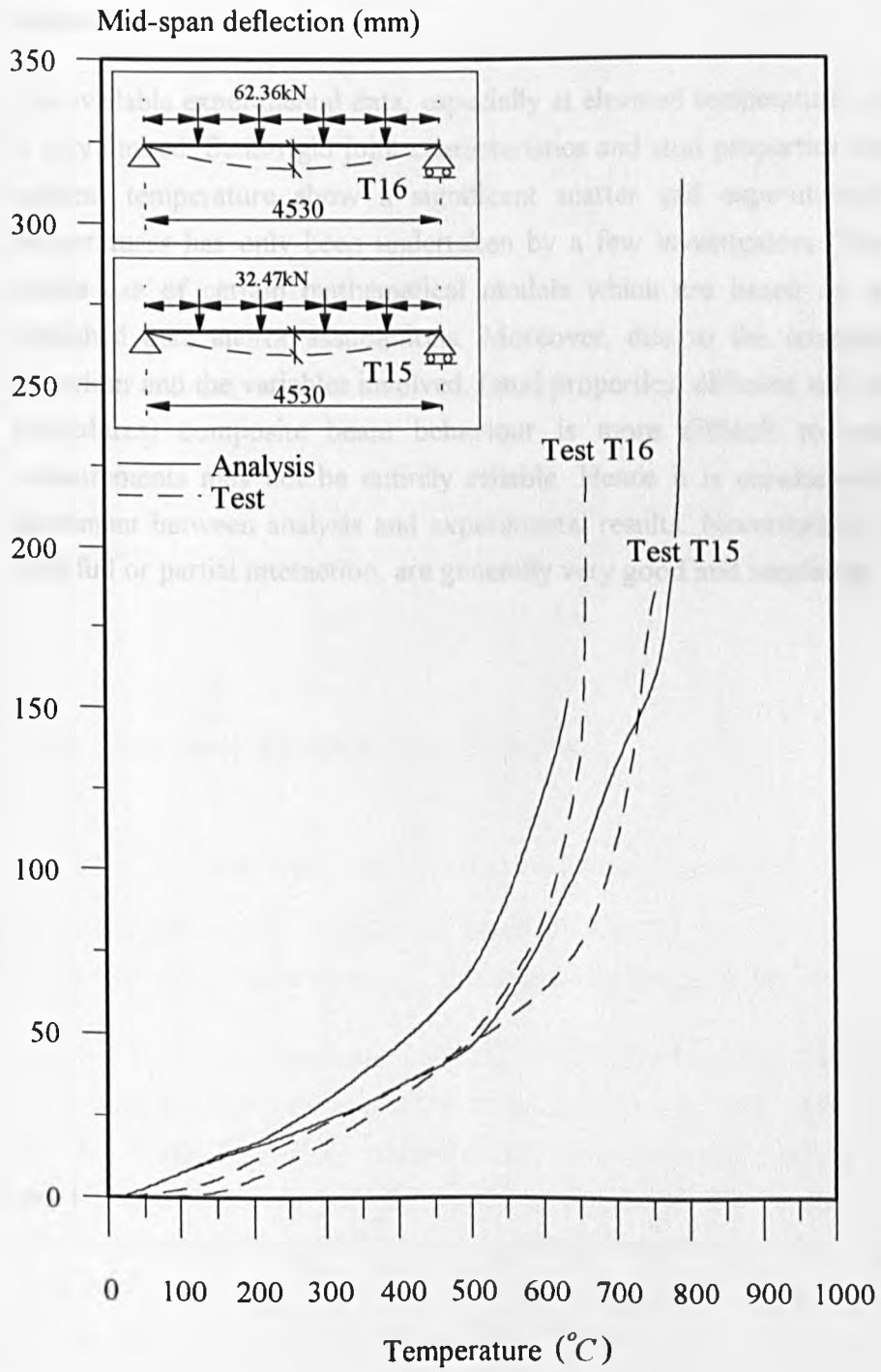

Fig. 6.42 Comparison between analysis and test beams T15 and T16.

6.5. Concluding Remarks

The convergence studies using both full and partial interaction analyses indicate that two elements are sufficient for representing the simply supported beam and four elements for representing the fixed ended or continuous beam. If too many elements are used the Gauss points along an element can become too closely positioned, leading to numerical instability.

The available experimental data, especially at elevated temperatures, on composite beams is very limited. Semi-rigid joint characteristics and stud properties from push-out tests at ambient temperature show a significant scatter and experimental work at elevated temperatures has only been undertaken by a few investigators. The program therefore makes use of certain mathematical models which are based on a limited amount of published data and/or assumptions. Moreover, due to the complexity of the material behaviour and the variables involved, (stud properties, different end conditions and testing procedures) composite beam behaviour is more difficult to monitor and the test measurements may not be entirely reliable. Hence it is unreasonable to expect perfect agreement between analysis and experimental results. Nevertheless, the comparisons for both full or partial interaction, are generally very good and consistent.

CHAPTER 7. PARAMETRIC STUDIES

7.1. Introduction

The studies in this chapter concentrate mainly on elevated temperature behaviour although some preliminary studies have been conducted at ambient temperature. Where appropriate, comparisons between fully and partially composite beam behaviour are included. The studies are divided into four categories:

1. The influence of shear connectors,
2. The influence of connection rigidity,
3. The influence of different temperature profiles,
4. The influence of reinforcement.

In most cases the beams used in these examples represent the typical main and secondary beams used in the large building test facility[110] constructed by BRE at Cardington as shown in Fig. 6.2.

7.2. Ambient Temperature Studies

7.2.1. The Effect of Number of Shear Connectors

The influence of the number of shear connectors has been investigated at ambient temperature for a 6m long simply supported beam and a 1.5m cantilever (Fig. 7.1).

Fig. 7.2 shows the predicted load-deflection behaviour for the simply supported beam with varying number of connectors ranging from 1 to 100. Also shown for comparison are the results from fully composite and non-composite analyses. The non-composite beam fails at 200kN and the fully composite beam at 480kN. As expected the results of the partial interaction analyses lie between these two extreme cases and the load-deflection paths progress steadily from non-composite to fully composite behaviour as the number of shear connectors is increased. The predicted failure load is most sensitive to the changes in the number of shear connectors between 10 and 25. Increasing the shear connectors beyond 75 or reducing them below 10 has little effect on the predicted ultimate loads.

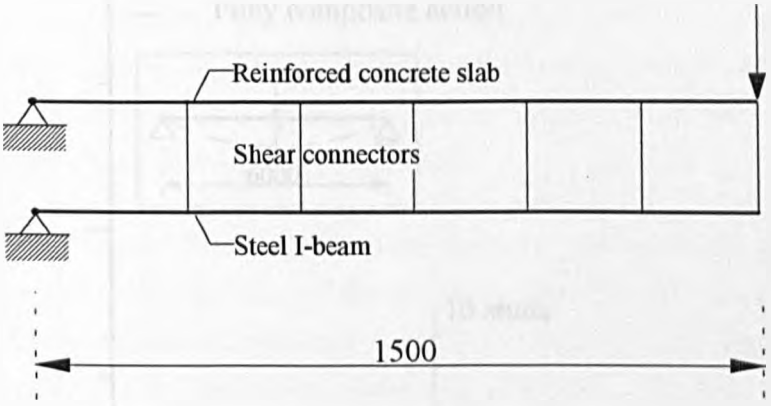

(a) Finite element representation of the cantilever beam

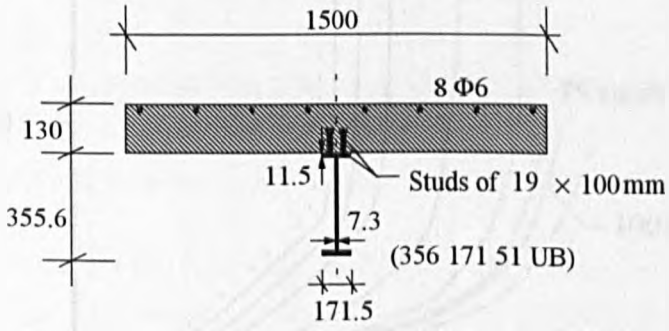

(b) Cross-sectional details of the cantilever beam

Fig. 7.1 Details of the cantilever beam.

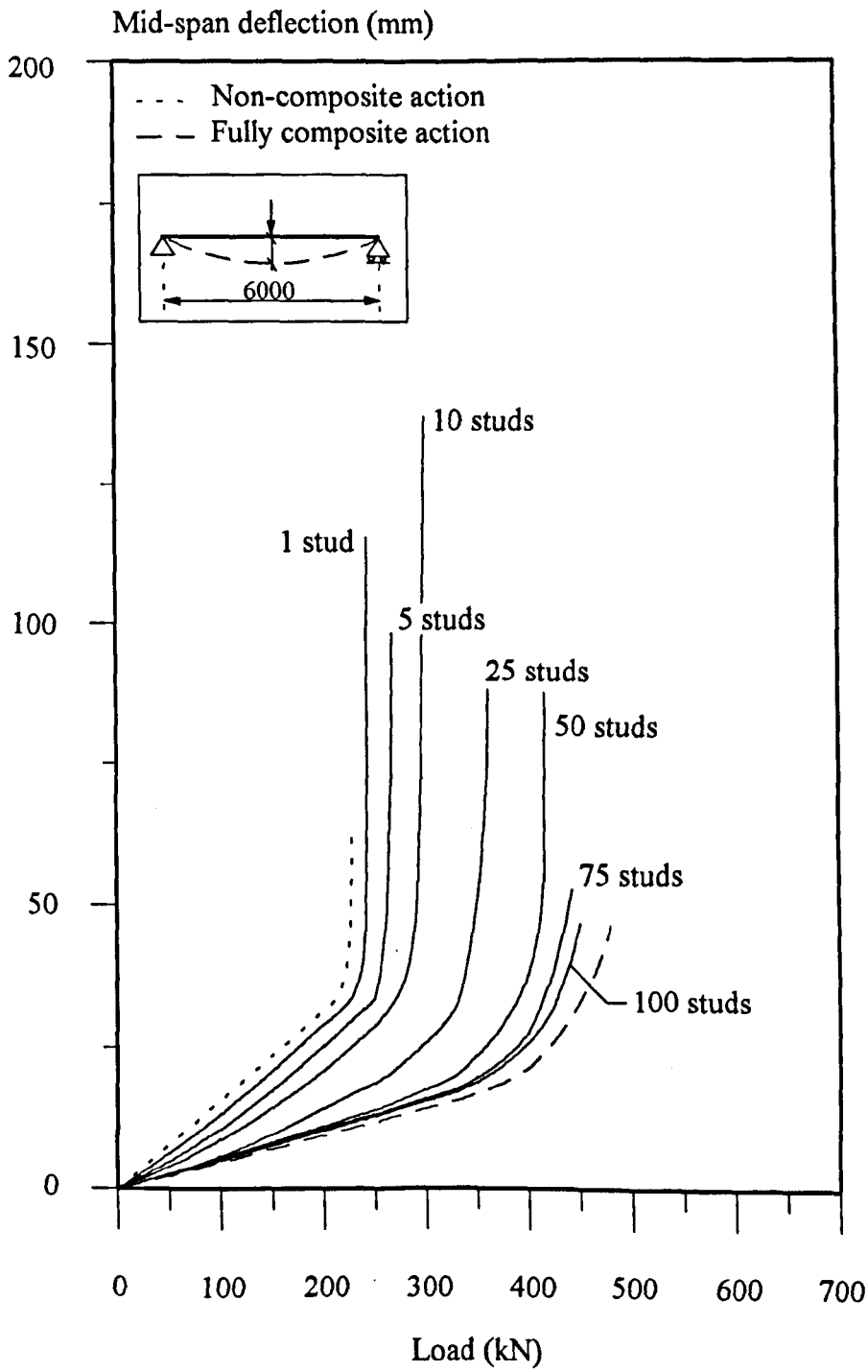

Fig. 7.2 The effect of number of studs on the behaviour of a simply supported beam.

Fig. 7.3 shows the effect of increasing the number of shear connectors on the load-deflection behaviour for the cantilever. A cantilever beam that is free to rotate at its support is unstable but in this case stability is afforded by the longitudinal shear strength between the two line elements used in the partial interaction model. The failure of this type of beam is dictated largely by the strength of the studs and it is therefore a useful example for examining this failure mode.

On the basis of this simplified representation, there are two possible modes of failure, namely, shearing of the studs and cracking of concrete in tension. For modest degrees of shear connection - fewer than 10 studs along the length - the failure mode was found to be the fracture of the studs. The failure load for 10 studs is 100kN and for fewer studs the failure load decreases in proportion.

If more than 10 studs are used, fracture of the studs is avoided and the failure mode becomes the cracking of the concrete slab followed by yielding of the reinforcing bars. The predicted ultimate load at which the concrete slab fails and instability occurs is 111kN regardless of how many additional studs are used. This is confirmed by considering a simple model in which the concrete slab and steel beam are subject to equal and opposite axial forces, compression and tension respectively. This system constitutes a couple which is equal to the applied bending moment. The minimum number of studs required to avoid shear failure can be determined by equating the shear force in the studs to the tensile force in the concrete. In this case it was found that a minimum of 10 studs was needed. The corresponding ultimate load for 10 studs was then calculated to be 105kN. Furthermore plastic analysis assuming the concrete is under pure tension and the steel section under pure compression was also used to determine the load level at which the concrete slab cracks in tension. This was found to be 112kN. The analytical results appear to be consistent with these simple calculations.

Up to 75kN the load-deflection behaviour for the fully composite cantilever is stiffer than the partially composite conditions. Beyond this load the concrete slab cracks in tension and a sudden increase in deflections is observed. Compared with the partial interaction case the concrete cracks at a lower load because it is subject to greater stresses. However since the beam is fully restrained against rotation, the reinforcement and steel section continue to carry load as a non-composite beam. The ultimate load capacity is reached when the steel section at the support yields at 250kN.

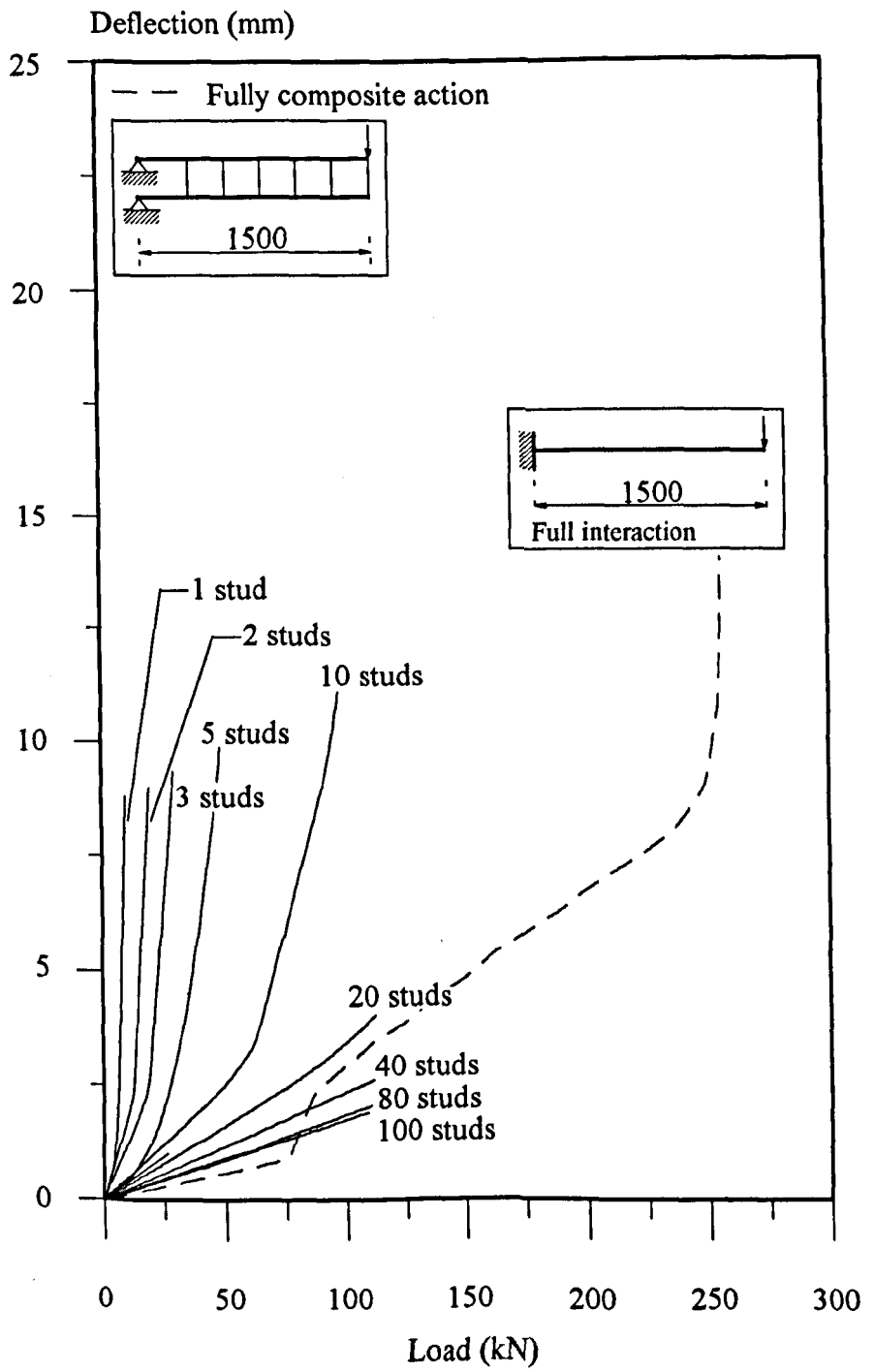

Fig. 7.3 The effect of number of studs on the behaviour of a cantilever beam.

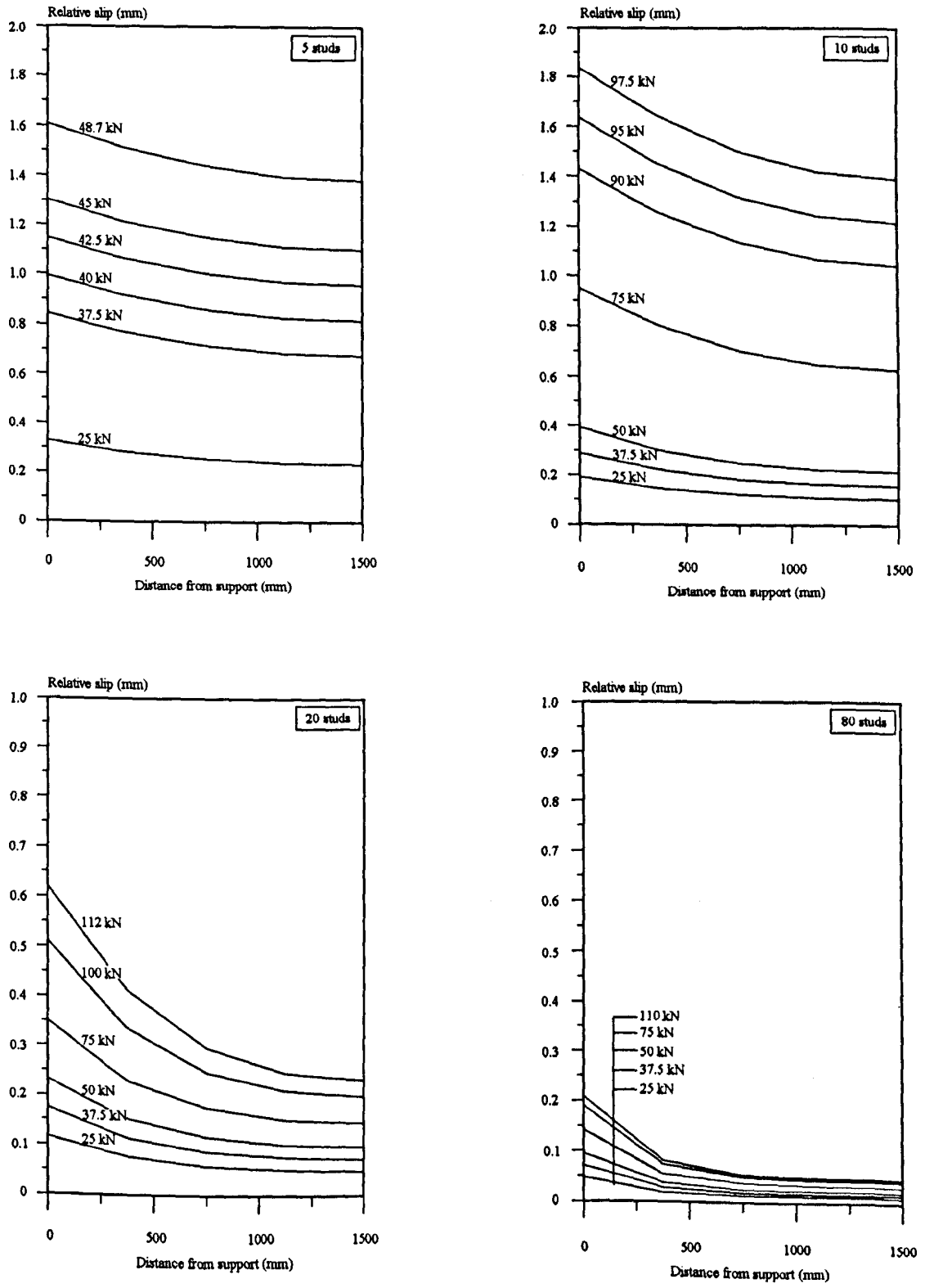

Fig. 7.4 The effect of number of studs on slip distribution for a cantilever beam.

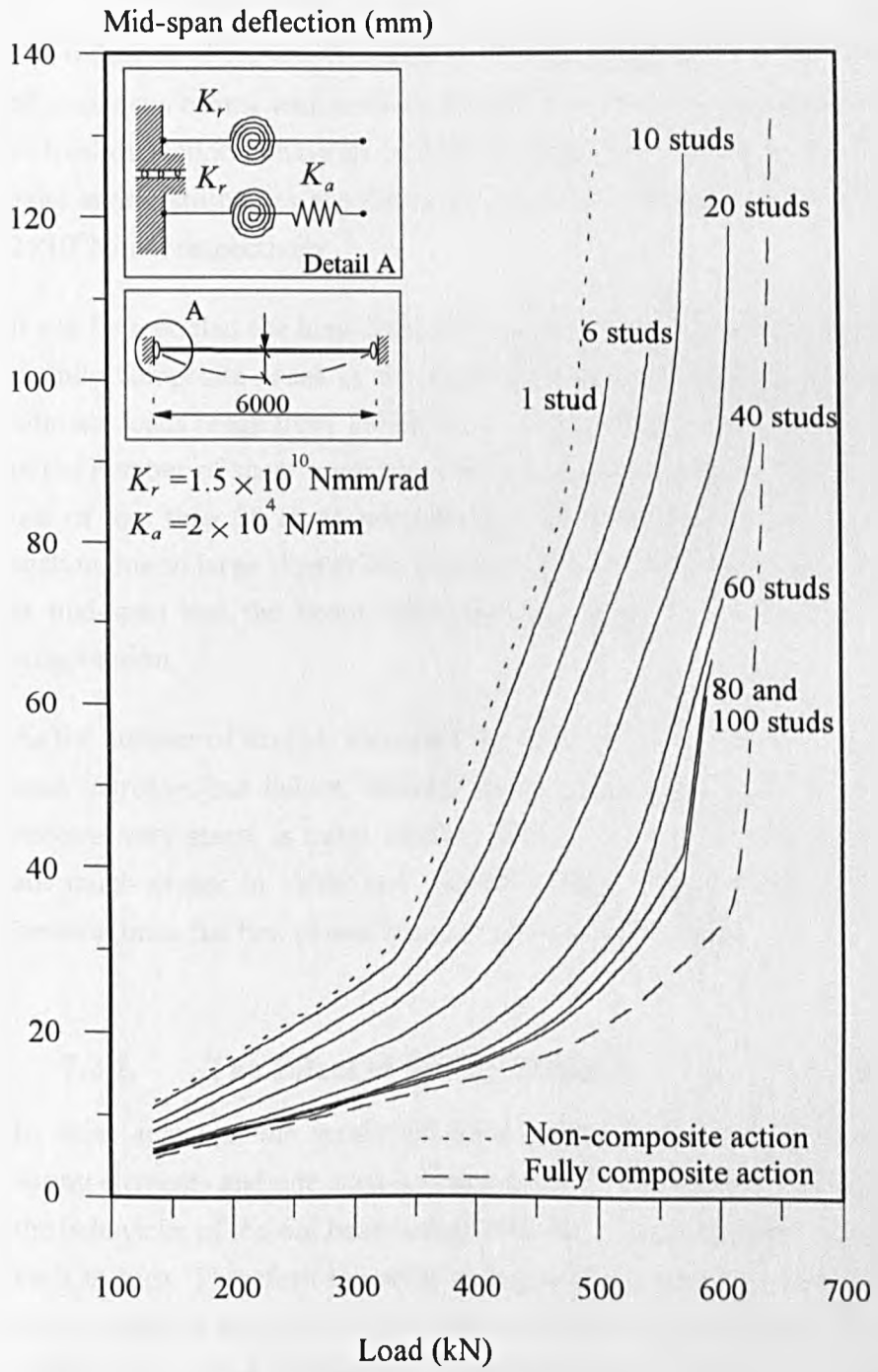

Fig. 7.5 The effect of number of studs on the behaviour of a semi-rigid beam.

The slip distributions along the length at various load levels for 5, 10, 20 and 80 studs are shown in Fig. 7.4. The slip distribution for stiffer shear connections varies significantly with greater slip at the support and very little slip near to the free end. In contrast the slip distribution for weaker shear connections is more linear with very large slips along the length of the beam.

The influence of varying the number of shear connectors on the load-deflection behaviour of composite beams with semi-rigid joints has also been examined and the results, in terms of load-deflection behaviour for the 6m beam, are shown in Fig. 7.5. The rotational and axial spring stiffnesses are kept constant with stiffness values of 1.5×10^{10}Nmm/rad and 2×10^{4}N/mm respectively.

It can be seen that the load-deflection paths progress consistently from the non-composite to fully composite cases as the number of shear connectors is increased. The predicted ultimate loads range from 511kN for a single stud to 630kN for 40 studs. Further increase in the number of shear connectors results in only negligible increase in ultimate load. The use of less than 20 studs prevents the full utilisation of the strength of the composite section due to large slips at the interface. For all cases failure is initiated by a plastic hinge at mid-span and the beam fails when the steel I-section yields at the support under compression.

As the number of studs is increased the load level at which the plastic hinge forms at mid-span increases but failure, defined by the point when the load-deflection curve start to become very steep, is more sudden. This is because the mid-span and support moments are much closer in value and therefore there is less opportunity for redistribution of bending once the first plastic hinge at mid-span is formed.

7.2.2. The Effect of Spring Stiffness

In these analyses, the semi-rigid joint model shown in Fig. 5.2(b) with two rotational spring elements and one axial spring was used. The influence of these spring stiffnesses on the behaviour of the 6m beam using 100, 40, 20 and 10 studs was investigated by varying each in turn. Therefore the axial spring stiffness was kept constant while the rotational spring stiffness was varied from zero to a very large numerical value (10^{20}Nmm/rad). The study was repeated by fixing the rotational spring stiffness to a maximum and varying the axial spring stiffness from zero to 10^{20}N/mm.

Results for varying rotational spring stiffness and using 100 studs along the length are presented in Fig. 7.6 in terms of load-deflection. This shows that when the beam is fully

restrained against rotation the predicted failure load is 777kN. Reducing the rotational spring stiffness to zero results in a failure load of 640kN, a reduction of about 20%.

Examination of the strains for a spring stiffness of 10^{20}Nmm/rad indicates that the steel section yields under negative bending at the supports at a load of 675kN. At the failure load (777kN) the steel section additionally yields at mid-span under positive bending. Using a rather more flexible spring stiffness (5×10^{10}Nmm/rad) the mode of failure differs in that the steel section yields first at mid-span at 603kN followed by failure at the supports at a load of 750kN. However as the spring stiffness is reduced further redistribution of bending from the middle of the beam to the supports is limited and the beam fails after the first plastic hinge forms at mid-span.

The range of spring stiffnesses in which a small change in stiffness produces the greatest variation in load-deflection behaviour is between $10^9$and 5×10^{10}Nmm/rad. These values correspond approximately to the initial stiffness of a flush and extended end plate connection respectively. The corresponding predicted failure loads are 654kN and 775kN, indicating an increase in failure load of 18%.

The influence of varying the rotational spring stiffness while keeping the axial stiffness constant was repeated using 40, 20 and 10 studs along the length of the beam. The results are shown in Fig 7.7 to 7.9 respectively. As expected beams with greater shear connection have a higher ultimate load level. For 40 studs and a fully restrained rotational spring the failure load is 698kN. This decreases by 38% to 431kN when the ends are free to rotate. For 20 studs the corresponding figures are 615kN (fully restrained) and 341kN (unrestrained). Further reducing the number of studs to 10 results in ultimate loads of 575kN and 308kN for the fully restrained and unrestrained cases respectively. In all cases, as the rotational stiffness is varied from fully fixed to pinned the reduction in failure load is approximately 45%.

Although the failure loads reduce as the slips at the interface increase, the failure mode in all cases is similar. For a constant rotational spring value of 10^{20}Nmm/rad and using 40 or 20 studs the supports are stressed slightly more than at mid-span while for 10 studs or with more flexible spring stiffnesses (10^{10}Nmm/rad) this is reversed. In situations where zero spring stiffness is used, the mode of failure is the yielding of the steel beam under positive bending at mid-span.

In all cases, the load-deflection behaviour appears to be more sensitive between stiffness values of 10^9Nmm/rad and 5×10^{10}Nmm/rad. In this range the increases in failure load for 40, 20 and 10 studs are 53%, 61% and 66% respectively.

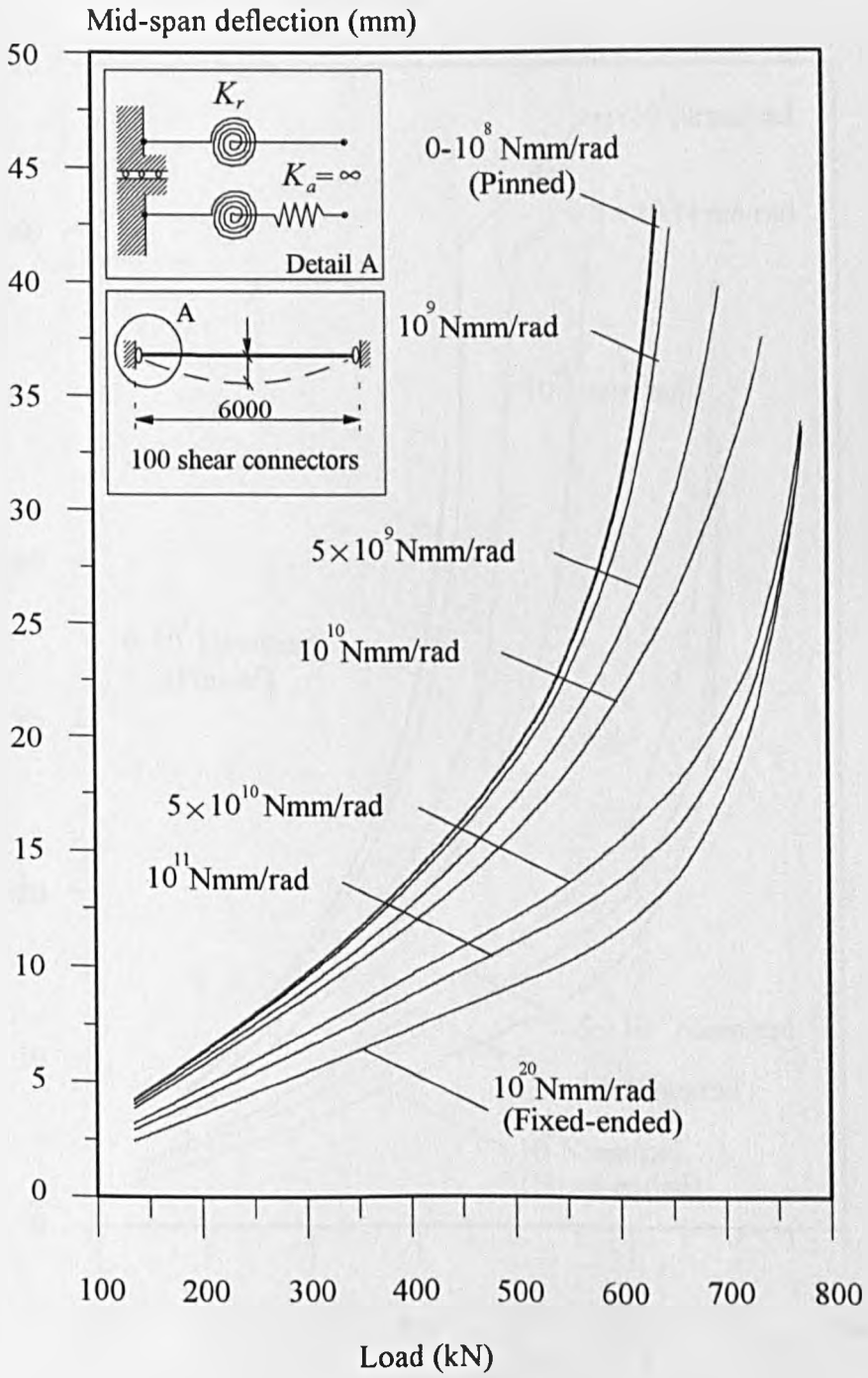

Fig. 7.6 The effect of rotational spring stiffness on the load-deflection behaviour.

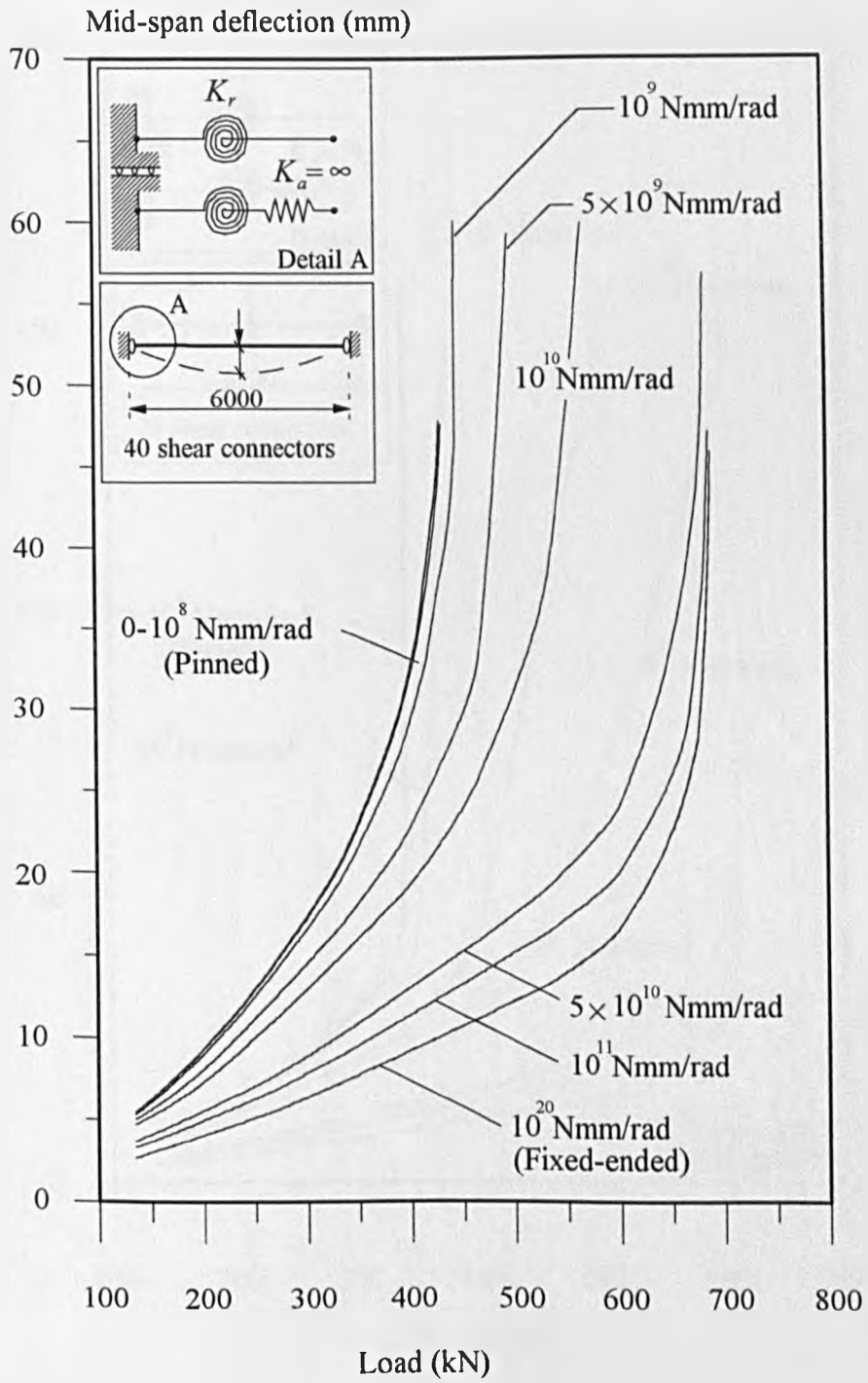

Fig. 7.7 The effect of rotational spring stiffness on the load-deflection behaviour.

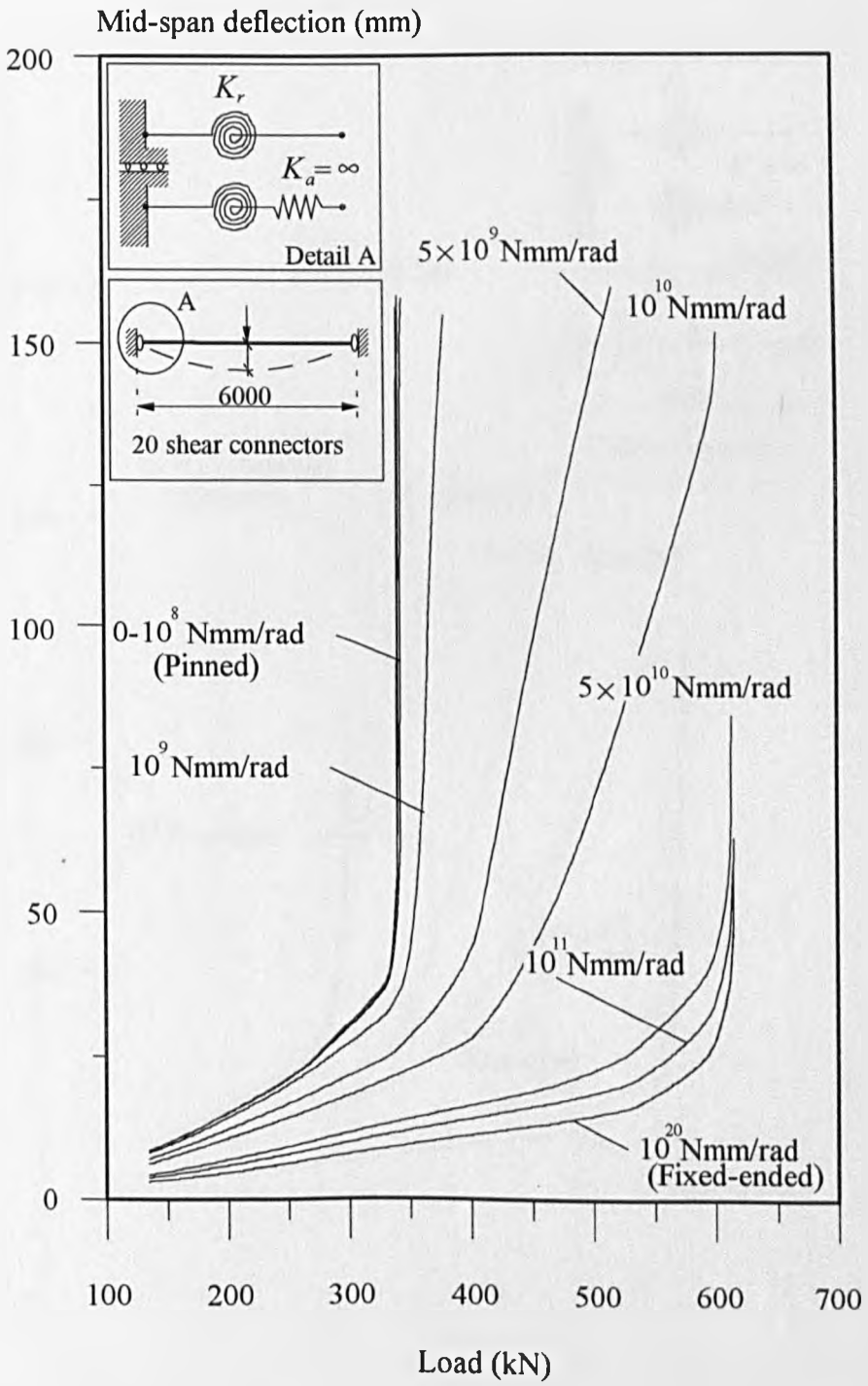

Fig. 7.8 The effect of rotational spring stiffness on the load-deflection behaviour.

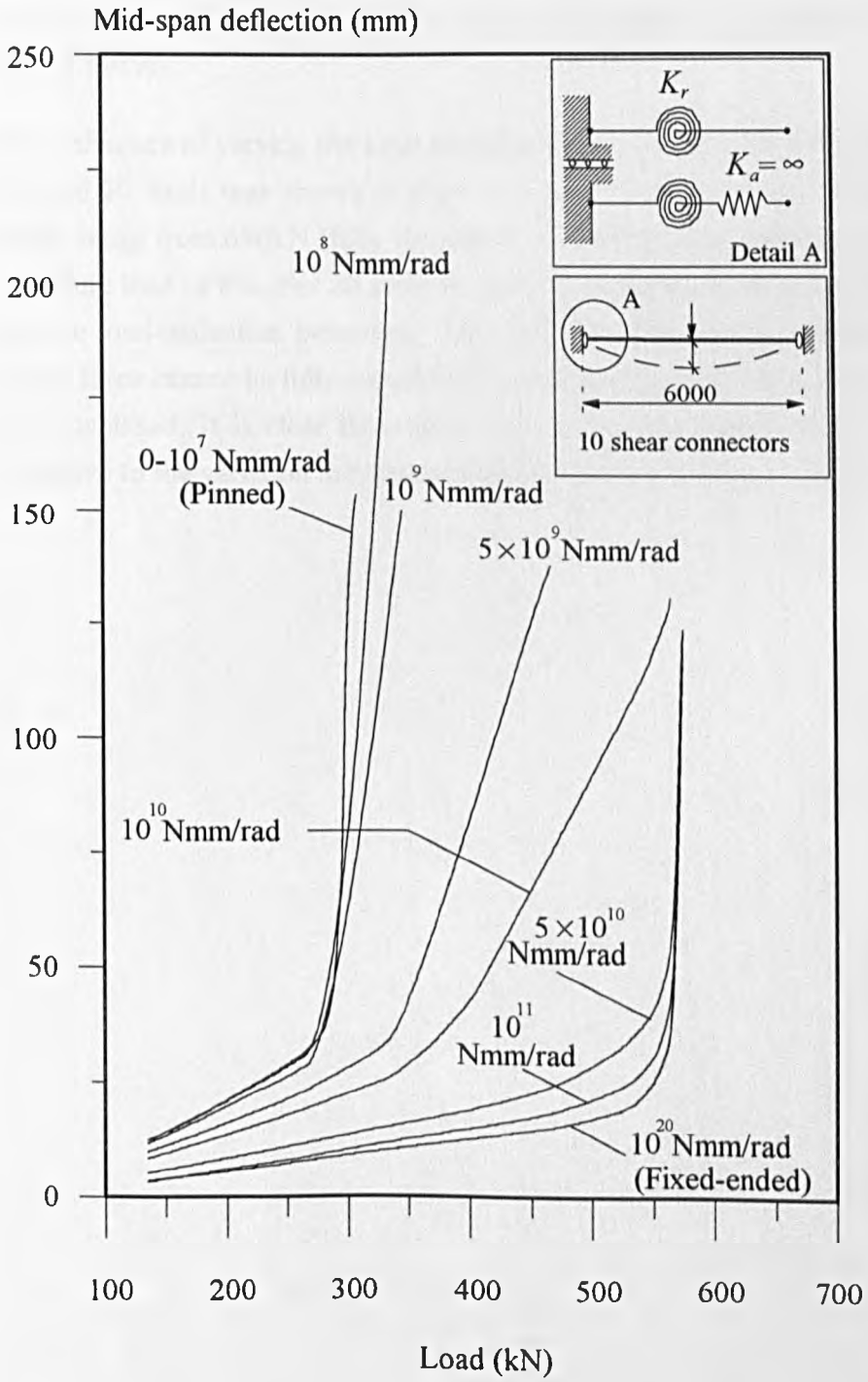

Fig. 7.9 The effect of rotational spring stiffness on the load-deflection behaviour.

Results for analyses with fixed rotational stiffness but variable axial stiffness and using 100 studs are shown in Fig. 7.10 in terms of load-deflection curves. It can be seen that analysis using a very large stiffness predicts a failure load of 776kN. When the axial spring is very flexible the predicted failure load is found to be 725kN, a reduction in failure load of 7%. The increase in failure load with increasing spring stiffness is progressive, although the most notable changes occur when the stiffness is increased from 10^5N/mm to 5×10^6N/mm.

The influence of varying the axial spring stiffness on the load-deflection behaviour for 40, 20 and 10 studs was shown in Figs. 7.11 to 7.13 respectively. The failure loads for 40 studs range from 690kN (fully restrained) to 635kN (unrestrained), indicating a reduction in failure load of 8%. For 20 studs or less, changing the axial spring stiffness has no effect on the load-deflection behaviour. This indicates that, due to inadequate interaction, the shear force cannot be fully transferred to the steel section and therefore the axial spring is not mobilised. It is clear from these results that the load-deflection behaviour is more sensitive to the variation in rotational spring stiffness than axial stiffness.

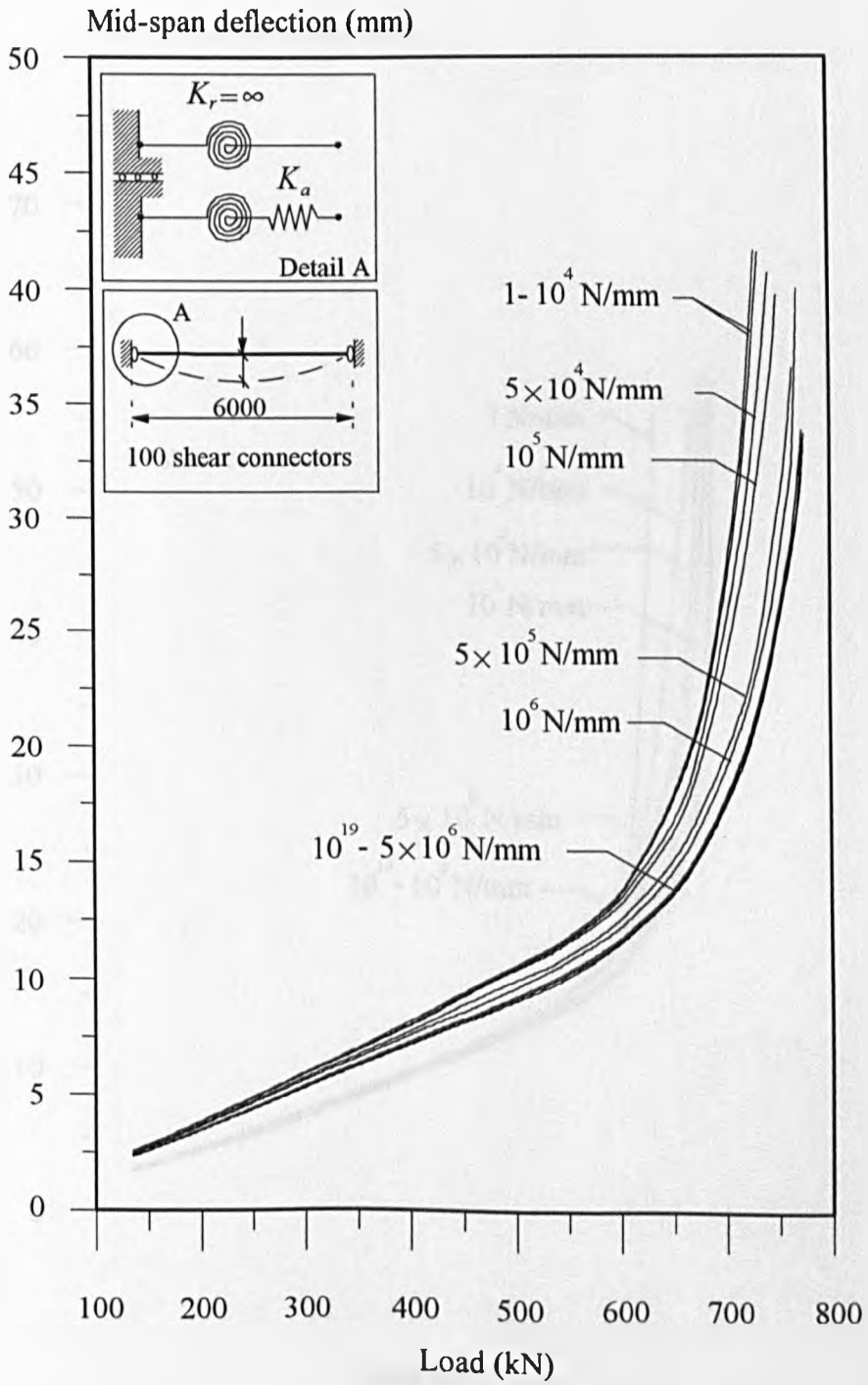

Fig. 7.10 The effect of linear spring stiffness on the load-deflection behaviour.

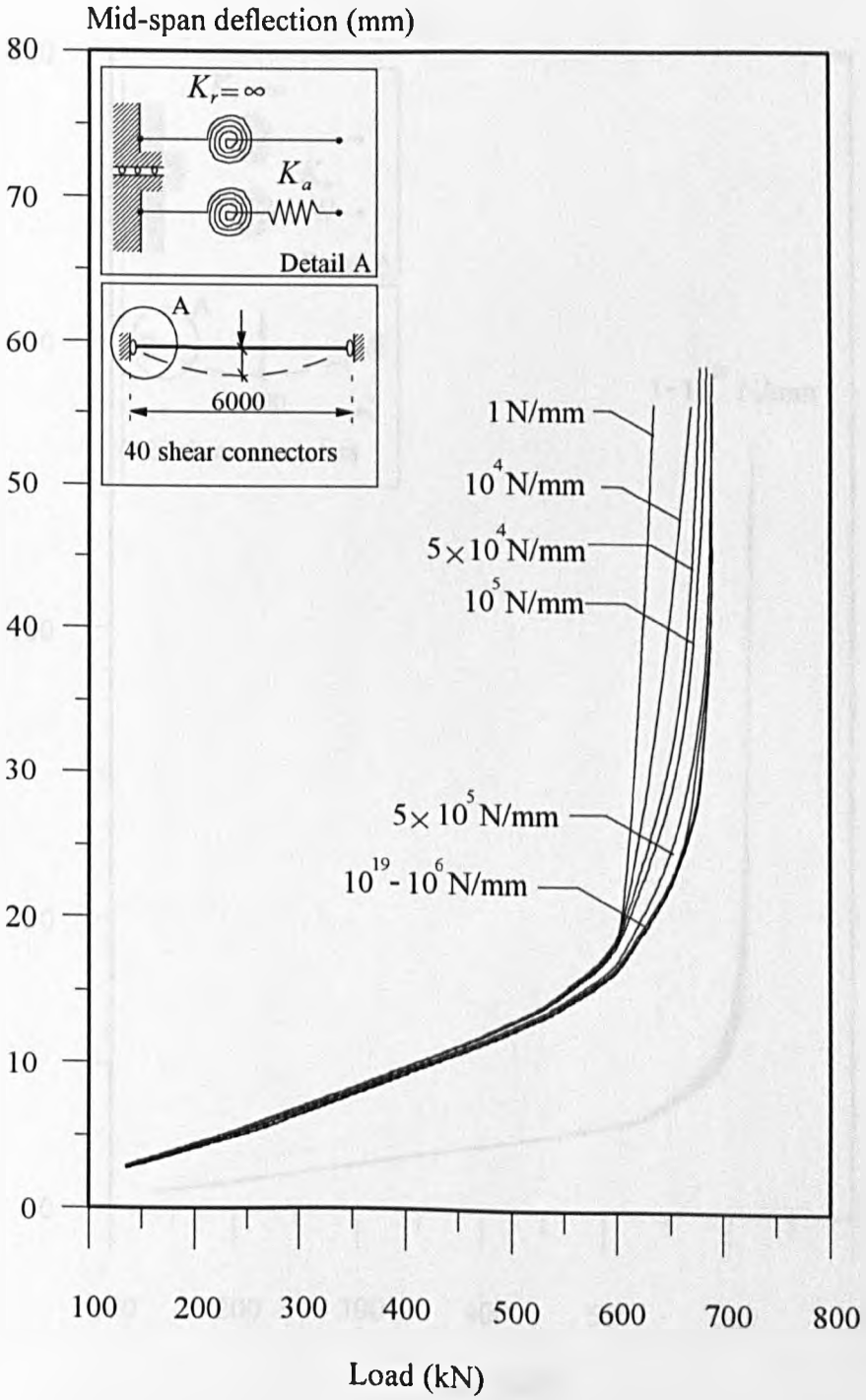

Fig. 7.11 The effect of linear spring stiffness on the load-deflection behaviour.

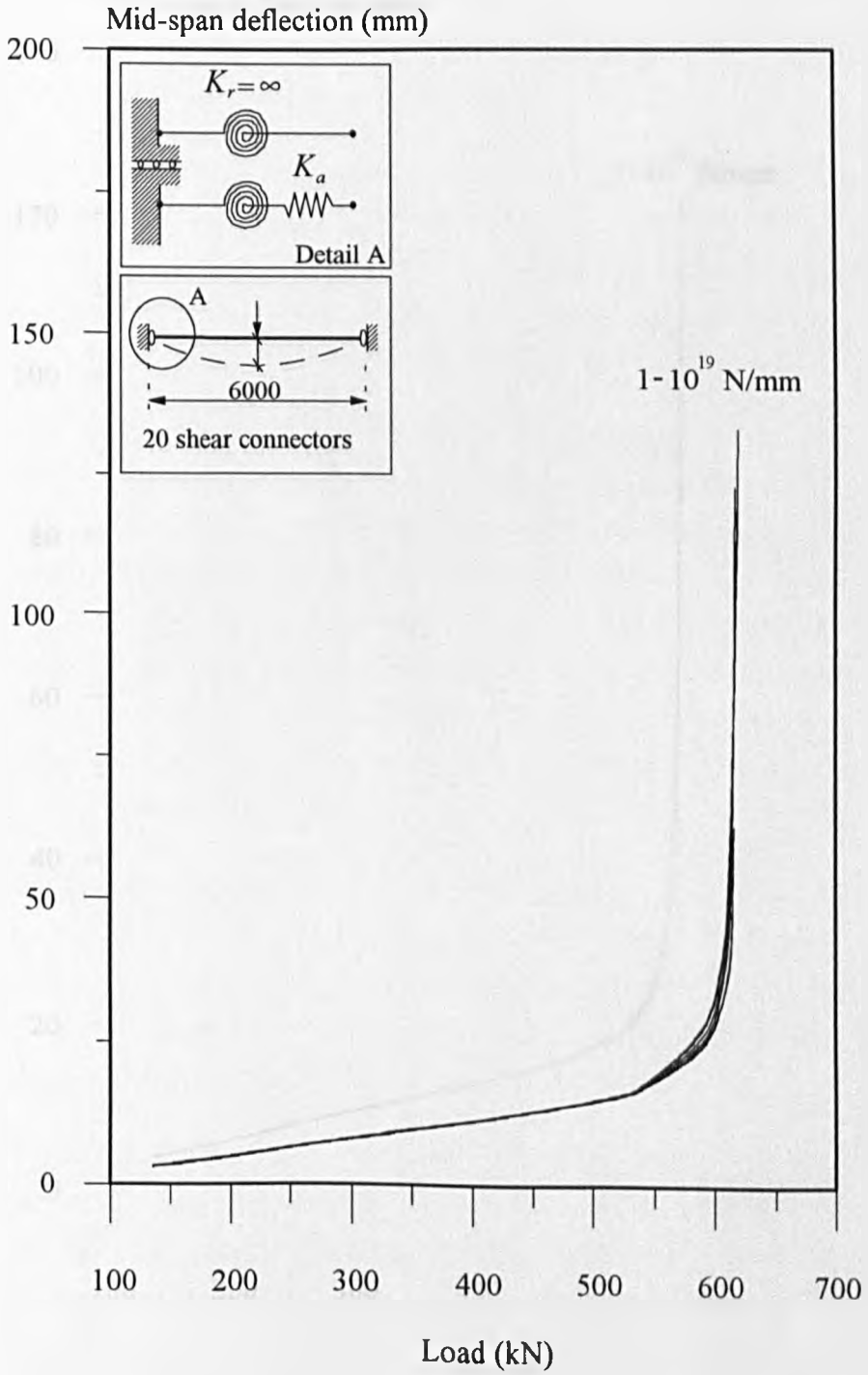

Fig. 7.12 The effect of linear spring stiffness on the load-deflection behaviour.

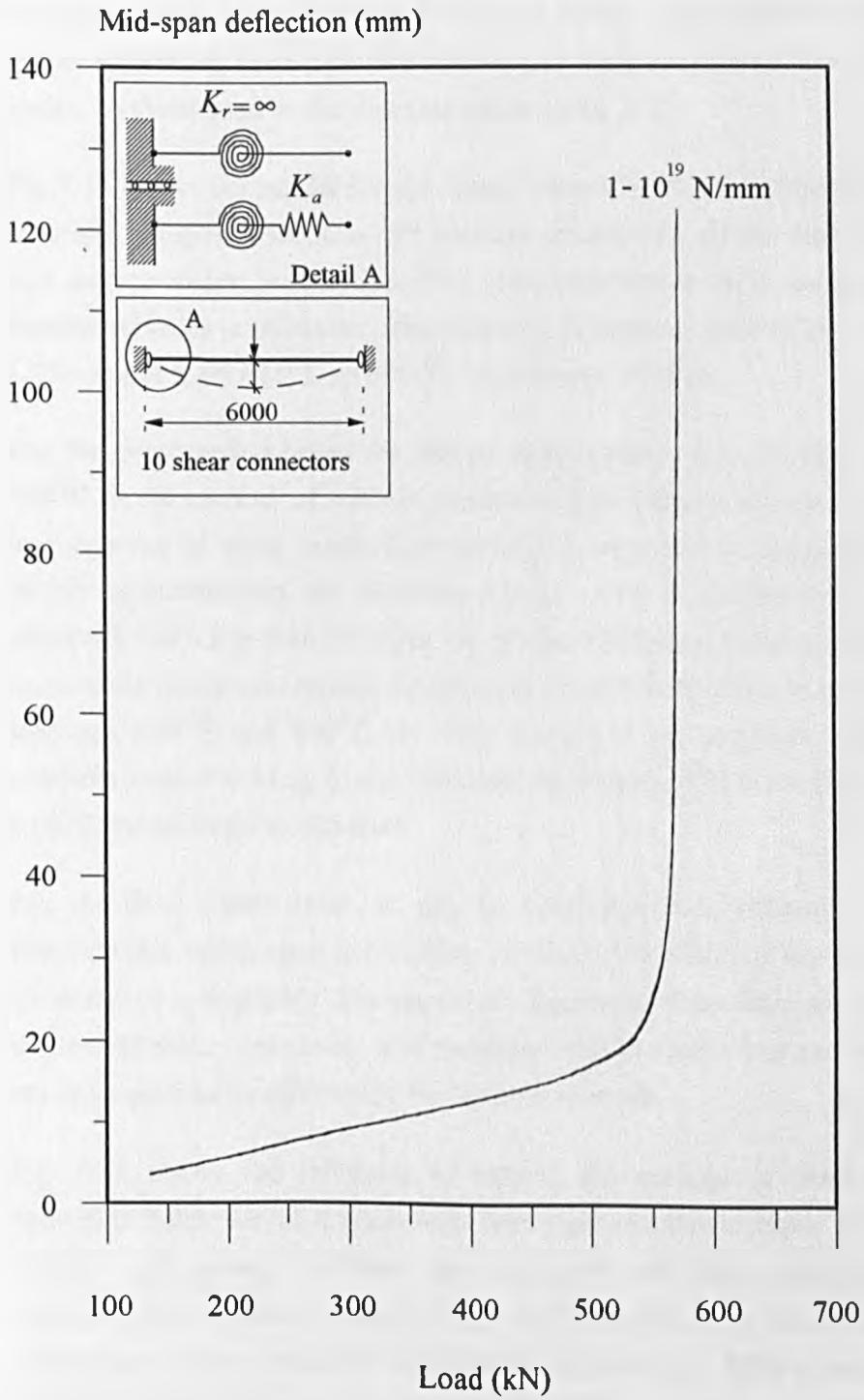

Fig. 7.13 The effect of linear spring stiffness on the load-deflection behaviour.

7.3. Elevated Temperature Studies

7.3.1. The Effect of Number of Shear Connectors

The influence of the degree of shear connection has been investigated by varying the number of studs from 1 to 100 for the 6m beam. Three different end conditions namely simply supported, semi-rigid and fixed ended were considered. The temperature regime is similar to those used in the previous studies (Fig. 6.2).

Fig 7.14 shows the results for the simply supported beam compared with non-composite and fully composite sections. All analyses extend beyond the limiting deflection of L/30, and show a steady progression from non-composite to fully composite behaviour as the number of studs is increased. The failure temperature, defined by a limiting deflection of L/20, ranges from 615^{o}C to 690^{o}C, an increase of 12%.

For the fixed ended beam the failure temperatures at L/20 vary between 680^{o}C and 700^{o}C as the number of studs is increased, indicating an increase of 3% (Fig. 7.15). For low degrees of shear connection the slip at supports is considerably greater than the simply supported case and therefore a bigger spread of behaviour at lower deflections is observed. With less than 20 studs, the mode of failure is shearing of the studs. With 20 or more studs the slip is reduced significantly and the deflections show a significant decrease. Between 400^{o}C and 450^{o}C the steel section at the supports yields and a subsequent redistribution of bending to the mid-span takes place. The beam fails with the formation of a third plastic hinge at mid-span.

For the fixed ended beam, it may be concluded that, although the behaviour at low temperatures varies with the number of studs, the effect of slip on the predicted failure temperature is negligible. For the simply supported beam little slip occurs, even with low degrees of shear connection, and therefore both the behaviour and the failure temperature are not significantly affected by the number of studs.

Fig. 7.16 shows the influence of varying the number of studs on the temperature-deflection behaviour of a beam with semi-rigid end connections. In order to examine the influence of shear connection, the rotational and axial spring stiffnesses were kept constant with stiffness values of 1.5×10^{10}Nmm/rad and 2×10^{4}N/mm respectively. A comparison with a similarly sized non-composite and fully composite section using a constant rotational spring stiffness of 1.5×10^{10}Nmm/rad is also shown. In these cases the axial expansion of the beam is freely allowed.

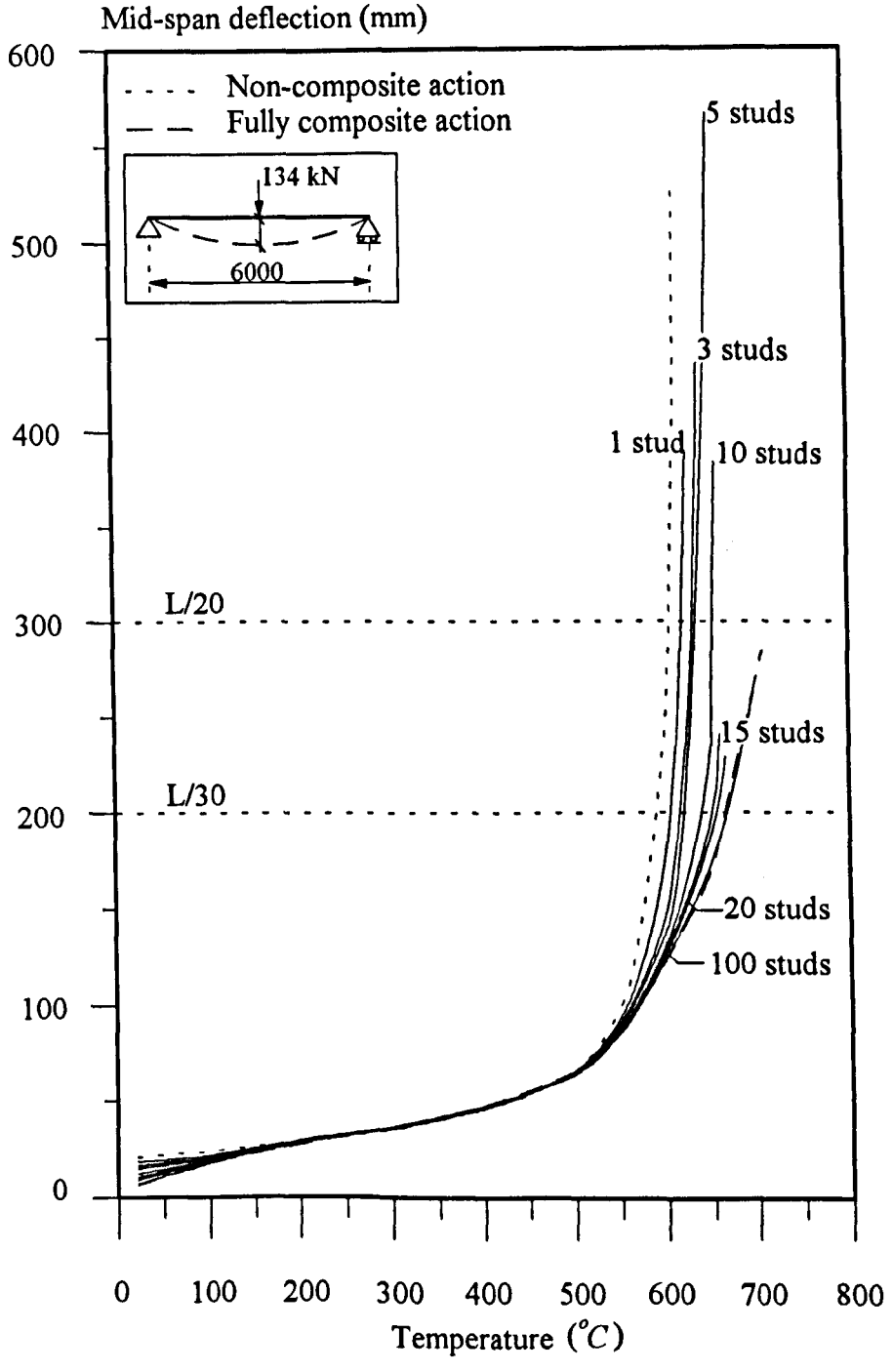

Fig. 7.14 The effect of number of studs at elevated temperatures for a simple beam.

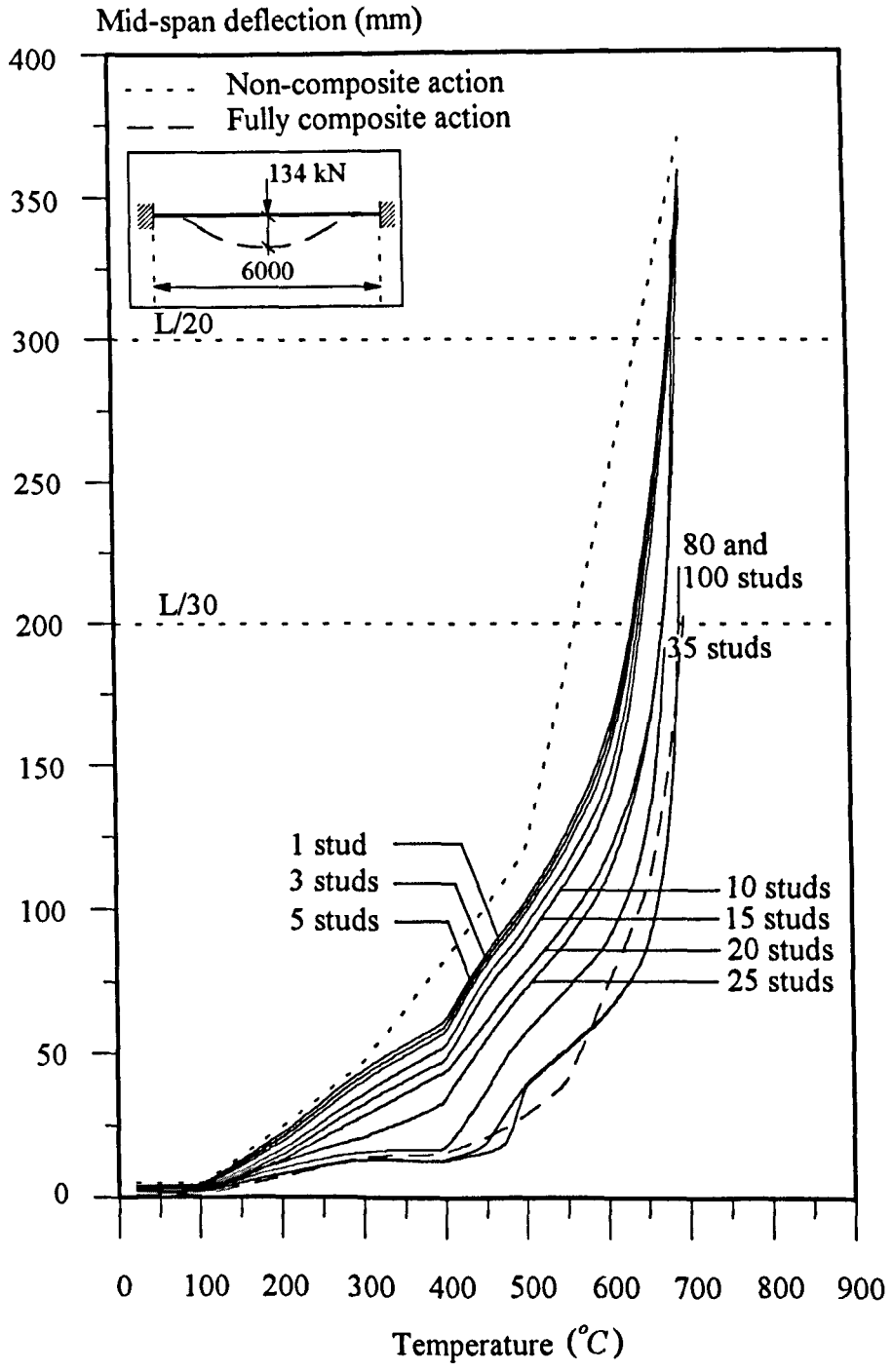

Fig. 7.15 The effect of number of studs at elevated temperatures for a fixed-end beam.

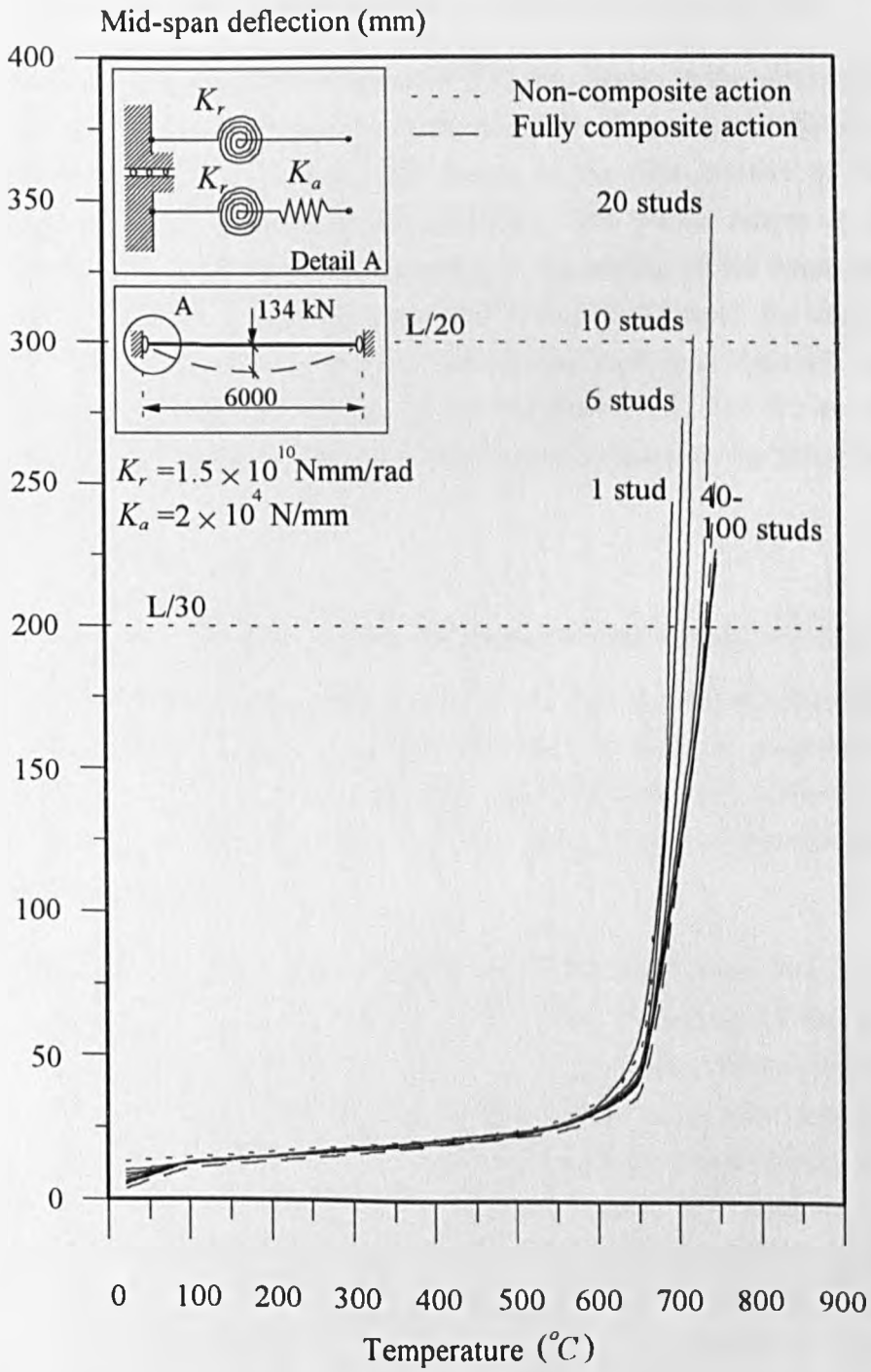

Fig. 7.16 The effect of number of studs at elevated temperatures for a semi-rigid beam.

Again an increase in failure temperature is observed as the number of studs is increased but the influence is very small. The predicted failure temperature, defined by a limiting deflection of L/30, ranges from 698°C to 750°C. This shows an increase in the failure temperature of 11% and 5% over the simply supported and fixed ended beams respectively. Compared with the semi-rigid beam, the lower failure temperature of the fixed ended beam is because of the restraint to thermal expansion.

In all cases at temperatures up to 650°C the stresses at the supports increase more rapidly than the stresses at mid-span. At this stage the slips are not sufficient to cause shearing of the studs and the concrete slab moves to the right relative to the beam due to both thermally and mechanically induced slips. The plastic hinges at the supports form at 660°C and redistribution of bending to the middle of the beam takes place. The beam starts to behave as a simply supported beam and as a result the slips change direction. The mode of failure for less than 20 studs is the shearing of the studs and the yielding of the steel at mid-span occurring almost simultaneously. For 20 or more studs failure is associated only with yielding of the steel and therefore the failure temperature is slightly greater.

7.3.2. The Effect of Force-Slip Characteristics of Shear Connectors

The force-slip characteristics of studs can vary significantly depending on their size and the strength of the surrounding concrete. In order to examine the effect of this on structural behaviour at elevated temperatures, five different types of force-slip characteristic, shown in Fig. 7.17, for various types of connector and concrete strength have been used[60].

Experimental results on composite beams and slabs show that the average concrete slab temperature at failure, is below 250°C[71,97-100]. Assuming that the temperature of the shear connectors is similar, the degradation in force-slip characteristics with temperature is negligible[71]. Therefore in elevated temperature analyses the required stiffness of the shear connectors can be defined simply by the force-slip characteristics at ambient temperature. The force-slip curves at ambient temperature (Fig. 7.17) used in this analysis are based on these obtained from experimental studies by Chapman and Balakrishnan[60]. The studs referred to as PA2, PA4 and PA5 are all 19mm in diameter 101.6mm in length. Their force-slip characteristics vary because of different strengths of concrete used in push-out tests. The stud T1 is a tee connector and PE1 is a more flexible stud of 12.7mm diameter and 50.8mm long.

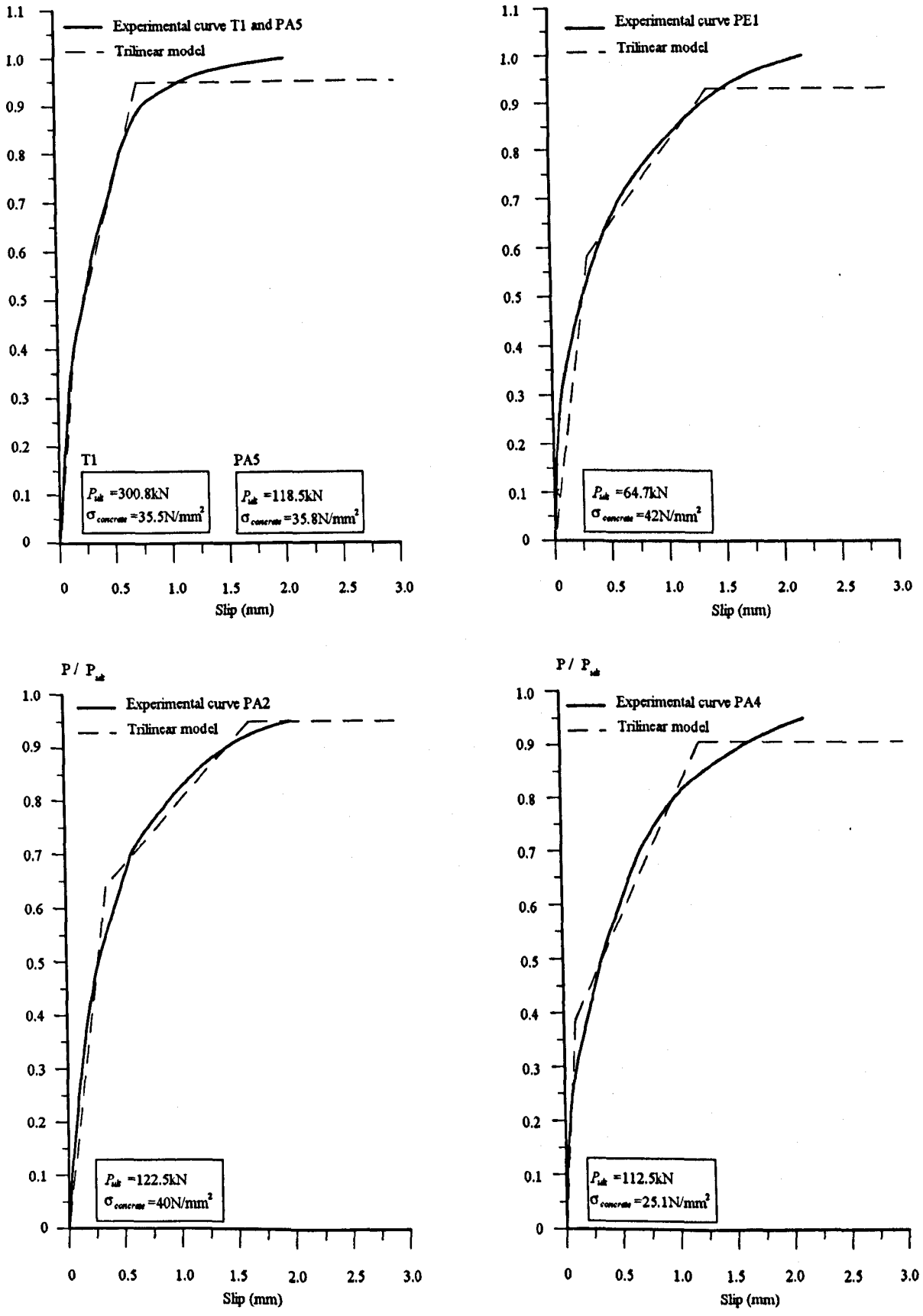

Fig. 7.17 Experimental force-slip characteristics of studs used in the parametric studies.

The studies have been carried out using a 9m beam - this is typical of the secondary beams used in the BRE large building test facility at Cardington[110] (Fig. 6.2) - with simply supported and semi-rigid end conditions under uniformly distributed load. Partial composite interaction is achieved by means of 36 uniformly spaced shear connectors. The temperature of the concrete slab, top flange and web is assumed to be constant and equal to 20%, 80% and 100% of the bottom flange temperature respectively (Fig 6.2).

The results are presented in Fig. 7.18 as temperature-deflection curves. For all cases the difference in structural behaviour is negligible. This implies that the shape of the force-slip characteristics and the ultimate strength of the connectors have very little influence on behaviour at elevated temperatures. This is due to the fact that the studs remain cool up to failure and they are not stressed beyond their elastic limit. Therefore the failure of the beam is dictated mainly by softening of the steel. Because of the negligible degradation of the stress-strain curve for steel between 300°C and 400°C the increase in deflection is very little for the semi-rigid beam. This, however, does not occur in the simply supported case because the axial and rotational displacements are freely allowed.

There has been very little information published on the force-slip characteristics of studs at elevated temperatures. However Kruppa[71] presented some experimental curves for a 19mm headed stud based on push-out tests at elevated temperatures. These have been approximated as trilinear relationships as shown in Fig. 3.5 in order to investigate the effect of the deterioration of the force-slip characteristics on beam behaviour. A 6m beam with simply supported and fixed-end conditions was the subject of these studies. As reported by Kruppa the stud temperature was increased at a ratio of 80% with respect to the temperature of the upper flange which in turn was 80% of the bottom flange temperature. The results are compared with those obtained assuming the studs remain at ambient temperatures in Fig. 7.19.

For the simply supported case it can be seen that degradation of the force-slip characteristics of the studs with increase in temperature has very little effect on the structural behaviour. The failure temperatures at a limiting deflection of L/30 are 638°C for degrading the stud properties and 650°C for constant stud properties at 20°C.

Results are similar for the fixed ended case with a failure temperature, corresponding to L/30, of 680°C for both heated and cool studs.

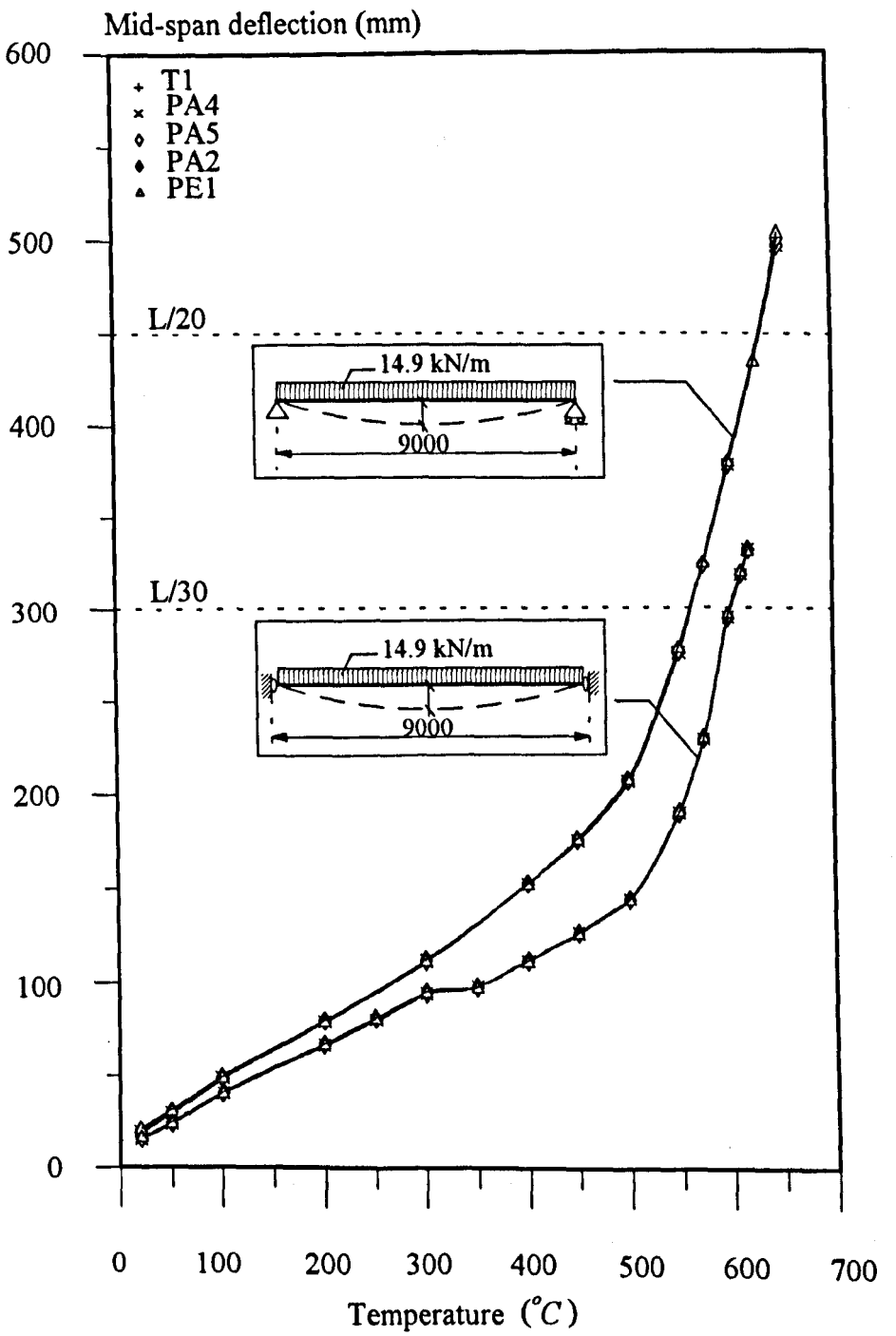

Fig. 7.18 The effect force-slip characteristics of studs at elevated temperatures.

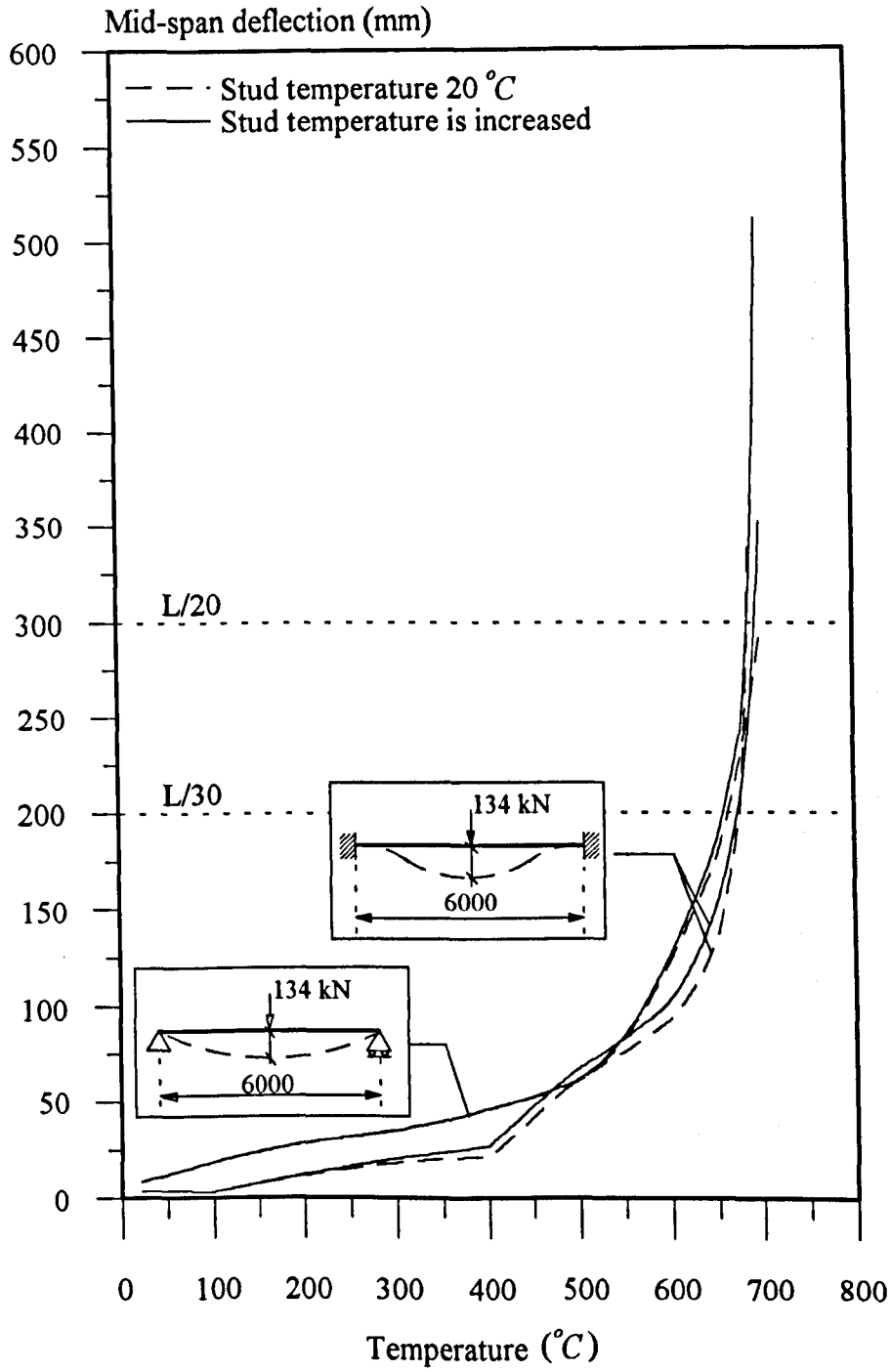

Fig. 7.19 The effect of degrading force-slip characteristics of studs with temperature.

In both cases the maximum stud temperature at failure is below 435°C. The force-slip-temperature curves in Fig. 3.5 show that at this temperature the studs lose only 15% of their ultimate shear strength and 30% of their initial stiffness compared with ambient temperature. The reduction in strength and stiffness is not significant until the temperature of the stud is in excess of 450°C. It may therefore be concluded that the shear connectors may not cause any significant deterioration in the fire resistance of composite beams unless the bottom flange temperature at failure is in excess of 700°C.

7.3.3. The Effect of Spring Stiffness

The effect of spring stiffness has been investigated for the 6m beam with 20 studs along its length. Details of the beam and the temperature profile across the cross-section are as shown in Fig. 6.2. Fig. 7.20 shows the influence of varying the rotational spring stiffness while keeping the axial stiffness fixed at 10^{20}N/mm and Fig. 7.21 shows the influence of axial stiffness while the stiffness of the rotational spring is kept at a maximum of 10^{20}Nmm/mrad.

The failure temperatures for pinned and fixed end conditions are 545°C and 687°C respectively, representing a 26% increase in failure temperature. Because of the high degree of restraint to thermal expansion afforded by the axial stiffness of the connection the beam is subject to an axial force. This is very different from the observations made in the ambient temperature studies for the same beam where the axial spring stiffness had only a negligible effect on the load-deflection behaviour. The thermally induced axial force causes a rapid increase in mid-span deflections especially for beams with flexible end conditions. For a constant rotational stiffness of 10^{9}Nmm/mrad or more the mode of failure is yielding of the steel at supports and at the middle of the beam. Plastic hinges form at the supports at 500°C and 600°C for rotational stiffnesses of 10^{20}Nmm/mrad and 10^{9}Nmm/mrad respectively and the corresponding failure temperatures, when the steel yields additionally at mid-span, are 687°C and 660°C. For rotational stiffnesses of less than 10^{9}Nmm/mrad, the failure mode is yielding of the steel under combined bending and compression at mid-span, and this occurs at approximately 550°C.

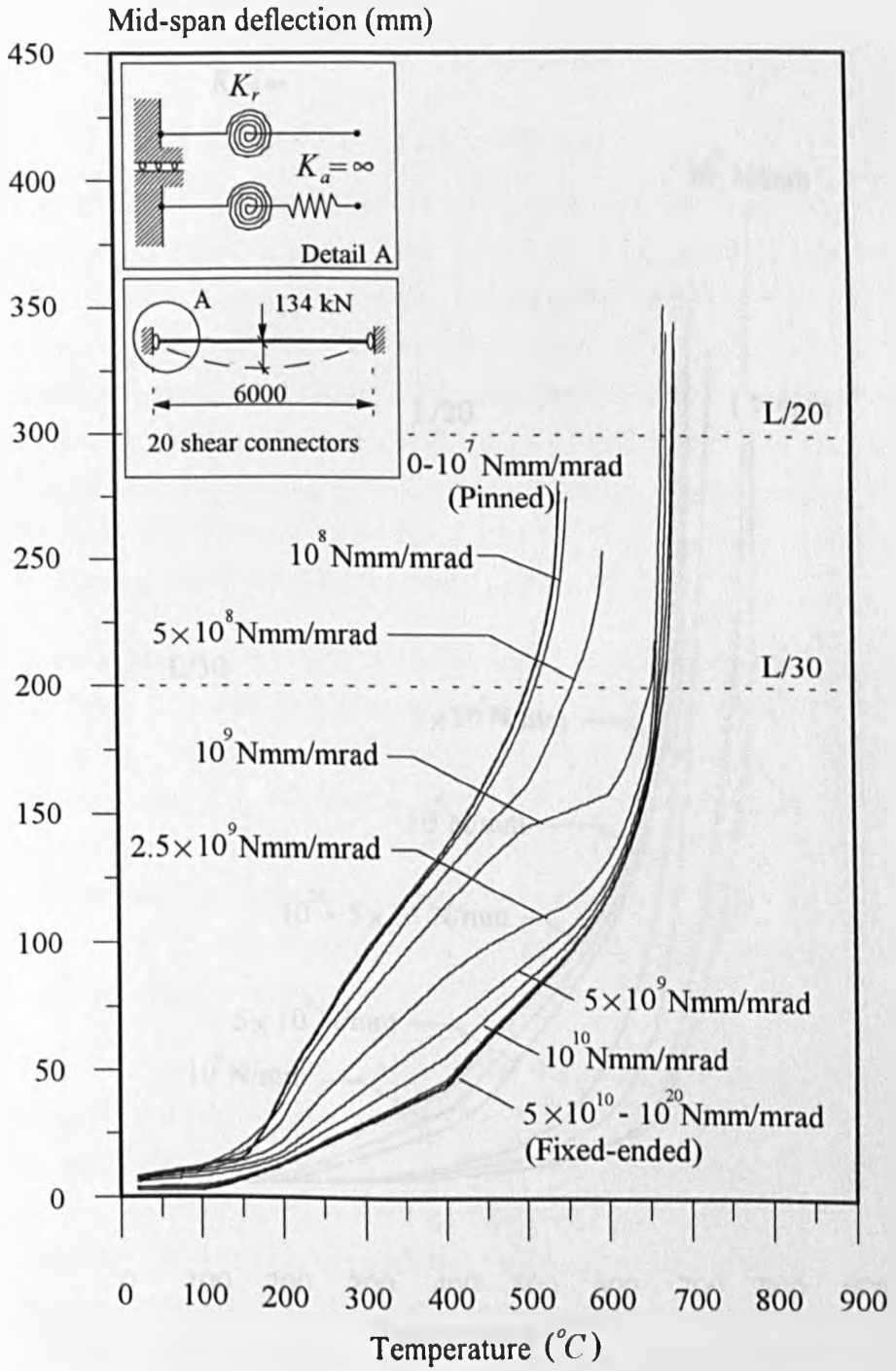

Fig. 7.20 The effect of rotational spring stiffness at elevated temperatures.

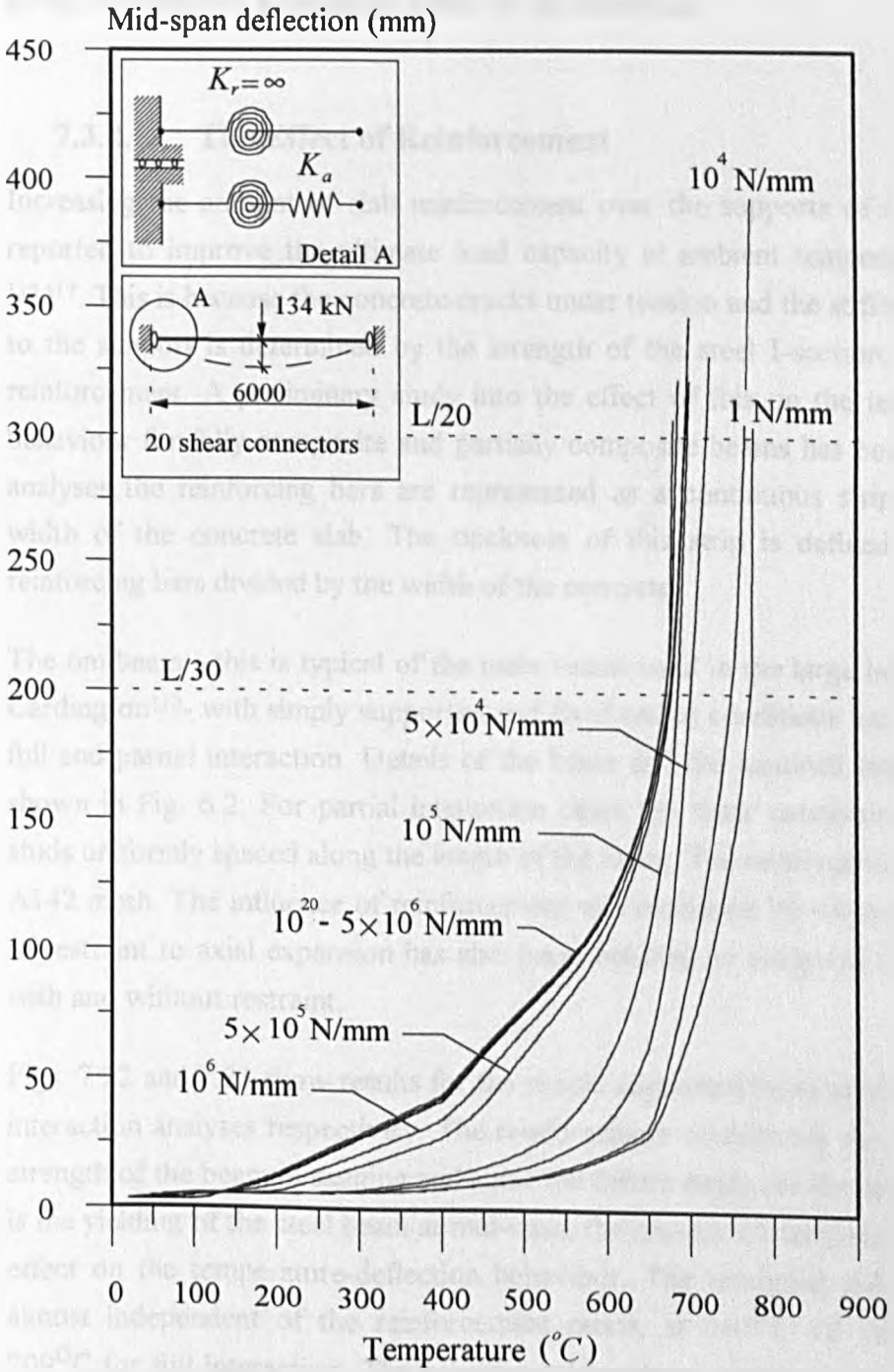

Fig. 7.21 The effect of linear spring stiffness at elevated temperatures.

As can be seen from Fig. 7.21, keeping rotational stiffness constant and increasing the axial stiffness results in a reduction in failure temperature because of the additional axial force caused by restraint to thermal expansion. For a large and very flexible stiffness the failure temperatures are 688°C and 775°C respectively, an increase of 13%. This contrasts with similar studies at ambient temperatures, where it was found that the axial spring stiffness had a negligible effect on the behaviour.

7.3.4. The Effect of Reinforcement

Increasing the amount of slab reinforcement over the supports of a composite beam is reported to improve the ultimate load capacity at ambient temperature significantly[113-115,117]. This is because the concrete cracks under tension and the stiffness of the beam near to the support is determined by the strength of the steel I-section, connection and the reinforcement. A preliminary study into the effect of this on the temperature-deflection behaviour for fully composite and partially composite beams has been conducted. In the analyses the reinforcing bars are represented as a continuous strip running across the width of the concrete slab. The thickness of this strip is defined as the area of the reinforcing bars divided by the width of the concrete.

The 6m beam - this is typical of the main beams used in the large building test facility at Cardington[110]- with simply supported and fixed ended conditions has been used assuming full and partial interaction. Details of the beam and the assumed temperature profile are shown in Fig. 6.2. For partial interaction cases the shear connection is provided by 20 studs uniformly spaced along the length of the beam. The reinforcement used in the slab is A142 mesh. The influence of reinforcement was examined by varying its area. The effect of restraint to axial expansion has also been included by analysing the fixed ended beam with and without restraint.

Figs. 7.22 and 7.23 show results for the simply supported beam case using full and partial interaction analyses respectively. The reinforcement contributes very little to the bending strength of the beam in sagging and since the failure mode for the simply supported beam is the yielding of the steel beam at mid-span, the amount of reinforcement has a negligible effect on the temperature-deflection behaviour. The predicted failure temperatures are almost independent of the reinforcement ratios, at 667°C for partial interaction and 709°C for full interaction. The behaviour throughout heating is also very similar with a small variation at temperatures between 200°C and 550°C due to greater thermal bowing with increased reinforcement.

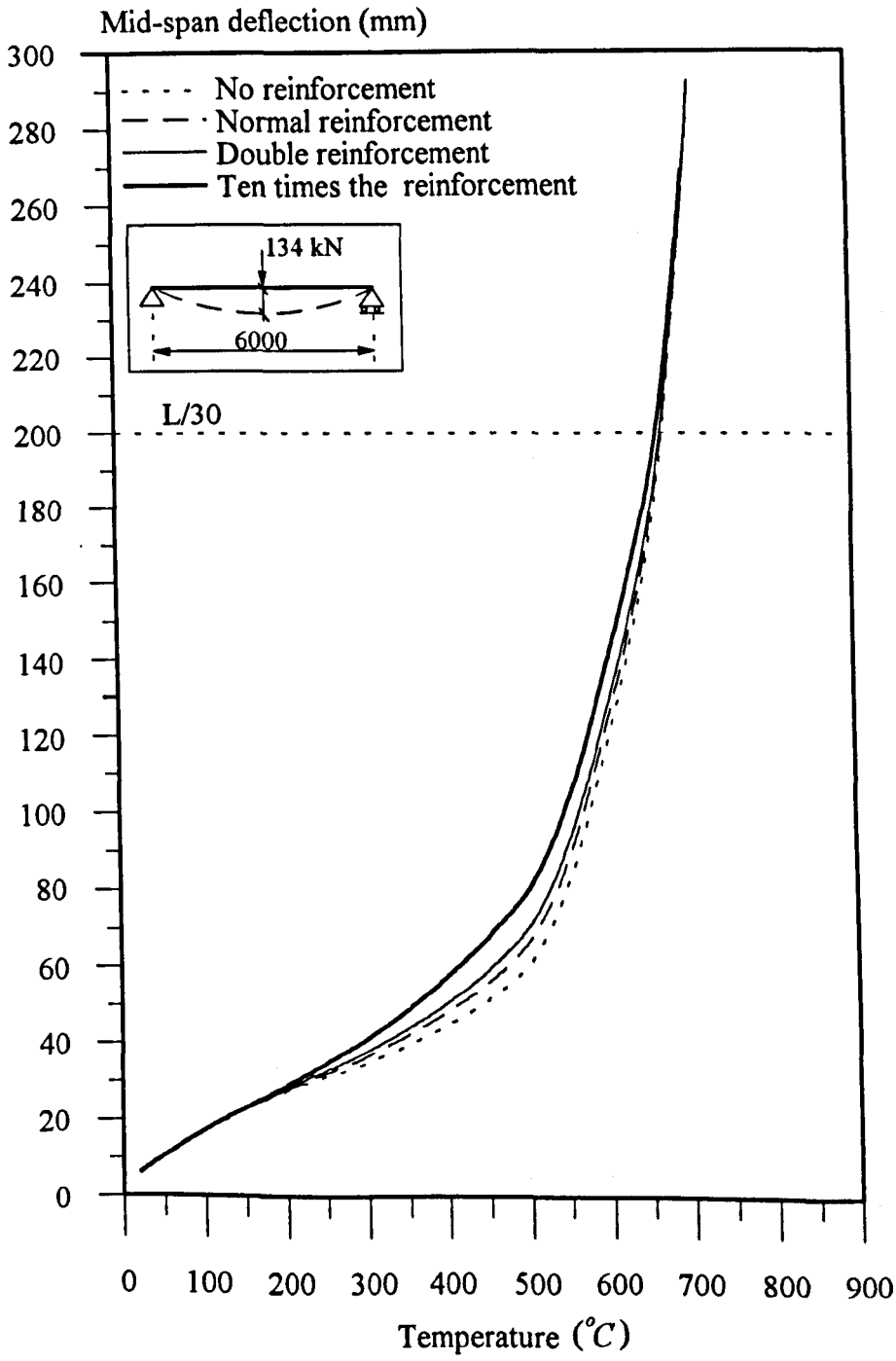

Fig. 7.22 The effect of reinforcement at elevated temperatures with full interaction.

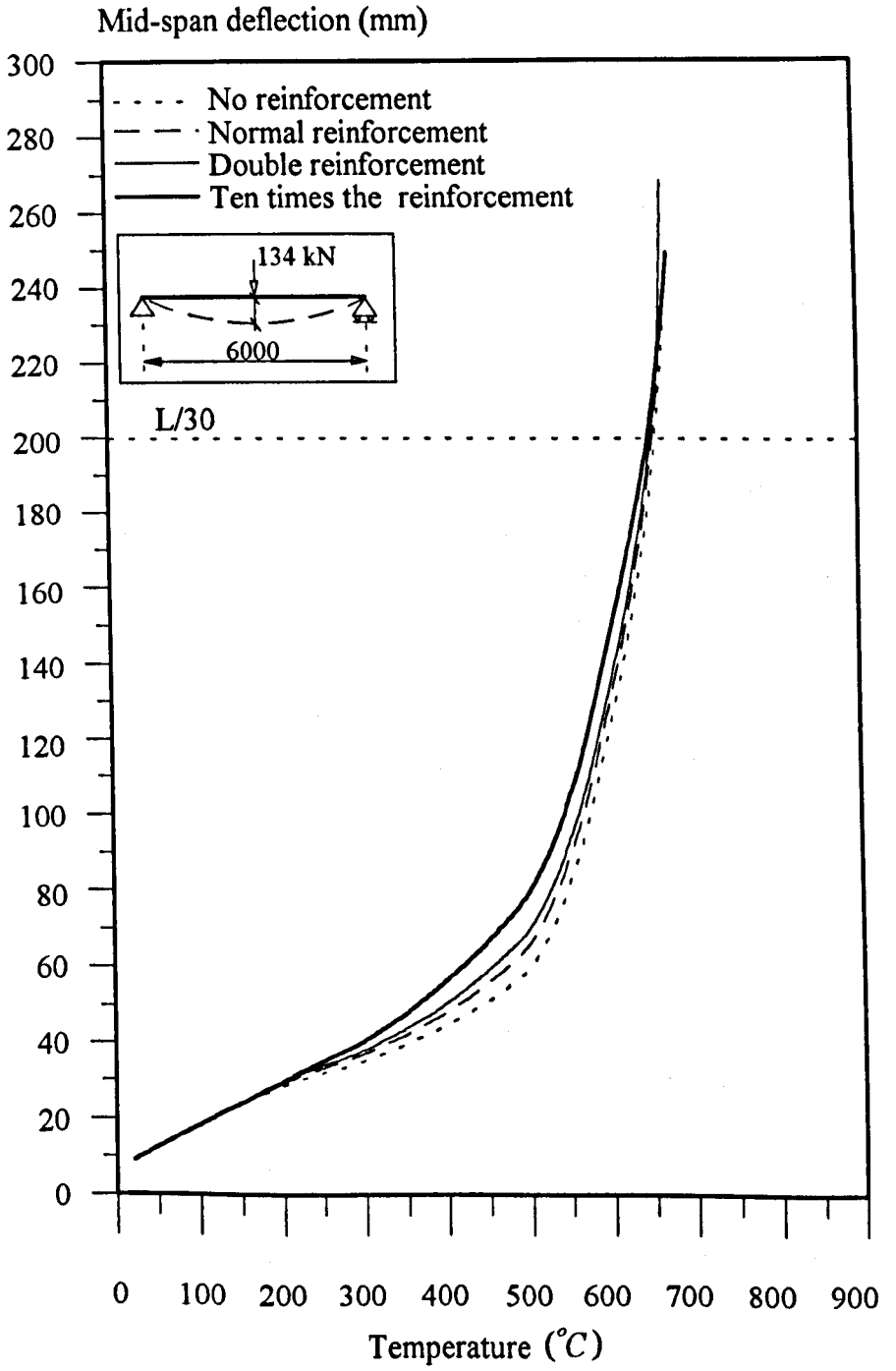

Fig. 7.23 The effect of reinforcement at elevated temperatures with partial interaction.

As shown in Fig. 7.24, the results for the axially restrained fixed ended beam assuming full interaction also reveal very little difference in temperature-deflection behaviour. This is mainly because of the additional axial force induced by restraint to thermal expansion. The predicted failure temperature varies from 690°C to 725°C with increased reinforcement, resulting in a maximum difference of 5%. The plateau between 300°C and 400°C in the temperature-deflection behaviour is due to the very slow rate of material degradation between these temperatures.

Also shown in Fig. 7.24 are the results of the axially unrestrained fixed ended beam. For normal and double reinforcement the improvement in failure temperature over the case with no reinforcement is very little but increasing the reinforcement by a factor of 10 leads to a failure temperature in excess of 900°C, an increase of 14%. In fact the beam still had a reserve of strength when analysis was terminated at 900°C due to inadequate material data beyond this temperature level.

Fig. 7.25 shows similar results assuming partial-interaction. In the axially restrained case the predicted failure temperature is 675°C for both normal and double reinforcement. Increasing the reinforcement by a factor of 10 results in a failure temperature of 750°C, an increase of 11% whereas with no reinforcement the failure temperature is 567°C, a reduction of 16%. Compared with full interaction analysis there is a greater variation in fire resistance as the amount of reinforcement is increased. This is due to the fact that in the partial interaction analysis the concrete slab is free to deform axially and therefore there is less thermally induced axial force than with the full interaction analysis.

Fig. 7.25 also shows the partial interaction analysis results for the axially unrestrained fixed ended beam. When the axial expansion of both the concrete slab and steel beam are freely allowed, the predicted failure temperatures for normal and double reinforcement corresponding to L/20 are 790°C and 816°C. Increasing the reinforcement by a factor of 10 raises the failure temperature to 867°C, an increase of approximately 8% whereas the failure temperature with no reinforcement is 750°C, a reduction of 6.5%.

The development of mechanical strains in the reinforcement as the temperature increases is shown in Fig. 7.26 for the axially restrained fixed ended beam assuming partial interaction. It is clear that at temperatures above 400°C the strains for normal and double reinforcement increase very rapidly due to the softening of the steel beam at supports. Yielding of the reinforcing bars occurs at a temperature of 500°C. Increasing the reinforcement by a factor of 10 allows it to remain in the elastic range throughout.

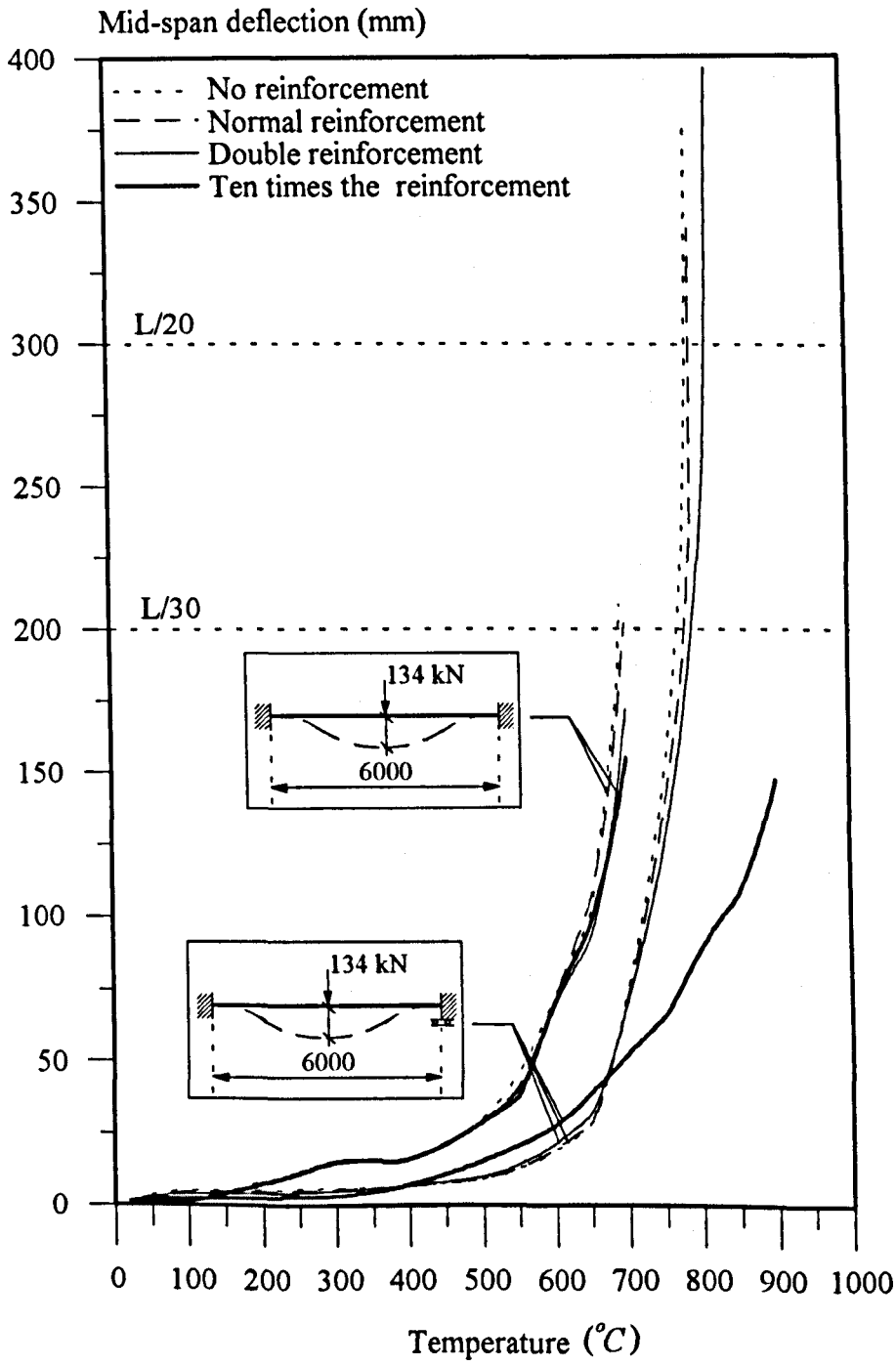

Fig. 7.24 The effect of reinforcement at elevated temperatures with full interaction.

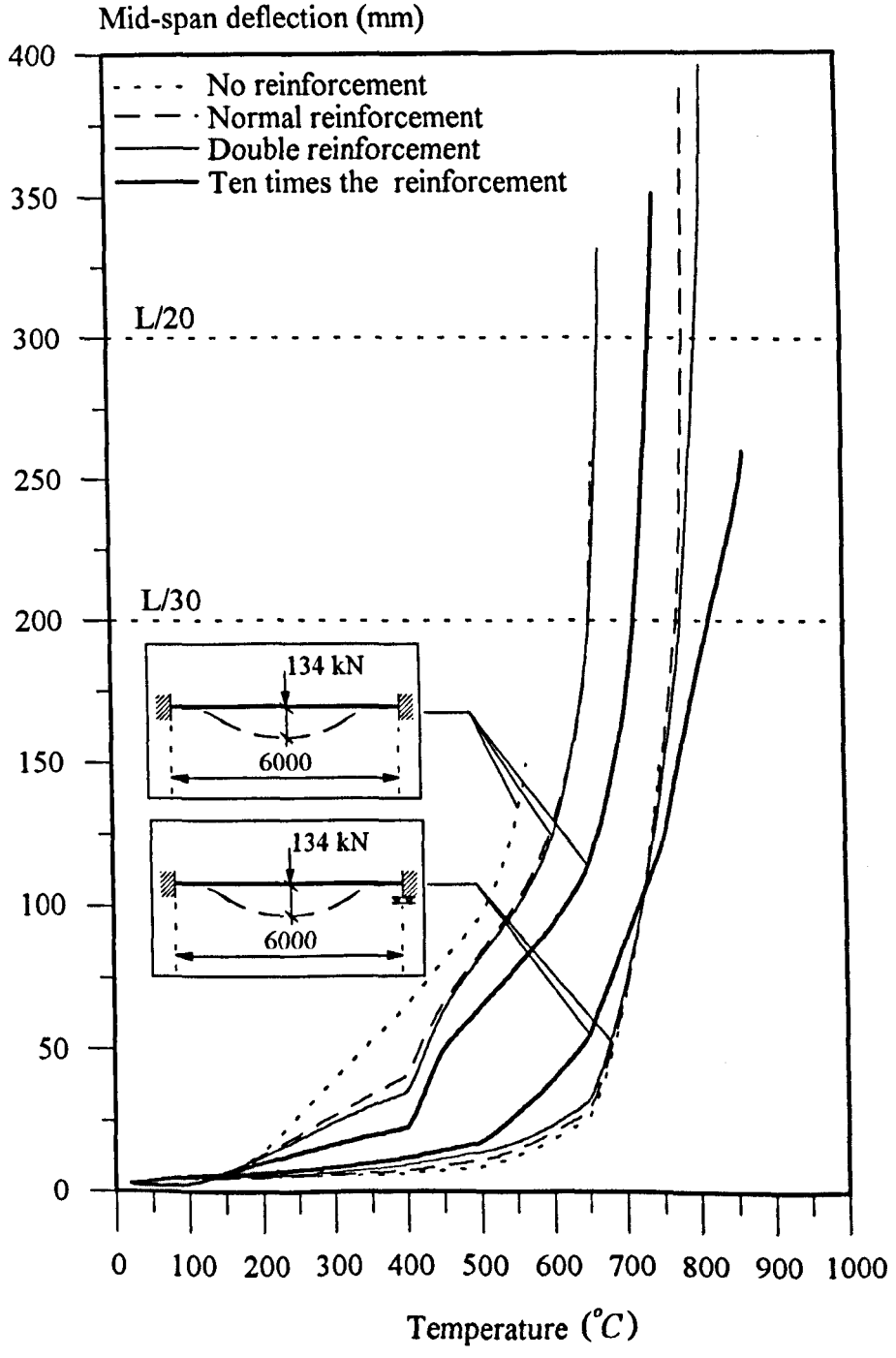

Fig. 7.25 The effect of reinforcement at elevated temperatures with partial interaction.

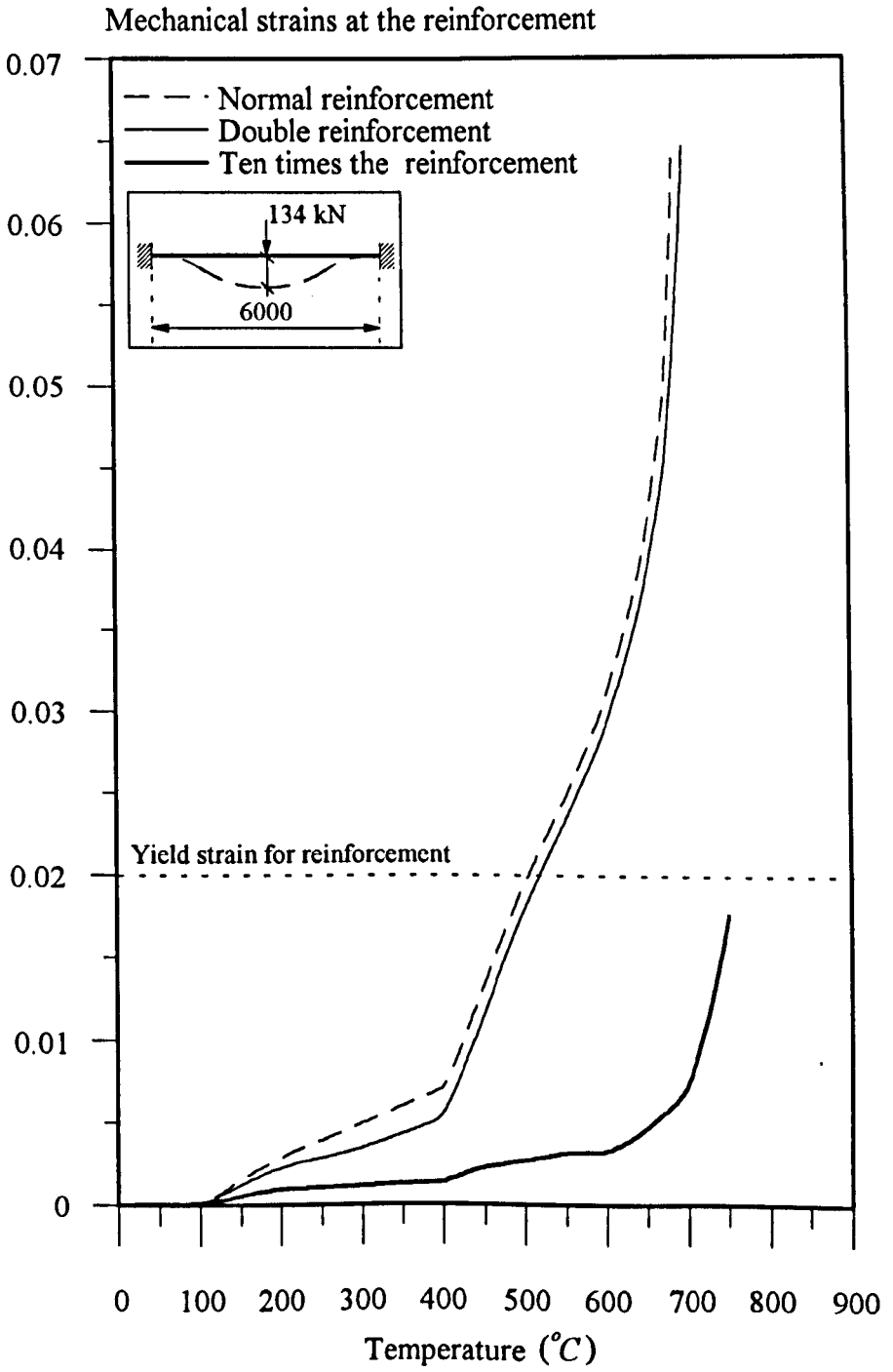

Fig. 7.26 Strains at the support at the reinforcement for a fixed-end beam.

7.3.5. The Effect of Temperature Distribution

The use of profiled metal decks has become increasingly popular in multi-storey steel framed construction. When the trough profiles are perpendicular to the beam, the top flange of the beam and the floor slab are only in intermittent contact, resulting in a series of 'voids'. These locally reduce the heat sink effect of the concrete slab and increase the heat flow around this region resulting in higher temperatures in the upper half of the steel I-section. Based on experimental results[110], the temperatures in the upper web and the top flange of the I-section are about 5% and 10% respectively hotter than the temperature in the bottom flange. In contrast where the top flange is in contact with the concrete slab, its temperature is typically 20% cooler than the rest of the steel section. Typical temperature profiles for these two different types of construction are shown in Fig. 7.27 and referred to as unfilled and filled void temperature profiles.

Partial interaction analyses have been conducted on two isolated beams namely the 6m and 9m beams, with simply supported and semi-rigid end conditions. Full-interaction analyses were carried out only for the 9m beam. The simply supported beam was analysed as an isolated beam whereas analysis with semi-rigid end connections was conducted in a sub-frame. The semi-rigid connection characteristics are defined using the moment-rotation curves for a flush end plate (Fig. 5.1(a)). Details of the isolated beams and subassemblies are shown in Figs. 6.2 and 7.27 respectively.

Figs. 7.28 to 7.31 show the temperature-deflection behaviour assuming partial interaction for beams with simply supported and semi-rigid end characteristics. The failure temperatures, defined by the limiting deflection of L/30, are clearly very little affected by temperature profiles. Analyses assuming unfilled voids predict slightly lower fire resistance than for filled voids but the difference in failure temperature is less than 5%. Using simply supported end conditions the mean failure temperatures for the 6m and 9m beam are 675°C and 692°C respectively whereas with semi-rigid end conditions the corresponding failure temperatures are 684°C and 706°C. For unfilled voids predicted deflections between 100°C and 600°C are smaller than for filled voids. This is because the hotter top flange causes thermal bowing in the opposite direction to normal deflections.

Full interaction results are compared in Fig. 7.32 for the 9m beam with simply supported end connections. Again it can be seen that the influence of the two different temperature patterns on predicted failure temperature at L/20 is negligible. The observed failure temperatures for filled and unfilled voids are 750°C and 738°C, a difference of less than 7%. The results for unfilled voids show a slight discrepancy in predicted deflections at

temperatures between 100°C and 550°C due to thermal bowing in the opposite direction to normal deflections.

Results for the 9m beam with semi-rigid end connections in a sub-frame are shown in Fig. 7.33. The temperature-deflection behaviour is consistent with that for the isolated beams, and predicted failure temperature with filled and unfilled voids is 700°C. Compared with the isolated beam with simply supported end connections the predicted failure temperature is 6.5% lower. This might be explained partly by the axial force due to restraint to thermal expansion in the semi-rigid beam and partly by large column deformations at the supports.

Although, at temperatures between 100°C and 600°C, the structural behaviour of composite beams with profiled metal decks shows a different pattern from composite beams with solid slabs, the failure temperatures remain the same. In this particular case isolated beams showed a slightly greater fire resistance than beams in a sub-frame. As expected analyses assuming full interaction predict slightly greater failure temperatures than analyses assuming partial interaction but the increase is less than 8%. In these analyses the effect of studs on failure temperatures is negligible and the use of less complicated full interaction analysis may be adequate.

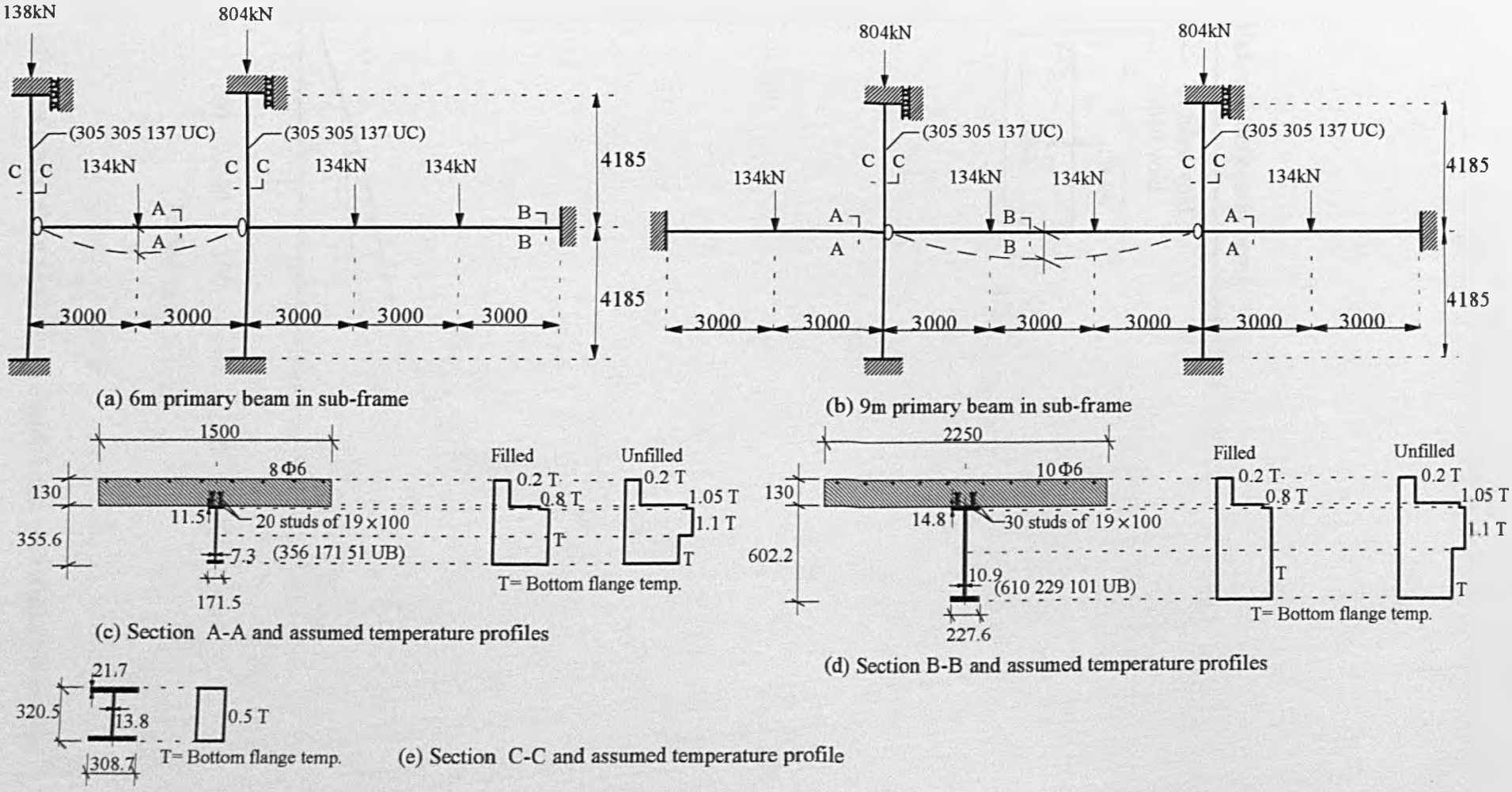

Fig. 7.27 Details of beams used in studies with different temperature profiles.

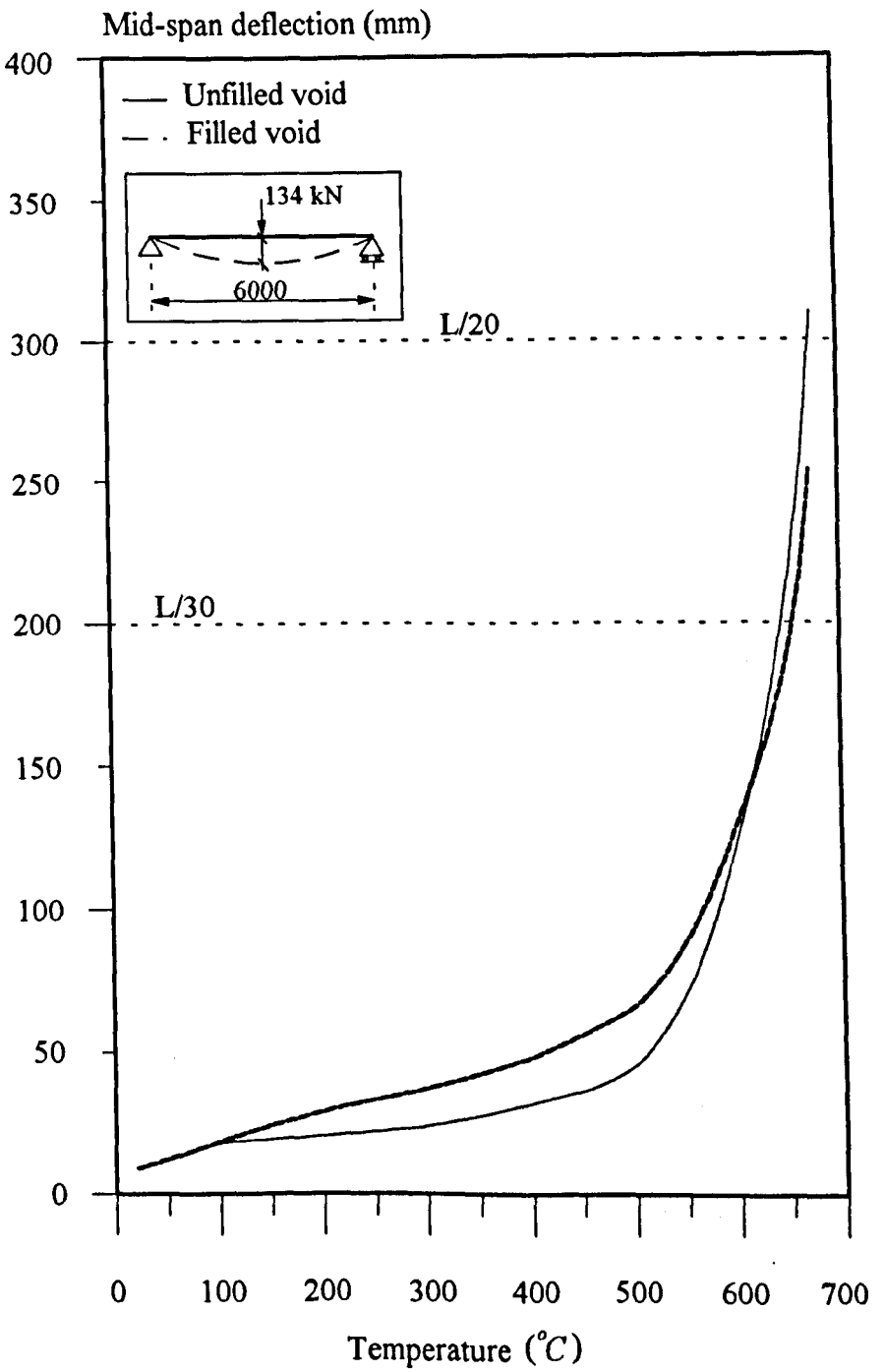

Fig. 7.28 Effect of temperature profile for a simple beam with partial interaction.

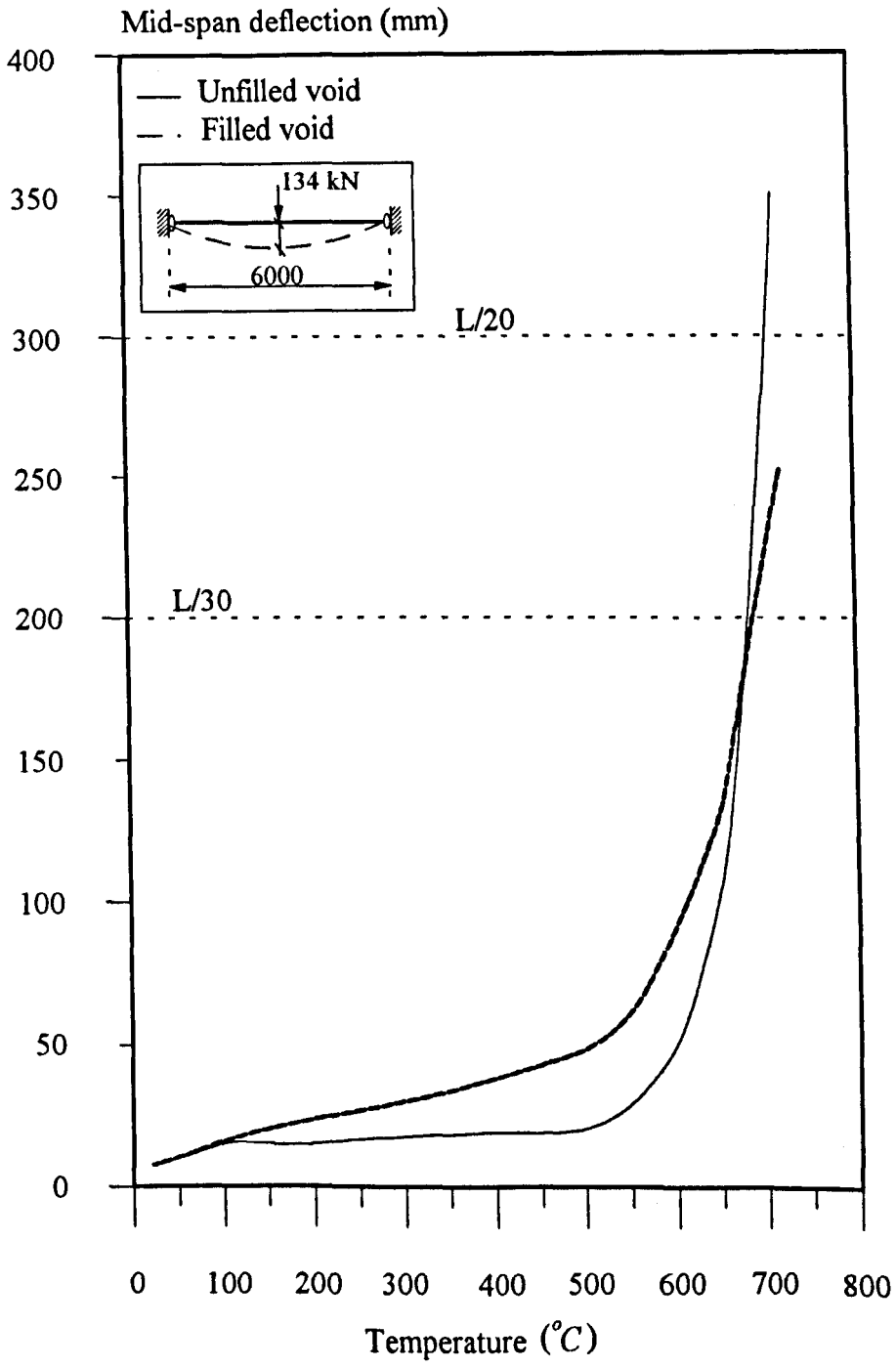

Fig. 7.29 Effect of temperature profile for a semi-rigid beam with partial interaction.

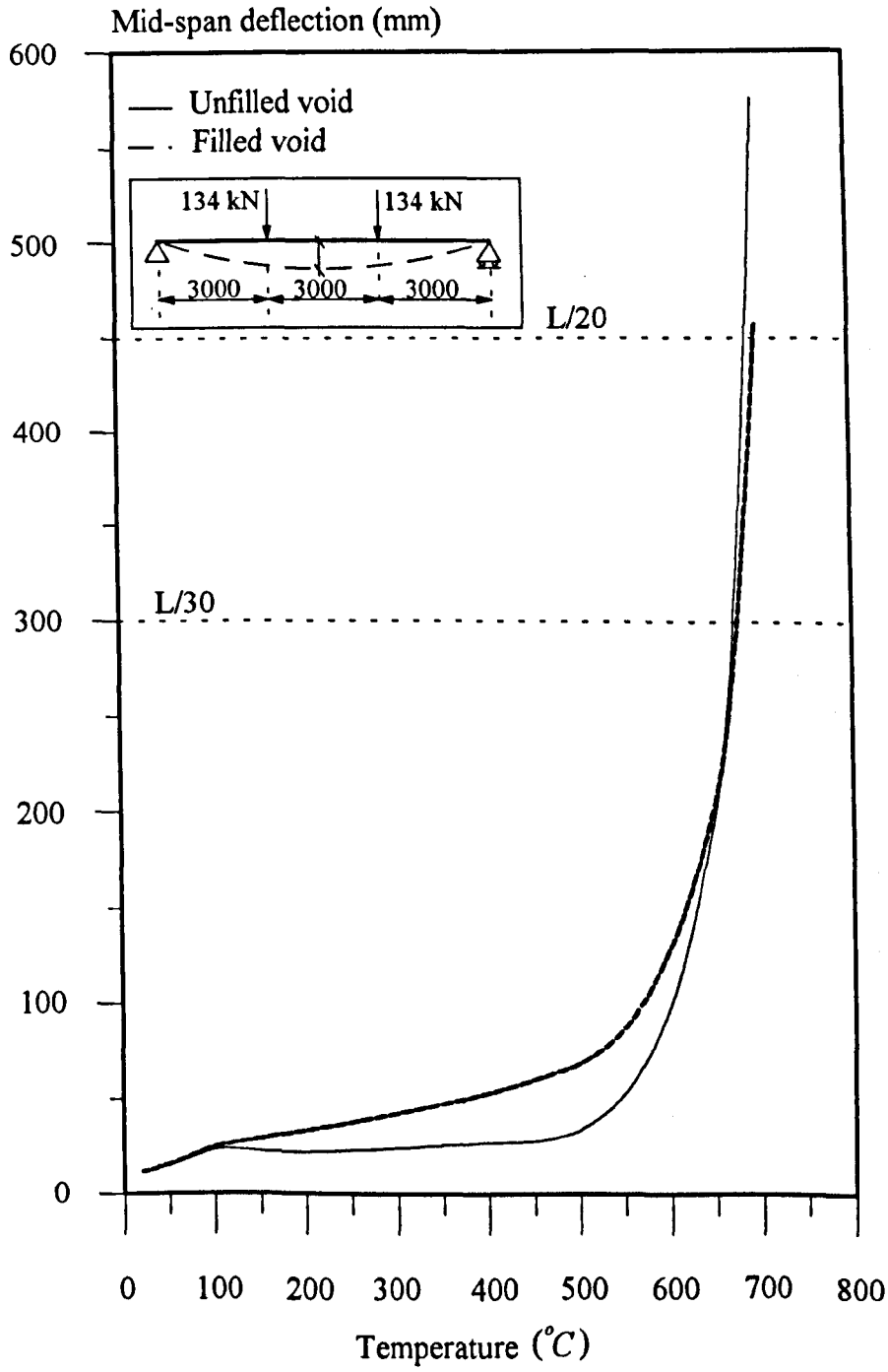

Fig. 7.30 Effect of temperature profile for a simple beam with partial interaction.

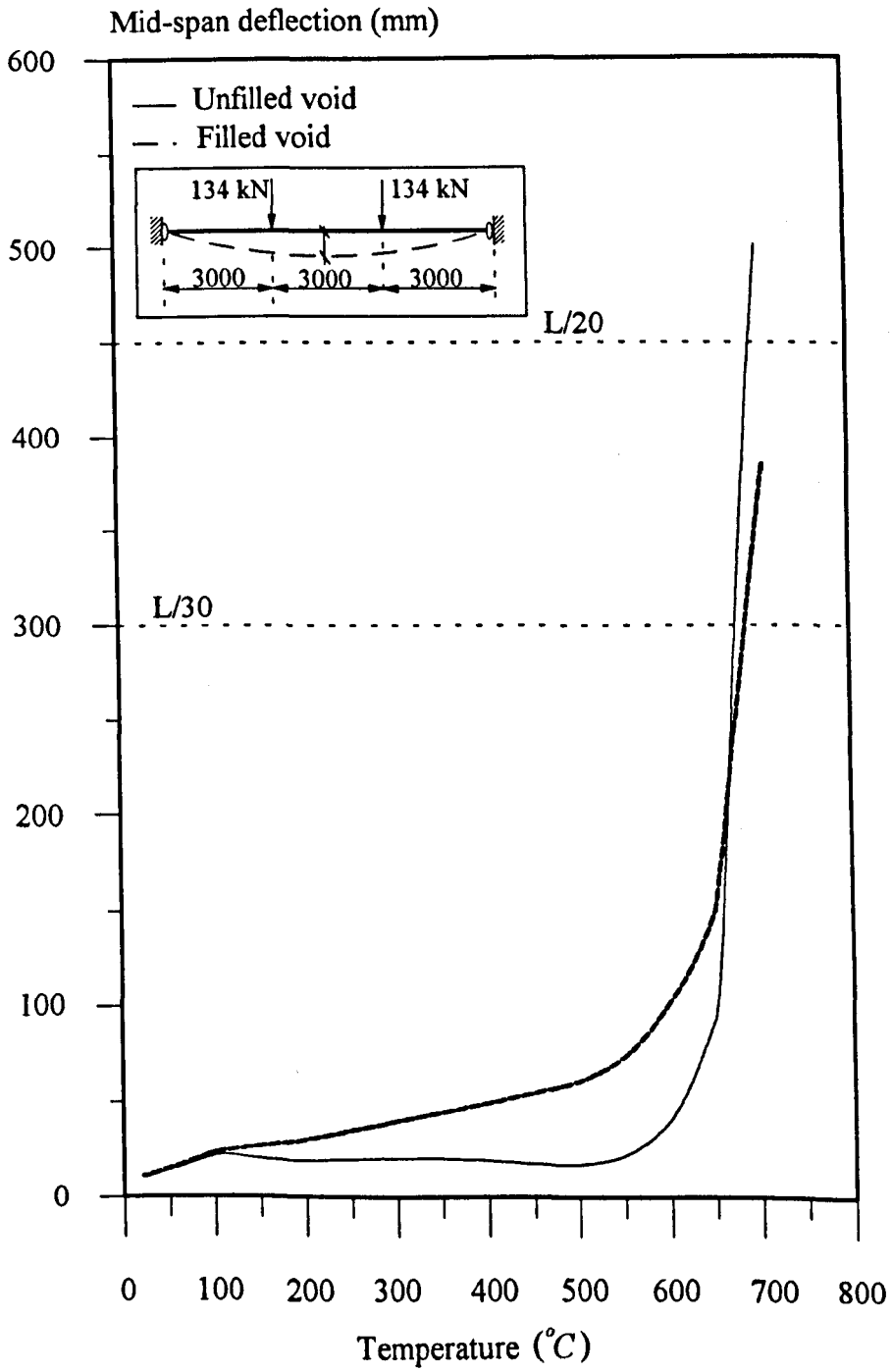

Fig. 7.31 Effect of temperature profile for a semi-rigid beam with partial interaction.

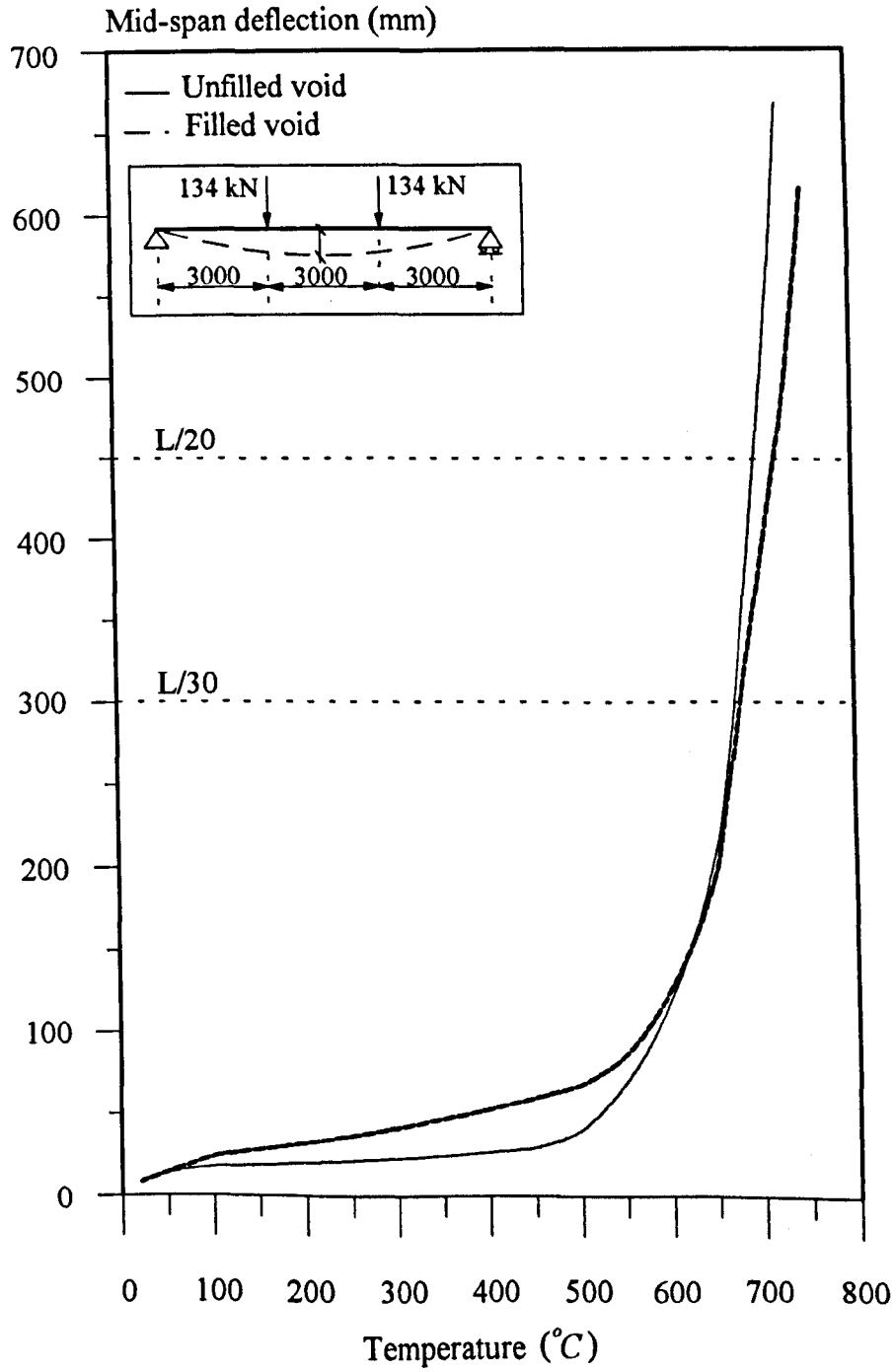

Fig. 7.32 Effect of temperature profile for a simple beam with full interaction.

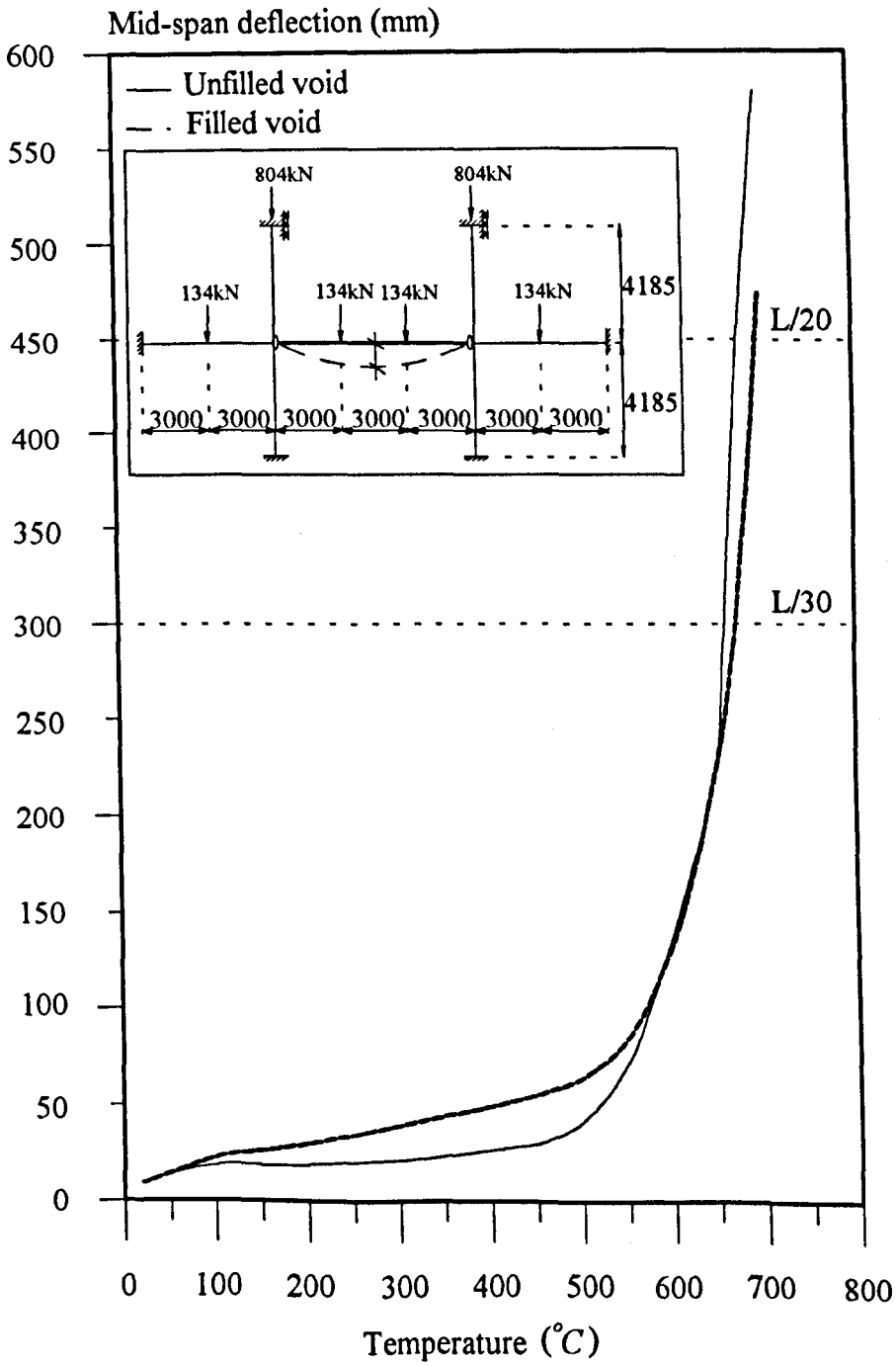

Fig. 7.33 Effect of temperature profile for a semi-rigid beam in a sub-frame.

CHAPTER 8. DISCUSSION AND CONCLUSIONS

In recent years there has been a growing trend towards using analytical methods to predict the performance of steel structures, protected or unprotected, under fire conditions. The work presented in this thesis is a development of this and is concerned mainly with the development of an analytical approach to investigate the structural behaviour of unprotected composite beams at elevated temperatures. In particular the influence of slip between the steel and concrete and the effect of semi-rigid connections have been incorporated. The analysis has been validated against published experimental data for various types of beam and subsequently used to determine the influence of various parameters which might affect the structural behaviour at elevated temperatures.

8.1. The Computer Model

The analysis is based on a non-linear finite element model 'INSTAF' originally developed for studying the behaviour of two-dimensional non-composite steel structures. This has been extensively modified to deal with composite beams at elevated temperatures for both full and partial interaction. The original program included geometrical and material non-linearity and a non-linear strain-displacement relationship but the influence of thermal strains and non-uniform temperature distribution across the cross-section and along the length of an element had to be incorporated. The procedures used for full and partial interaction analyses were essentially different, and hence two separate computer programs were developed using FORTRAN 77 for IBM compatible personal computers.

In the case of full interaction the influence of slip is neglected and the finite element model consists of a single line element representing both the reinforced concrete slab and steel beam. The original program INSTAF was extended to include the reinforced concrete slab, the degradation of material properties at high temperatures and semi-rigid connections. The basic formulation is similar to INSTAF and therefore the program is capable of analysing both frames and isolated composite beams, although the current work has largely concentrated on beams only.

In the partial interaction model the influence of slip between the concrete slab and the steel beam was considered by introducing two parallel line finite elements connected together by a continuous shearing medium along the length of the beam, characterised by

an assumed force-slip relationship. The treatment of slip allowed for conditions involving large displacements, since under fire exposure, beam deformations which are much bigger than under normal circumstances must be considered. Numerical procedures were developed to account for this effect and then incorporated into the original formulation of INSTAF.

The connections have been modelled as zero length spring elements corresponding to the degrees of freedom in the beam elements. In the full interaction model only a rotational spring, characterised by the moment-rotation relationship of a steel-to-steel connection, was used. In the partial interaction model the treatment of the semi-rigid connections requires more care due to its more complicated representation. The rotational stiffness of the connection was represented by a pair of rotational springs one connected to the concrete slab and the other to the steel I-section. Applying the full rotational stiffness from the moment-rotation curve will effectively double the stiffness of the connection. In order to avoid this the rotational spring stiffness was assumed to be divided equally between the concrete slab and the steel beam. Because of the truss-like behaviour of the two line elements used in the partial interaction analysis, a normal reaction force is induced in the bottom line element corresponding to the steel I-section and this increases the connection rigidity significantly. This necessitates the introduction of a linear spring connected to the steel beam which will allow for the relative movement between the steel and concrete at the beam ends. The force-elongation characteristics assumed in this study were based, for convenience, on the reinforcement. In both analyses the coupling effect between rotational, shear and axial displacements was ignored.

The behaviour for this semi-rigid model was consistent with similar cases using full interaction analysis both at ambient and elevated temperatures. However the distribution of stiffness used in this model is indicative rather than representative of actual conditions.. A more detailed study including additional tests is required in order to establish a rational basis for representing the connection.

In order to validate the computer model some convergence studies and comparisons with published experimental data were carried out. The convergence studies also helped determine an appropriate mesh density, demonstrating acceptable accuracy. Typically it was found that good accuracy could be obtained with four to six elements and this helped to define modelling arrangements for subsequent studies.

Although a number of fire tests have been conducted on bare and protected steel beams, there is very little test data published for composite beams at elevated temperature. Even for those tests which have been reported, the slip between the steel and concrete was not measured. This would be very difficult and the primary purpose of the tests was to

establish survival times rather than study any deterioration in composite action. Therefore most validation studies for partial composite action were carried out with published experimental data at ambient temperature.

For the purpose of analysis semi-rigid connections are represented as a series of moment-rotation curves. The precise form of this relationship can influence the analytical results very significantly. Although ambient temperature characteristics for a range of bare steel connections are available, experimental data for composite connections is rather limited and shows considerable scatter. Moreover most ambient temperature test reports on composite beams with partial interaction and realistic (semi-rigid) support conditions do not include details of the connection characteristics.

Even at ambient temperature there are a number of sources of discrepancy when comparing analysis and test results. In many cases reports of tests on partially composite beams do not include the force-slip characteristics of the studs used in the specimen. Even when they are reported the force-slip characteristics of studs from standard push-out tests may differ in bending and the small measurements of slip deformations might not be entirely reliable, especially when the beam is near to failure and its deflection is increasing very rapidly.

Research on the degradation of connection, stud and concrete properties with increasing temperature is very limited. In the present analysis the temperature in the concrete slab rarely exceeds 200^{o}C and therefore the change in the properties of the studs and concrete may be less significant than that of the steel. However in situations where the concrete slab is heated more severely these may have a greater effect on the behaviour. More fire tests on partially composite beams including measurement of slip deformations would be valuable for fully validating the analysis at high temperatures.

Despite all these uncertainties comparisons both at ambient and elevated temperatures were generally good. The analysis predicts a logical response to variations in parameters, and also to changes in the finite element mesh density used. It may therefore be claimed that the model provides a reliable means of predicting the behaviour of partially composite beams in fire, in the context of the current state of knowledge.

8.2. Studies Using the Computer Model

A range of idealised connection representations were studied to establish the most appropriate form, and this was then used to conduct a parametric study in order to examine the influence of shear connectors, varying semi-rigid connection stiffness and

reinforcement ratio, and temperature profile across the section. For the purpose of comparison, the studies concerning the shear connectors and semi-rigid connections were carried out both at ambient and elevated temperatures.

The partial interaction analyses varying the number of studs along the length from a very small to a very large number showed a logical progression from non-composite to fully composite conditions, with a corresponding increase in failure temperature defined by a limiting deflection of L/20 or L/30. However, this range was surprisingly small. For a simply supported beam the fully composite beam failed at a temperature 12% higher than the non-composite beam, whilst for the fixed ended beam the difference was even smaller at 3%. As might be expected, results for the beam with semi-rigid end restraints were intermediate between these two figures. This suggests that the effect of the number of studs is less influential at high temperatures than at ambient temperature and may be explained by the relatively rapid deterioration of material properties of the steel causing yielding earlier than the shearing of the studs.

For fully fixed end conditions in which horizontal movement as well as rotation is prevented an axial force is induced due to restraint to thermal expansion. This in turn leads to a reduction in failure temperature of 7% compared with the semi-rigid beam where the linear spring allows some thermal expansion.

Fully fixed end restraints and differential thermal expansion between the steel I-section and concrete slab can cause severe slip deformations of the studs even with higher degrees of shear connection, reducing the benefits of composite behaviour significantly. Consequently increasing the number of studs has negligible influence on the failure temperature which is largely determined by the high temperature strength of the steel I-section acting non-compositely. The difference in failure temperature for a fully composite and non-composite section is also very little because in both cases the mode of failure is the same.

For simply supported end conditions the slip deformations are very small because thermal slips are opposite to the direction of mechanical slips. This suggests that simply supported beams behave essentially as fully composite, even with low degrees of shear connection. Therefore, for practical degrees of shear connection, the full interaction analysis may provide adequate accuracy in predicting composite beam behaviour at elevated temperatures but not at ambient temperature.

The influence of the strength of the shear connectors on structural behaviour was investigated, assuming stud temperatures remained cool. The results indicated that for simply supported beams the failure temperature was not affected because the common

mode of failure was yielding of the steel. This is entirely consistent with the observation that the number of studs has only a small influence on failure temperature.

Further analyses were carried out to investigate the effect of degrading the force-slip characteristics of the studs as this temperature increases. Comparisons were made with cases where the stud temperature remained cool, showing a negligible difference in predicted failure temperatures. The stud temperatures at failure were found to be below 435°C at which the stud has lost only 15% of its strength at ambient temperature.

It is possible to study frames with full interaction only. This introduces a range of additional parameters, namely relative size, length, load ratio of the beam and column, connection stiffness and also other failure modes, notably column failure. Limited studies on isolated beams assuming partial interaction showed a slight improvement (6% greater) in failure temperature compared with beams in a sub-frame assuming full interaction. This was possibly due to column failure (column exposed) in the sub-frame analysis. Clearly the behaviour of composite beams within a more extensive frame requires further detailed study, but this is largely beyond the scope of the current work.

The influence of the connection on the behaviour of beams has been studied by conducting a series of sensitivity studies varying the values of the spring stiffnesses used to model the connection. These showed that at ambient temperature the structural behaviour was more sensitive to the rotational stiffness with an increase in failure load of about 80% for an effectively fixed ended beam compared with the simply supported case. However at elevated temperatures it was equally sensitive to both rotational and axial stiffness. For low degrees of shear connection increasing the axial stiffness resulted in negligible effect on the failure load because it can only be mobilised when there is adequate interaction between the concrete slab and steel beam. For higher degrees of interaction however, increasing the axial stiffness led to a significant improvement in failure load. In contrast, the studies at elevated temperatures showed that the axial stiffness had a significant influence even with low degrees of shear connection. This is due to the restraint provided to thermal expansion. This induces an axial force which in turn reduces the fire resistance temperature. Compared with the axially unrestrained fixed-end condition, the failure temperature of 688°C is reduced by 14%.

Preliminary studies were conducted to investigate the effect of continuous reinforcement over the supports on the behaviour at elevated temperatures by varying the reinforcement ratio. This has very little effect on the failure temperature for the simply supported case whereas the effect for the unrestrained fixed ended case is significant due to the increased strength in hogging at the support. The increase in failure temperature was 15% as the reinforcement ratio was increased from 0 to 1.16%. For the axially restrained fixed ended

beam, however, the reinforcement ratio does not affect the failure temperature. In this case the axial force due to restraint to thermal expansion leads to a more rapid deterioration of the steel and reinforcement at the supports.

The temperature profile across the cross-section of a composite beam with a profiled metal deck is different from a beam with a solid concrete slab. This effect was investigated by comparing the analytical results for temperature distributions corresponding to filled and unfilled 'void'. For unfilled void temperatures thermal bowing in the direction opposite to normal deflections was observed. As a result predicted deflections between $100^{o}C$ and $600^{o}C$ were slightly lower than for filled void temperatures but for both cases the difference in predicted failure temperature was negligible.

8.3. Concluding Remarks

It has been shown that the computer model developed provides a useful and efficient tool for predicting composite beam behaviour at elevated temperatures. Experimental studies on composite beams, connections and studs at elevated temperatures are very scarce and additional experimental data on these would enable more complete validation of the computer model. The new parts regarding the concrete slab, shear connection, semi-rigid connections and high temperature aspects were incorporated into self-contained subroutines so that future modifications can be introduced easily.

Due to the heat sink effect of the concrete slab, the steel beam in composite floor construction may not need full fire protection. The studies presented here indicated failure temperatures in excess of $660^{o}C$, an increase of 20% compared with the critical temperature of $550^{o}C$ for bare steel beams.

Future work might involve the development of the partial interaction analysis into a three dimensional frame analysis with composite or bare steel columns. This would enable the conduct of an intensive parametric study to provide guidance on simplified approaches to modelling the behaviour of composite frames in fire. However indications are that incomplete interaction is relatively unimportant and that the beam behaviour is relatively insensitive to this. It may therefore be assumed that for practical degrees of shear connection, full-interaction is adequate for the analysis of composite beams under fire conditions.

REFERENCES

1. *Fire Grading of Buildings, Part 1, General Principles and Structural Precautions, Post-War Building Studies* No 2, London, HMSO, 1946.

2. *Fire Grading of Buildings, Part 2, Fire Fighting Equipment, Part 3 Personal Safety*, Part 4 Chimneys and Flues, Post-War Building Studies No 29, London, HMSO, 1952.

3. *Building and Buildings, Building Regulations 1965*, SI 165 No 1373, HMSO, London, 1965.

4. *Building and Buildings, Building Regulations 1985*, SI 1985 No 1065, HMSO, London, 1985.

5. Malhotra, H.L., *Fire Safety in Buildings*, Building Research Establishment Report, December 1986.

6. Shields, T.J. and Silcock, G.W.H., *Buildings and Fire*, Longman Scientific & Technical, John Wiley & Sons, Inc., New York, 1987.

7. *British Standard BS476: Fire tests on Building Materials and Structures, Part 20, Method for the Determination of the Fire Resistance of Elements of Construction (General Principles), Part 21, Method for the Determination of the Fire Resistance of Load Bearing Elements of Construction*, 1987.

8. Kirby, B.R., *Modern Fire Protection Systems and Design Methods, Fire Resistance of Steel Structures*, British Steel Corporation, January 1985.

9. Uddin, T. and Culver, C.G., Effects of Elevated Temperatures on Structural Members, *Journal of the Structural Division*, **101**, (ST7), July 1975.

10. Smith, C.I., Structural Steel Fire Protection for Multi-Storey Buildings-Recent Developments, *Steel Construction*, **20**, (2), 1986.

11. Cooke, G.M.E., Session 1, *Developments in Multi-Storey Buildings, Practical Fire Engineering: Part A: The Context*, National Structural Steel Conference, 1984.

12. Latham, D.J., *Developments in Multi-Storey Buildings, Practical Fire Engineering: The Use of Unprotected Steelwork in Buildings*, National Structural Steel Conference, 1984.

13. Witteveen, J., *Design Methods for Fire Exposed Steel Structures, Steel in Building*, IABSE-ECCS Symposium, Luxembourg, 1985.

14. Lie, T.T. and Stanzak, W.W., Structural Steel in Fire, -More Realistic Analysis, ASCE National Structural Engineering Meeting, Cincinnati, April 1974, *Engineering Journal*, American Institute of Steel Construction, Second Quarter, 1976.

15. *RPS Report, No. 08/90*, Arbed Recherches, Luxembourg, 1990.

16. Becker, J., Bizri, H. and Bresler, B., *FIRES-T A Computer Program for the Fire Response of Structures-Thermal*, Report No. UCB FRG 74-1, Fire Research Group, Structural Engineering, University of California, Berkeley, 1974.

17. Hill., A.J., *Fire Tests and the Response of Structural Steelwork*, M.Phil. Thesis, Department of Civil and Structural Engineering, University of Sheffield, March 1990.

18. Wickstrom, U., *TASEF-2 A Computer Program for Temperature Analysis of Structures Exposed to Fire*, Report No. 79-2, Department of Structural Mechanics, Lund Institute of Technology, Sweden, 1979.

19. Schleich, J.B., Dotreppe, J.C. and Franssen, J.M., *Numerical Simulations of Fire Resistance Tests on Steel and Composite Structural Elements or Frames*, Fire Safety Science, Proceedings of the First International Symposium, October, 1985.

20. Schleich, J.B., Fire Engineering Design of Steel Structures, *Steel Construction Today*, **2**, 1988, pp. 39-52.

21. Preston, R.R. and Kay, T.R., Deformation of Steel Beams During Fire Tests, *Metals and Materials*, **2**, (5), May, 1986.

22. Burgess, I.W., El-Rimawi, J.A. and Plank, R.J., A Secant Stiffness Approach to the Fire Analysis of Steel Beams, *Journal of Constructional Steel Research*, **11**, (2), 1988, pp. 105-122.

23. El-Rimawi, J.A., *The Behaviour of Flexural Members Under Fire Conditions*, Ph.D. Thesis, Department of Civil and Structural Engineering, University of Sheffield, April 1989.

24. Burgess, I.W., El-Rimawi, J.A. and Plank, R.J., Analysis of Beams with Non-Uniform Temperature Profile Due to Fire Exposure, *Journal of Constructional Steel Research*, **16**, (13), 1990, pp. 169-192.

25. Johnson, R.P., *Composite Structures of Steel and Concrete, Beams, Columns, Frames and Applications in Building*, Vol. 1, Granada Publishing Ltd., London, 1982.

26. Langdon-Thomas, G.J., *Fire Safety in Buildings-Principle and Practice*, Adam & Charles Black, London, 1972.

27. Lu, S.Y., Trubert, M. and Nash, W.A., Elevated Temperature Characteristics of Type 347 Stainless Steel, *American Society for Testing and Materials*, Proceedings, **61**, 1961.

28. Willhelm, A.C. and Kattus, J.R., Stress-strain Characteristics of Metals Under Conditions of Transient Heating and Loading, *American Society for Testing and Materials*, Proceedings, **63**, 1963.

29. Jorgensen, J.R. and Sorensen, A.H., *Fire Resistance of Load-Bearing Structures Testing Procedures and Test Results, Project 4, Mechanical Properties of Structural Steel at Elevated Temperatures*, Institute for Bygningsteknik, July 1980.

30. Anderberg, Y., *Behaviour of Steel at High Temperatures, RILEM*, Lund Institute of Technology, Sweden 1983.

31. Holmes, M., Anchor R.D., Cook G.M.E., and Crook R.N., The Effects of Elevated Temperatures on the Strength properties of Reinforcing and Prestressing Steels, *The Structural Engineer*, **60B**, (1), March 1982.

32 Baba, S. and Nagura, H., Effect of Material Properties on the Deformation of Steel Frame in Fire, *Proc. of JSCE Structural Eng./Earthquake Eng.*, **2**, (1), April 1985.

33. Purkiss, J.A., Developments in the Fire Design of Structural Steelwork, *Journal of Constructional Steel Research*, **11**, 1988, pp. 149-173.

34. Harmathy, T.Z. and Stanzak, W.W., Elevated-Temperature Tensile and Creep Properties of Some Structural Prestressing Steel, Fire Test Performance, *American Society for Testing and Materials*, (STP 464), 1970, pp. 186-208.

35. Harmathy, T.Z. and Stanzak, W.W., *Behaviour of Steel Flexural Members in Fire, Application of Solid Mechanics, Study no. 7*, University of Waterloo, 1972.

36. Stanzak, W.W., *Fire Tests on Wide-Flange Steel Beams Protected with Gypsium Sanded Plaster, Fire Study No. 16 of the Division of Building Research*, National Research Council of Canada, June 1967.

37. Harmathy, T.Z., Deflection and Failure of Steel-Supported Floors and Beams in Fire, *ASTM*, (Special Technical Publication 422), 1967, pp. 40-62.

38. Stanzak, W.W. and Harmathy, T.Z., Effect of deck on Failure Temperature of Steel Beams, *Fire Technology*, **4**, 1968, pp. 265-270.

39. Witteveen, J., Twilt, L. and Bijlaard, F.S.K., *Theoretical and Experimental Analysis of Steel Structures at Elevated Temperatures*, IABSE, 10th Congress, Tokyo, Final Report, Zurich, 1977.

40. Kirby, B.R., and Preston, R.R., High Temperature Properties of Hot Rolled Structural Steels For Use in Fire Engineering Studies, *Fire Safety Journal*, **13**, 1988.

41. Popovics, S., A numerical Approach to the Complete Stress-Strain Curve of Concrete, *Cement and Concrete Research*, **3**, (5), 1973, pp. 583-599.

42. Wang, P.T., Shah, S.P. and Naaman, A.E., Stress-Strain Curves of Normal and Lightweight Concrete in Compression, *Journal of the American Concrete Institute*, **75**, (11), November 1978.

43. Noor, F.A. and Wijayasri, S., Modelling the Stress-Strain Relationship of Structural Concrete, *Magazine of Concrete Research*, **34**, (118), March 1982.

44. Carreira, D.J. and Chu, K.H., Stress-Strain Relationship for Plain Concrete in Compression, *Journal of the American Concrete Institute*, **82**, (6), November-December 1985.

45. Tomaszewics, A., Stress-Strain Relationship for Concrete in Compression, *Journal of the American Concrete Institute*, **83**, (5), September-October 1986.

46. Hsu, T.T.C., Slate, F.O., Sturman, G.M. and Winter, G., Microcracking of Plain Concrete and the Shape of the Stress-Strain Curve, *Journal of the American Concrete Institute*, **60**, February 1963, pp. 209-223.

47. Krishnaswamy, K.T., Microcracking of Plain Concrete Under Uniaxial Compressive Loading, *Indian Concrete Journal*, **66**, April 1969, pp. 143-145.

48. Kupfer, H., Hilsdorf, H.K. and Rusch, H., Behaviour of Concrete Under Biaxial Stresses, *Journal of the American Concrete Institute*, **66**, August 1969, pp. 656-665.

49. Furamura, F., *The Stress-Strain Curve of Concrete at High Temperatures*, Annual Meeting of the Architectural Institute of Japan, Paper No. 70004, Part 1, 1966.

50. *Fire Resistance of Concrete Structures*, Report of a Joint Comittee, The Instituion of Structural Engineers, The Concrete Society, August 1975.

51. Anderberg, Y. and Thelandersson, S., A Constitutive Law for Concrete at Transient High Temperature Conditions, Douglas McHenry International Symposium on Concrete and Concrete Structures, *American Concrete Institute*, Publication SP-55, Detroit, 1978.

52. Anderberg, Y., Magnusson, S.E., Pettersson, O., Thelandersson, S. and Wickstrom, U., An Analytical Approach to Fire Engineering Design of Concrete Structures, Douglas McHenry International Symposium on Concrete and Concrete Structures, *American Concrete Institute*, (Publication SP-55), Detroit, 1978.

53. Anderberg, Y., Fire-Exposed Hyperstatic Concrete Structures: An Experimental and Theoretical Study, Douglas McHenry International Symposium on Concrete and Concrete Structures, *American Concrete Institute*, (Publication SP-55), Detroit, 1978.

54. Malhotra, H.L., The Effect of Temperature on the Compressive Strength of Concrete, *Magazine of Concrete Research*, **8**, (23), August 1956, pp. 85-94.

55. Mohamedbhai, G.T.G., The Residual Strength of Concrete Subjected to Elevated Temperatures, *Concrete*, December 1983, pp. 22-27.

56. Fahmi, H.M. and Nuri, D., Influence of High Temperatures on Compressive and Tensile Strengths of Concrete, *Journal of Building Research*, **5**, (2), 1986, pp. 86-102.

57. Ahmed, A.E., Al-Shaikh, A.H. and Arafat, T.I., Residual Compressive and Bond Strengths of Limestone Aggregate Concrete Subjected to Elevated Temperatures, *Magazine of Concrete Research*, **44**, (159), June 1992, pp. 117-125.

58. Philleo, R., Some Physical Properties of Concrete at High Temperatures, *Journal of the American Concrete Institute*, **29**, (10), April 1958, pp. 857-867.

59. Cruz, C.R., Elastic Properties of Concrete at High Temperatures, *Journal of the PCA*, Research and Development Laboratories, **8**, (1), January 1966, pp. 37-45.

60. Chapman, J.C. and Balakrishnan, S., Experiments on Composite Beams, *The Structural Engineer*, **42**, (11), November 1964.

61. Slutter, R.G. and Driscoll, G.C., Flexural Strength of Steel-Concrete Composite Beams, *Journal of the Structural Division*, Proceedings of the American Society of Civil Engineers, **91**, (ST2), Part 1 of 2 Parts, April 1965.

62. Menzies, J.B., CP117 and Shear Connectors in Steel-Concrete Composite Beams Made with Normal-Density or Lightweight Concrete, *The Structural Engineer*, **49**, (3), March 1971.

63. Ollgaard, J.G., Slutter, R.G. and Fisher, J.W., Shear Strength of Stud Connectors in Lightweight and Normal-Weight Concrete, *American Institute of Steel Construction Engineering Journal*, **8**, (2), April 1971.

64. Oehlers, D.J and Coughlan, C.G., The Shear Stiffness of Stud Shear Connection in Composite Beams, *Journal of Constructional Steel Research*, **6**, 1986, pp. 273-284.

65. Oehlers, D.J. and Johnson, R.P., The Strength of Stud Shear Connection in Composite Beams, *The Structural Engineer*, **65B**, (2), June 1987.

66. Robinson, H., Multiple Stud Shear Connections in Deep Ribbed Metal Deck, *Canadian Journal of Civil Engineering*, **15**, 1988.

67. Mottram, J.T. and Johnson, R.P., Push Tests on Studs Welded through Profiled Steel Sheeting, *The Structural Engineer*, **68**, (10), May 1990.

68. Lawson, R.M., *Shear Connection in Composite Beams*, Composite Construction in Steel and Concrete: Proceedings of an Engineering Foundation Conference, Trout Lodge, Potosi, Missouri, June 1992, American Society of Civil Engineers, 1993.

69. Oehlers, J. and Sved, G., Composite Beams with Limited-Slip-Capacity Shear Connectors, *Journal of Structural Engineering*, **121**, (6), June 1995, pp. 932-938.

70. Crisinel, M., Partial-Interaction Analysis of Composite Beams with Profiled Sheeting and Non-welded Shear Connectors, *Journal of Constructional Steel Research*, **15**, 1990, pp. 65-98.

71. Kruppa, J. and Zhao, B., Fire Resistance of Composite Beams to Eurocode 4 Part 1.2, *Journal of Constructional Steel Research*, **33**, 1995, pp. 51-69.

72. Donell, L.H., Suggested New Definitions for Proportional Limit and Yield Point, *Mechanical Engineering*, **60**, (11), 1938, pp. 837-838.

73. Esser, H. and Ahrend, H., Kann die 0.2 Uberin Kommenfreie Dehngrenze Ersetzt Werden, *Arch. f. Eisenhuttenw.*, **13**, (13), 1939-40, pp. 425-428.

74. Holmquist, J.L. and Nadai, A., *A Theoretical and Experimental Approach to the problem of Collapse of Deep-Well Casing*, Paper Presented at 20th Annual Meeting, American Petroleum Institute, Chicago, November 1939.

75. Ramberg, W. and Osgood, W.R., *Description of Stress-Strain Curves by Three Parameters*, National Advisory Committee for Aeronautics, Technical Note No. 902, 1943.

76. Kruppa, J., Collapse Temperature of Steel Structures, *Journal of Steel Structural Division*, **105**, (ST9), September 1979.

77. *British Standard BS5950, Code of Practice for the Fire Protection of Structural Steelwork, Part 8*, 1985.

78. Proe, D.J., Thomas, I.R. and Bennetts, I.D., Simulation of the Fire Testing of Structural Elements by Calculation- Mechanical Response, *Steel Construction*, **19**, (4), February 1986

79. Dounas, S. and Golrang, B., *Stals Mekaniska Egenskaper vid Hoga Temperaturer*, Lund Institute of Technology, Sweden, 1982.

80. *Eurocode4, Design of Composite Steel and Concrete Structures, Part 1.2: Structural Fire Design*, Second Draft 1992.

81. Hognestad, E. and Hanson, N.W., Mc. Henry D., Concrete Stress-Distribution in Ultimate Strength Design, *Proceedings of the ACI*, **52**, (Pt. 1), December 1955.

82. Desayi, P. and Krishnan, S., Equation for the Stress-Strain Curve of Concrete, *Journal of the American Concrete Institute*, **61**, (3), March 1964.

83. Kabaila, A., Equation for the Stress-Strain Curve of Concrete, Discussion of the Paper by Desayi, P. and Krishnan, S., *Journal of the American Concrete Institute*, Proceedings, **61**, (9), September 1964.

84. Tulin, L.G. and Gerstle, K.H., Equation for the Stress-Strain Curve of Concrete, Discussion of the Paper by Desayi, P. and Krishnan, S., *Journal of the American Concrete Institute*, Proceedings, **61**, (9), September 1964.

85. Saenz, L.P., Equation for the Stress-Strain Curve of Concrete, Discussion of the Paper by Desayi, P. and Krishnan, S., *Journal of the American Concrete Institute*, Proceedings, **61**, (9), September 1964.

86. Tsai, W.T., Uniaxial Compressional Stress-Strain Relation of Concrete, ASCE, *Journal of Structural Engineering*, **114**, (9), September 1988.

87. Bresler, B. and Iding, R.H., Effects of Normal and Extreme Environment on Reinforced Concrete Structures, Douglas McHenry International Symposium on Concrete and Concrete Structures, *American Concrete Institute*, (Publication SP-55), Detroit, 1978.

88. Baldwin, R. and North, M.A., A Stress-Strain Relationship for Concrete at High Temperatures, *Magazine of Concrete Research*, **25**, (85), December 1973.

89. Kishysh, K.O., *Finite Element Analysis of Fire Exposed Reinforced Concrete Column*, Ph.D. Thesis, Department of Civil and Structural Engineering, University of Sheffield, July 1986.

90. Yam, L.C.P and Chapman, J.C., The Inelastic Behaviour of Continuous Composite Beams of Steel and Concrete, *Proc. of Institution of Civil Engineers*, **53**, December 1972, pp. 487-501.

91. Witteveen, J. and Twilt, L., Behaviour of Steel Column Under Fire Action, International Colloqium of Column Strength, Paris 1972, *Proc. IABSE*, **23**, 1973.

92. Witteveen, J., Twilt, L. and Bijlaard, F.S.K., *The Stability of Braced and Unbraced Frames at Elevated Temperatures, Stability of Steel Structures*, Preliminary Report, Liege, April 1977.

93. Cooke, G.M.E., *Session 1: Developments in Multi-Storey Buildings, Practical Fire Engineering: Part D: Applications of Steel Models Research*, National Structural Steel Conference, 1984.

94. Wainman, D.E. and Kirby, B.R., *Compendium of UK Standard Fire Test Data, Unprotected Structural Steel-1*, British Steel Corporation, Swinden Laboratories, Ref. No. RS/RSC/S10328/1/87/B, Rotherham, 1988.

95. Rubert, A. and Schaumann, P., Structural Steel and Plane Frame Assemblies Under Fire Action, *Fire Safety Journal*, **10**, 1986, pp. 173-184.

96. Dotreppe, J.C., Structural Models for Fire Analysis, *IABSE Periodica*, **3**, 1986, pp. 101-111.

97. *Construction Industry Research and Information Association, Data Sheet: Fire Resistance of Composite Slabs*, CIRIA Special Publication 42, London, 1986.

98. *British Steel Corporation, Report on the Results of Fire Tests on Three Composite Concrete Steel Floor Decks and Verification of the Design Recommendations*, BSC Welsh Labs., Report WL/FP/1464/87/D, 1987.

99. Cooke, G.M.E., Lawson, R.M. and Newman, G.M., Fire Resistance of Composite Deck Slabs, *The Structural Engineer*, **66**, (16/16), August 1988.

100. Hamerlinck R. and Twilt L., Fire Resistance of Composite Slabs, *Journal of Constructional Steel Research*, **33**, 1995, pp. 71-85.

101. Teraszkiewicz, J.S., *Static and Fatigue Behaviour of Simply Supported and Continuous Composite Beams of Steel and Concrete*, Ph.D. Thesis, Department of Civil Engineering, University of London, 1967.

102. Wright, H.D. and Francis, R.W., Tests on Composite Beams with Low Levels of Shear Connection, *The Structural Engineer*, **68**, (15), August 1990, pp. 293-298.

103. Chapman, J.C., Composite Construction in Steel and Concrete-the Behaviour of Composite Beams, *The Structural Engineer*, **42**, (4), April 1964.

104. Barnard, P.R., A Series of Tests on Simply Supported Composite Beams, *Journal of the American Concrete Institute*, **62**, April 1965, pp. 443-456.

105. Barnard, P.R. and Johnson, R.P., Ultimate Strength of Composite Beams, *Institution of Civil Engineers*, Proceedings, **32**, 1965.

106. Barnard, P.R. and Johnson, R.P., Plastic Behaviour of Continuous Composite Beams, *Institution of Civil Engineers*, Proceedings, **32**, 1965.

107. Johnson, R.P., Longitudinal Shear Strength of Composite Beams, *Journal of the American Concrete Institute*, Proceedings, **67**, (6), June 1970.

108. Cooke, G.M. and Latham, D.J., The Inherent Fire Resistance of Loaded Steel Framework, *Steel Construction Today*, **1**, 1987, pp. 49-58.

109. Lloyd, R.M. and Wright, H.D., In Situ Testing of A Composite Floor System, *The Structural Engineer*, **70**, (12), June 1992.

110. Armer, G.S.T. and Moore, D.B., Full-Scale Testing on Complete Multi-Storey Structures, *The Structural Engineer*, **72**, (2), January 1994, pp. 21-24.

111. Aggarwal, A.K., Behaviour of Flexible Endplate Beam-to-Column Joints, *Journal of Constructional Steel Research*, **16**, 1990, pp. 111-134.

112. Aggarwal, A.K., Comparative Tests on Endplate Beam-to-Column Connections, *Journal of Constructional Steel Research*, **30**, 1994, pp. 151-175.

113. Leon, T.R., Semi-Rigid Composite Connection, *Journal of Constructional Steel Research*, **15**, 1990, pp. 99-120.

114. Dalen, K.V. and Godoy, H., Strength and Rotational Behaviour of Composite Beam-Column Connections, *Canadian Journal of Civil Engineering*, **9**, (2), 1982, pp. 313-322.

115. Davison, J.B., Lam, D. and Nethercot, D.A., Semi-Rigid Action of Composite Joints, *The Structural Engineer*, **68**, (24), 1990, pp. 489-499.

116. Kemp, A.R., Trinchero, P. and Dekker, N., *Ductility Effects of End Details in Composite Beams:* Proceedings of an Engineering Foundation Conference, Trout Lodge, Potosi, Missouri, June 1992, American Society of Civil Engineers, 1993.

117. Xiao, Y., Choo, B.S. and Nethercot, D.A., Composite in Steel and Concrete, Experimental Behaviour of Composite Beam-Column Connections, *Journal of Constructional Steel Research*, **31**, 1994, pp. 3-30.

118. Anderson, D. and Najafi, A.A., Performance of Composite Connections: Major Axis End Plate Joints, *Journal of Constructional Steel Research*, **31**, 1994, pp. 31-57.

119. Puhali, R., Smotlak, I. and Zandonini, R., Semi-Rigid Composite Action: Experimental Analysis and a Suitable Model, *Journal of Constructional Steel Research*, **15**, 1990, pp. 121-151.

120. Jarrett, N.D. and Lennon, T., *Composite Sub-frame Tests, Report No.3, Results From Test NR2*, Building Research Establishment Note N141/92, 1992.

121. Lawson, R.M., Behaviour of Steel Beam-to-Column Connections in Fire, *The Structural Engineer*, **68**, (14), 1990, pp. 263-271.

122. Lawson, R.M. and Newman, G.M., Fire Resistance of Steel Beam-to-Column Connections and Composite Beams, *Steel Construction Today*, November 1991.

123. Lennon, T. and Jones, L.C., *Elevated Temperature Moment Rotation Tests*, Building Research Establishment, Note N135/94, October 1994.

124. Preston, R.R. and Kay, T.R., Fire Resistance of Structural Steel Beams, *Metals and Materials*, **2**, (1), January 1986.

125. Gehri, E., The Fire Resistance of Steel Structures, *Fire Technology*, **21**, (1), February 1985.

126. Newman, G.M., *Session 1: Developments in Multi-Storey Buildings, Practical Fire Engineering: Part B: Structural Applications*, National Structural Steel Conference, 1984.

127. Proe, D.J., Thomas, I.R. and Bennets, I.D., Simulation of the Fire Testing of Structural Elements by Calculation, -Overall Behaviour, *Steel Construction*, **19**, (4), February 1986.

128. Oven, V.A., *The Behaviour of Shelf-Angle Beams at Elevated Temperatures*, M.Phil. Thesis, School of Architectural Studies, University of Sheffield, May 1992.

129. Petterson, O. and Witteveen, J., On the Fire Resistance of Structural Steel Elements Derived From Standard Fire Test or by Calculation, *Fire Safety Journal*, **2**, 1979/80, pp. 73-87.

130. Luckyram, J. and Vardy, A.E., Shear Displacement in Bonded Structures, *Journal of Constructional Steel Research*, **16**, 1990, pp. 71-84.

131. Bradford, M.A. and Gilbert, R.I., Composite Beams with Partial Interaction Under Sustained Loads, *Journal of Structural Engineering*, **118**, (7), July 1992, pp. 1871-1882.

132. Cunnigham, R., Some Aspects of Semi-Rigid Connections in Structural Steelwork, *The Structural Engineer*, **68**, (5), 1990.

133. Jaspart, J.P. and Maquoi, R., Guidelines for the Design of Braced Frames with Semi-Rigid Connections, *Journal of Constructional Steel Research*, **16**, 1990, pp. 319-328.

134. Li, T.Q., Choo, B.S. and Nethercot, D.A., Determination of Rotation Capacity Requirements for Steel and Composite Beams, *Journal of Constructional Steel Research*, **32**, 1995, pp. 303-332.

135. Zandonini, R. and Zanon, P., *Semi-Rigid Joint Action in Composite Frames: Numerical Analysis and Design Criteria:* Proceedings of an Engineering Foundation Conference, Trout Lodge, Potosi, Missouri, June 1992, American Society of Civil Engineers, 1993.

136. Plank, R., *The Collapse Behaviour of Steel Beams in Fire -An Analytical Treatment*, International Conference on Steel and Aluminium Structures, Cardiff, 1987, pp. 110.

137. El-Rimawi, J.A., Burgess, I.W. and Plank, R.J., *The Analysis of Steel Beams in Fire*, International Conference on Steel and Aluminium Structures, ICSAS 91, Singapore, 22-24 May 1991.

138. El-Rimawi, J.A., Burgess, I.W. and Plank, R.J., The Analysis of Semi-Rigid Frames in Fire-A Secant Approach, *Journal of Constructional Steel Research*, **33**, 1995, pp. 125-146.

139. Cheng, W. and Mak, C.K., Computer Analysis of Steel Frame in Fire, *Journal of the Structural Division*, **101**, (ST4), April 1975.

140. Furamura, F. and Shinohara, Y., *Inelastic Behaviour of Protected Steel Beams and Frames in Fire*, Report of the Research Laboratory of Engineering Materials, Tokyo Institute of Technology, No. 3, 539.433:6999:81, Tokyo, Japan, 1978.

141. Cheng, W.C., Theory and Application on the Behaviour of Steel Structures at Elevated Temperatures, *Computers and Structures*, **16**, (1-4), 1983, pp. 27-35.

142. Jain, P.C. and Rao, M.N.G., Analysis of Steel Frames Under Fire Environment, *International Journal for Numerical Methods in Engineering*, **19**, 1983, pp. 1467-1478.

143. Saab, H.A. and Nethercot, D.A., Modelling Steel Frame Behaviour Under Fire Conditions, *Engineering Structures*, **13**, October 1991, pp. 371-382.

144. El-Zanaty, M.H., Murray, D.W. and Bjorhovde, R., *Inelastic Behaviour of Multi-Storey Steel Frames, Structural Engineering Report No. 83*, Department of Civil Engineering, University of Alberta, Canada, April 1980.

145. El-Zanaty, M.H. and Murray, D.W., Non-Linear Finite Element Analysis of Steel Frames, *ASCE Journal of Structural Division*, **109**, (ST2), 1983, pp. 353-368.

146. Najjar, S.R., *Three-Dimensional Analysis of Steel Frames and Subframes in Fire*, Ph.D. Thesis, Department of Civil and Structural Engineering, University of Sheffield, 1994.

147. Bailey, C.G., *Simulation of the Structural Behaviour of Steel-Framed Buildings in Fire*, Ph.D. Thesis, Department of Civil and Structural Engineering,, University of Sheffield, May 1995.

148. Siess, C.P., Tests and Analysis of Composite Beams With Incomplete Interaction, *Proc. Soc. Exp. Stress Analysis*, **9**, (1), 1951, pp. 75-92.

149. Yam, L.C.P and Chapman, J.C., The Inelastic Behaviour of Simply Supported Composite Beams of Steel and Concrete, *Institution of Civil Engineers Proceedings*, **41**, 1968.

150. Hirst, M.J.S. and Yeo, M.F., The analysis of Composite Beams Using Standard Finite Element Programs, *Computers and Structures*, **11**, 1980, pp. 233-237.

151. Roberts, T.M., Finite Difference Analysis of Composite Beams with Partial Interaction, *Computers and Structures*, **21**, (3), 1985, pp. 469-473.

152. Al-Amery, R.I.M. and Roberts, T.M., Non-linear Finite Difference Analysis of Composite Beams with Partial Interaction, *Computers and Structures*, **35**, (1), 1990, pp. 81-87.

153. Aribert, J.M., *Application and Recent Development of a Numerical Model for Composite Beams with Partial Shear Connection:* Proceedings of an Engineering Foundation Conference, Trout Lodge, Potosi, Missouri, June 1992, American Society of Civil Engineers, 1993.

154. Arizumi, Y., Hamada, S. and Kajita, T., Elastic-Plastic Analysis of Composite Beams with Incomplete Interaction by Finite Element Method, *Computers and Structures*, **14**, (5-6), 1981, pp. 453-462.

155. Abdul Wali, A.A., *The Behaviour of Semi-Continuous Composite Beams*, Ph.D. Thesis, Department of Civil and Structural Engineering, University of Sheffield, September 1992.

156. Wright, H.D., The Deformation of Composite Beams with Discrete Flexible Connection, *Journal of Constructional Steel Research*, **15**, 1990, pp. 49-64.

157. Lee, S.L. and Basu, P.K., Secant Method for Non-linear Semi-Rigid Frames, *Journal of Constructional Steel Research*, **14**, 1989, pp. 273-299.

158. El-Rimawi, J.A., Burgess, I.W. and Plank, R.J., *NARR2 A Program for the Structural Analysis of 2-D Steel Frames at Elevated Temperatures*, Department of Civil and Structural Engineering, University of Sheffield, Version 1.0, July 1992.

159. Poggi, C., A Finite Element Model for the Analysis of Flexibly Connected Steel Frames, *International Journal for Numerical Methods in Engineering*, **26**, 1988, pp. 2239-2254.

160. Li, T.Q., Choo, B.S. and Nethercot, D.A., Connection Element Method for the Analysis of Semi-Rigid Frames, *Journal of Constructional Steel Research*, **32**, 1995, pp. 143-171.

161. Wegmuller, A.W. and Amer, H.N, Non-linear Response of Composite Steel-Concrete Bridges, *Computers and Structures*, **7**, 1977, pp. 161-169.

162. Elkelish, S. and Robinson, H., Effective Widths of Composite beams with Ribbed Metal Deck, *Canadian Journal of Civil Engineers*, **13**, January 1986, pp. 575-582.

163. Choi, C.K. and Kwak, H.G., The Effect of Finite Element Mesh Size in Non-linear Analysis of Reinforced Concrete Structures, *Computers and Structures*, **36**, 1990, pp. 807-815.

164. Saada, A.S., *Elasticity Theory and Applications*, Pergamon Press Inc., New York, 1974.

165. Macon, N., *Numerical Analysis*, John Wiley and Sons Inc., New York, 1963.